Final Report

STUDY OF EXTERNAL PRESSURIZATION SYSTEMS FOR CRYOGENIC STORAGE SYSTEMS

71-7537
September 10, 1971

Prepared for
Manned Spacecraft Center
National Aeronautics and Space Administration
Houston, Texas

Under Contract NAS 9-10453

GARRETT

AIRESEARCH MANUFACTURING COMPANY
Los Angeles, California

Final Report

EXTERNAL PRESSURIZATION SYSTEMS FOR CRYOGENIC STORAGE SYSTEMS

71-7537

September 10, 1971

PREPARED FOR

ROBERT R. RICE
MANNED SPACECRAFT CENTER
NAT'^NAL AERONAUTICS AND SPACE ADMINISTRATION

Prepared by
P. G. Wapato, A. W. Keeley, L. N. Jew, And C. F. Young

GARRETT

AIRESEARCH MANUFACTURING COMPANY
Los Angeles, California

PRECEDING PAGE BLANK NOT FILMED

FOREWORD

In a study conducted under Contract NAS 9-10453 initiated in December 1969, the AiResearch Manufacturing Division of The Garrett Corporation has investigated the design of external pressurization systems for cryogenic storage systems. The external pressurization concept allows pressure control of cryogenic storage systems to be accomplished without installation of dynamic components in the storage vessel.

The primary objective of the study was the establishment of a handbook-type approach to design of external pressurization systems. The results of the program are presented in three reports, as follows:

> External Pressurization Systems for Cryogenic Storage Systems - Design Reference Manual, Report 71-7535, September 10, 1971
>
> Study of External Pressurization Systems for Cryogenic Storage Systems - Contract Summary Report, Report 71-7536, September 10, 1971
>
> Study of External Pressurization Systems for Cryogenic Systems - Final Report, Report 71-7537, September 10, 1971

This volume, the last listed above, describes the total program carried out under this contract and provides background information on the characterizations presented in the Design Reference Manual.

PRECEDING PAGE BLANK NOT FILMED

CONTENTS

CONTENTS (Continued)

ILLUSTRATIONS

ILLUSTRATIONS (Continued)

ILLUSTRATIONS (Continued)

ILLUSTRATIONS (Continued)

TABLES

SECTION 1

INTRODUCTION AND SUMMARY

This report describes a study of recirculation-type external pressurization systems for use in pressure control of cryogenic hydrogen, oxygen and nitrogen storage systems. The subject concept provides an alternative to internal heating devices or injection of gaseous pressurants as a means of tank pressurization during delivery of fluid.

OBJECTIVE

The objective of the study was to investigate the external pressurization concept sufficiently to establish the tools and techniques needed by system planners for estimation of weight and cost of pressurization systems for hydrogen, oxygen and nitrogen storage systems. This information has been assembled in the form of a Design Reference Manual published as AiResearch Report 71-7535 (Reference 1).

In order to establish a system design procedure, characterization information and design procedures were developed for all major system elements. These fall into the following categories:

- Energy addition devices
- Fluid-moving devices
- Transfer lines
- Controls

The system considerations and their effect on component selection is discussed in Section 2 of this report. The thermodynamic analyses carried out are presented in Section 3. The development of individual component data is the subject of Sections 4 through 7. An appendix to the report briefly considers another alternative fluid delivery technique--the use of decay of storage pressure. It is noted that for delivery of liquid cryogen from a subcritical (two-phase) storage system, pressure decay can allow large quantities of the stored fluid to be delivered at high flow rates.

Detailed information on the use of the material developed in this program is provided in Reference 1. There, extensive graphical design data is presented, together with step-by-step procedures and a completely worked example problem.

In the remainder of this section, the program scope and approach is summarized, and recommendations for efforts related to this study are presented.

SCOPE

In dealing with dynamic systems, it is generally possible to conceive many system arrangements, component type selections and transient situations which will be of interest in particular applications. The intent here is to provide analytical techniques based on a basic system model having application to most pressurization requirements and employing component types selected during the course of this study. Selection of components for the various functions is discussed in Section 2.

The system designs, which are obtained from the Design Reference Manual, are based on steady-state operating conditions. The transient phenomena involved with external pressurization systems are not amenable to a handbook-type treatment and require more knowledge of the overall cryogenic storage system than is presumed for use of the manual. In any case, the effect of the transients is primarily on the selection of values for pressure control bands. Thus, the system weight and cost estimates derived for steady-state functional requirements can be taken to be little affected by the transient analysis which ultimately must be accomplished in the development of an external pressurization system.

As mentioned earlier, this study considered systems operating on three cryogenic fluids: hydrogen, oxygen, and nitrogen. The operational ranges applicable to each fluid are defined in Table 1-1.

The characterizations provided for the energy addition devices allow several sources to be considered for heat input. The available heat sources are:

<u>Electrical power</u>--assumed to be 28 vdc or 115-v, 400-Hz ac.

Heat transport fluid stream--taken to be FC-75 (a 3M fluorochemical) received at 30 to 100 psia and 500° to 700°R.

Hot gas stream--taken to be H_2-O_2 combustion products received at 100 psia and 2000°R.

TABLE I-I

EXTERNAL PRESSURIZATION SYSTEM
OPERATIONAL RANGES

Parameter	Hydrogen	Fluid Oxygen	Nitrogen
Tank pressure range, psia	14.7 to 1000	14.7 to 1000	14.7 to 1000
Tank volume range, cu ft	5 to 1000	5 to 1000	5 to 1000
Fluid delivery rates			
Vapor, lb per hr	0 to 2	0 to 20	0 to 20
Liquid, lb per sec	0 to 10	0 to 20	--

The pump, which supplies the fluid motion potential for the recirculation loop, is considered to be driven by an electrical motor. Two motor types have been characterized: the cage rotor induction motor and the samarium-cobalt, permanent-magnet brushless dc motor.

GENERAL APPROACH

In developing the system characterization, analyses were carried out to define the range of component characteristics implied by the system operational ranges noted in Table I-I. Component studies were then undertaken to establish means of representing each component over the required range. Here, the goal was definition of design approaches suitable for presentation in handbook form. The system model, interface relationships, and study ground rules governing this effort are summarized in the following paragraphs.

System Model

In Figure 1-1, a schematic is presented of a recirculation-type external pressurization system which has application to pressure control of both sub-critical (two-phase) and supercritical (single-phase) cryogenic storage systems. The schematic indicates a flow control valve which opens at some pressure defining the lower limit of the pressure control band for the cryogenic storage system. Sensing of valve movement causes the control unit to energize those components requiring electrical power; these are the pump and, if chosen, the electrical fluid heater unit. Flow is thus initiated in the loop, with energy being added to the recirculation stream W_R by the pump and heating device. The stream, returning to the storage tank at an increased energy level, maintains tank pressure while fluid delivery is taking place at the rate W_D. As tank pressure rises to the upper limit of the control band, the flow control valve closes and electrical devices of the loop are deenergized. The check valve shown in the return line serves to isolate the loop during no-flow periods to minimize thermal pumping in this line.

At steady-state flow conditions, the lines supplying the heat exchanger contain fluid at conditions essentially equivalent to those existing in the storage tank, and the return line fluid state is approximately that defined by the heat exchanger outlet conditions. This situation allows the flow in the lines to be treated as incompressible.

Figure 1-1 also contains a tabulation of the system components, indicating the type selected for characterization.

System Interfaces

For the purposes of this study, the external pressurization system is considered to consist of only those elements installed in the recirculation loop, including the cryogen supply and return lines. The nature of the interfaces differ somewhat as a function of the heat source employed, as is shown on Figure 1-2.

Where the fluid heat sources (the FC-75 or H_2-O_2 combustion products streams) are used, it is assumed that the proper flow rate, at the inlet conditions desired, is available at any time the external pressurization is

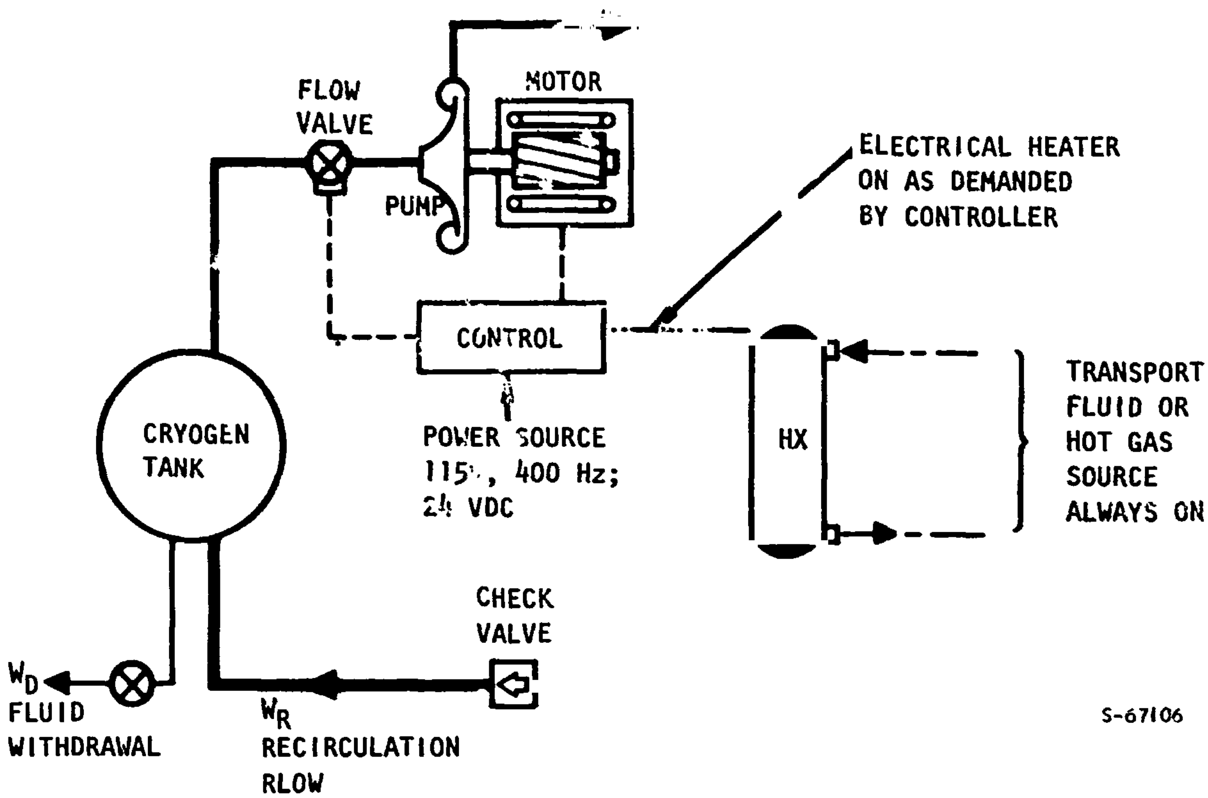

Major Components	Type Characterized
Flow Valve	Pressure actuated poppet.
Control Unit	Senses flow valve position. Actuates pump motor and electrical heater, if used.
Pump	Barske or centrifugal, as required by flow conditions
Motor	400 hz cage rotor induction or permanent magnet brushless dc.
Heat Exchanger	Resistance heater unit or tubular fluid-to-fluid heat exchanger.
Check Valve	Poppet.
Lines	Stainless steel.

Figure 1-1. Definition of External Pressurization System Model

actuated. This implies that these streams flow through the hot side of the heat exchanger continuously or that the systems supplying these streams possess controls such that the interface conditions are satisfied.

At the vehicle electrical interface, it is assumed that the quantity of power indicated in the system analysis is available either as 28 vdc or 115 v, 400 Hz ac.

The cryogenic storage tank interface is considered to supply fluid at the conditions specified by the tank pressure and recirculation mode (vapor or liquid) chosen, in the case of a subcritical storage system. For supercritical storage systems the state of the fluid supplied is given by the tank pressure and the stored fluid density, or quantity. Fluid returning to the tank is at a state given by the heat exchanger outlet conditions. It is assumed that complete mixing of the tank contents occurs during operation of the pressurization system. This results in selection of a conservative value for the recircula-flow rate.

A further assumption is made relative to subcritical storage systems: the fluid phase chosen by the user for recirculation is considered to be available at the supply line inlet at all times when system operation is required. This implies that the tank contains provisions for proper orientation of the liquid or vapor phases or that the vehicle acceleration is such that location of the phases is known.

The vehicle mounting interface was not considered in detail in this study, although nominal allowances for mounting arrangements were considered in the system installation weight and cost characterizations.

Study Ground Rules

The following set of ground rules, which guided development of the manual, are important to observe:

- The design manual is intended to provide a simple, rapid method of estimating system characteristics for planning purposes.
- Design of components assumes steady-state flow conditions with recirculation flow rate based on a homogeneous tank state.

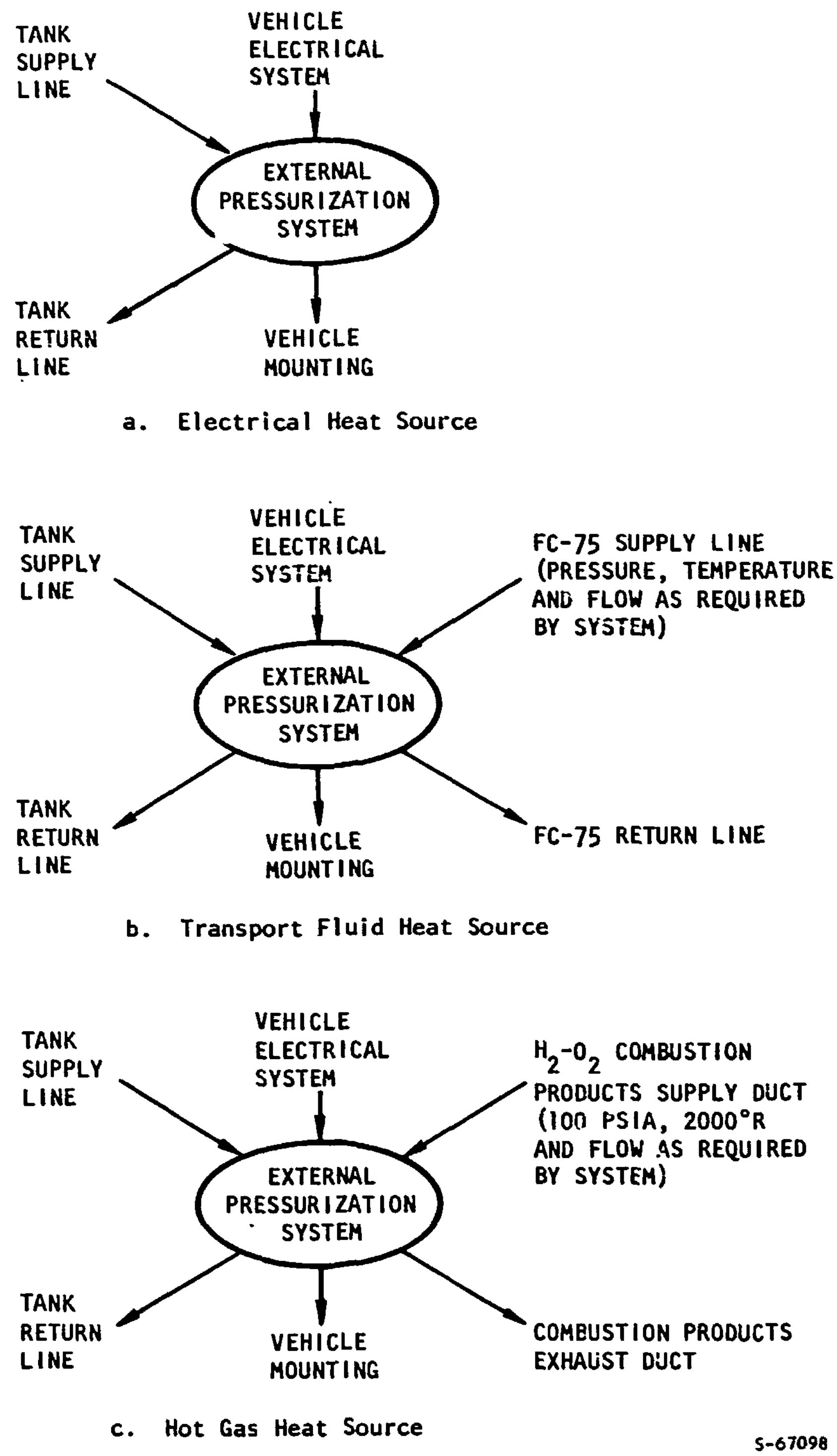

Figure 1-2. Definition of System Interface for Various Heat Sources

- Flow in transfer lines is treated as being imcompressible, with the density evaluated at either tank conditions or heat exchanger outlet conditions.
- The electrical heat source is considered applicable only to low power input requirements; thus, characterization of this device was restricted to ranges corresponding to the vapor delivery flow rates of Table 1-1.
- The transport fluid heat source is considered useful for low-to-moderate rates of energy input; therefore, the FC-75 heat exchanger characterization allows recirculation flows as follows:

Hydrogen	50 lb per hr
Oxygen	100 lb per hr
Nitrogen	20 lb per hr

- The hot gas heat source is considered to apply to the entire flow range.

In addition to the points noted above, the user should be aware of the basis established for the cost information presented in this report.

There are very little published data on the costs of components used in this study. Consequently, the cost data provided in later sections are based on AiResearch cost records for similar components, practical experience in the design and development of such components, and estimates of the man hours required to produce the components. An hourly rate of $15 per hr is assumed. The cost estimates are based on technology existing in 1971 and on the 1971 value of the dollar.

The component costs suggested here represent cost to the seller, not to the buyer; therefore, profit and general and administration costs are not included in the cost analysis. Furthermore, only predictable costs in the design, development and manufacture of the components are included. This includes design, development, manufacture, and acceptance testing of each component, but does not include qualification testing, documentation, or provision for expenses incurred in contract changes. These last three items can vary greatly from contract to contract and are highly dependent on the intended use of the system. Hence, characterizing their costs in a handbook is extremely difficult, if not impossible.

The cost analysis was based on a production quantity of 15 to 20 units. The cost can be expected to decrease if more units are produced; however, the values given will remain relatively constant up to 50 units. Above this quantity, the costs will decrease by approximately 10 percent for each 100-percent increase in units produced beyond 50.

RECOMMENDED RELATED EFFORTS

The studies conducted in this program did not indicate a need for basic research; however, a need for applied research was indicated in two areas: (1) development of more sophisticated tools for detail system design, and (2) development of combustion products-to-cryogen heat exchangers, should combustion products be selected as a source of energy for specific applications. Each of these areas of suggested additional effort are discussed below.

Detailed System Design Tools

The design procedures developed in this program are based on steady-state conditions as well as complete mixing of the recirculated fluid with the stored fluid. As previously mentioned, these design procedures lead to conservative results for most applications; in the detail design phase and for performing mission simulations for specific systems, dynamic modeling will be required. It is therefore suggested that generalized dynamic modeling of cryogenic storage systems employing recirculation-type pressurization be undertaken.

The dynamic modeling of this type of a system,can be logically divided into three parts: (1) modeling the dynamic behavior of the stored fluid as influenced by the environmental conditions, vessel configuration, vessel dimensional changes, the exiting fluid stream,and the returning recirculation stream; (2) dynamic modeling of the external recirculation loop and its components including control responses; and (3) integrating the two items above into an overall system dynamic model. Some of the effort required to accomplish the first item--by far the most difficult of the three items--has been accomplished in past NASA efforts. The major task required in this area is the extension of the existing analytical approaches to handle two-phase fluid situations, including interface heat and mass transfer.

Approaches to developing the external recirculation loop and integrated system model, though complex, are well understood and could be developed in a generalized format to provide analysis over a wide variation of system operating parameters and component types.

Combustion Products-to-Cryogen Heat Exchangers

For many applications, combustion products offer the most suitable source of energy for cryogenic storage pressurization systems· the Space Shuttle is one such application. The combustion products-to-cryogen heat exchanger is considered the critical component for such pressurization systems due to the large temperature gradients within the unit and the thermal cycling to which it is subjected. For this reason it is suggested that development work be undertaken on this type of heat exchanger.

Initial efforts toward developing combustion products-to-cryogen heat exchangers have been undertaken at AiResearch. These efforts have resulted in the selection of a heat exchanger configuration consisting of an annular tube bundle contained within a shell. Sample tube bundles have been fabricated and tested with promising results. The weight of heat exchangers based on this configuration are significantly lighter than other approaches considered to date; for this reason, further development appears warranted.

SECTION 2

SELECTION OF SYSTEM AND COMPONENT MODELS

The first task required by the study was adoption of a system model. From this the component requirement can be established, allowing work to proceed on the selection of components and data-gathering for the various analytical efforts. To ensure a proper frame of reference for this task, the available information relative to external pressurization systems was reviewed.

LITERATURE SEARCH

A search of the published literature was undertaken making use of the resources of the AiResearch technical library and the NASA Scientific and Technical Information Division. Although considerable information is available in the field of cryogenic storage system pressurization, no citations were found which were directly applicable to recirculation-type systems. However, sources of basic information for the various system elements are available. Where applicable, these are referenced in the appropriate component discussions.

SYSTEM MODEL

In general, delivery of fluid from a cryogenic storage tank will require that energy be added to the thermodynamic system represented by the tank and its contents. The rate of energy addition is defined by the desired tank pressure and flow characteristics and the first law of thermodynamics. Tank pressure in most applications is desired to be a constant value. For small flow rates, the energy addition due to heat leak through the tank thermal protection media may be adequate; larger flow rates will require that provisions for additional energy addition become a part of the overall storage system design.

In many cryogenic storage systems active heating devices have been installed within the fluid storage vessel. In addition, some systems have included equipment for convecting fluid over or through the heating device.

Such installations pose problems with regard to safety, maintainability and modification of flow characteristics. These problems may be alleviated by use of an external flow loop which recirculates stored fluid, returning warmed cryogen to the storage vessel. In an external pressurization system of this type, all dynamic components associated with the energy addition are located external to the tank system. Safety is improved and components may be maintained or modified without major rework of the storage tank.

Selection of Model

The concept considered in this study consists of a recirculation flow loop containing a pump or fan which induces flow from the tank through a heat exchange device and, thence, back into the fluid vessel. Other components needed include valves, sensors, and control elements for flow control and a means of driving the pump or fan. For this study, the sources of heat were specified as electrical, transport fluid, and hot gas. Electric motor drive was specified for the pump.

For accomplishment of the basic function of the system, tank pressurization during delivery of fluid, a simple series arrangement of the system elements is most satisfactory. Specific applications, of course, can call for use of more complex system arrangements. The basic system arrangement and four specialized circuits are shown in Figure 2-1.

The basic arrangement of Figure 2-1a is suitable for all applications considered in this study. The flow control valve has the function of initiating flow in the loop when storage tank pressure falls below the selected lower operational limit. Although valve operation can be pneumatic, control elements are required to energize the pump motor when the flow valve opens. Fluid is then circulated through the heat exchanger, and returned to the tank at an increased energy level through the check valve. The check valve serves to isolate the external loop to prevent heat transfer due to thermal pumping effects during no-flow periods. In many instances, the check valve may not be required; however, if the return stream is routed to the liquid region of the tank in order to provide agitation of the stored fluid, isolation of the external loop will be necessary.

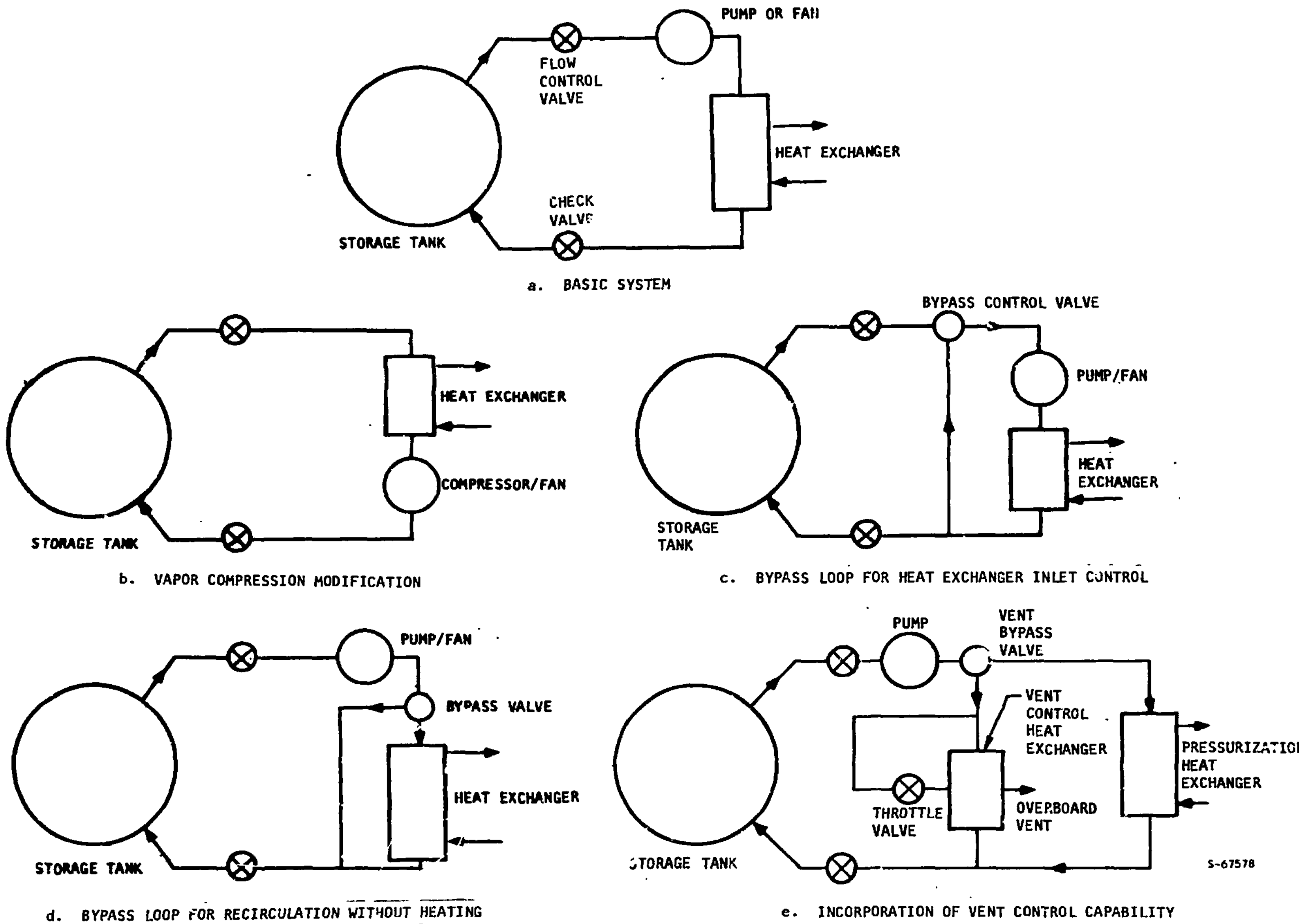

Figure 2-1. Possible Arrangements for Recirculation-Type External Pressurization Systems

The vapor compression arrangement shown in Figure 2-1b differs only in the location of the fluid moving device, which now must be considered to be a compressor or fan. This approach has merit only where cavitation considerations lead to very difficult pump design requirements. Use of vapor compression at the heat exchanger outlet condition will result in much higher power consumption and may also increase component cost. Since the systems dealt with in this study will require only small or moderate pressure rise for circulation in the external loop, cavitation at the pump inlet does not present a serious problem. In this case, the approach of Figure 2-1b appears to apply primarily to situations where an existing compressor unit is to be adapted to a system.

The system presented in Figure 2-1c adds a bypass loop and control valve to the basic system arrangement; the valve allows warm fluid from the heat exchanger outlet to be mixed with the stream from the tank to control the heat exchanger inlet temperature. This technique can be employed where heat exchanger freeze-up is a problem. For a specific design point, it is generally possible to select the heat exchanger design such that freezing does not occur; however, this may not be possible where the cryogen or heat source fluid inlet conditions vary over a wide range during operation.

Figure 2-1d indicates an arrangement which allows the recirculation flow to bypass the heat exchanger. This feature would permit the fluid dynamic potential provided by the pump to be employed for agitation of the tank contents. Heating of the stream in this case would be limited to that due to the heat leak and the pump head rise. While this technique may be of value in some situations, it would not appear to have general applications.

The system of Figure 2-1e incorporates a vent control feature into the pressurization loop. The concept presented has applications to two-phase storage systems where venting of the high-energy vapor phase is preferable, since this results in the desired pressure decrease at the expense of less fluid loss. To achieve this, the flow control valve must be actuated at both the lower operational pressure and at the vent pressure limit. In the first case, functioning of the loop is as for the basic system; in the latter case, the vent bypass valve diverts flow through the vent control loop, where a portion of the stream is routed through a throttling device; due to the temperature decrease accompanying this expansion, the throttle stream is able to absorb heat from the unthrottled stream, thus being vaporized in the vent control heat exchanger prior to venting overboard. The cooled, unthrottled stream is then returned to the tank.

Several conditions must be met to make use of this approach. First, the vent control loop must be arranged to ensure that the energy increase due to recirculation (i.e., heat leak and pump head rise) is less than the energy removal effected by the vent stream. In addition, it is necessary that the venting and pressurization requirements be such that the pump design is applicable to both. In many cases, it may be found that a separate vent control subsystem is preferable to integration of these functions.

Consideration of the foregoing possible arrangements, together with the system interfaces defined in Section I, leads to the conclusion that only the basic system of Figure 2-1a is germane to generalized characterization of external pressurization systems. The limited applicability of more complex arrangements makes consideration of these more appropriate to the preliminary design phase of the design of specific systems. For development of system characteristics over a wide range, it is more appropriate to employ the basic system arrangement as a baseline.

Operational Considerations

As noted above, the external pressurization system operates between two pressure levels which encompass the nominal tank pressure. System operation is initiated when the pressure falls to the lower limit; shutdown of the system takes place when the upper limit is reached. Clearly, operation of a real system involves transients with respect to the lines and the heat exchanger during a duty cycle and with respect to thermal soak-back to the tank following a duty cycle. Analysis of these involves the performance and mass characteristics of both the pressurization system and the tank system. While the analysis of a specific system presents no conceptual problem, use of fairly sophisiticated computer techniques are mandatory.

For generalized handbook presentation, only procedures based on a steady-state design point are feasible. This, however, does not invalidate the results thus obtained. Since the major effect of the transients will be to determine the limiting pressure values and characteristics required of the controls, the weight and cost derived from steady-state conditions will remain representative for the system.

System Design Approach

The characteristics of a system design are determined by the characteristics of the components which make up the system. Thus, establishment of the design approach upon which the Design Reference Manual was to be based required that the component design relationships be considered because the various procedures must intermesh such that a valid system design is defined without excessive effort.

To this end, Table 2-1 is useful. The matrix presented here categorizes the information desired from each of the areas and defines the information necessary to obtain these results. Table 2-1 makes clear what forms of individual and system design procedures are possible.

For instance, Table 2-1 shows that knowledge of the recirculation loop flow rate is essential to the analyses. However, this quantity is a function of the heat exchanger outlet temperature. Thus, it is necessary to choose one of these variables at the outset of the analysis. The outlet temperature is most conveniently fixed, so this approach was chosen. Since no method could be found which would guarantee the correctness of the a priori selection, iteration with respect to outlet temperature became necessary at the system design level.

Returning to Table 2-1, it can be seen that pressure loss (or its inverse, with respect to the pump, pressure rise) is among the information necessary to the determination of the desired component characteristics. However, consideration of the line and heat exchanger characteristics leads to the conclusion that this variable can be treated somewhat loosely. Since the pressure loss is related to the flow area of both these components, the

TABLE 2-I

REQUIRED SYSTEM AND COMPONENT INPUT INFORMATION

Item	Results Desired	Input Information Desired
System	Total weight Power consumption Total cost	Fluid species Fluid quantity Storage pressure Delivery schedule (flow rate as function of quantity) Heat source characteristics Electrical power source Transfer line length Total pressure loss allowable
Transfer Equipment	Line size Weight of lines and associated equipment Cost	Recirculation flow rate Line length and routing configuration Allowable pressure loss
Heat Addition Equipment	Size Weight Cost	Recirculation flow rate Heat transfer required Heat source characteristics Allowable pressure loss
Pumps	Size Weight Power Cost	Recirculation flow rate Pressure rise required Rotational speed
Motors	Weight Power Cost	Shaft output power Rotational speed Power source

design procedures can be chosen to allow freedom to vary geometry and, ultimately, pressure loss. In the final analysis, it was decided to employ a target overall loss in the system procedure. This could then be apportioned to the components and used as a guide in those analyses. However, it was clear that this target loss should not be closely adhered to; otherwise, completely unacceptable geometric results could be forced on the designer.

Through analysis of the requirements and results as indicated above, a detailed system design procedure was established. This technique is presented in logic diagram form in Figure 2-2. The dashed boxes on this chart refer to the sections of the Design Reference Manual which contain the necessary design data.

Selection of Heat Sources

At this point it is necessary to more closely define the sources of energy to be employed in the pressurization system. Three types--electrical, transport fluid, and hot gas--were specified for inclusion in this study. The electrical source does not require further definition; for the two fluid sources, specific selections are needed.

1. Transport Fluid Heat Source

Here, it was assumed that the availability of warm heat transport fluid loops implied the use of fuel cell power systems. Thus, typical fuel cell coolants were considered as candidate transport fluids. Past usage has indicated that the most likely fluids for this application are:

Water-glycol
Freon-21
FC-75

Of these, water-glycol presents the greatest potential for heat exchanger freeze-up. Although the remaining two are usable to temperatures below -100°F, FC-75 possesses a lower vapor pressure characteristic, and is thus preferred for fuel cell coolant service. Therefore, the transport fluid considered in this study was taken to be FC-75. Consistent with the fuel cell assumption, the FC-75 was assumed to be available at temperatures in the range 500°R to 700°R, and at pressures from 30 to 100 psia.

FOLDOUT FRAME 1

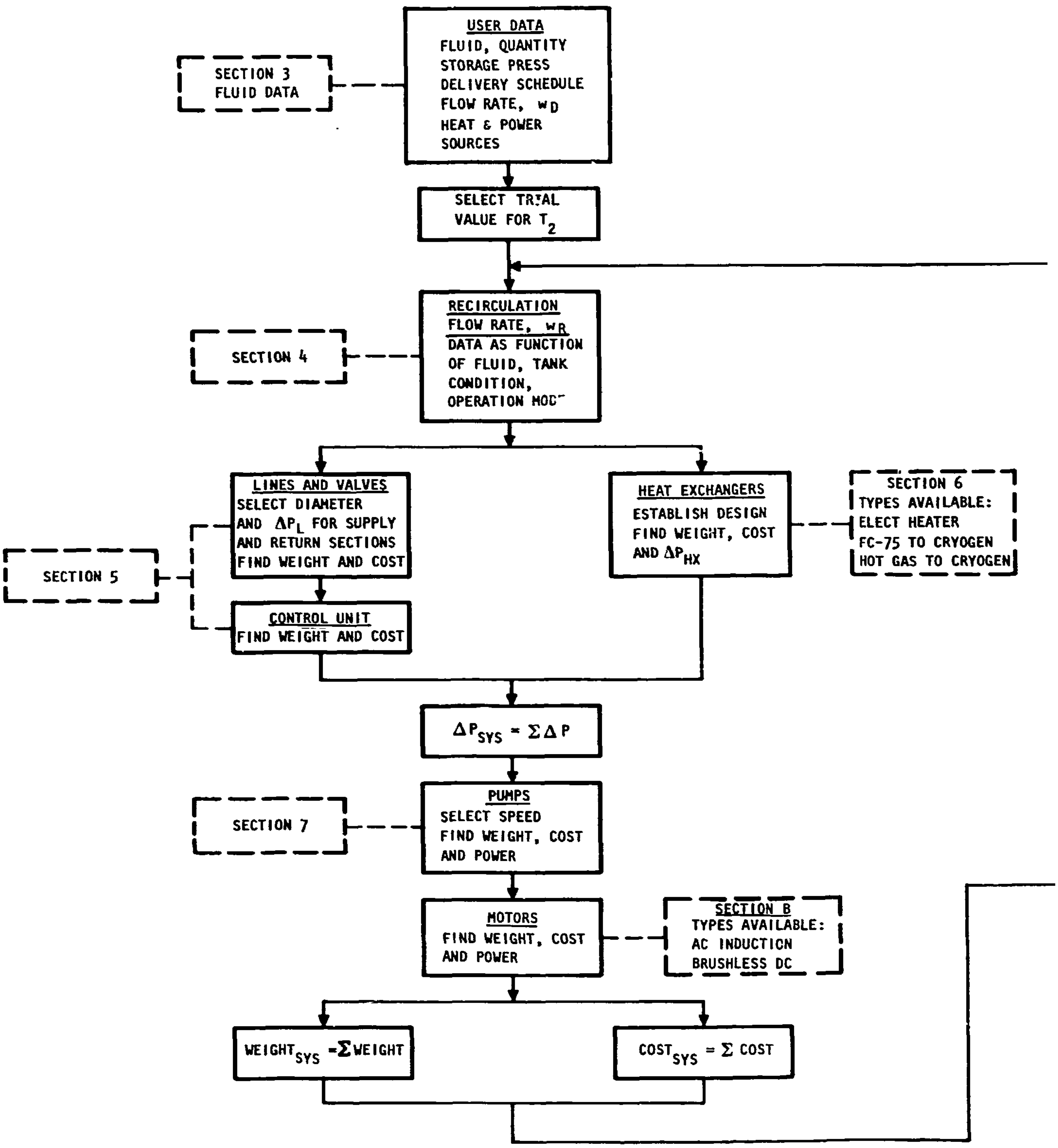

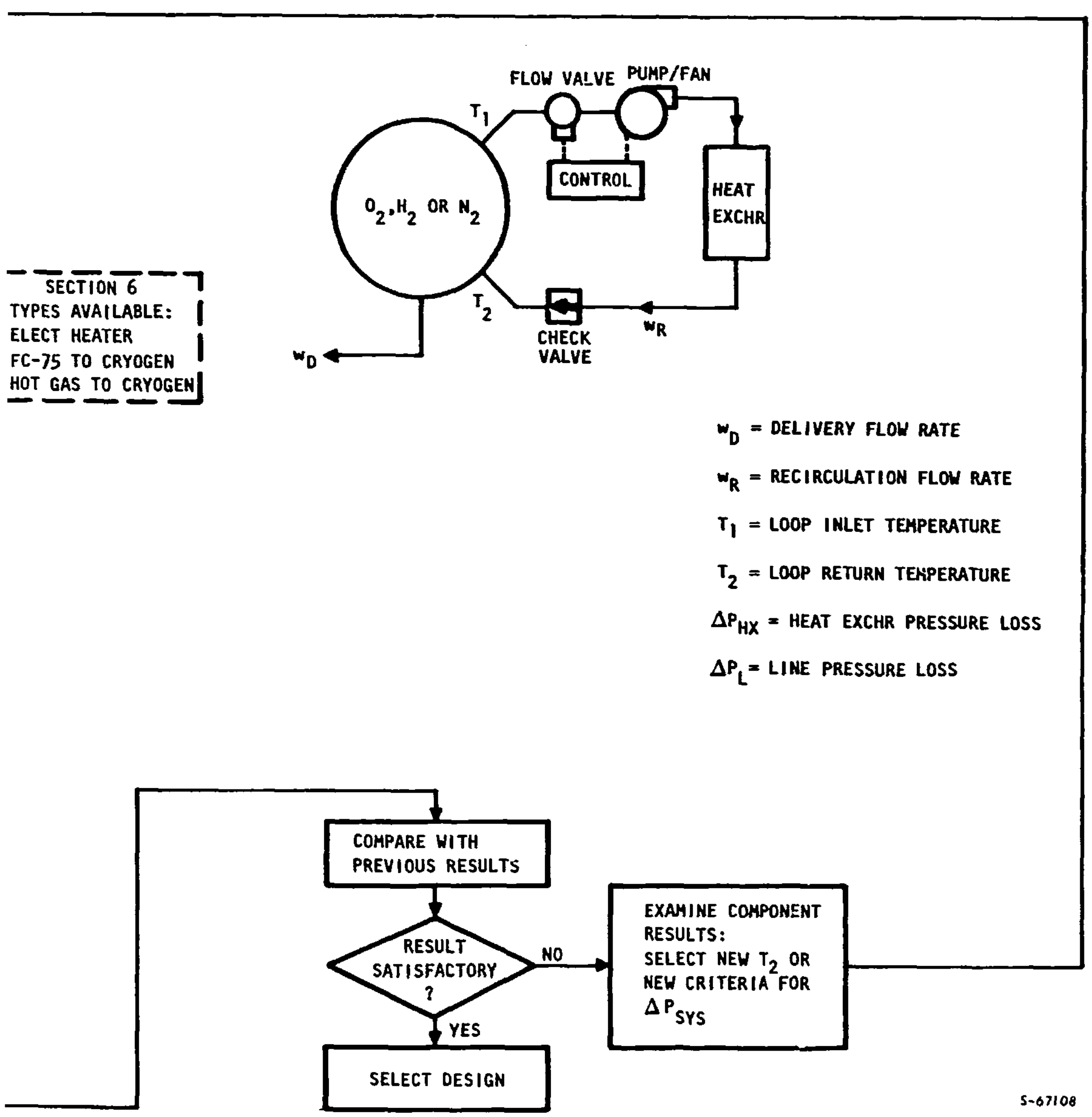

Figure 2-2. Basic Algorithm for External Pressurization System Design

PRECEDING PAGE BLANK NOT FILMED

2. Hot Gas Heat Source

Availability of waste hot gas as a heat source was interpreted as implying the use of hydrogen-oxygen fueled auxiliary power units. In this case, the fluid is hydrogen-oxygen combustion products consisting largely of superheated water vapor. Studies of cryogenic heat exchanger designs employing this fluid, conducted under Contract NAS 9-11330, have indicated that 2000°R is a reasonable maximum inlet temperature. A further conclusion is that minimum heat exchanger weight is generally obtained at hot gas pressures near 100 psia. These results were adopted for the hot gas heat exchanger procedure prepared for this study. The oxidizer-to-fuel ratio implied by these selections is 1.0.

COMPONENT MODELS

After establishment of a system design basis, the requirements of the individual components were investigated, leading to adoption of approaches and selection of the types to be characterized.

As a guide to this effort, the maximum recirculation flow rate corresponding to the upper delivery flow rates of Table 1-1 was estimated based on tank pressures of 1000 psia for the vapor delivery cases and 150 psia for liquid delivery; the return temperature was assumed to be 400°R, the minimum considered for this variable. The results of this worst-case analysis are presented in Table 2-2.

TABLE 2-2

MAXIMUM RECIRCULATION FLOW RATES

	Tank Pressure psia	Recirculation Flow					
		Oxygen		Hydrogen		Nitrogen	
		T_I, °R	$\dot{w}_R$, lb/hr	T_I, °R	$\dot{w}_R$, lb/hr	T_I, °R	$\dot{w}_R$, lb/hr
Vapor Delivery	1000	350	0 to 70	300	0 to 6	350	0-90
Liquid Delivery	150	216.4	0 to 2000	56.6	0 to 1250	---	---

Transfer Lines and Related Equipment

Flow in the transfer lines is treated as being incompressible. At steady-state flow conditions, the flow from the tank to the heat exchanger is best represented by the stored fluid density, and the density at the heat exchanger outlet is representative of the flow from the heat exchanger to the tank. To fully validate this assumption, it is necessary to assure that the Mach number existing in vapor lines is 0.2 or less.

The lines are taken to consist of stainless steel tubing made up with threaded fluid connections. Both the flow control valve and check valve are poppet-type valves, a design concept suitable for cryogenic service. The flow control valve is assumed to sense tank pressure, opening fully at the lower operational pressure band limit and closing at the upper limit. These features are obtainable with proper pneumatic design.

Electrical controls have been minimized, consisting primarily of a relay contactor unit that energizes the pump motor and electrical heater circuits (if employed) in response to a signal from a flow control valve poppet position sensor.

Heat Exchangers

Three types of heat exchangers are required to permit employment of the three specified heat sources.

1. Electrical Heater

This concept calls for a simple unit combining an annular fluid passage with a sheathed resistance heating element. Features are incorporated to limit heater temperature rise in no-flow situations and to isolate the heating element from the fluid; the last is necessary only for oxygen heaters.

2. Transport Fluid Heat Exchangers

The design situation encountered here can be satisfied by straight-forward direct-exchange heat exchanger approaches. To minimize the possibility of freeze-up, a shell-and-tube design with a cross-parallel flow configuration is most desirable. More compact heat transfer surfaces or the use of counter-flow will result in lower wall temperatures than the selected approach, increasing danger of freezing the transport fluid.

3. Hot Gas Heat Exchanger

This heat source presents the most difficult heat exchanger design problem. The structural design is most important because of the low design allowables at the 2000^{0}R inlet condition and the extreme thermal gradients encountered in the unit. In addition, close attention must be paid to wall temperature because the heat source fluid consists primarily of water.

To counter the freezing problem, the cross-parallel flow arrangement is again adopted. For this unit, however, the traditional shell and tube concept is not satisfactory from a structural standpoint. The large temperature gradients which would result through the tube bank and around the shell periphery are not acceptable. Instead, another tubular exchanger concept that has undergone development at AiResearch for high-temperature applications has been selected. This is the annular tube bundle design in which flow is directed radially outward and inward on successive passes through a tube bundle arrangement in a hollow cylindrical configuration. Tube bank length presented to the flow is decreased, and shell temperatures vary only in the longitudinal direction.

While this concept has been the subject of developmental effort and appears to represent the state-of-the-art in lightweight, high-temperature heat exchangers, it is not fully developed. Although the characterization of heat exchanger size and weight is realistic, the cost characterization is based on the assumption of a development status similar to that existing for the other heat exchangers, thus providing a projection of the cost likely for this unit after completion of the needed technology development.

Pumps

Under the system model and the specified system operational ranges, the pumps may be called on to handle liquid cryogen, saturated vapor, or supercritical gas. The pressure rise required of the recirculation loop appears to be small, typically of the order of 10 psi or less. To assure adequate coverage of the design range, pump characterizations were established over the expected recirculation flow range for pressure rises up to 100 psi.

The desired pump capability was found to call for pump specific speeds ranging from 150 to 5,000 rpm, based on a maximum rotational speed of 100,000 rpm. The bulk of this range can be satisfied by centrifugal pumps, which provide good efficiency in the range from 400 to 5,000 rpm. The lower specific speeds (from 150 to 400 rpm) can be obtained by inclusion of the Barske pump as a candidate. Specific speeds above 5,000 rpm are in the regime of axial-flow machines. Although such high specific speeds do not appear likely for the problem conditions considered, it was decided to extend the pump characterization to a specific speed of 10,000 rpm.

Motors

Two motor types have been selected for inclusion in this study to provide flexibility with respect to electrical power source and rotational speed. These are the 3-phase induction motor considered to operate on 400-Hz power and the brushless dc motor, which may operate on either the ac or dc power sources. Induction motor speeds are constrained to those corresponding to even numbers of poles. Pole numbers from 2 to 12 were considered. Brushless dc motor speed can be chosen at any value required up to 100,000 rpm.

Examination of the pump operational range indicates that approximately 40 hp is the maximum motor shaft output likely to be needed. The characterizations presented, however, have been extended to the 100-hp level.

USE OF THE COST CHARACTERIZATIONS

The basis of the cost characterizations for the components discussed above has been defined in Section I. Here, some observations on the nature and use of this information are offered.

For each component, two cost elements are provided: the recurring cost and the nonrecurring cost. The recurring cost occurs each time the component is produced and is related to the cost of materials, the time required for manufacture, the complexity of the manufacturing process, and the nature of the acceptance test required for the component. The nonrecurring cost element occurs only once during the design, development, and production of a specific component design, and is related to the man hours required for the design and development of the component, plus the manhours and material cost required to produce the tooling required by the component.

The cost information can be applied by the user in several ways:

(a) The individual cost elements can be summed, providing system recurring and non-recurring elements:

$$C_{rs} = \Sigma C_r \tag{2-1}$$

where C_{rs} = system recurring cost

C_r = component recurring cost

and:

$$C_{ns} = \Sigma C_n \tag{2-2}$$

where C_{ns} = system non-recurring cost

C_n = component non-recurring cost

(b) The system cost elements can be combined into a measure of cost per system if the total number of systems (n) is known, by prorating the non-recurring element over the n systems:

$$C_s = C_{rs} + \frac{C_{ns}}{n} \tag{2-3}$$

where C_s = cost per system procured

(c) The total expenditure involved can be evaluated from:

$$C_T = nC_{rs} + C_{ns} \tag{2-4}$$

Obviously, the technique chosen will depend on the objectives of the user; however, flexibility to satisfy many objectives is provided by the method of presentation.

SECTION 3

THERMODYNAMIC ANALYSIS

CHARACTERIZATION APPROACH

This section presents the cryogenic fluid thermodynamic functions needed to evaluate the energy input required during fluid withdrawal and the corresponding recirculation flow rate which must be processed by the external pressurization system.

The emphasis of this project was to provide a design reference manual for rapid design characterization and estimation of the performance and cost of external pressurization systems. For this reason it was necessary to limit the treatment of fluid thermodynamics to those conditions which are amenable to handbook treatment and bear most directly on the design of pressurization systems. The major assumptions made relative to operation of the cryogenic storage system consist of:

(1) The storage pressure is maintained at a constant level during delivery of fluid to the using system.

(2) Fluid recirculated through the external pressurization loop mixes completely with the tank contents on return to the tank.

The first assumption embodies the usual approach to tank pressure control; the second implies that thermal stratification of the tank contents does not take place. Should stratification result from operation of the external pressurization system, the recirculation flow requirements are markedly decreased except for the case of supercritical storage of hydrogen in the low density region. In this case the recirculation flow requirements for most extreme stratified conditions--no mixing at all--are slightly greater than for the complete mixing conditions assumed; this difference does not significantly affect the pressurization system design, however. Thus, as far as the components of the external pressurization are concerned, the homogeneous stored fluid assumption provides a reasonable and generally conservative design point.

As to operation of the pressurization system, if designed for the homogenous condition, the following observations can be made:

(1) Short duty cycles by the recirculation loop would supply most withdrawal periods; for long withdrawal periods, intermittent operation would occur.

(2) Limited stratification within the storage volume could be intentionally permitted; in the case of large subcritical tanks, this feature could be used to provide a net positive suction head (NPSH) to downstream pumps. The homogenous model still provides a conservative design point of the components of the pressurization system.

(3) As mixing occurs after development of a stratified condition, the tank pressure will decay (either slowly or rapidly); thus, recirculation loop duty cycles can be expected between withdrawal periods to correct the pressure decay.

Detail description of the behavior of the integrated cryogenic storage/external pressurization systems requires complete modeling of both systems and the use of computer programs for thermal stratification simulation and external pressurization system transient analysis. This type of system modeling is considered essential in the detail design phase of developing an external pressurization system.

The remainder of this section consists of an introduction of the thermodynamic functions for energy addition and recirculation flow requirements for constant pressure and homogenous operation of the storage system. This is followed by a presentation of the pressurization flow requirements for nonmixing stratified operation.

THERMODYNAMIC RELATIONSHIPS

For the constant pressure, homogeneous tank model treated here, the relationship between the delivery flow and recirculation flow is determined from a first-law energy balance. For development of this expression, the thermodynamic system considered consists of the mass of stored fluid at any time. The first law of thermodynamics applied to this system can be written as:

$$q = mdH + Hdm - \underline{V}\, dp - Pd\underline{V} - H_a dm + H_a dm_r - H_2 dm_r \tag{3-1}$$

where

q = a differential quantity of heat energy

m = the stored mass of fluid

H = the specific enthalpy of the fluid

$\underline{V}$ = the tank volume

H_a = the specific enthalpy of the exiting fluid

dm_r = a differential quantity mass recirculated in the external pressurization loop

H_2 = enthalpy of fluid returning to the storage tank from the pressurization loop

Considering constant pressure operation and neglecting tank volume changes due to temperature changes, Equation 3-1 reduces to:

$$q = mdH + Hdm - H_a dm + H_a dr_r - H_2 dm_r \tag{3-2}$$

In the case of homogenous supercritical storage, the enthalpy of the exiting fluid can be taken as equal to that of the stored fluid, and Equation 3-2 reduces to:

$$q = mdH - (H_2 - H_a)\, dm_r \tag{3-3}$$

which can be rewritten as:

$$q = -\rho\left(\frac{\partial H}{\partial \rho}\right)_P dm - (H_2 - H_a)\, dm_r \tag{3-4}$$

The most conservative case results if it is assumed that all energy added to the system is supplied by the external pressurization system (i.e., $q = 0$). Then noting:

$$\frac{dm_r}{dm} = \frac{\dot{w}_R}{\dot{w}_D} \tag{3-5}$$

where:

$\dot{w}_R$ = the pressurization loop flow rate

$\dot{w}_D$ = the delivery rate

and making the following change in notation:

$H_a = H_1$ = the tank exit enthalpy or inlet enthalpy to the external pressurization loop

Equation 3-4 can be rewritten as:

$$\frac{\dot{w}_R}{\dot{w}_D} = \frac{-\rho \left(\frac{\partial H}{\partial \rho}\right)_P}{H_2 - H_1} \tag{3-6}$$

which is the desired relation for supercritical operation.

In the case of subcritical operation, either liquid or vapor can be delivered from the tank and/or recirculated in the pressurization loop. Following the same general lines of development as above yields the following relations for subcritical operation:

For liquid delivery

$$\frac{\dot{w}_R}{\dot{w}_D} = \frac{\lambda \left[\frac{\nu_L}{\nu_V - \nu_L}\right]}{H_2 - H_1} \tag{3-7}$$

For vapor delivery

$$\frac{\dot{w}_R}{\dot{w}_D} = \frac{\lambda \left[\frac{\nu_V}{\nu_V - \nu_L}\right]}{H_2 - H_1} \tag{3-8}$$

where

λ = the latent heat of vaporization at the particular operation pressure

ν_L and ν_V = the specific volume of the saturated liquid and vapor respectively

It is noted that the numerator in the right hand side of Equations 3-6 through 3-8 is the expression commonly referred to as the specific heat input; these equations can therefore be rewritten as:

$$\frac{\dot{w}_R}{\dot{w}_D} = \frac{\dot{q}/\dot{w}_D}{H_2 - H_1} \qquad (3\text{-}9)$$

where

$\dot{q}/\dot{w}_D$ = the specific heat input for the particular operation conditions

The energy addition requirements for the pressurization system is then given by:

$$Q_{in} = \dot{w}_R\,(H_2 - H_1) = \dot{w}_D\left(\frac{\dot{q}}{\dot{w}_D}\right) \qquad (3\text{-}10)$$

Both $q/\dot{w}_D$ and $\dot{w}_R/\dot{w}_D$ are needed in design of external pressurization systems; this data is furnished in Figures 3-1 through 3-7. Figures 3-1, 3-2, and 3-3 apply to supercritical oxygen, nitrogen, and hydrogen, respectively. Here, $q/\dot{w}_D$ is presented as a function of pressure and density, while $\dot{w}_R/\dot{w}_D$ is a function of pressure, density and loop discharge temperature, T_2 (which corresponds to H_2).

For subcritical storage situations, only liquid delivery of oxygen and hydrogen is considered. Two modes of recirculation loop operation are characterized: the loop can be taken to receive either saturated vapor or saturated liquid at its inlet.

For liquid delivery of oxygen, the vapor and liquid recirculation options are treated on Figures 3-4 and 3-5, respectively. Figures 3-6 and 3-7 cover the same two conditions for hydrogen.

The fluid properties data used to develop Figures 3-1 through 3-7 are presented in Section 3 of the Design Reference Manual (Report 71-7535).

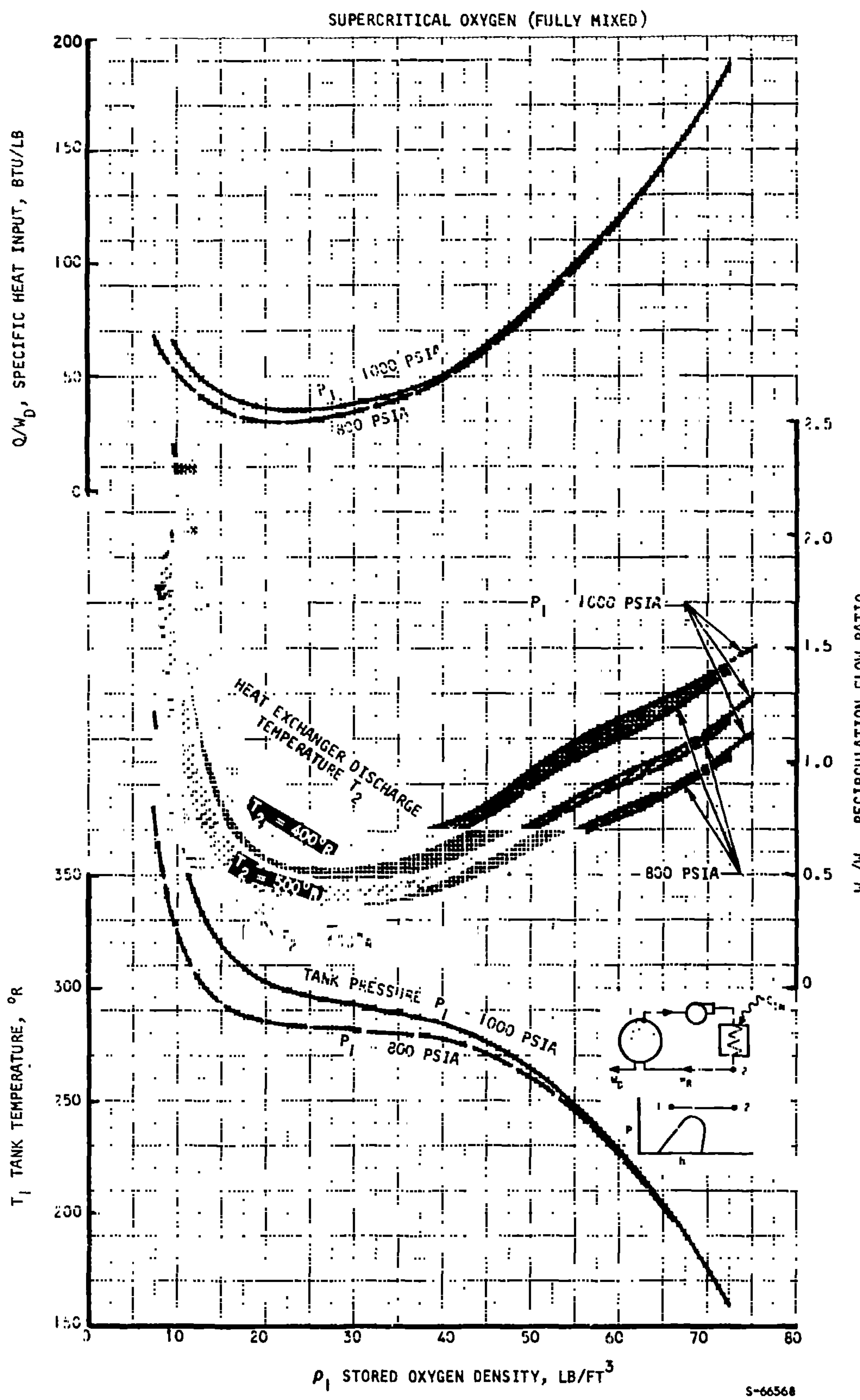

Figure 3-1. Recirculation Flow Requirements of Supercritical Oxygen

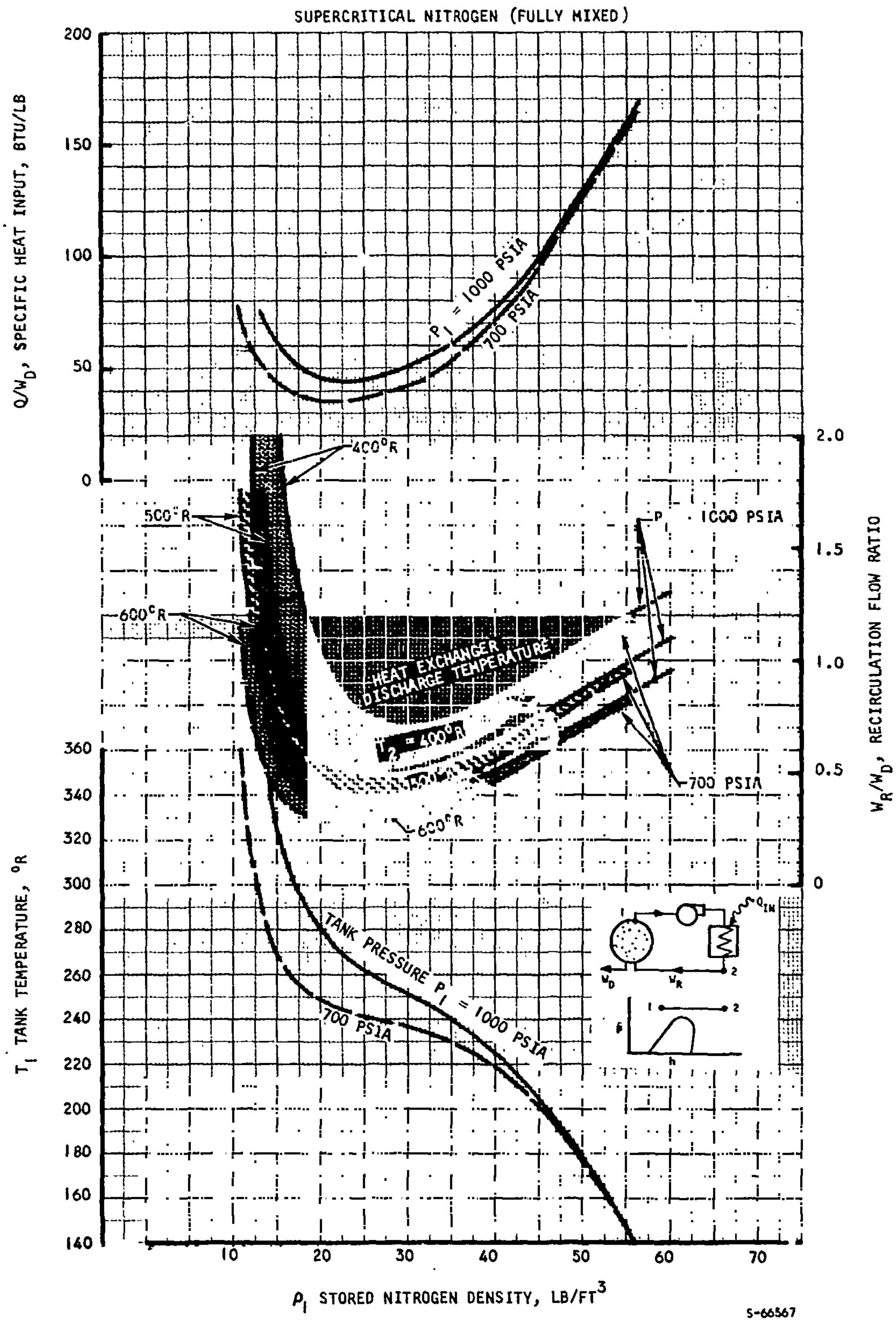

Figure 3-2. Recirculation Flow Requirements of Supercritical Nitrogen

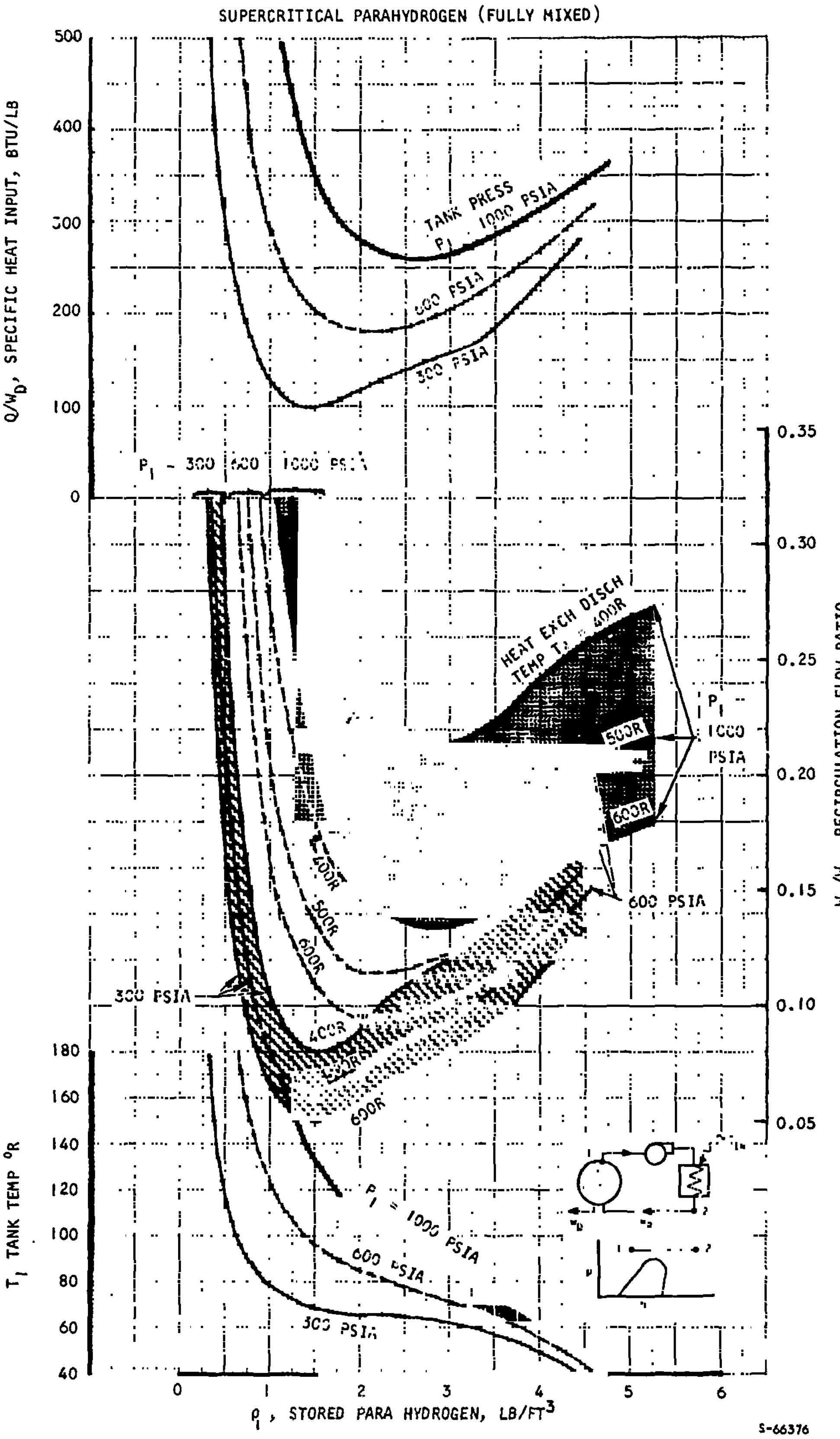

Figure 3-3. Recirculation Flow Requirements of Supercritical Parahydrogen

OXYGEN LIQUID DELIVERY-VAPOR RECIRCULATION
(FULLY MIXED)

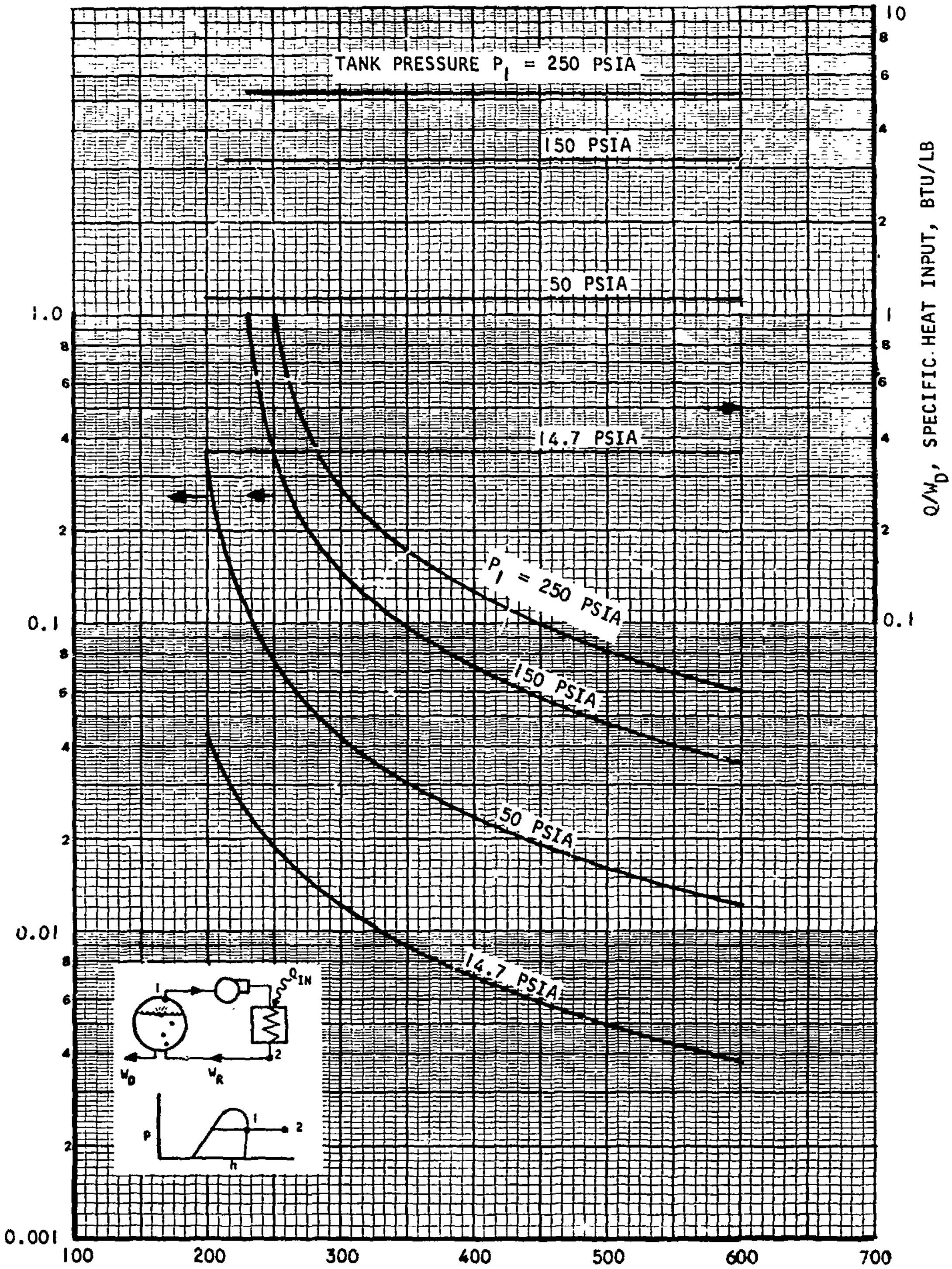

Figure 3-4. Recirculation Flow Requirements of Oxygen, Liquid Delivery - Vapor Recirculation

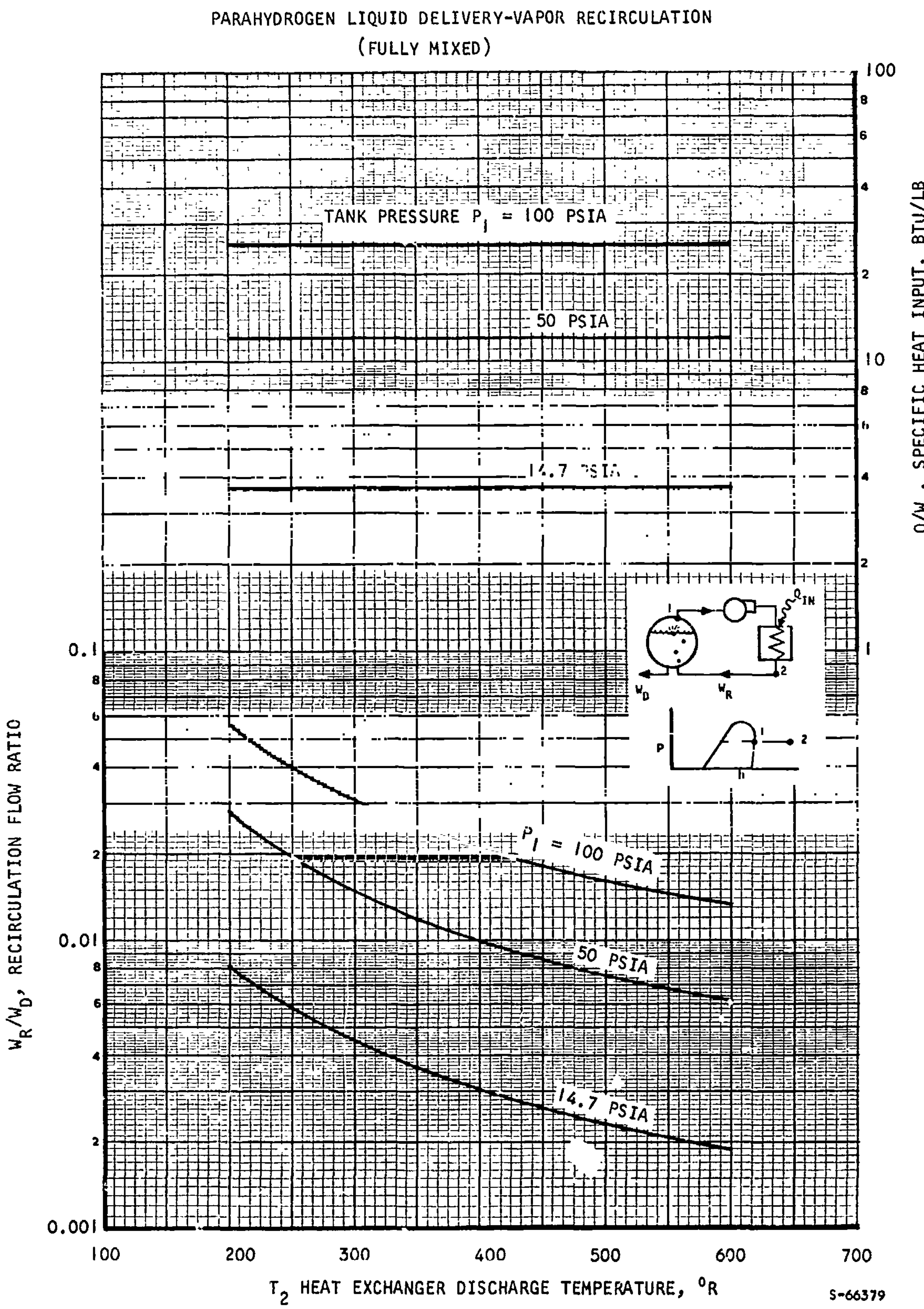

Figure 3-5. Recirculation Flow Requirements of Parahydrogen, Liquid Delivery - Vapor Recirculation

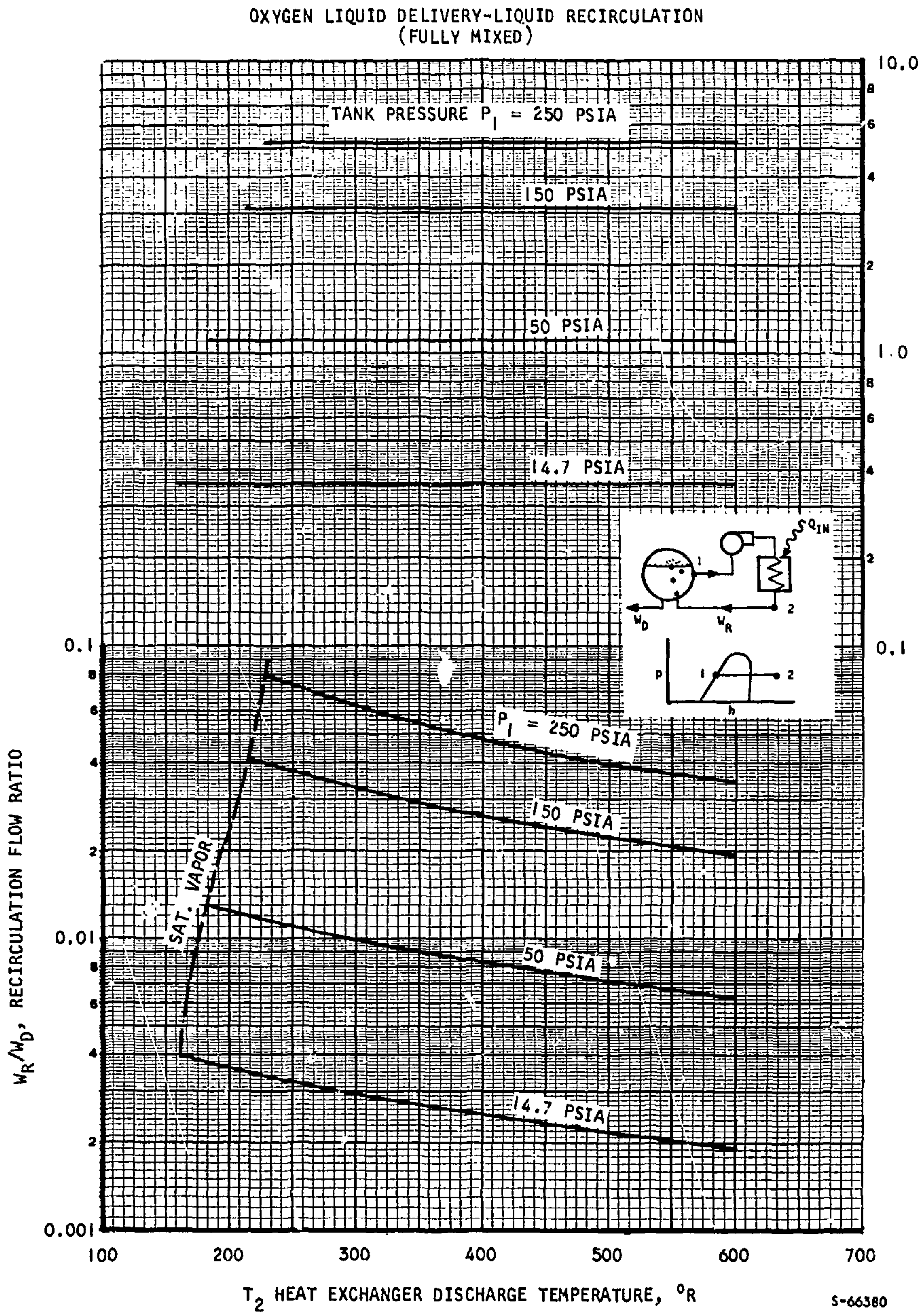

Figure 3-6. Recirculation Flow Requirements of Oxygen, Liquid Delivery - Liquid Recirculation

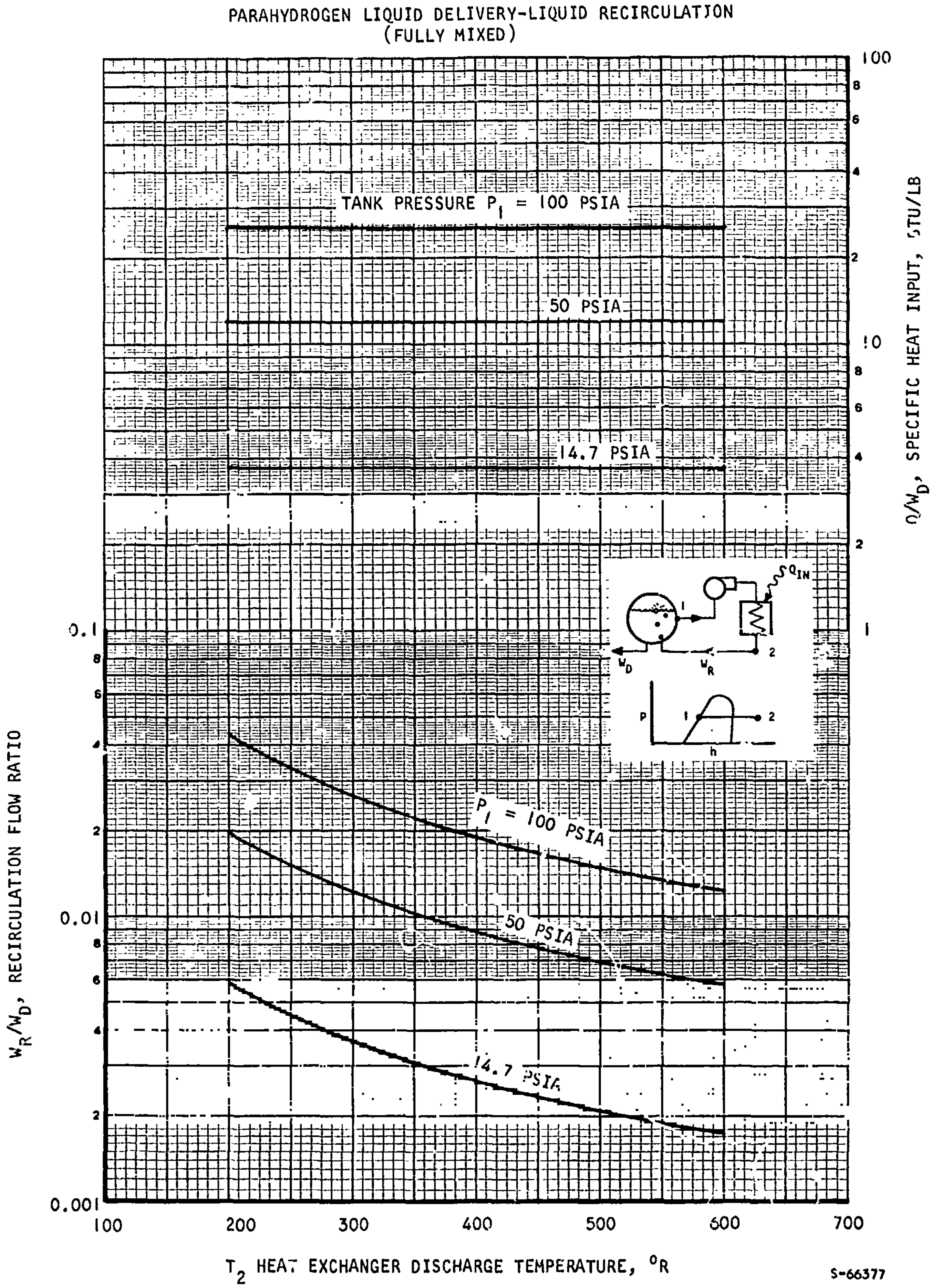

Figure 3-7. Recirculation Flow Requirements of Parahydrogen Liquid Delivery - Liquid Recirculation

STRATIFICATION CONSIDERATIONS

Thermal stratification of the stored contents can result from ground servicing, extended ground hold times in a one-g environment, operation in a low-to-zero-g environment, and operation of the external pressurization system. The following discussion is limited to consideration of the influence of stratification on pressurization loop flow requirements.

To investigate the potential influence of stratification on recirculation flow requirements, a simple two fluid model was used. This model represents the extreme case with respect to the degree of stratification resulting from operation of the pressurization loop.

The fluid recirculated to the tank was assumed to act as a separate body of fluid, void of heat and mass transfer between the recirculated fluid and the stored fluid. For constant pressure operation this condition leads to two active volumes within the storage tank: (1) the volume of fluid from which the delivered fluid is being supplied, termed V_A, and (2) the volume into which the recirculation flow is entering, termed V_B. Both of these volumes are changing during delivery of fluid and by definition for constant pressure operation:

$$dV_A = dV_B \qquad (3\text{-}11)$$

The rate at which mass is leaving the storage volume at the exit port is given by:

$$\dot{w}_{out} = \rho_A dV_A \qquad (3\text{-}12)$$

where

ρ_A = density of the stored fluid being delivered

Similarly, assuming the pressurization system heats the recirculation flow to a fixed temperature, the recirculation flow is given by:

$$\dot{w}_R = \rho_B dV_B \qquad (3\text{-}13)$$

where

ρ_B = the density of the recirculation flow stream as it reenters the storage volume

Then noting that delivery rate $\dot{w}_D$ is given by:

$$\dot{w}_D = \dot{w}_{out} - \dot{w}_R \qquad (3\text{-}14)$$

and combining Equations 3-11 through 3-14 yields

$$\frac{\dot{w}_R}{\dot{w}_D} = \frac{\dot{w}_R}{\dot{w}_{out} - \dot{w}_R} = \frac{\rho_B}{\rho_A - \rho_B} \qquad (3\text{-}15)$$

Recirculation flow rate data are provided in Figures 3-8 through 3-12. Figures 3-8, 3-9, and 3-10 apply to supercritical oxygen, nitrogen, and hydrogen, respectively. The recirculation ratio $\frac{\dot{w}_R}{\dot{w}_D}$ is a function of pressure, density, and pressurization loop discharge temperature T_2 as indicated in these figures.

For subcritical storage situations, only liquid delivery of oxygen and hydrogen is considered. Two modes of recirculation loop operation can be characterized: the loop can be taken to receive either saturated vapor or liquid at its inlet. Only the latter of these two is considered here; the data is given in Figures 3-11 and 3-12. The solution for the case of vapor recirculation in the stratified model is time and volume dependent. Additionally this situation can lead to unrealistic results where small ullage volumes are initially present.

Figures 3-8 through 3-12 provide a comparison between the pressurization loop flow requirements for the homogenous model used in developing data for the design reference manual and the stratified model discussed above. An examination of these figures show that with the exception of supercritical hydrogen storage in the low density region, use of the homogenous model gives conservative results. For supercritical hydrogen storage in the low density region (densities below approximately 2.5 lb/ft^3, see Figure 3-10), the recirculation flow required as given by the stratification model is slightly greater than that predicted by the homogenous model. Due to the relatively small difference between the flow requirements predicted by the two models

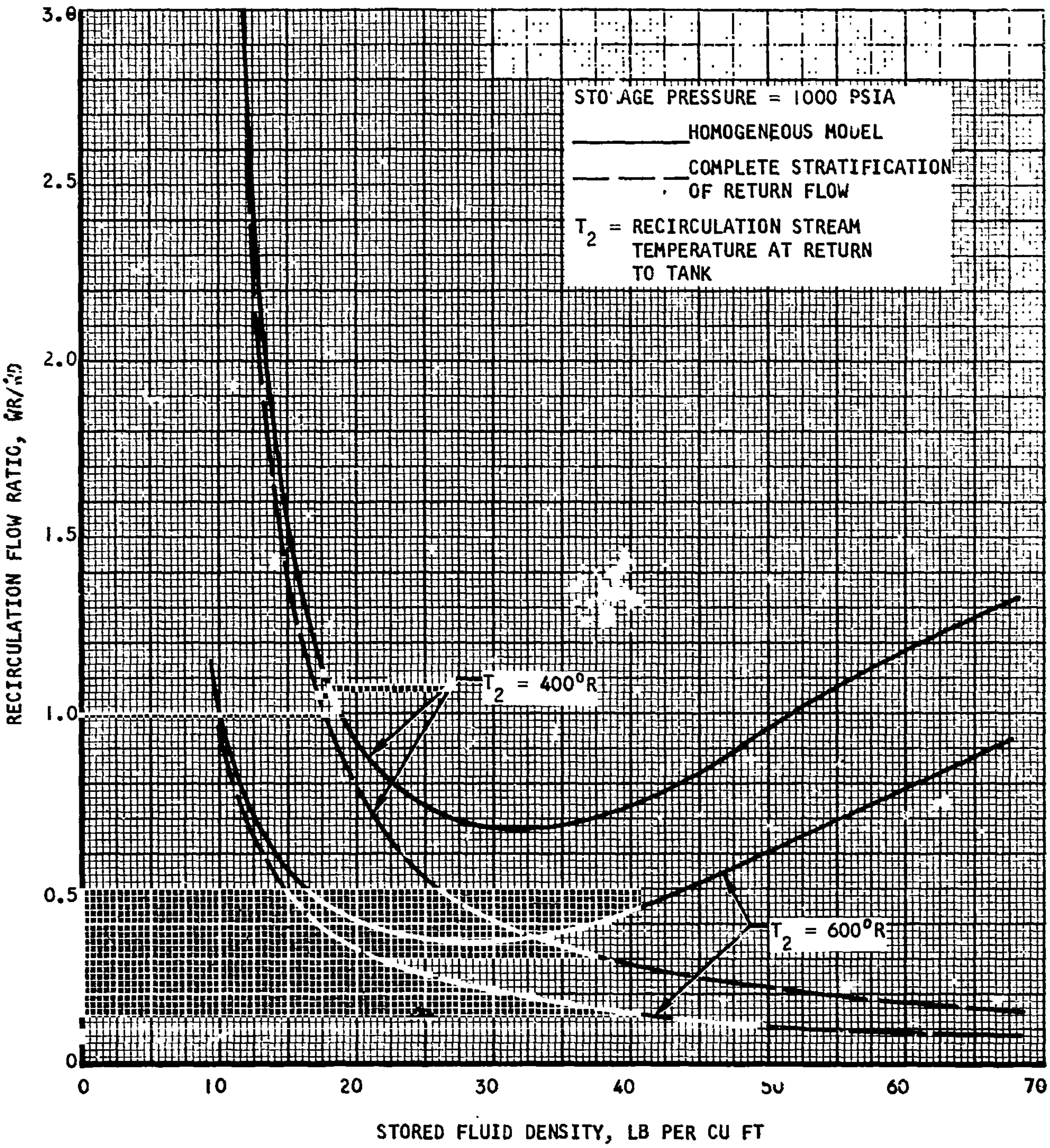

Figure 3-8. Recirculation Flow Rates for Supercritical Oxygen for Homogeneous and Stratified Models

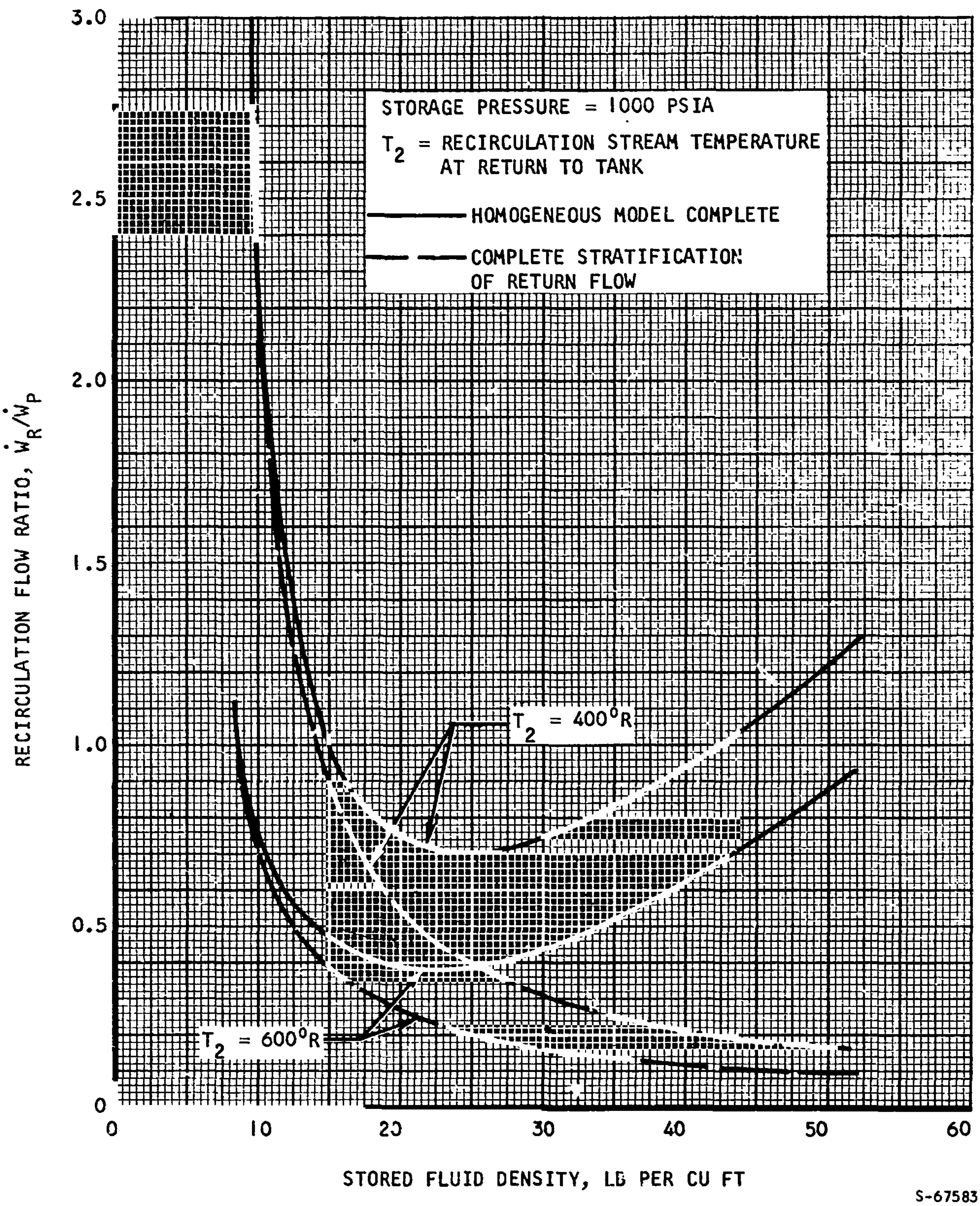

Figure 3-9. Recirculation Flow Rates for Supercritical Nitrogen for Homogeneous and Stratified Models

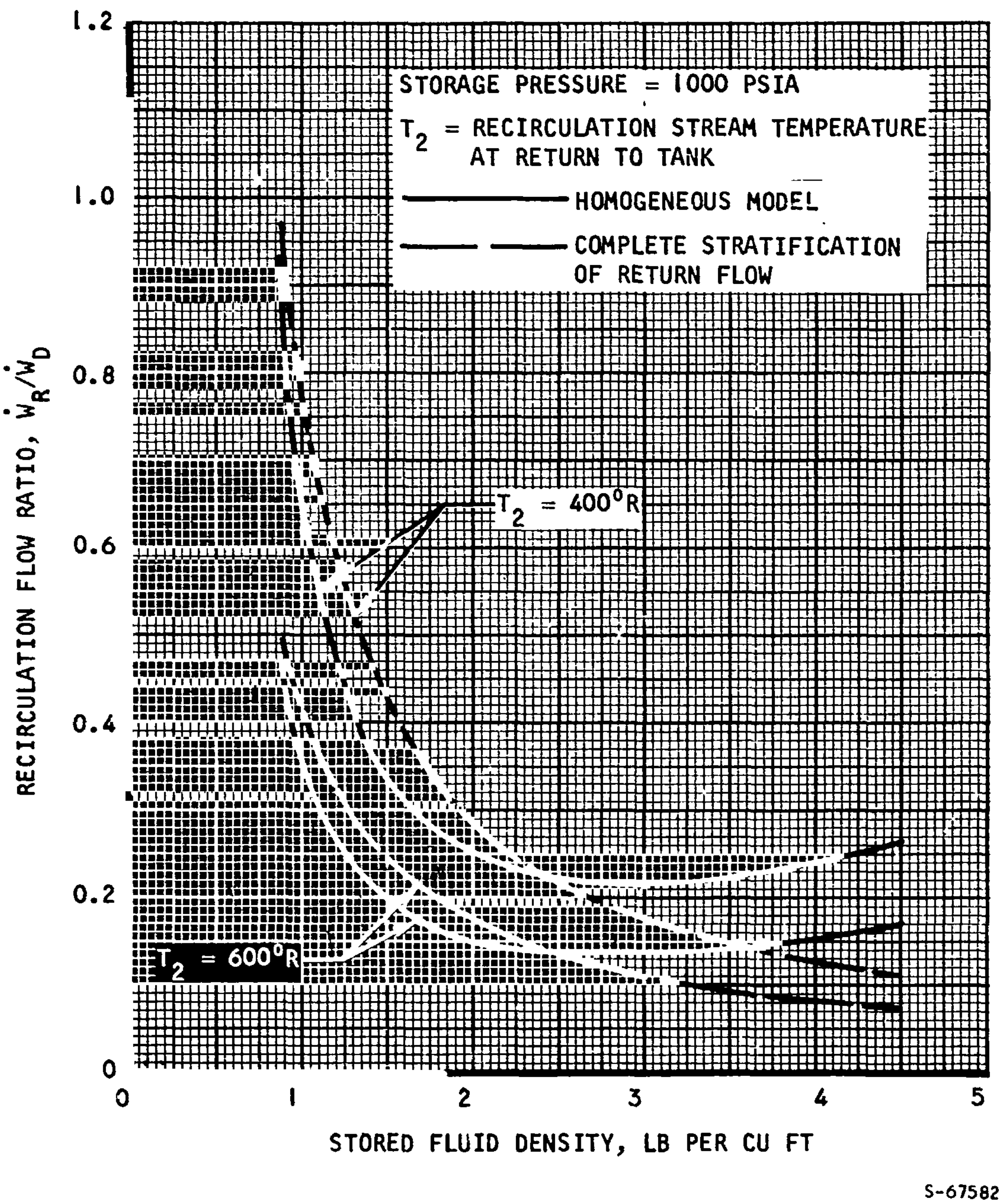

Figure 3-10. Recirculation Flow Rates for Supercritical Hydrogen for Homogeneous and Stratified Models

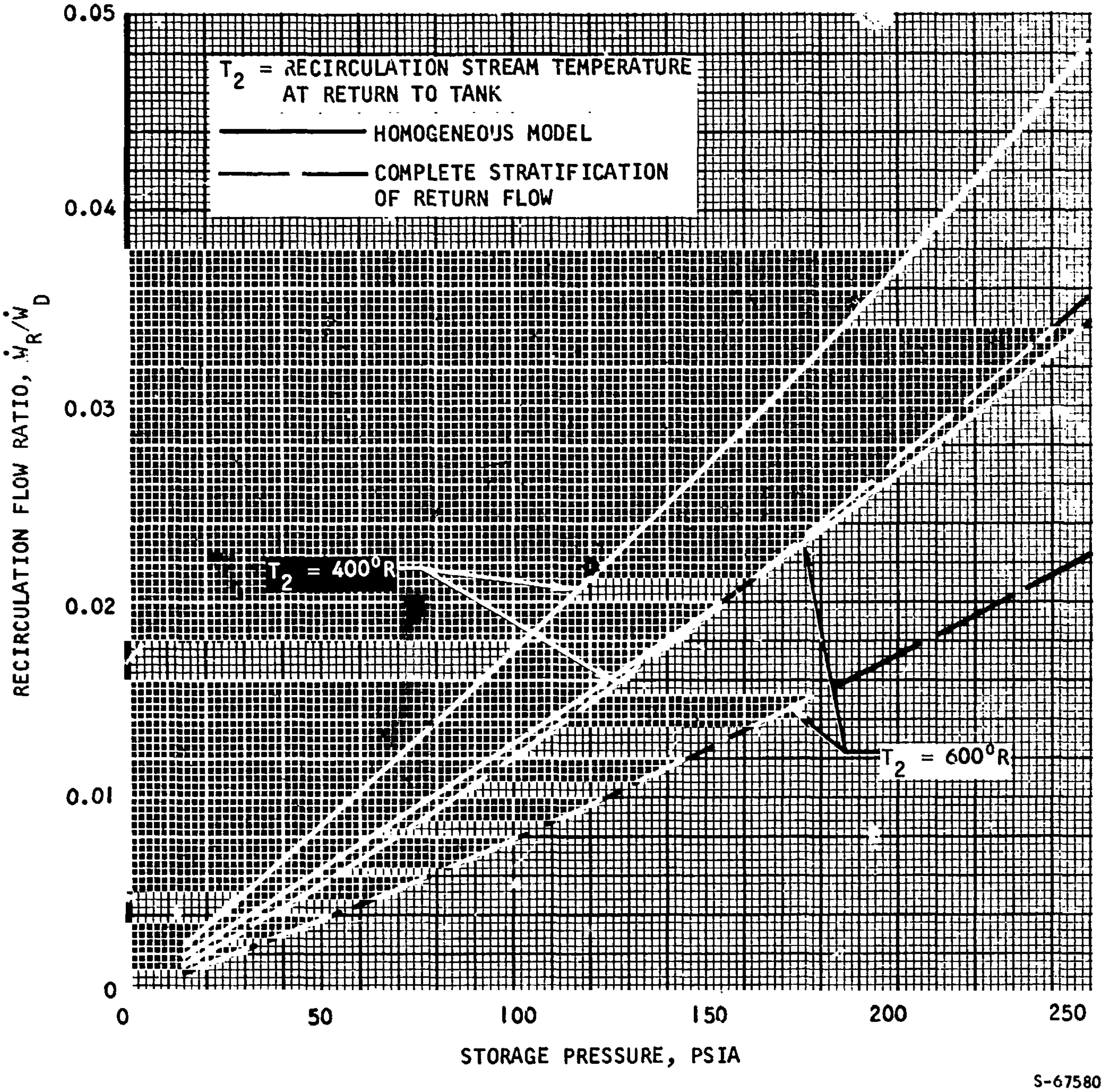

Figure 3-1ꞌ circulation Flow Rates for Liquid Delivery of ge with Recirculation of Liquid

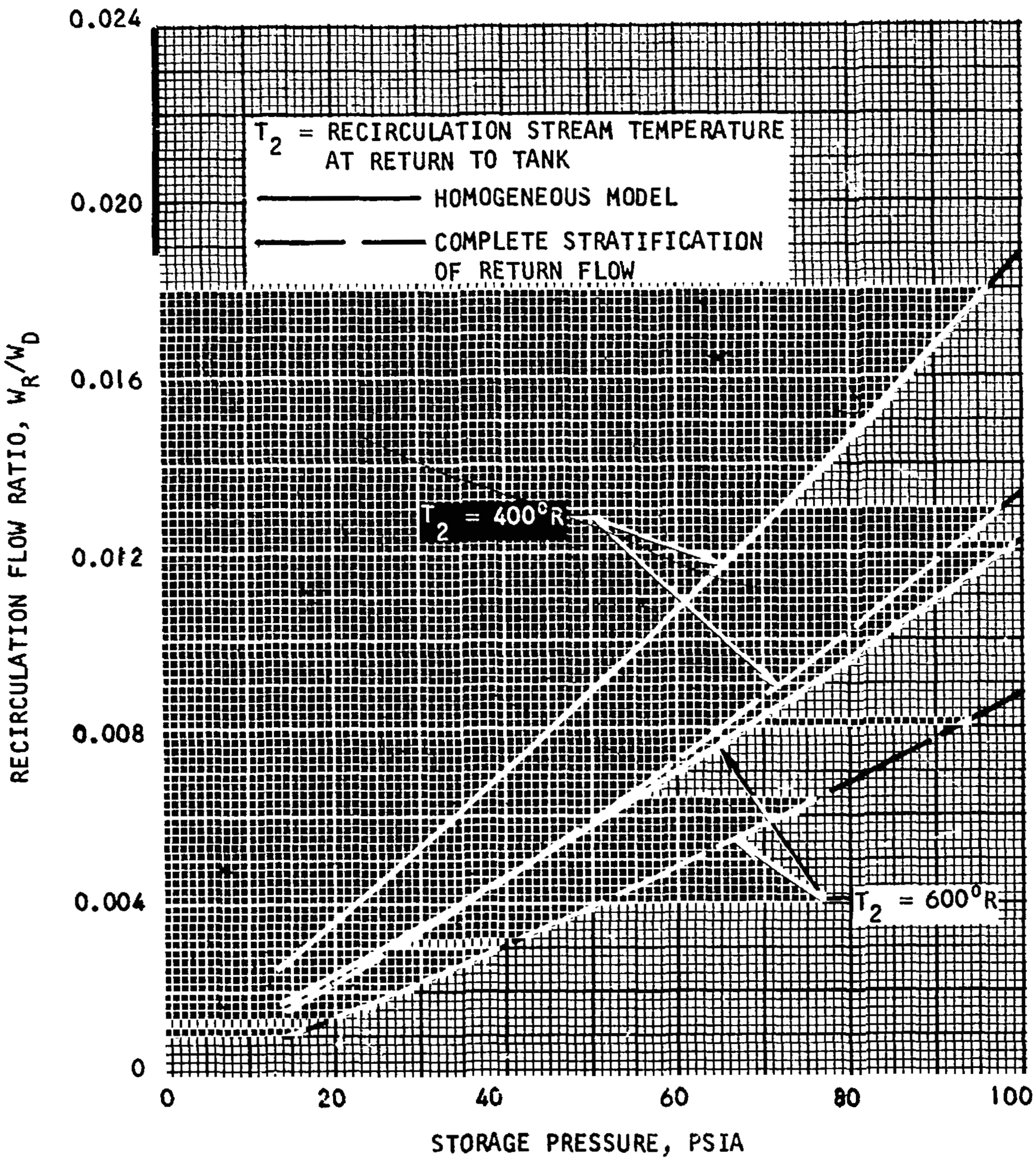

Figure 3-12. Recirculation Flow Rates for Liquid Delivery of Hydrogen with Recirculation of Liquid

in this region, the use of the homogenous model for development of design point data is not expected to affect the pressurization system design. Additionally, it should be remembered that the two-fluid stratification model represents an extreme case; this degree of stratification would not actually result for operation of the system.

SECTION 4

LINES, VALVES AND CONTROLS

Design of external pressurization systems requires that techniques be established for sizing the fluid transfer and control elements. To supply this need, a generalized graphical procedure was developed for incompressible flow in circular ducts. This section describes the procedure and presents related information that defines the characteristics of this group of components.

LINE SIZING PROCEDURE

Selection of line size and the associated pressure drop under the assumed incompressible flow conditions does not present a difficult problem. However, the calculations can become tedious, particularly if iteration of diameter is necessary to satisfy a specified pressure drop. To alleviate this aspect of the analysis, a simplified procedure was defined for use in the Design Reference Manual.

Sizing Charts

The technique adopted is based on the following expression for friction loss in a circular duct:

$$\Delta p = f \frac{L}{D} \frac{\rho V^2}{2 g_c} \qquad (4\text{-}1)$$

where f = Blasius (or Darcy) friction factor

L = duct length

D = duct diameter

ρ = fluid density

V = fluid velocity

By introducing the equation of continuity and considering the circular cross-section of the duct, Equation 4-1 can be rewritten as

$$\Delta p = \frac{8}{g_c \pi^2} \frac{f L \dot{w}^2}{\rho D^5} \qquad (4\text{-}2)$$

where $\dot{w}$ = fluid mass flow rate. The duct diameter, then, is given by

$$D = \left[\frac{8}{g_c \pi^2} \frac{f L \dot{w}^2}{\rho \Delta p} \right]^{1/5} \qquad (4\text{-}3)$$

If in Equation 4-3 reference values are assigned to the friction factor, duct length, and pressure loss, a reference diameter, which will be noted as D_3, can be defined as a function of mass flow rate and fluid density:

$$D_3 = \left[\frac{8 f_{ref} L_{ref}}{g_c \pi^2 \Delta P_{ref}} \frac{\dot{w}^2}{\rho}\right]^{1/5} \tag{4-4}$$

Another reference diameter D_2 can be defined as a function of D_3 and a general duct length L as follows:

$$D_2 = D_3 \left(\frac{L}{L_{ref}}\right)^{1/5} \tag{4-5}$$

Clearly, D_2 is a function of L, $\dot{w}$, and ρ. Thus, D_2 is a less restricted diameter function than D_3. In the same manner, a function D_1 can be defined as

$$D_1 = D_2 \left(\frac{f}{f_{ref}}\right)^{1/5} \tag{4-6}$$

and finally,

$$D = D_1 \left(\frac{\Delta P_{ref}}{\Delta P}\right)^{1/5} \tag{4-7}$$

where Equation 4-7 is now equivalent to Equation 4-3, representing a general expression for duct diameter.

The above results indicate that four related graphs can be prepared that when used in sequence allow duct to be graphically evaluated as a function of the variables on the right-hand side of Equation 4-3. Figure 4-1 presents an example of such a series of generalized curves; the curves have been arranged so that common axes are used for the intermediate diameter fuctions D_1, D_2, and D_3. This permits direct projection from one curve to the succeeding curve. In the Design Reference Manual, two sizing charts are provided to better cover the range of possible flows.

Evaluation of Line Sizes

Curve 1 of Figure 4-1 is generated by Equation 4-4 and curve 2 by Equation 4-5. In curve 3, advantage is taken of the fact that the friction factor for smooth tubing is a function of only the Reynolds number as shown on Figure 4-2. Thus, it is possible to present the Reynolds number as the parameter on this

FOLDOUT FRAME 1

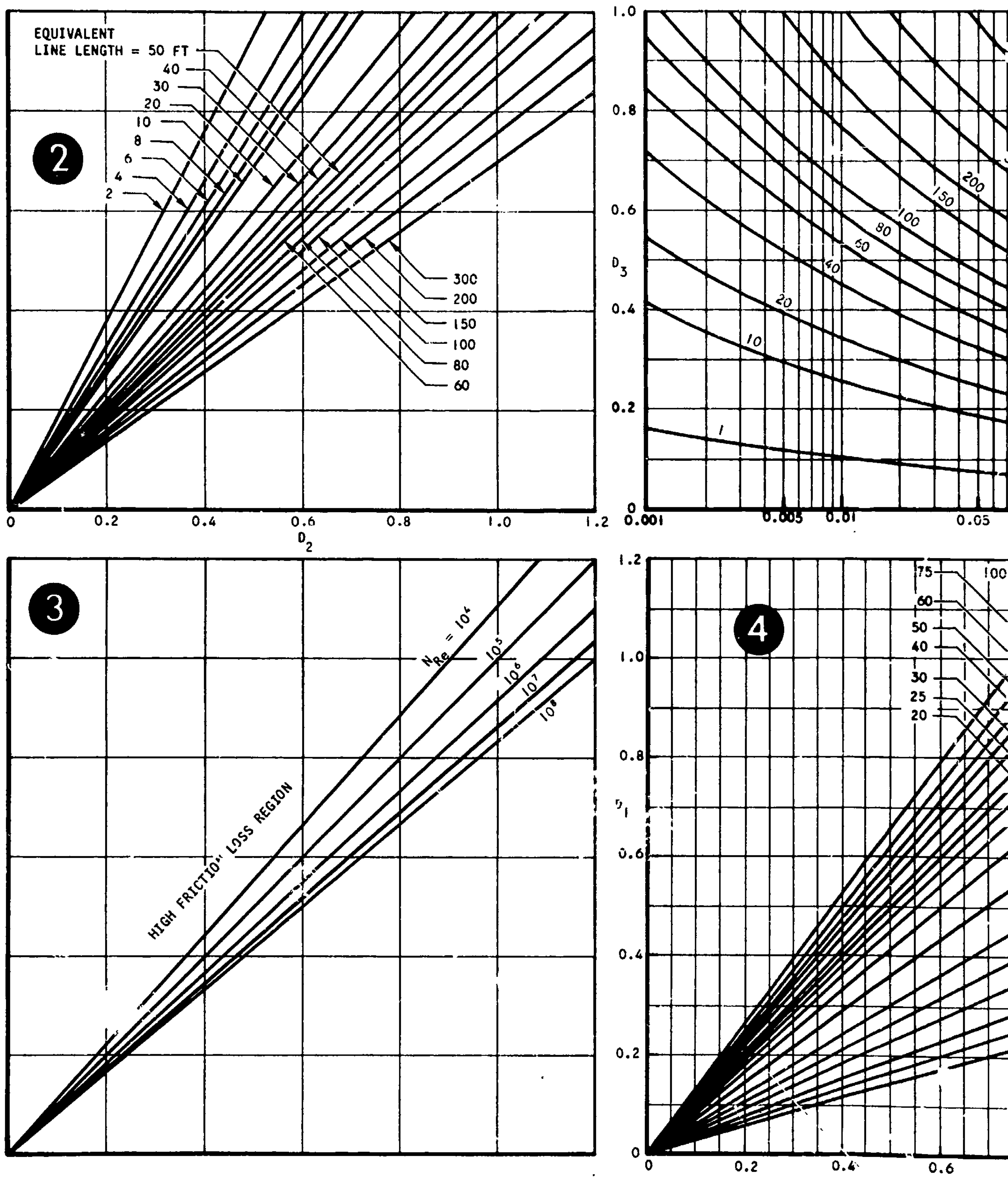

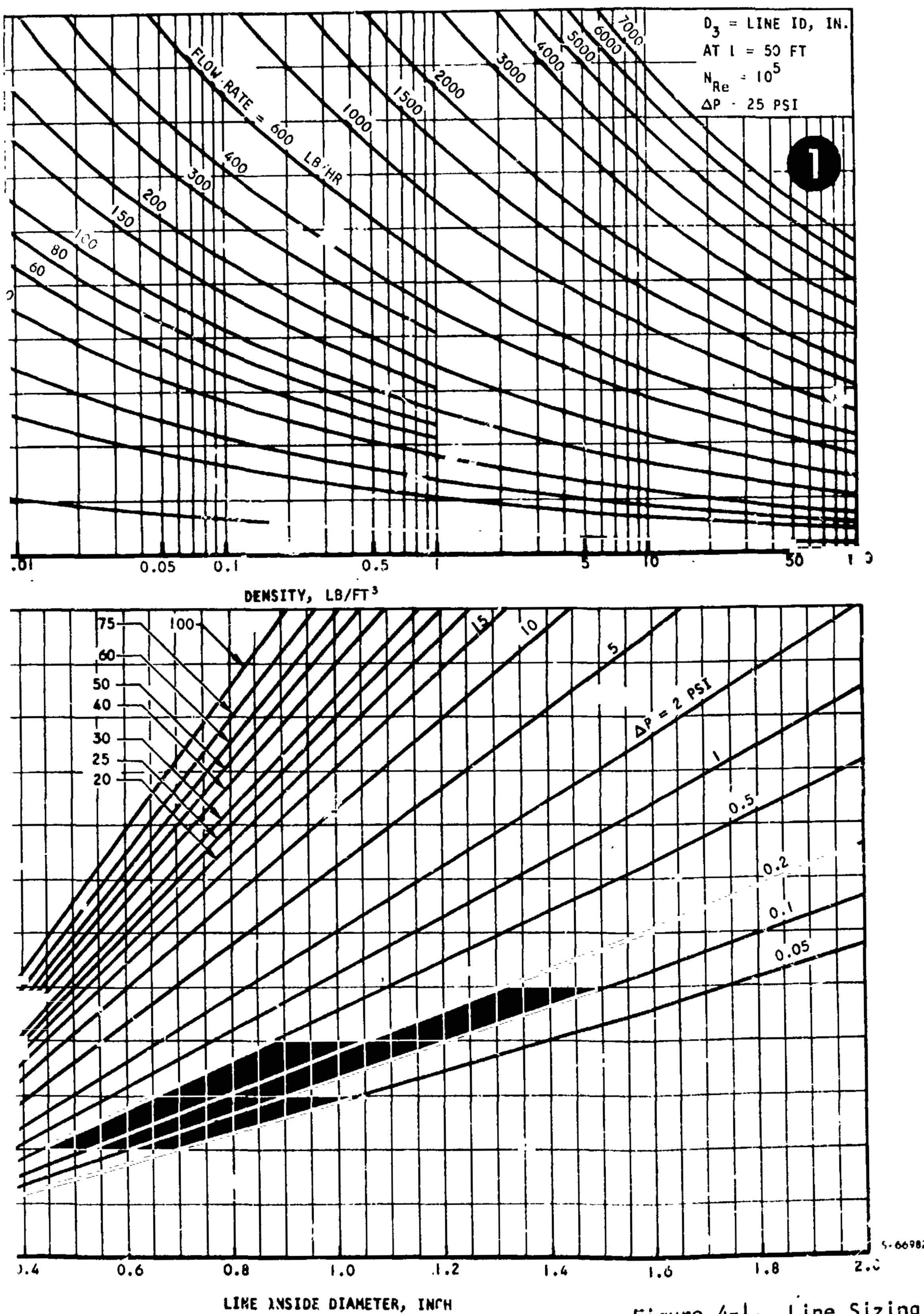

Figure 4-1. Line Sizing Plots for Small Tubing

PRECEDING PAGE BLANK NOT FILMED

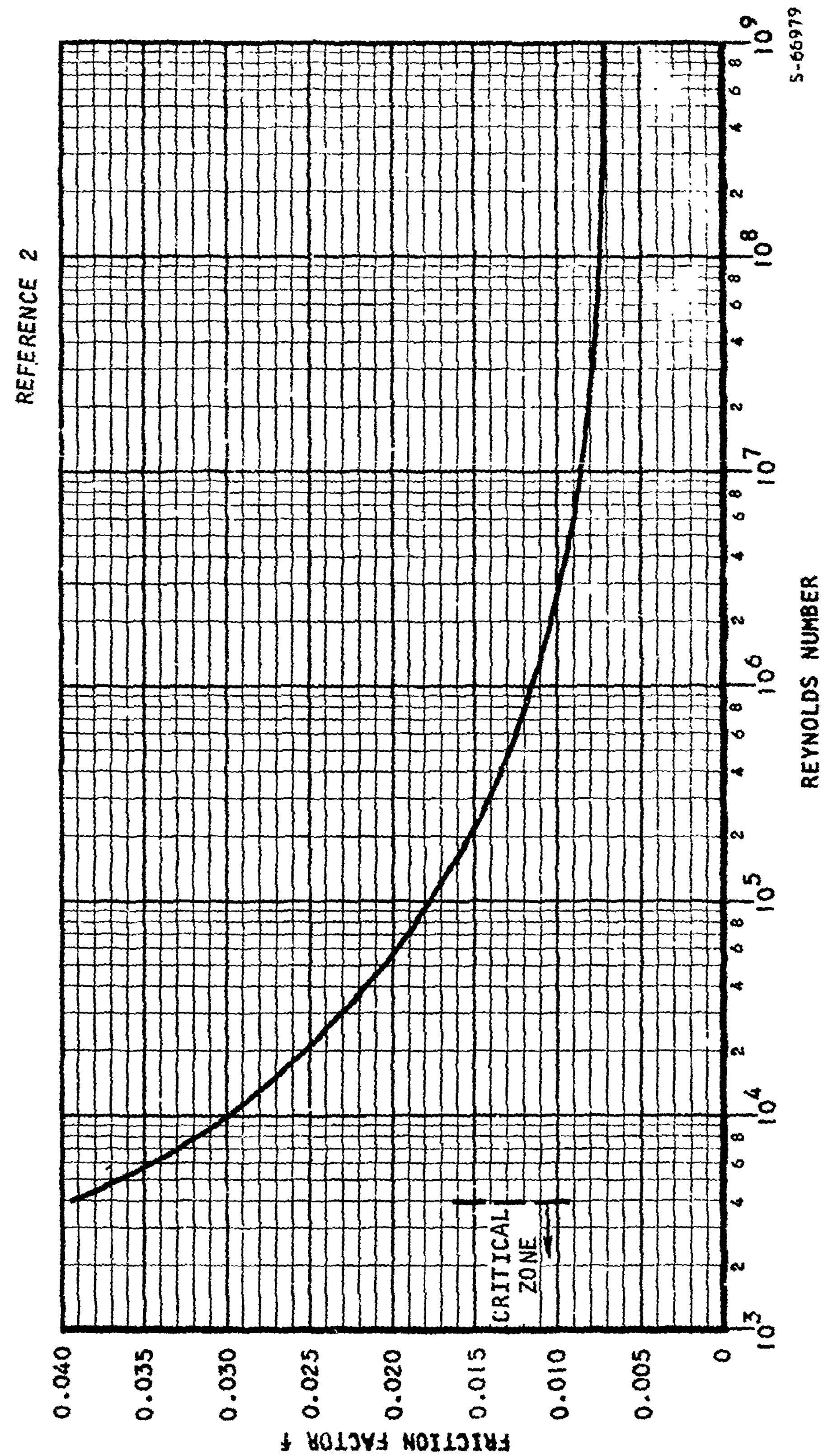

Figure 4-2. Friction Factor for Smooth Tubing

curve rather than the friction factor, as would be expected from Equation 4-6. The final curve (curve 4) is derived from Equation 4-7. The Reynolds number used here is based on line inlet conditions and is defined by

$$R_e = \frac{4\,\dot{w}}{\pi D \mu} \tag{4-8}$$

where μ = dynamic viscosity.

The lengths on curve 2 are labeled as equivalent lengths. By representing other line losses, such as those due to area change, bends, fittings and valves, as equivalent lengths of straight circular tubing, the loss experienced by a complete tubing run can be evaluated on Figure 4-1. Calculation of the appropriate equivalent length will be discussed later.

In using Figure 4-1, curve 1 is entered with the applicable flow rate and density, yielding a value for D_3. This is used as a first-guess line size in calculation of the Reynolds number and equivalent length. Curve 2 is then entered with D_3 and the equivalent length to define D_2, which allows curve 3 to be consulted with D_2 and the Reynolds number. The value found for D_1 is then used with the desired pressure loss to obtain the necessary line size on curve 4. The diameter found is compared with the first-guess size (D_3) from curve 1. If these are not within 10 or 15 percent of each other, the Reynolds number and equivalent length should be recalculated based on the diameter found from curve 4. Curves 2, 3 and 4 are then employed to reevaluate D. This process should continue until reasonably close agreement between subsequent values of D is obtained.

If it is not mandatory that a specific pressure loss be satisfied, curve 4 can be entered with D_1, and the pressure loss at the guess diameter can be determined. If this result is acceptable, the analysis can be considered complete, and no further iteration is required.

In applying this procedure to the external pressurization system, two line segments generally of different size are considered. The lines from the tank to the heat exchanger, identified as the cold leg, are treated as having a fluid density defined by the tank conditions. The hot leg comprises those lines and elements between the heat exhanger and the tank. Here, the density is determined by the heat exchanger outlet conditions. Thus, two line size evaluations are necessary for each pressurization system design.

Where vapor flows in the line segment, it is necessary to ensure that the incompressible flow assumption embodied in Figure 4-1 is valid. Thus, the hot leg always must be investigated; the cold leg must be investigated if vapor recirculation is being employed. The necessary verification is supplied by evaluation of the stream Mach number. If the Mach number is found to be less than 0.2, compressibility effects can be taken to be negligible (Reference 3). In the Design Reference Manual, Mach number evaluation is accomplished by calculation of a flow parameter, which is defined as

$$FP = \frac{\dot{w}\sqrt{T}}{2827\rho D^2} \tag{4-9}$$

where T is the line segment inlet temperature. The Mach number is then found graphically as a function of the flow parameter.

The procedure discussed above, including the compressibility check, is presented in logic diagram form on Figure 4-3. After obtaining a satisfactory line-size, pressure-loss combination, the overall line assembly characteristics are readily evaluated from information presented later in this section.

EQUIVALENT LENGTH CALCULATION

Determination of the total line segment pressure loss with the charts described above requires that an equivalent length be defined for the segment. The total pressure loss of a line containing bends, fittings, and valves can be expressed as

$$\Delta p = \left[f\frac{L_a}{D} + K_g + \left(\frac{K}{\rho}\right)_v \rho\right] \frac{\rho V^2}{2g_c} \tag{4-10}$$

where L_a = actual length of line of diameter D

K_g = sum of loss coefficients due to line geometry (bends, area changes, etc.)

$\left(\frac{K}{\rho}\right)_v$ = density-dependent valve loss coefficient

In Equation 4-10, the loss coefficients K are expressed as fractions of the head $\frac{\rho V^2}{2g_c}$.

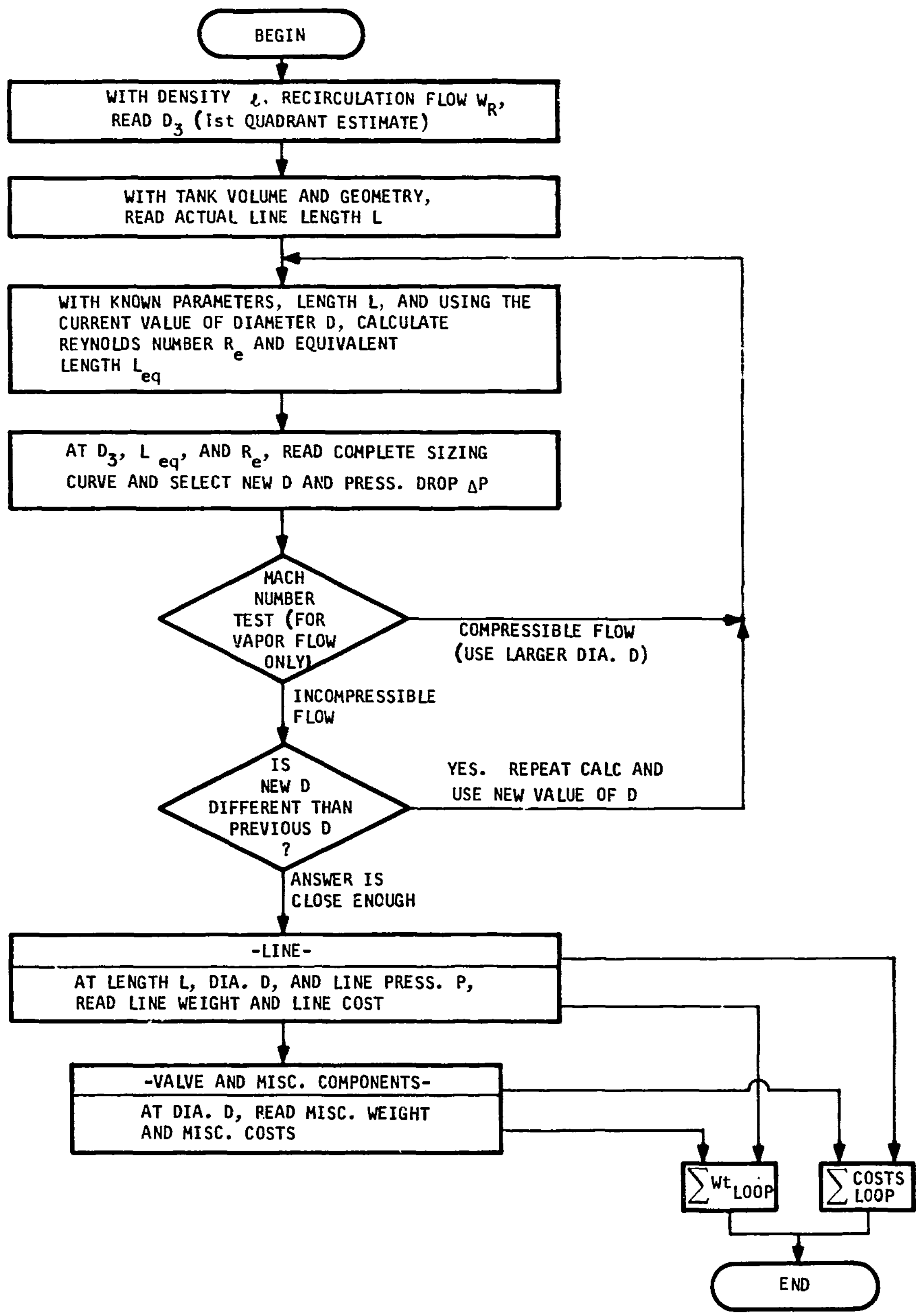

Figure 4-3. Line Sizing Design Procedures

If the equivalent length is defined as

$$L_{eg} = L_a + \frac{D}{f}\left[K_g + \left(\frac{K}{\rho}\right)_v \rho\right] \qquad (4-11)$$

Equation 4-9 can be written as

$$\Delta p = f \frac{L_{eg}}{D} \frac{\rho V^2}{2_{gc}} \qquad (4-12)$$

Thus, assumption of a value of D followed by calculation of the Reynolds number and evaluation of the friction coefficient f allows the equivalent length to be determined for the line segment.

Loss coefficients for various geometric situations and common valve types may be found in many fluid dynamics handbooks and texts such as References 2, 4 and 5. A representative collection of such data is provided in the Design Reference Manual; these curves will not be reproduced here.

Some data sources provide loss information in the form of equivalent length-to-diameter ratios L/D_{ref}. Figure 4-4 is useful in reducing these quantities to the form of head loss coefficients K. This curve assumes that the friction factors presented in Figure 4-2 apply.

Calculation of the equivalent length of pressurization system hot and cold legs implies that routing of these transfer lines has been completely defined. Since this generally may not be the case with a handbook procedure, users of the manual are furnished with a means of estimating a reasonable equivalent length.

For the actual line length, expressions were defined for the cold and hot legs as a function of tank volume and geometry. These were:

$$L_{a_{cold}} = \frac{1}{2}\left(\frac{6}{\pi} V_t\right)^{1/3}\left[\frac{x}{d} + \frac{\pi}{2} + 1\right] \qquad (4-13)$$

$$L_{a_{hot}} = \frac{1}{2}\left(\frac{6}{\pi} V_t\right)^{1/3}\left[\frac{x}{d} + \frac{\pi}{2}\right] \qquad (4-14)$$

where V_t = tank volume

x/d = tank length-to-diameter ratio (1.0 for a spherical vessel)

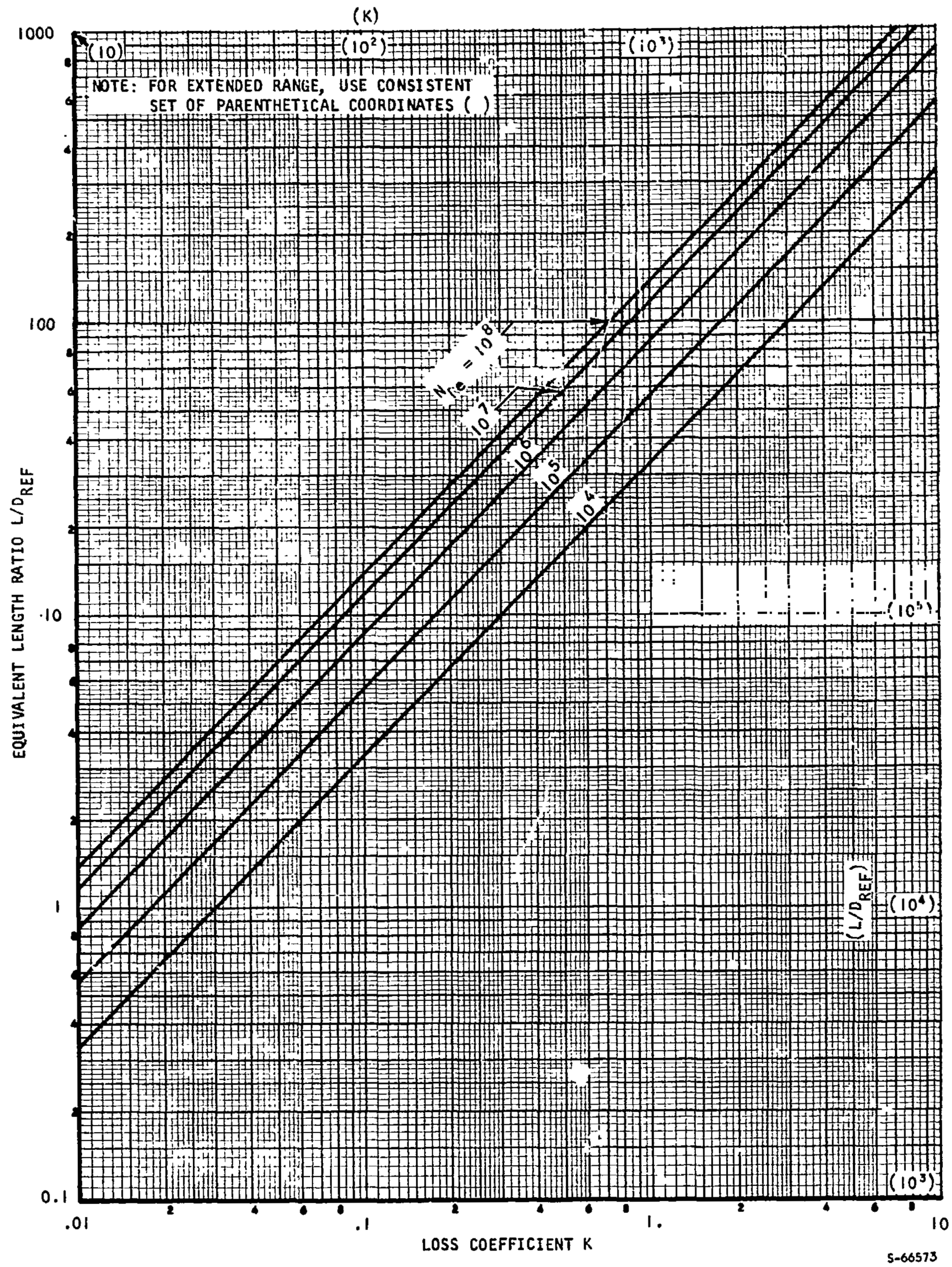

Figure 4-4. Reference Loss Coefficient Conversion Chart

These lengths represent the peripheral distance from one end of the tank to the other, plus one tank diameter for the cold leg or one-half a tank diameter for the hot leg. More line length is allowed for the cold leg to account for routing to the pump located in that leg. Equations 4-13 and 4-14 are presented graphically on Figure 4-5.

A typical set of geometric loss coefficients was also adopted for use in the absence of more detailed information. These are presented in Table 4-1.

TABLE 4-1

TYPICAL LINE

GEOMETRIC LOSSES

LOSS	COEFFICIENT, K
COLD LEG	
Entrance	0.46
Area change	
Pump inlet	0.36
Pump exit	0.28
Heat exchanger inlet	0.36
Bends -- nine 90°*	1.80
One miter fitting	1.20
TOTAL LOSS	4.46
HOT LEG	
Exit	1.0
Area change, heat exchanger outlet	0.28
Bends -- four 90°*	0.80
TOTAL LOSS	2.08

*$R/_D$ = 2.0

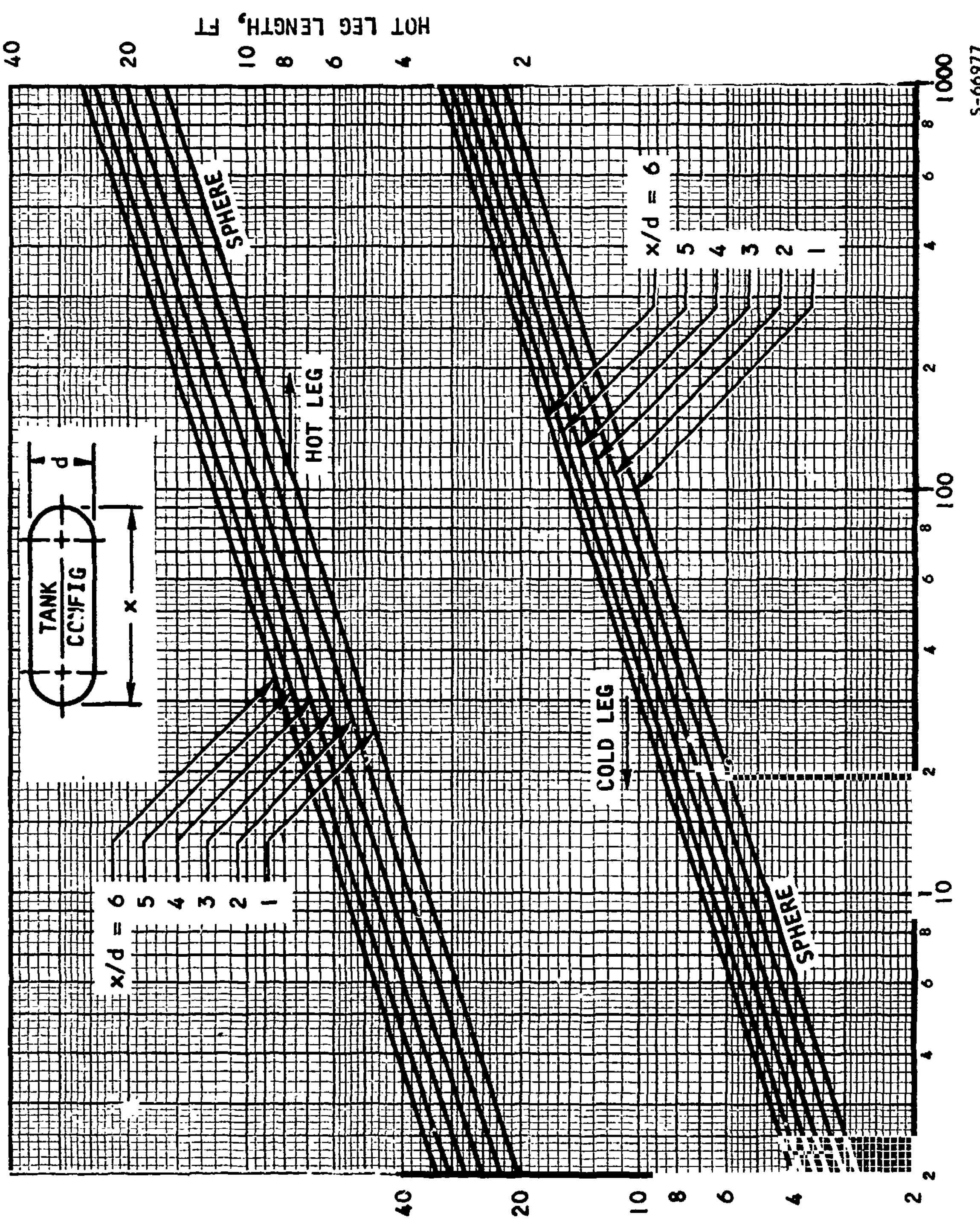

Figure 4-5. Actual Line Length Requirements

VALVES

The system model includes two valves: (1) a flow control valve, which initiates flow in the external loop, and (2) a check valve, which may be necessary for isolation of the loop hot leg. Both are exposed to cryogenic fluid, although the check valve experiences higher temperatures during system flow periods. Thus, the concept adopted for general characterization of these valves must be compatible with low temperature service. As a general type, poppet valves are suitable for such applications. Typical poppet control and check valves are shown in Figure 4-6.

Weight and pressure loss characteristics for poppet valves over a range of line sizes were obtained from the AiResearch division of Phoenix, Arizona for use in the Design Reference Manual. Pressure loss data was provided as a function of flow rate and nominal line size for various fluids. The pressure loss can be represented as

$$\Delta p = K_v \frac{\rho V^2}{2g_c} \tag{4-15}$$

where K_v = valve head loss coefficient

Introducing the line size D and mass flow rate $\dot{w}$, this can be written as

$$\Delta p = \frac{8}{\pi^2 g_c} \left(\frac{K_v}{\rho}\right) \frac{\dot{w}^2}{D^4} \tag{4-16}$$

Thus, the ratio of K_v to the density ρ can be found from

$$\left(\frac{K}{\rho}\right)_v = \frac{\pi^2 g_c}{8} \; \frac{\Delta p D^4}{\dot{w}^2} \tag{4-17}$$

For the three fluids discussed, it was found that the K/ρ ratio for poppet valves is well represented by the values given in Table 4-2.

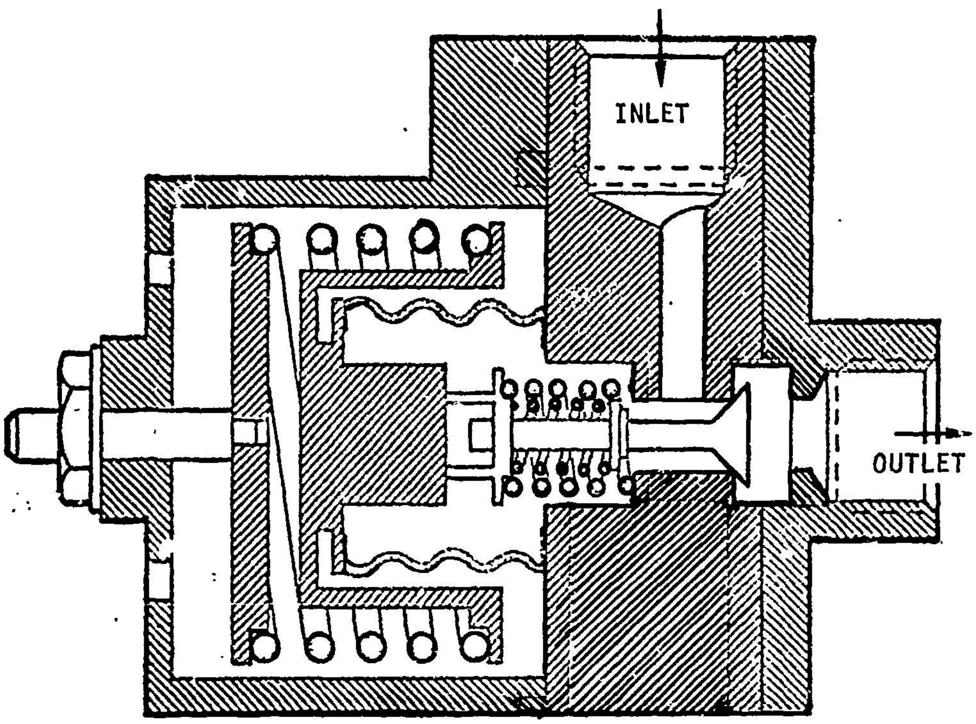

a. Flow Control Valve

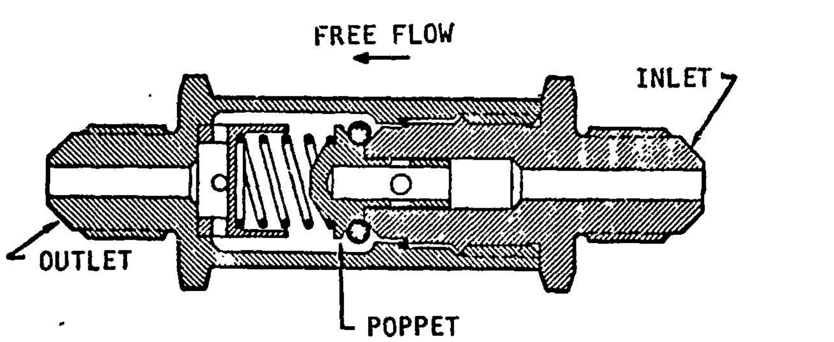

b. Check Valve

Figure 4-6. Valve Configurations

TABLE 4-2

POPPET VALVE

LOSS COEFFICIENTS

Fluid	$\left(\frac{K}{\rho}\right)_V$
Hydrogen	0.790
Oxygen	0.046
Nitrogen	0.052

ELECTRICAL CONTROLS

The electrical control equipment contemplated by the system model are minimal because control of flow initiation is taken to be accomplished pneumatically by the flow control valve. Coincident with flow initiation, energization of the pump motor is required, and if the electrical heat source is employed, the heater resistance element also must be energized. These functions can be performed by a simple, relay-type contactor that is actuated by a signal; the signal is provided by sensing the flow control valve poppet position. This type of device is depicted schematically in Figure 4-7.

WEIGHT AND COST CHARACTERIZATIONS

Weight and cost of the fluid transfer elements are treated in two categories: (1) the actual tubing elements are treated separately as a function of line size and length, and (2) all other weight and cost contributions are lumped together as a function of line size.

Line weight may be determined from Figure 4-8, which is based on the use of stainless steel tubing with a safety factor of 4.0. The curves at the right-hand section of Figure 4-8 allow weight per unit length to be found from line inside diameter and pressure; the total weight is given on the left side as a function of weight per unit length and actual line length. The material cost per unit length of line is available in Figure 4-9. The total line cost is found from

$$C_L = \left(\frac{C}{L}\right) L + 450 \text{ dollars} \qquad (4-.8)$$

where $\left(\frac{C}{L}\right)$ is the cost per unit length found on Figure 4-9. The 450 dollar term represents an allowance for line assembly preparation.

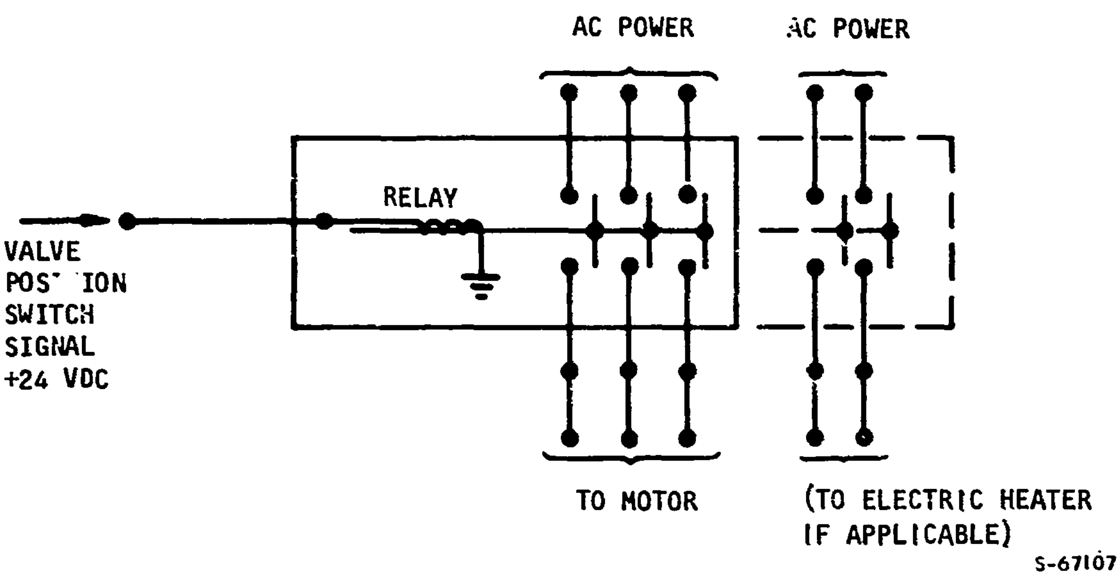

Figure 4-7. Control Schematic

FOLDOUT FRAME 1

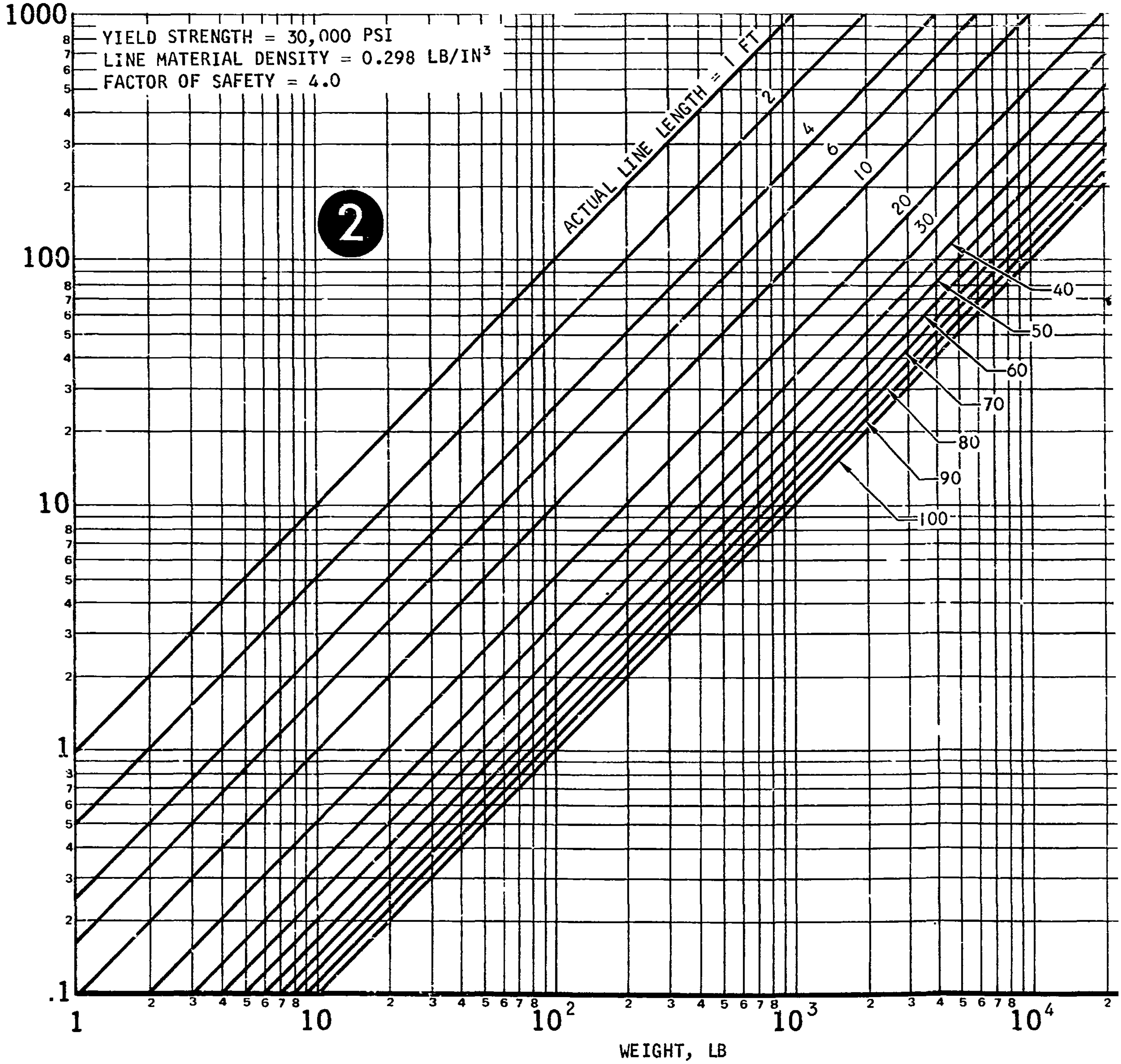

FOLDOUT FRAME 2

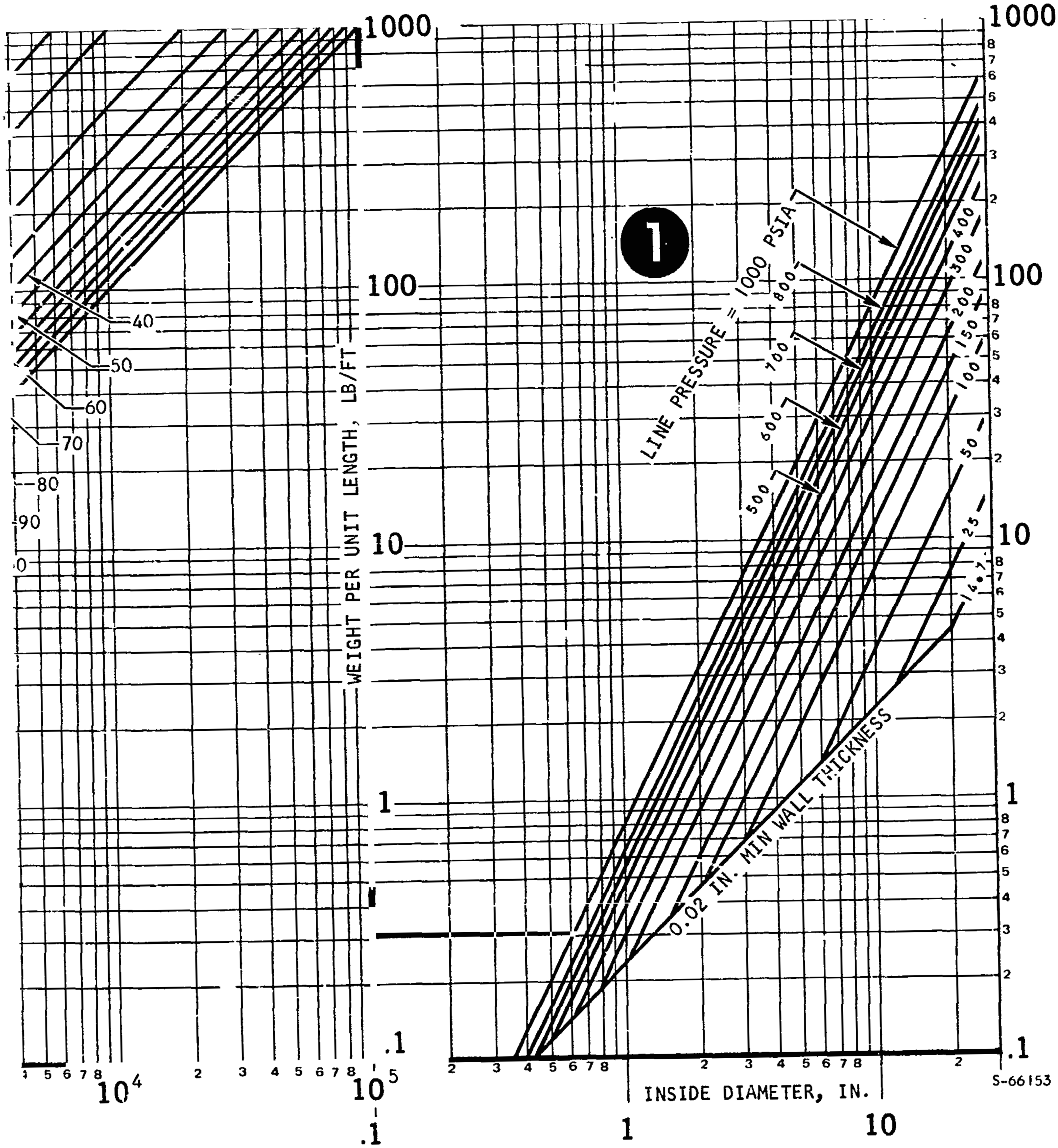

Figure 4-8. Line Weight per Unit Length and Total Weight Evaluation

PRECEDING PAGE BLANK NOT FILMED

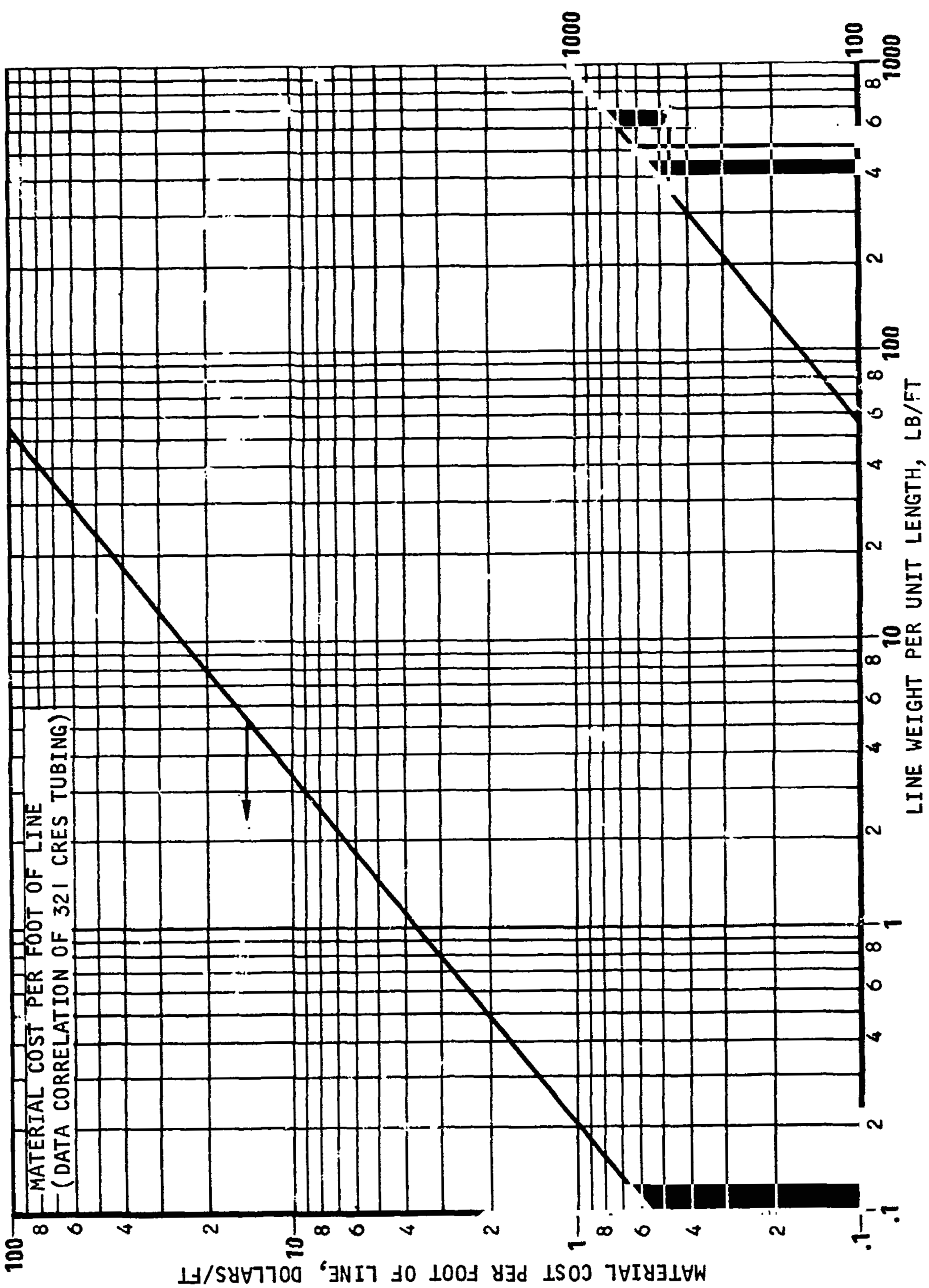

Figure 4-9. Line Material Cost

The weight of the remaining transfer components are found from Figure 4-10. The cold leg and hot leg weight totals are based on the assumed components tabulated on the figure. The individual component weights included are provided for reference on Figure 4-11. Some pressure dependence is shown for the valve weights for sizes above 4 in. Below this size, pressure does not exert a strong influence on valve design.

The recurring and nonrecurring costs of elements other than lines are presented in Figure 4-12. The recurring cost curves represent the hardware cost estimated for the components listed for each leg. The major elements of the nonrecurring cost are design and development of the valves and system analysis, coordination, and test costs. The basis for Figure 4-12 is the individual cost trends shown on Figure 4-13. Here, the solid curves are the recurring costs, while the nonrecurring costs are presented as dashed lines.

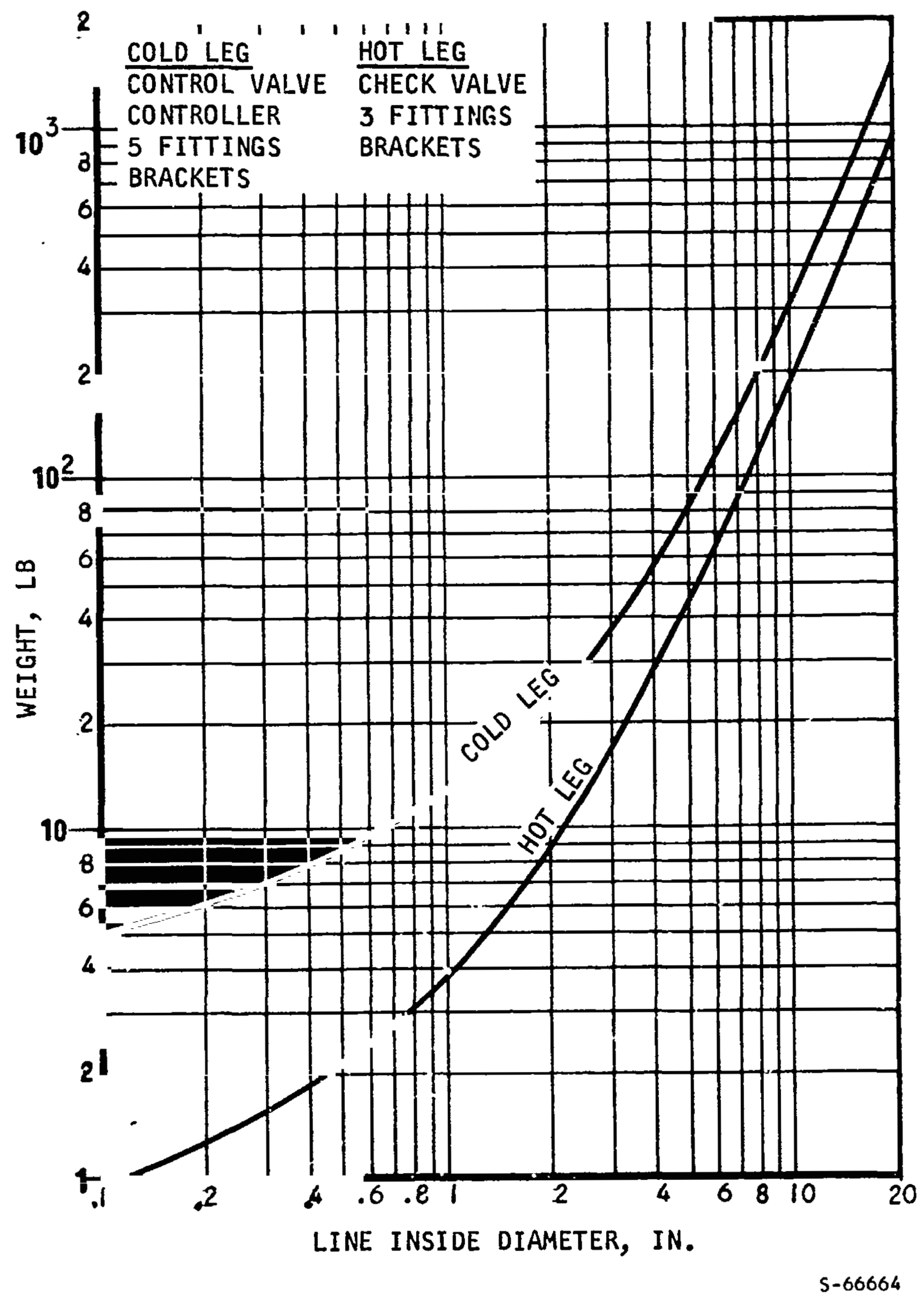

Figure 4-10. Line Components Miscellaneous Weights

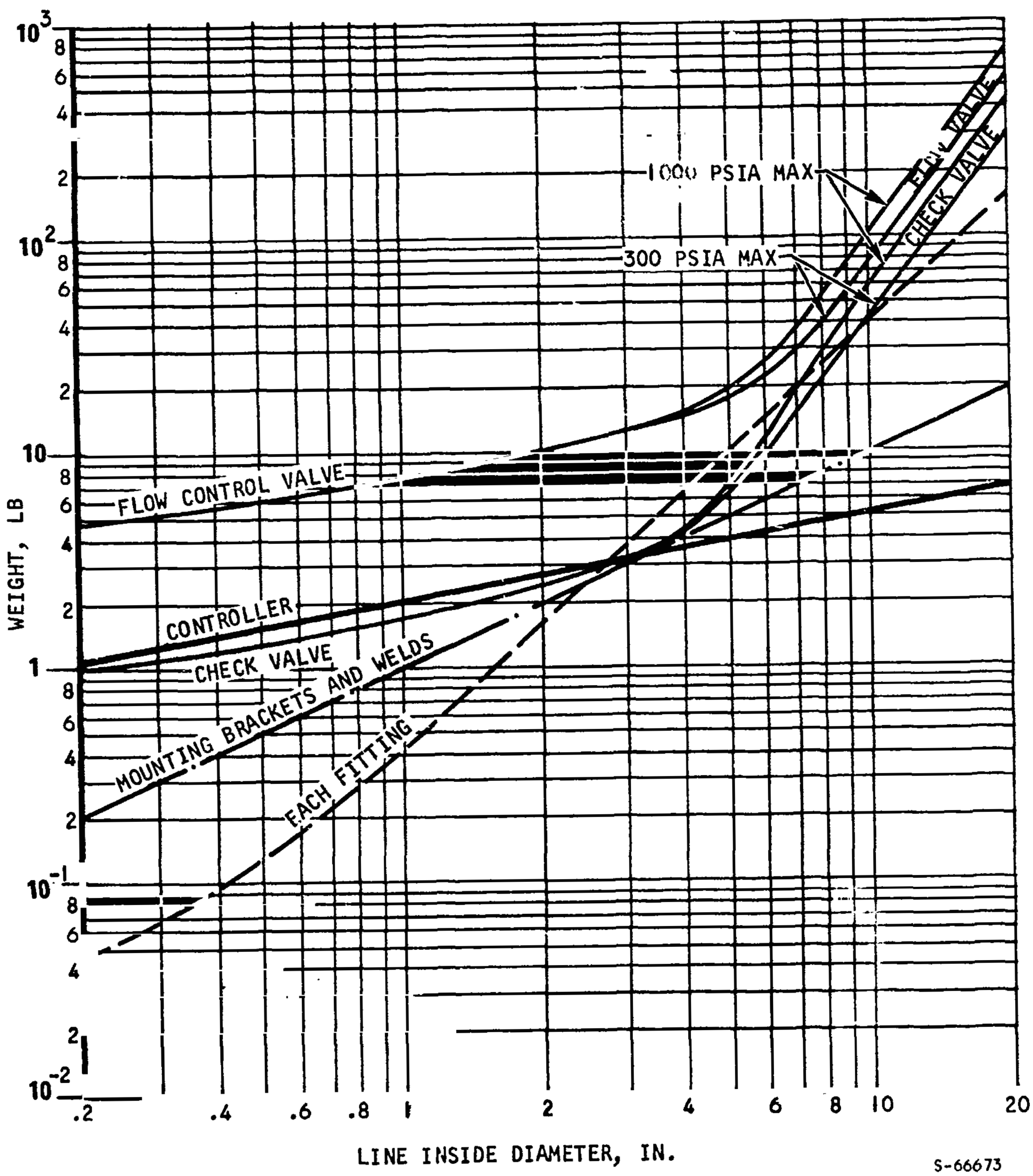

Figure 4-11. Individual Component Weights for Fluid Transfer Equipment

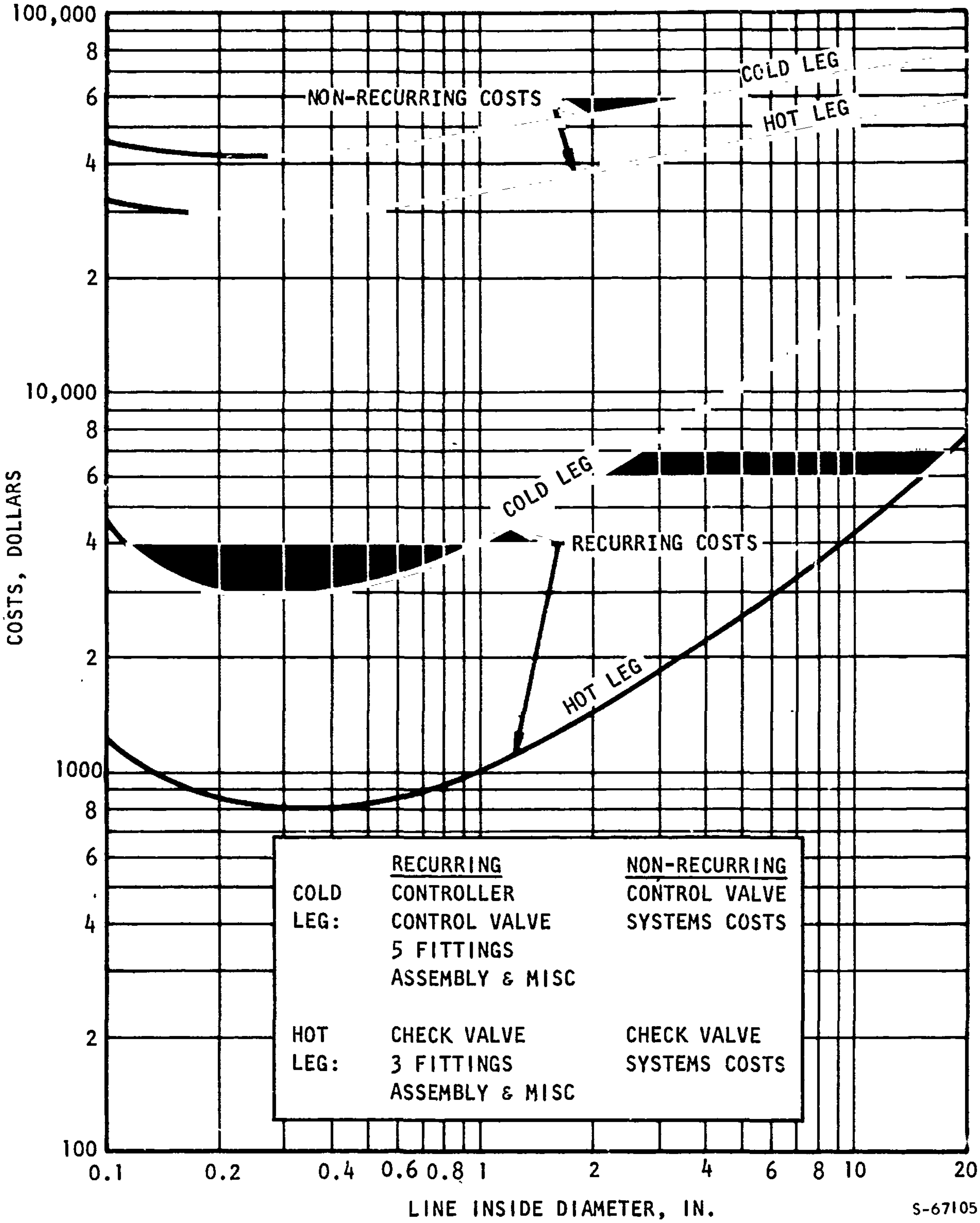

Figure 4-12. Loop Miscellaneous Component Cost

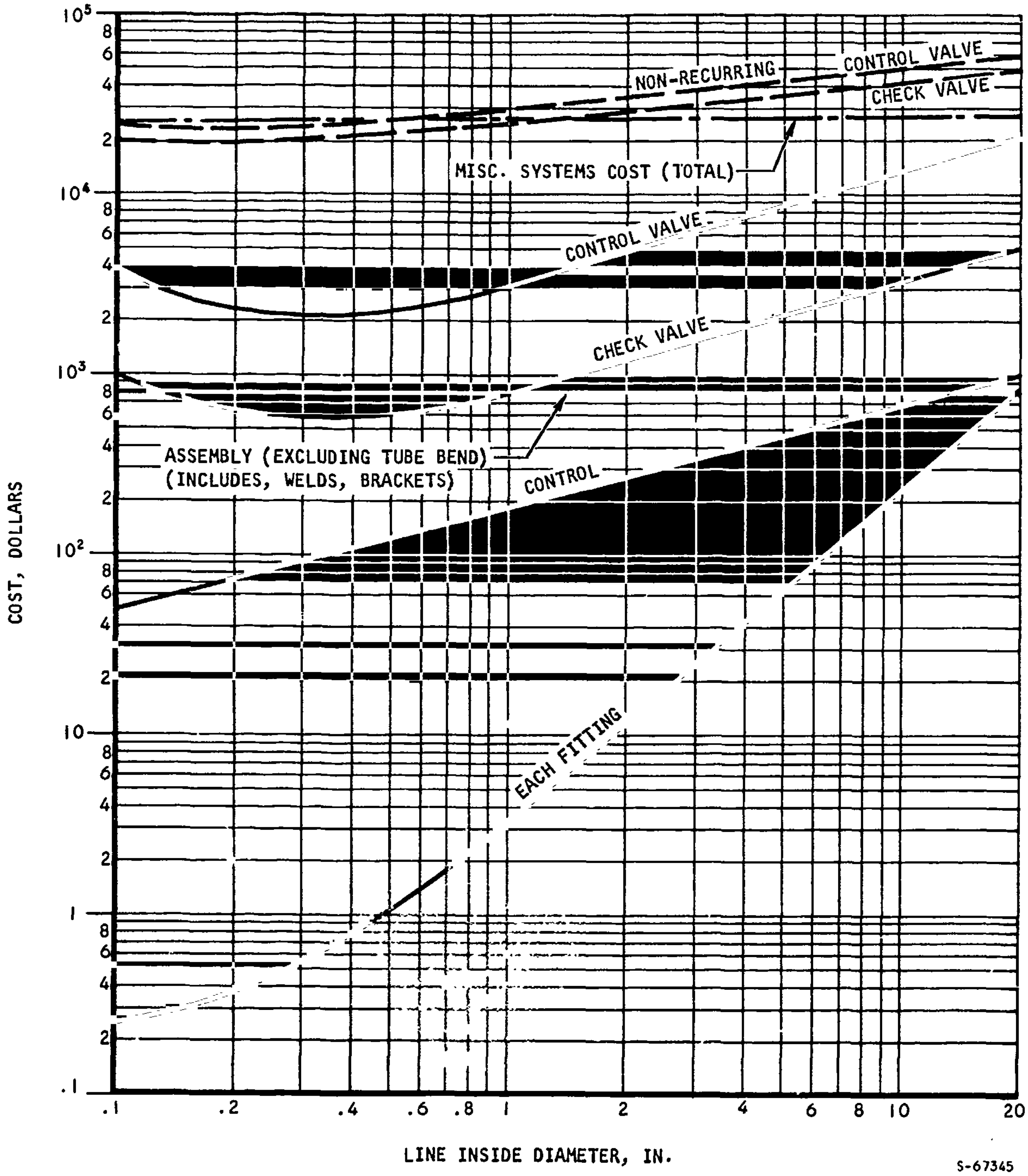

Figure 4-13. Individual Cost Elements for Fluid Transfer Equipment

SECTION 5

HEAT EXCHANGERS

Three sources of heat are specified as candidates for the energy addition function. These are:

(1) Electrical Power--28 vdc or 115-v, 400-Hz ac

(2) Transport Fluid--Represented by an FC-75 stream received at 30 to 100 psia and 500° to 700°R

(3) Hot Gas--Represented by an H_2-O_2 combustion products stream received at 100 psia and a nominal temperature of 200°R

Utilization of these sources calls for three entirely different heat exchanger concepts, each requiring a specific design procedure. All three sources cannot be considered to apply over the entire operational range covered by this study. The following comments are made relative to areas of application:

- The electrical heater units are particularly applicable to the lower range of energy inputs where the more complex system interface of the fluid heat sources is not justifiable. As the power level increases, the use of resistance heating will be discouraged by system designers. Thus, the information presented has been aimed at satisfaction of the energy inputs corresponding to the vapor delivery flow ranges defined in Table 1-1.
- The FC-75 to cryogen heat exchangers are useful for low to moderate heat input rates. Thus, the following recirculation flow rates have been used as a guide in preparing the procedure:

Hydrogen	50 lb per hr
Oxygen	100 lb per hr
Nitrogen	20 lb per hr

  The last figure is the maximum flow noted for nitrogen in Table 1-1.
- The hot gas-to-cryogen heat exchanger is applicable to the entire range if this source is available to the designer. However, minimum-size units will be encountered as the lower flows are approached.

The development of the three design techniques is discussed below, with the electrical heater being presented first followed by the transport fluid and hot gas heat exchangers. The procedures require iteration on at least one variable. This is unavoidable because of the number of variables involved in defining a heat exchanger design point. For example, eleven variables must be fixed to fully describe a direct-exchange, fluid-to-fluid heat exchanger. Effort has been made to simplify the procedures as much as possible without seriously limiting their accuracy and flexibility.

ELECTRICAL HEATER UNITS

The component type used here is an electrical resistance heater unit. The configuration, as shown on Figure 5-1, employs a cylindrical annular cryogen flow passage with the heater element attached to the outer cylindrical shell.

The heater element is Ni-Fe alloy, which was chosen because of the direct proportionality between resistance rise and temperature rise provided by this material. This characteristic acts to reduce power dissipation as heater temperature rises. This feature, coupled with extended external surfaces to enhance radiative heat rejection, allows heater temperature to be limited to $1000^{\circ}R$ even under conditions of zero cryogen flow. Danger of heater burnout is thus virtually absent.

Heat transfer from the heated outer shell to the cryogen is improved by use of a rectangular offset fin within the annular flow passage. This fin, a 16-per-in., 0.006-in. thickness aluminum configuration, fixes the annulus radial thickness at 0.10 in.

The concept adopted for the oxygen heater unit differs from that of the hydrogen and nitrogen units in that an additional cylindrical shell is located between the outer surface, to which the resistance element is brazed, and the oxygen flow passage. The barrier space thus formed is evacuated; the outer wall of the flow passage and the outer shell are thermally connected by a 0.05-in.-high triangular copper fin surface. This standoff construction prevents a single failure (of either the surface to which the heater is attached or the flow passage wall) from causing the heating element to be exposed to oxygen.

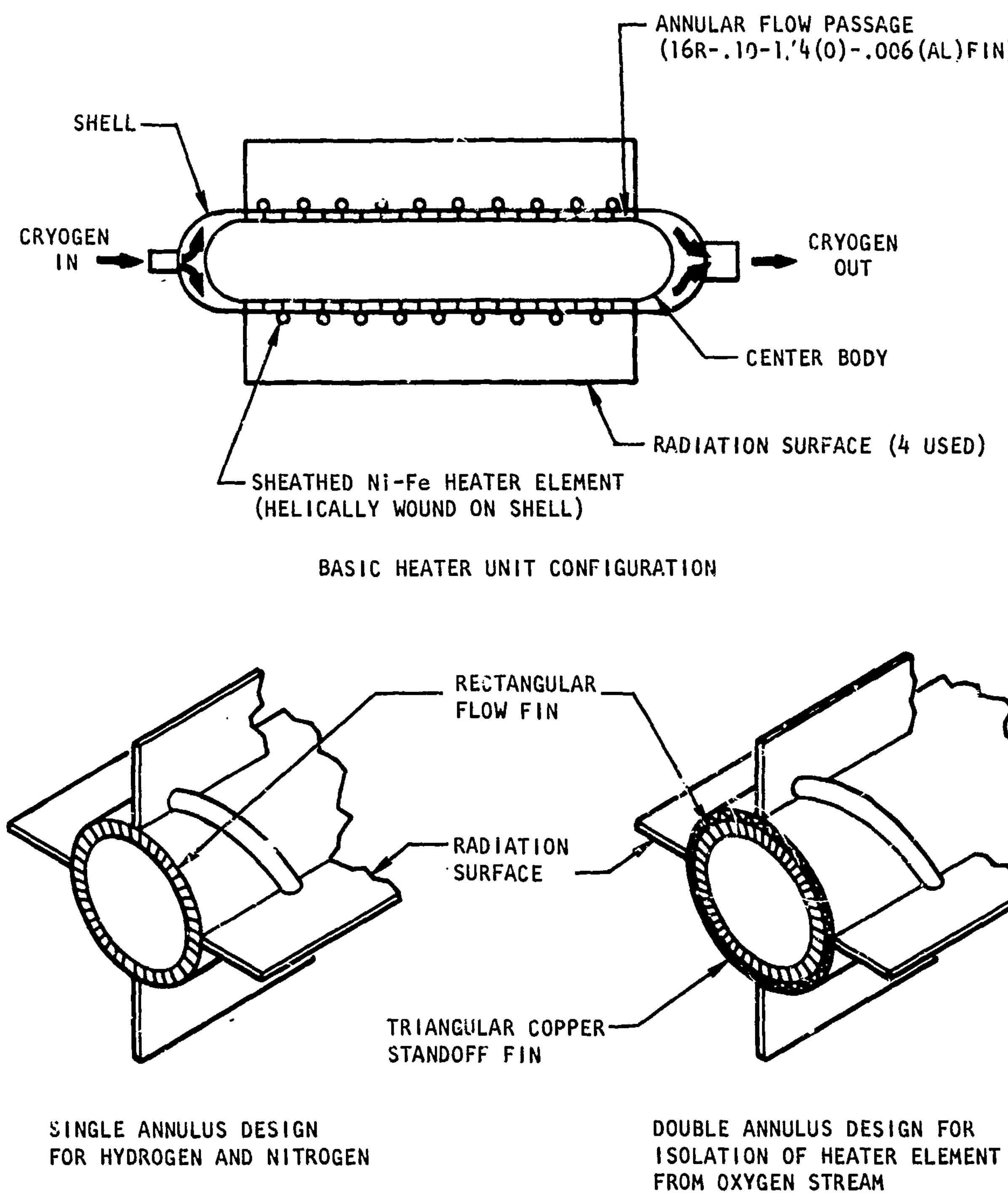

Figure 5-1. Electrical Heater Configuration

The procedure for design of electrical heater units is essentially closed-form, having a single degree of geometric freedom. It is necessary to select the outside diameter of the flow passage. For each diameter chosen, a heater design is defined. However, experimentation with this dimension may be needed in order to choose the most beneficial value for a particular application.

Heating Element Considerations

For this application, it is desirable to have a resistance element capable of providing a large heat flux per unit wall area and having a resistivity characteristic that rises rapidly with temperature. This last requirement causes power dissipation to be decreased as heater temperature rises, a valuable trait with respect to safety of operation and radiator surface requirements. The most common material for resistance heaters is Nichrome, a nickel-chromium alloy having a very weak dependence of resistivity on temperature. While this is preferred for most electrical heating applications, a material with a stronger temperature dependence was sought.

The resistivity of several alloys is compared in Figure 5-2 in the form of resistivity ratio R/R_{360} versus temperature, where R is the resistivity at the variable temperature and R_{360} is the resistivity at a 360°R reference condition. For the purposes of this program, the nickel-palladium alloy would be most desirable because the resistivity trend of this material would result in heater power dissipation at 1000°R, which is less than one-sixth of that at 360°R. However, consultation with heating element manufacturers indicated that neither the nickel-palladium nor nickel-manganese alloys were available in commercial sheathed elements. The 5.24-percent, nickel-iron alloy is a standard material; therefore, this material was chosen for use in the heater unit characterization developed. The nickel-iron alloy provides a 63-percent decrease in power dissipation as temperature rises from 360°R to 1000°R, compared with the 27-percent decrease to be expected with Nichrome over the same interval.

In Figure 5-2, curves are presented that relate the resistivity ratio to temperature in the exponential form:

$$\left(\frac{R}{R_{360}}\right) = \left(\frac{T}{360}\right)^n \qquad (5-1)$$

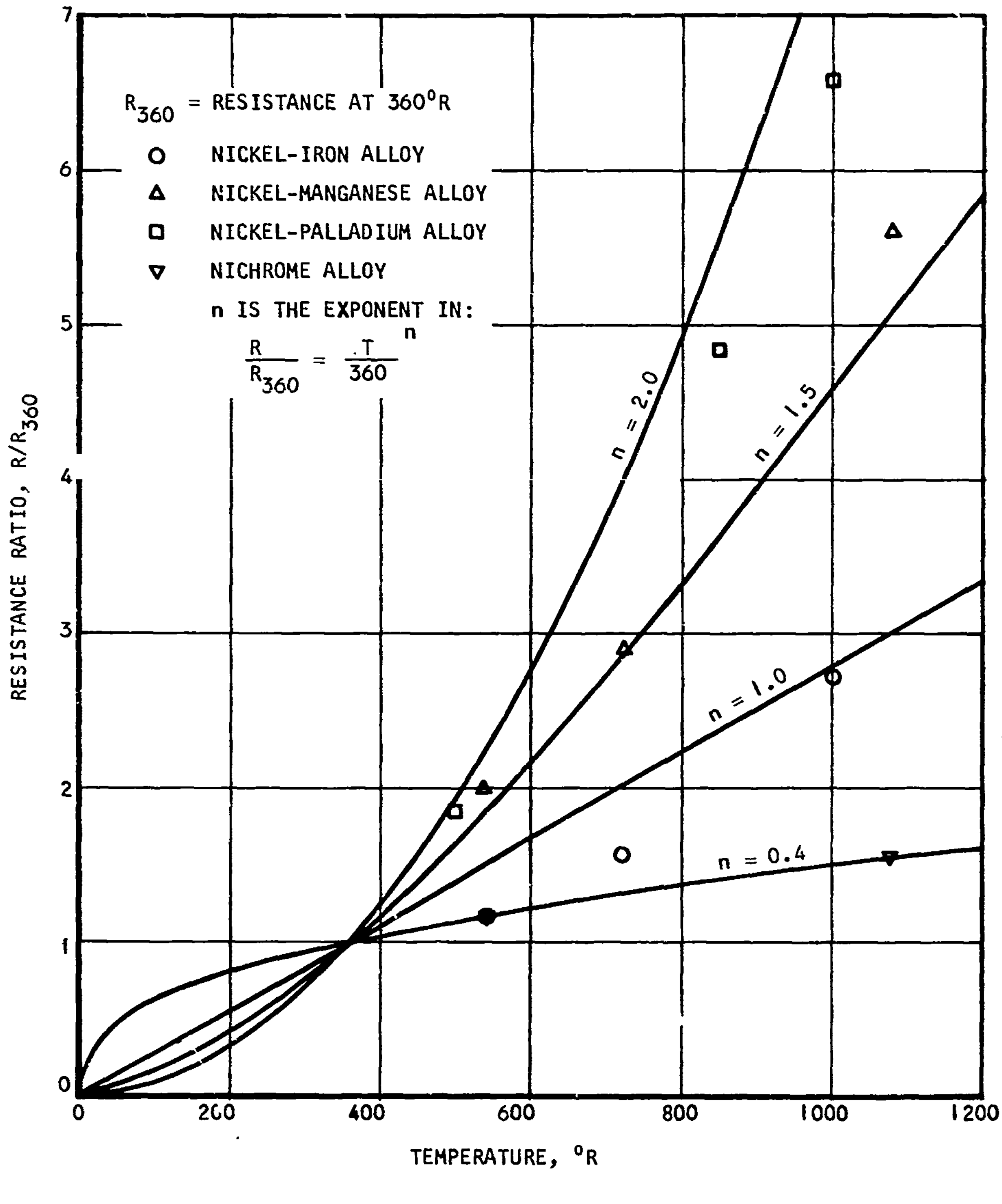

Figure 5-2. Comparison of Resistivity of Several Alloys.

The values of n shown on Figure 5-2 represent the resistivity ratio of the four materials with fair accuracy in the region above 360°R. Under this approach, the selected nickel-iron alloy would be characterized by $n = 1$, while $n = 0.4$ would be typical of Nichrome. This type of representation will be found useful in the analysis of the heater unit.

Determination of Heater Unit Size

At the outset of the electrical heater analysis, the heater configuration of Figure 5-1 was modeled on a thermal analyzer computer program. Several flow passage fins and heater resistance relationships were investigated for fluids and flow conditions throughout the range applying to this unit. This resulted in establishment of designs for each point considered. The data obtained allowed selection of the flow passage fin. The 16-fin-per-in. rectangular fin chosen was the largest examined. The smaller fins studied tended to require large unit diameters to prevent choking at the higher flow rates. There appeared to be no advantage in using a configuration larger than 16 fins per in.

The computer design study showed that establishment of parametric size, weight, and pressure loss data over the full range would be very time consuming. But, due to the single degree of geometric freedom in the heater design concept, it appeared that the computer results could be employed to establish a closed-form solution for the heater length. If the diameter of the annular flow passage is fixed, the heat transfer area per unit length is defined, and through the height of the chosen fin, the cross-sectional area for flow is also known. Thus, if means of defining the overall thermal conductance U can be found, a closed form solution can be obtained.

1. Overall Thermal Conductance

The heat transfer rate of the heater unit is given by:

$$q = UA_o(T_h - T_c) \tag{5-2}$$

where U = overall thermal conductance

A_o = heater unit outer wall surface area

T_h = heater temperature

T_c = cryogen temperature

In this case, the overall conductance is defined by

$$\frac{1}{U} = \frac{A_o}{\eta h A_i} + \frac{x}{k} \tag{5-3}$$

where η = overall heat transfer efficiency of flow passage extended surface

h = cryogen stream thermal conductance

A_i = total flow passage surface area

x = heater wall thickness

k = heater wall thermal conductivity

For the cryogen stream, the thermal conductance is available from heat transfer data for the chosen flow passage configuration. This information is supplied by Figure 5-3, which presents the Colburn modulus and Fanning f. ıction factor for the 0.10-in.-high, 16-per-in. fin. The Colburn modulus is

$$j = \frac{h}{c_p G} Pr^{2/3} \tag{5-4}$$

where Pr = cryogen stream Prandtl number $\frac{c_p \mu}{K_c}$

G = cryogen stream mass velocity $\frac{\dot{w}}{A_c}$

$\dot{w}$ = mass flow rate

A_c = flow area

c_p = mean specific heat capacity of cryogen stream

μ = mean dynamic viscosity of cryogen stream

K_c = mean thermal conductivity of cryogen stream

The data of Figure 5-3 was employed in the heater unit computer studies.

From the above, U is dependent on fluid properties, the inside surface characteristics, and the conduction characteristic of the wall. However, study of the computer results indicated that for the various fluid, U was well represented as a function of mass velocity and pressure level alone. This is evidently a consequence of the fixed flow geometry and the apparent fact that flows at a given pressure can be represented with reasonable accuracy by a single set of average fluid properties. The results obı ned are presented in Figure 5-4 for hydrogen and Figure 5-5 for oxygen and

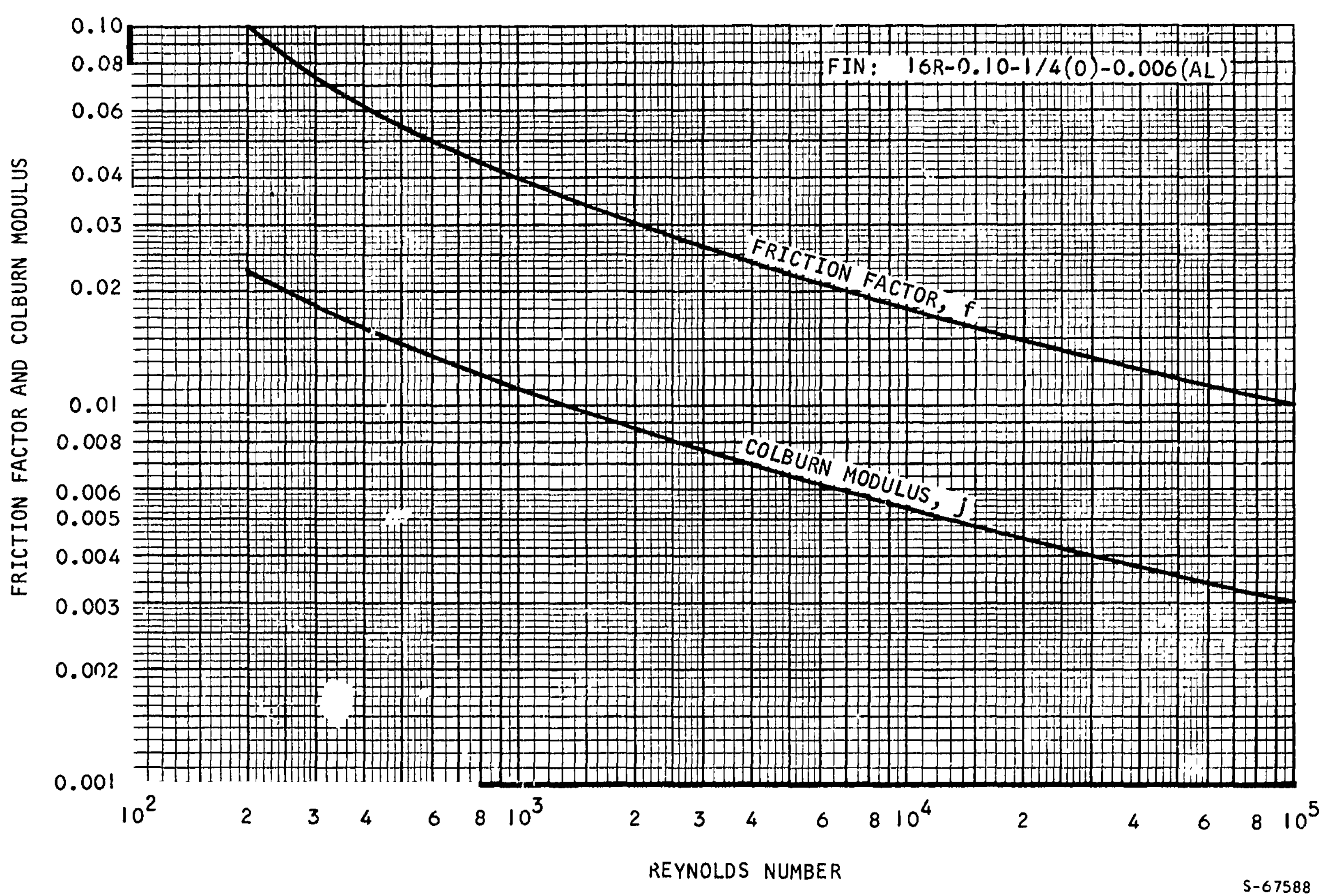

Figure 5-3. Heat Transfer and Friction Characteristics of Flow Passage Fin

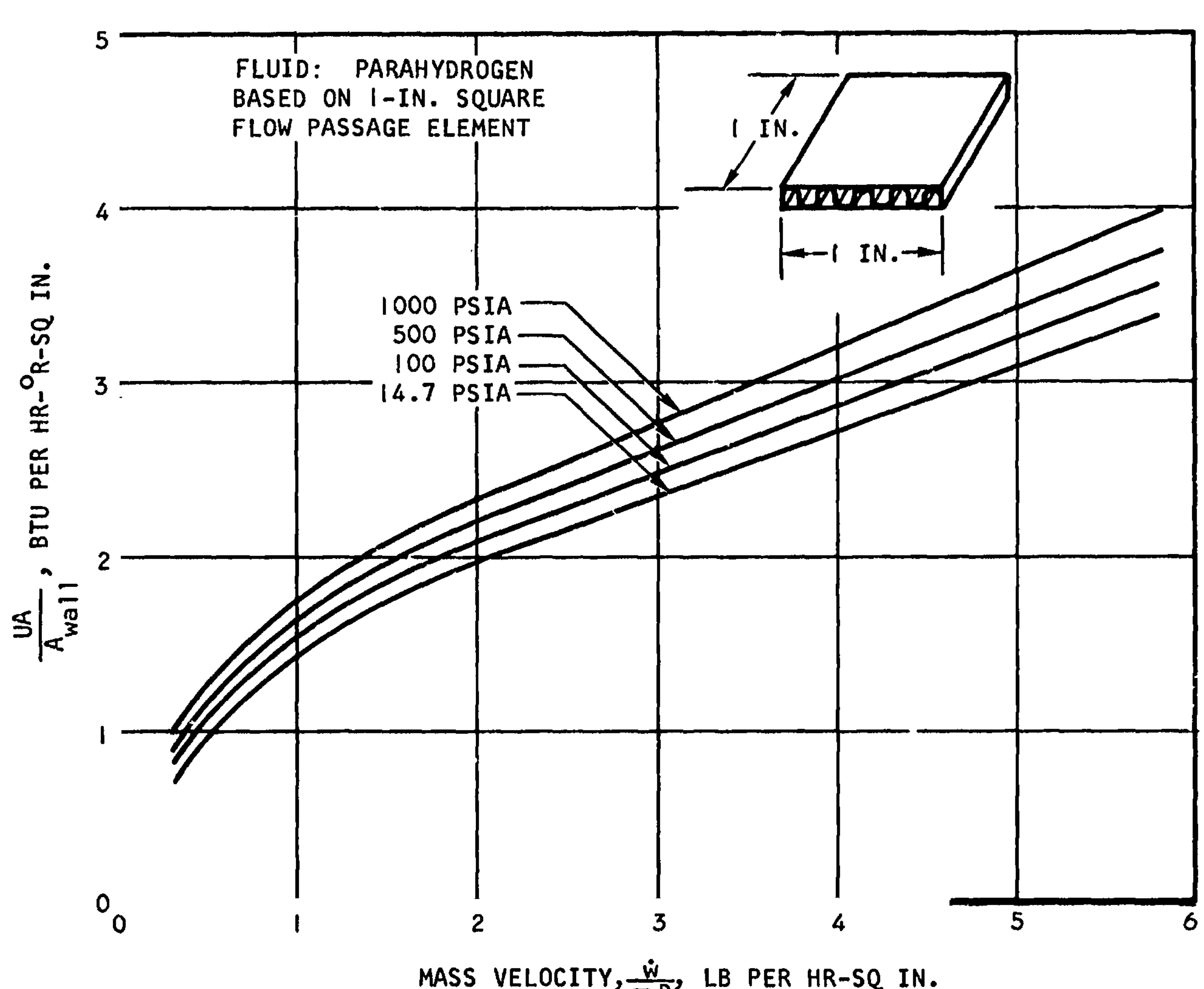

Figure 5-4. Hydrogen Electrical Heater Heat Transfer Performance

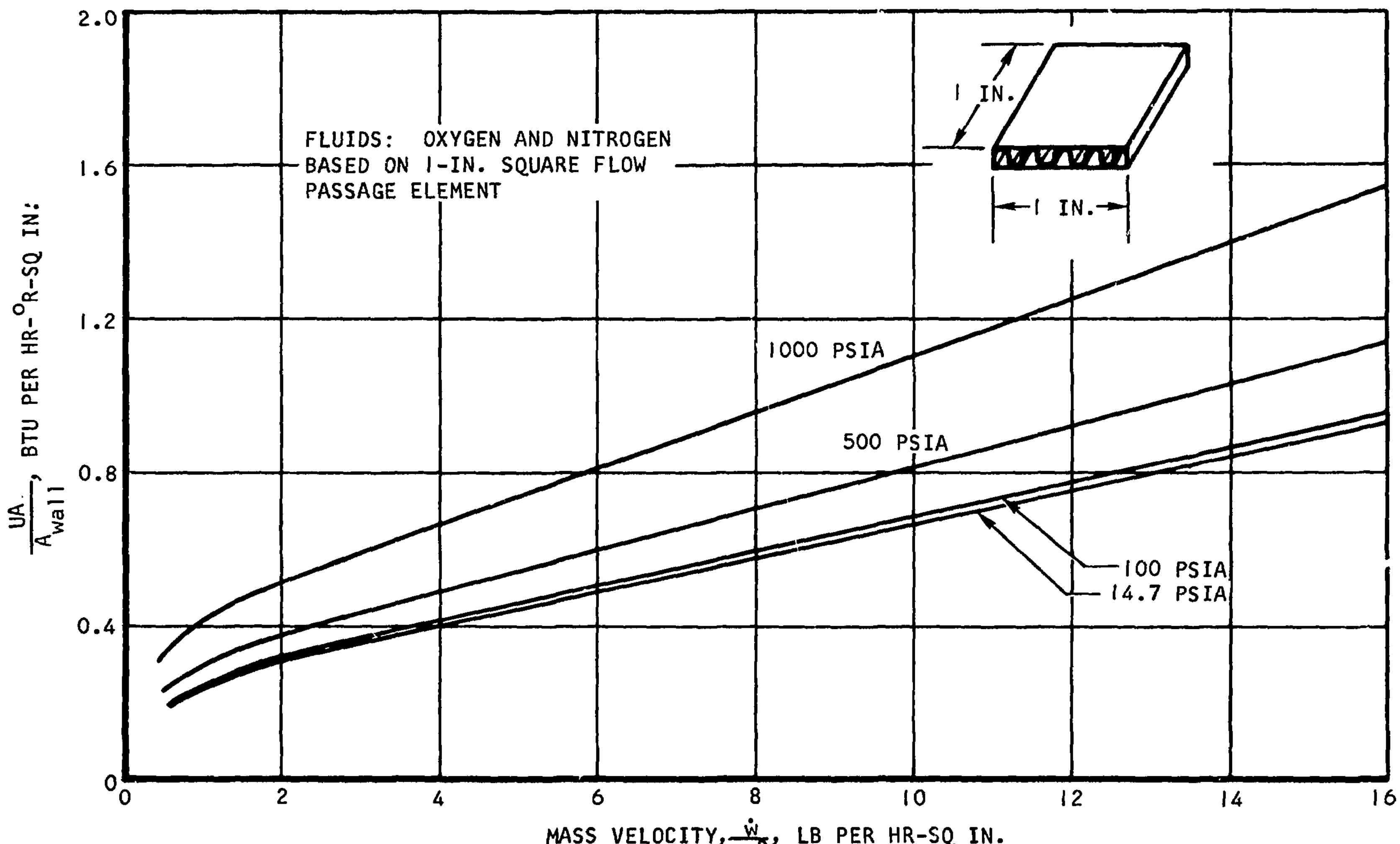

Figure 5-5. Oxygen and Nitrogen Electrical Heater Heat Transfer Performance

and nitrogen. Oxygen and nitrogen properties are so similar that a single set of curves is satisfactory for both fluids.

On Figures 5-4 and 5-5, advantage has been taken of the flow geometry to present U as a function of $\dot{W}/\pi D$ rather than $\dot{W}/A$. This is made possible by the constant annular dimension imposed by the fin.

2. Heater Length Equation

By employing the exponential approximation for the heater resistance, the heat flux supplied by the heating element can be written as:

$$\frac{q}{A} = \frac{B_o}{T^n} \tag{5-5}$$

where A = heat transfer area πDL

$B_o = (q/A)_{ref}\, T^n_{ref}$

L = heater length

$(q/A)_{ref}$ = heater flux at T_{ref}

For elements of the heater of length Δx, the heat transferred through the wall surface element $\pi D \Delta x$ in a time period $\Delta\theta$ is

$$Q = \frac{B_o}{T^n} \pi D \Delta x \Delta\theta \tag{5-6}$$

Let $$B = \pi D B_o \tag{5-7}$$

Thus, $$Q = \frac{B}{T^n} \Delta x \Delta\theta \tag{5-8}$$

The mass of fluid contained in the element is $\Delta M = \rho A_c \Delta x$; the energy balance is therefore:

$$\rho A_c \Delta x C_p \Delta T_c = \frac{B}{T^n} \Delta x \Delta\theta \tag{5-9}$$

where ΔT_c = fluid temperature rise due to transfer of Q

Equation 5-9 can be written as:

$$\rho A_c C_p \frac{\Delta T_c}{\Delta\theta} = \frac{B}{T^n}$$

which, in the limit, is

$$\rho A_c C_p \frac{dT_c}{d\theta} = \frac{B}{T^n} \tag{5-10}$$

Or, transforming to stationary coordinates;

$$\rho A_c C_p \frac{dT_c}{dx} \frac{dx}{d\theta} = \frac{B}{T^n}.$$

But $\frac{dx}{d\theta}$ is the fluid velocity and $\rho A_c \frac{dx}{d\theta}$ is the mass flow rate $\dot{w}$. Thus, we have

$$\dot{w} c_p \frac{dT_c}{dx} = \frac{B}{T^n} \tag{5-11}$$

The heater temperature T and fluid temperature T_c must be constrained by

$$\frac{dq}{dx} = U \left(T - T_c\right) \frac{dA}{dx} \tag{5-12}$$

Since the cross-section is constant, $\frac{dA}{dx} = \frac{A}{L}$, resulting in

$$\frac{dq}{dx} = \frac{UA}{L} \left(T - T_c\right) \tag{5-13}$$

Equation 5-8 shows that $\frac{dq}{dx} = \frac{B}{T^n}$.

Thus, Equation 5-13 allows the cryogen temperature to be expressed as

$$T_c = T - \frac{B}{T^n} \left(\frac{UA}{L}\right)^{-1} \tag{5-14}$$

The derivative of T_c with respect to x (assuming that U is constant) is

$$\frac{dT_c}{dx} = \left[1 + \frac{nB}{T^{n+1}} \left(\frac{UA}{L}\right)^{-1}\right] \frac{dT}{dx} \tag{5-15}$$

Inserting Equation 5-15 in Equation 5-11 and rearranging yields:

$$\left[T^n + nB \left(\frac{UA}{L}\right)^{-1} \frac{1}{T}\right] dT = \frac{B}{\dot{w} c_p} dx \tag{5-16}$$

If c_p is taken as a constant, Equation 5-16 can be integrated over the length of the heater, where at $x = 0$, $T = T_1$, the fluid inlet temperature and at $X = L$, $T = T_2$, the outlet temperature:

$$\int_{T_1}^{T_2} \left[T^n + nB\left(\frac{UA}{L}\right)^{-1} \frac{1}{T}\right] dT = \int_0^L \frac{B}{\dot{w}c_p}\, dx$$

This results in:

$$\frac{1}{n+1}\left[T_2^{n+1} - T_1^{n+1}\right] + \frac{nB}{\left(\frac{UA}{L}\right)} \ln \frac{T_2}{T_1} = \frac{BL}{\dot{w}c_p} \tag{5-17}$$

The heater length is thus expressed by

$$L = \dot{w}c_p \frac{T_2^{n+1} - T_1^{n+1}}{(n+1)B} + \frac{n}{\left(\frac{UA}{L}\right)} \ln \frac{T_2}{T_1} \tag{5-18}$$

For the specific circumstances of this study,

$$\frac{A}{L} = \pi D$$

and for the nickel-iron alloy heating element, $n = 1$. The length equation thereby becomes

$$L = \left(\frac{\dot{w}}{\pi D}\right) c_p \frac{T_2^2 - T_1^2}{2B/\pi D} + \frac{\ln (T_2/T_1)}{U} \tag{5-19}$$

If the substitutions

$$\phi_1 = \frac{T_1^2 - T_1^2}{2B/\pi D} \tag{5-20}$$

$$\phi_2 = \frac{\ln (T_2/T_1)}{U} \tag{5-21}$$

are made, the compact form below may be written:

$$L = \left(\frac{\dot{w}}{\pi D}\right) c_p (\phi_1 + \phi_2) \tag{5-22}$$

The two functions ϕ_1 and ϕ_2 are readily calculated; plots of these are presented in Figures 5-6 and 5-7. In Figure 5-6, B is based on a heater flux of 144 Btu per hr - sq in. at 360°R.

3. Design Procedure

Since Equation 5-22 was obtained by assuming that the thermal conductance U was constant, it was not surprising to find that this expression provided a poor prediction of the lengths found in the detailed computer designs. To correct the effect of this assumption, the length equation was written as

$$L = \left(\frac{\dot{w}}{\pi D}\right) c_p \left(\phi_1 + \beta\phi_2\right) \tag{5-23}$$

where B is a correction factor for ϕ_2, which is a function of fluid inlet and outlet temperatures and the overall conductance. Evaluation of B with the use of the lengths defined by thermal analyzer results is illustrated in Figure 5-8. Since β behaved as a constant for both hydrogen and oxygen at low pressures and very high pressures, this factor was employed as a function of critical pressure ratio, as shown on Figure 5-9.

Establishment of the corrected equation provided the tools needed for rapid design of electrical heater units. By choosing a heater diameter, the mass velocity may be calculated. Then Figure 5-4 or 5-5 may be entered with $\dot{w}/\pi D$ to obtain U; with the pressure, terminal temperatures, and U known, ϕ_1, ϕ_2, and β may be evaluated, allowing calculation of the length. This technique is shown schematically on Figure 5-10. As indicated, some iteration of the diameter D is generally required to obtain a desirable configuration.

Basic Heater Unit Pressure Drop and Weight

The flow passage pressure drop is assumed to be entirely due to the skin friction and the volumetric expansion of the fluid. This is true even for the case involving subcritical boiling. The loss associated with boiling is assumed to be accountable entirely by volumetric change. The pressure loss is presented in Figure 5-11 in the form of $\sigma\Delta p$ as a function of length and the mass velocity parameter $\dot{w}/\pi D$.

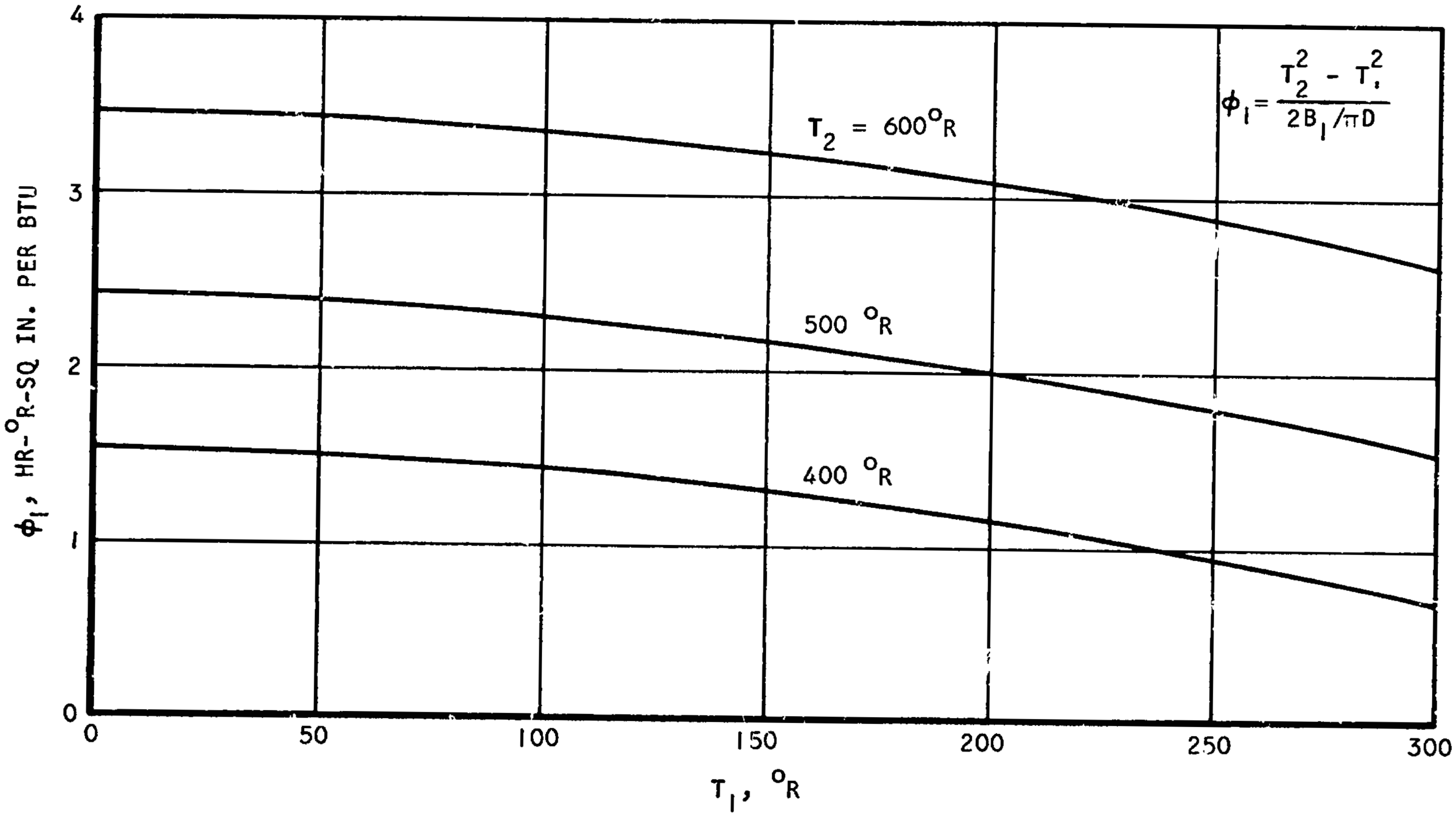

Figure 5-6. First Function of the Heater Length Equation

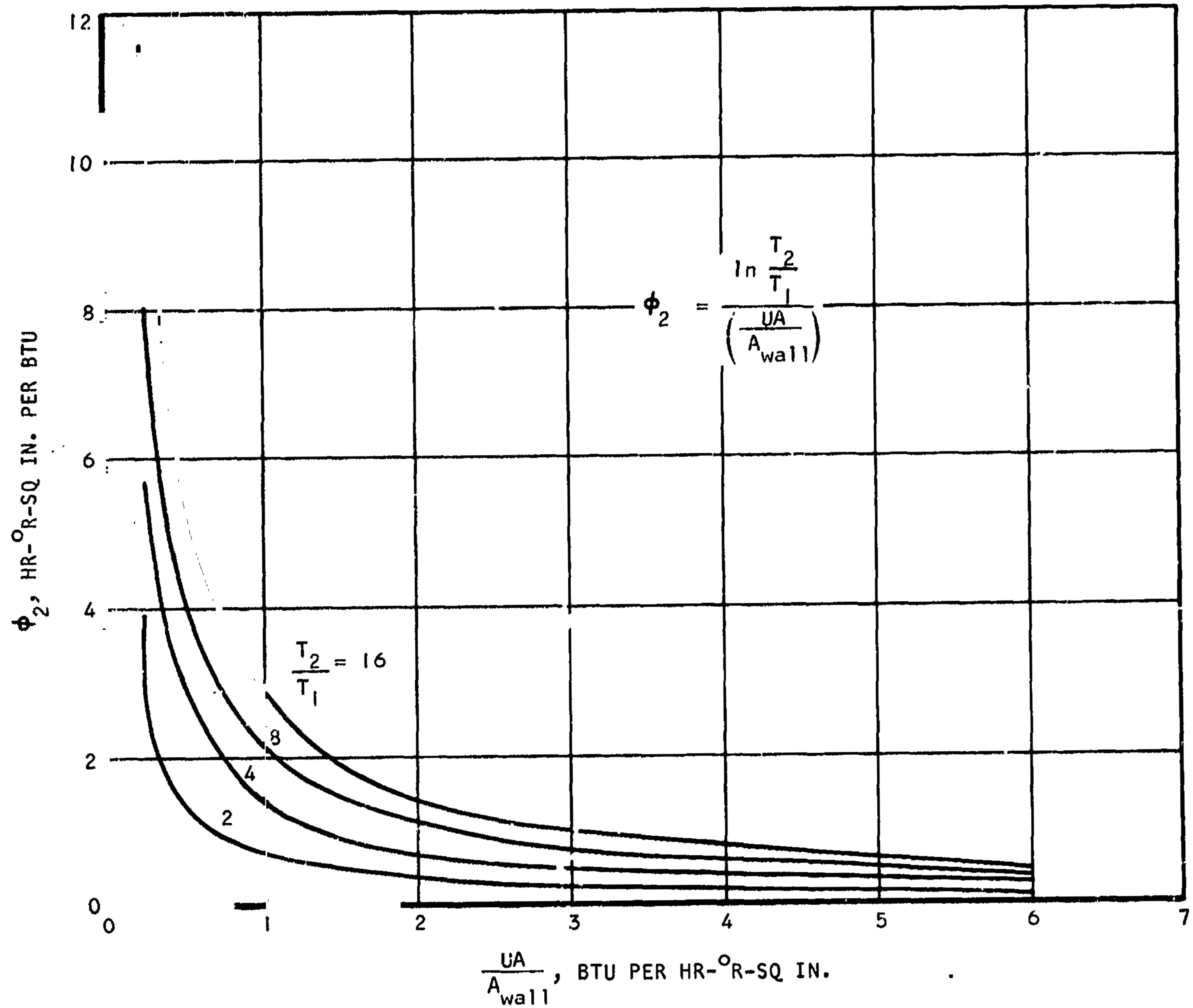

Figure 5-7. Second Function for the Heater Length Equation

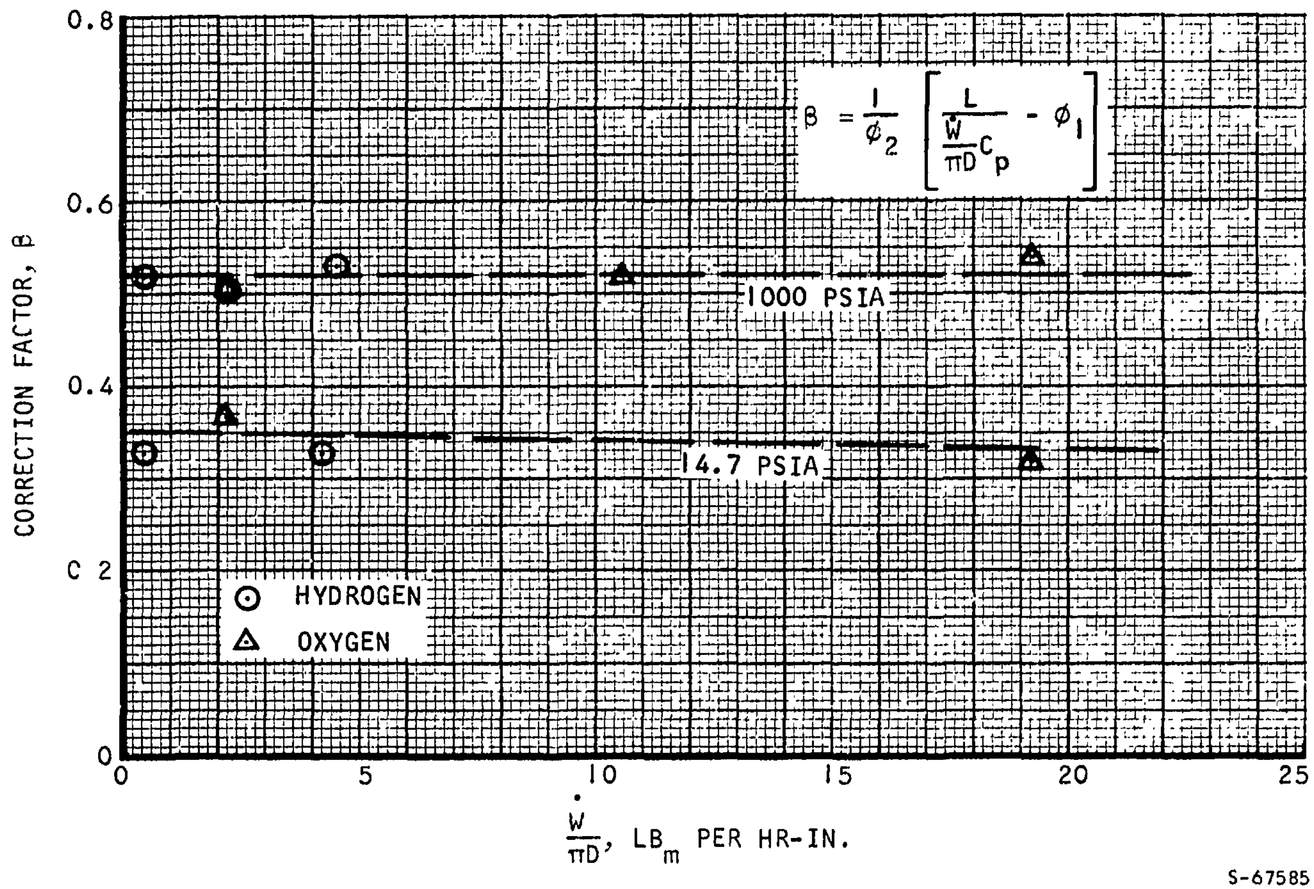

Figure 5-8. Evaluation of Correction Factor, β

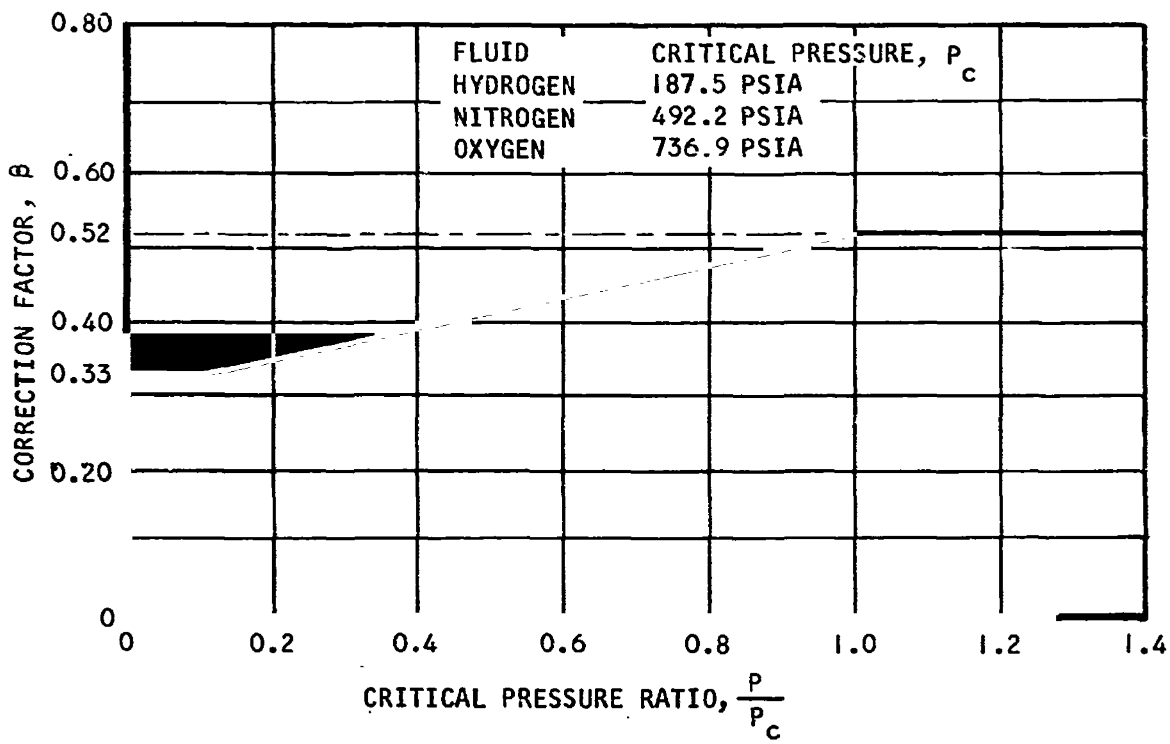

Figure 5-9. Pressure Correction Factor for Heater Length Equation

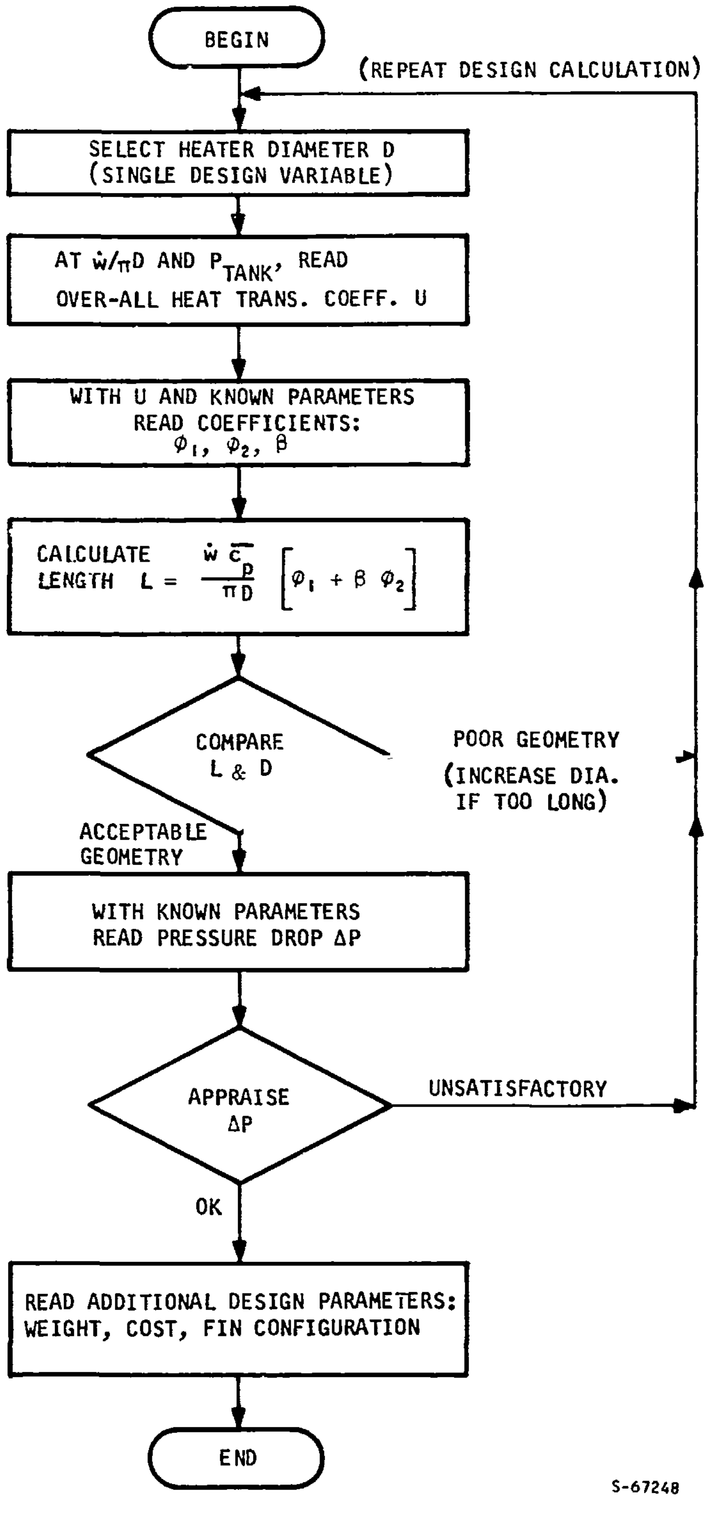

Figure 5-10. Electrical Heater Design Procedure

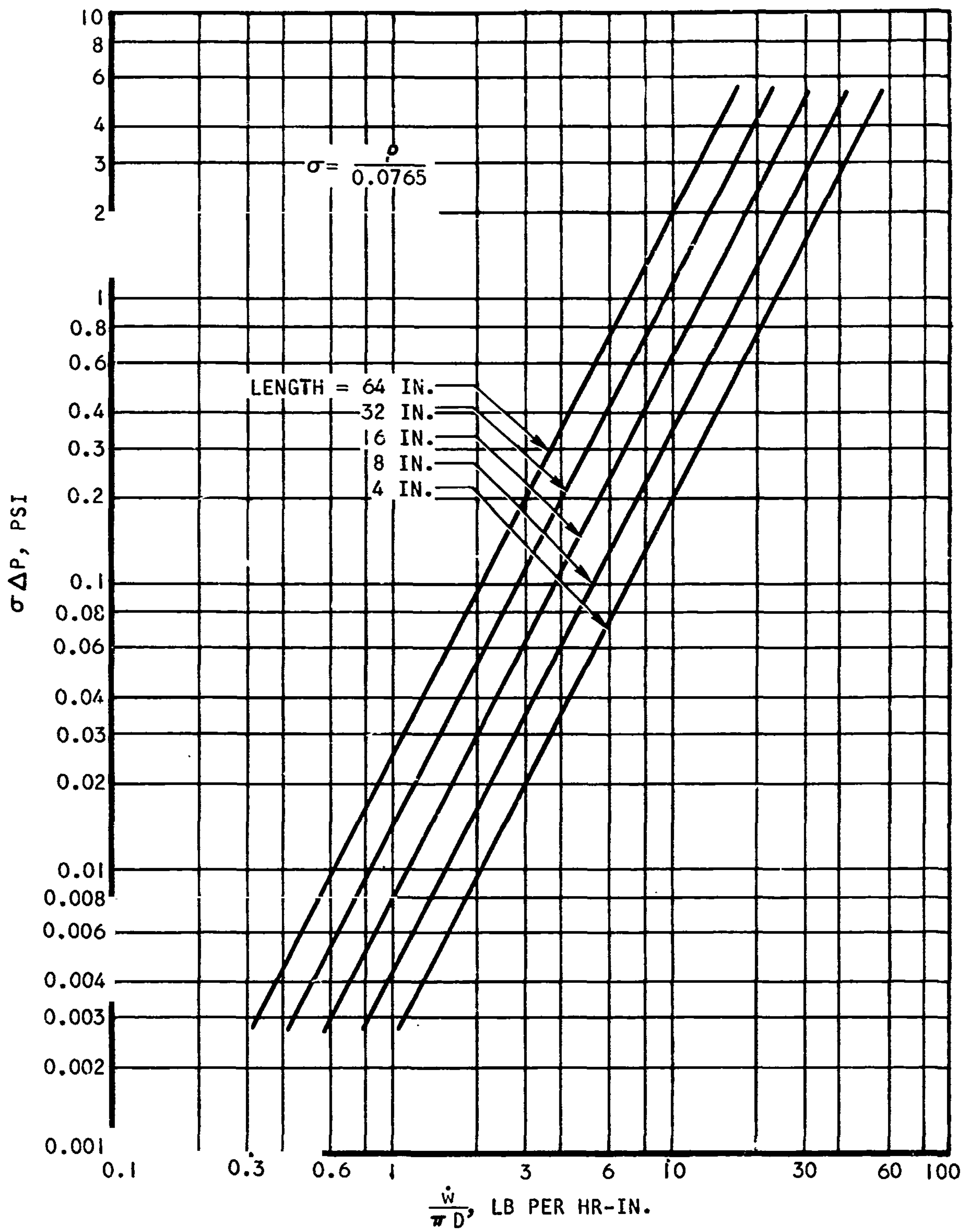

Figure 5-11. Electrical Heater Pressure Loss Characteristics

Weight of the basic heat unit exclusive of the radiation fins is provided in Figure 5-12, where the weight penalty of the double-wall construction employed for the oxygen heaters is apparent. The basic heater is taken to be constructed of stainless steel with an aluminum flow passage fin. The outer standoff wall of the oxygen units is fabricated from 0.05-in.-thick copper with copper standoff fins being employed.

Extended Radiation Surface

If sufficient external surface is available, the heater unit will be capable of dissipating the entire heating element output to the surroundings while remaining at an acceptable maximum temperature. In this manner, burnout as a result of zero cryogen flow while the heater is energized can be avoided. The heating element resistance - temperature relationship is important because reduction of the power dissipated at the maximum temperature markedly reduces the size and weight of the required radiation surface.

For this study, it was desired to provide a simple technique for selection of surfaces which would limit the heater temperature to 1000°R when operating in surroundings permitting radiative rejection to 500°R. The radiation surfaces are taken to be four copper fins parallel to the heater unit longitudinal axis and located at 90-deg intervals about the cylindrical cross-section. The fins are of length L, height y, and have a constant thickness δ.

Since the length L is defined by the basic heater design procedure, the required information is a technique for selection of the fin height y and thickness δ. To size the fin, the temperature distribution on the radiative surface must be known, or assumed to be known. To simplify the solution, the temperature distribution is assumed linear, being given by

$$T = a_o + a_1 y \tag{5-24}$$

where at y = 0, the following conditions exist:

The fin root temperature is

$$T_{y=o} = T_r \tag{5-25}$$

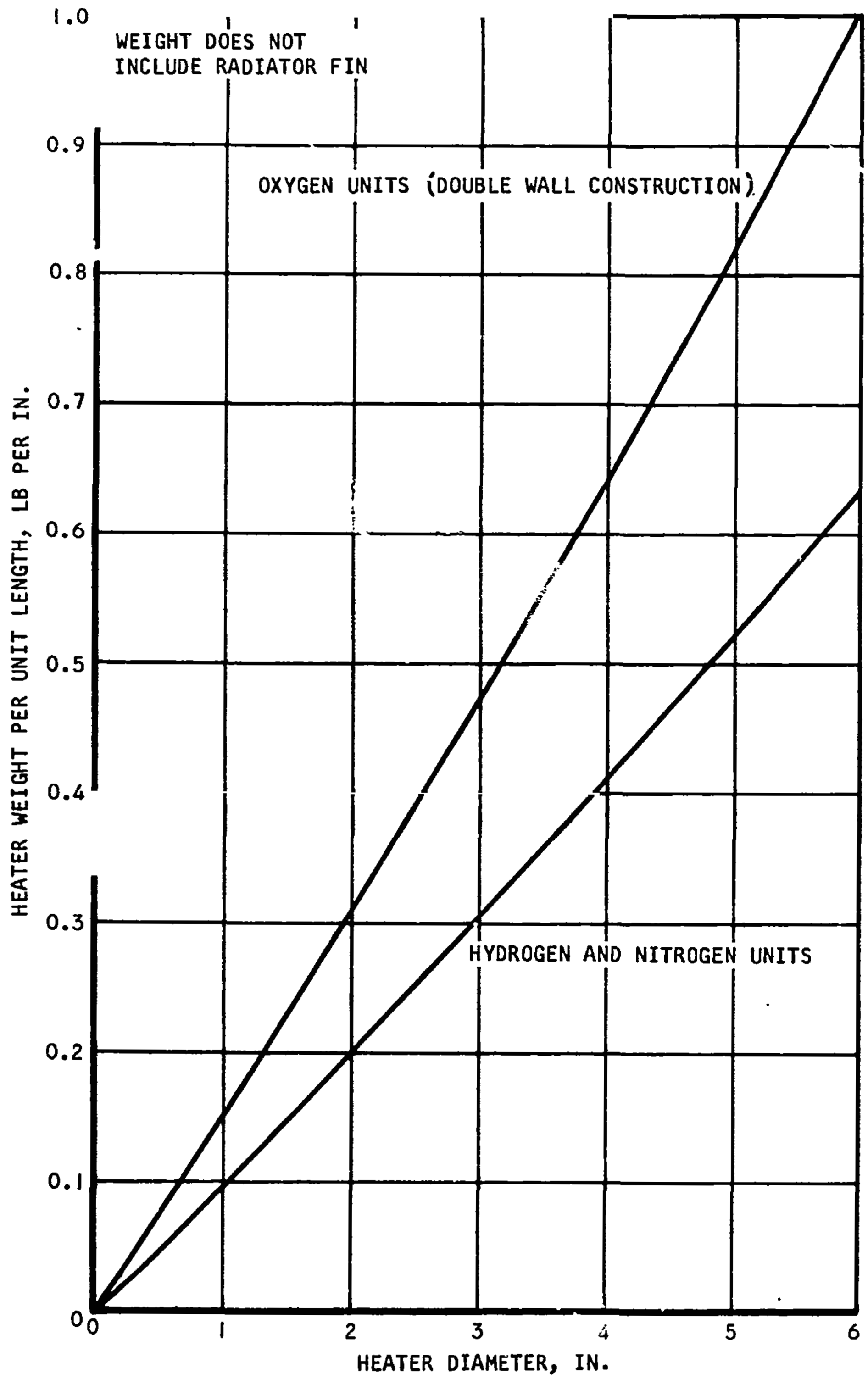

Figure 5-12. Basic Electrical Heater Weight Characteristics

The heat to be rejected is

$$q_r = -AK \left(\frac{dT}{dy}\right)_{y=0} \tag{5-26}$$

where A = fin root cross-section area
K = fin thermal conductivity

For each of the four fins, the heat to be rejected per unit length of fin is

$$q_r = \frac{\pi D}{4E} \left(\frac{q}{A}\right)_{ref} \tag{5-27}$$

where D = basic heater unit diameter
$\left(\frac{q}{A}\right)_{ref}$ = heater flux at T_{ref}
E = ratio of $(q/A)_{ref}$ to heater flux of fin root design temperature

Applying the condition of Equation 5-25 to the temperature distribution gives:

$$a_o = T_r$$

With the use of Equation 5-27 and the observation that the fin conduction area per unit length is equal to δ (the fin thickness), Equation 5-26 can be express as

$$\left(\frac{dT}{dy}\right)_{y=o} = - \frac{q_r}{AK} = - \frac{\pi D}{4E\delta K} \left(\frac{q}{A}\right)_{ref} \tag{5-28}$$

Since a_1 in Equation 5-24 is given by Equation 5-28, the temperature distribution is found to be:

$$T = T_r - \left[\frac{\pi D}{4E\delta K} \left(\frac{q}{A}\right)_{ref}\right] y \tag{5-29}$$

The heat radiated from both surfaces of the fin to surroundings at a temperature of T_a is given for a unit fin length by the Stefan-Boltzmann law as:

$$q_r = 2\sigma\epsilon F_a \int_o^{y_{max}} (T^4 - T_a^4)\, dy \tag{5-30}$$

where σ = Stefan-Boltzmann constant

ϵ = fin surface emissivity

F_a = geometric factor for radiation from fin

y_{max} = total fin height

The derivative of the surface temperature with respect to y is:

$$dT = -\left[\frac{\pi D}{4E\delta K}\left(\frac{q}{a}\right)_{ref}\right] dy$$

Thus, Equation 5-30 can be written as

$$-\frac{q_r}{2\sigma\epsilon F_a}\left[\frac{\pi D}{4E\delta K}\left(\frac{q}{A}\right)_{ref}\right] = \int_{T_r}^{T_e} (T^4 - T_a{}^4)\, dT \tag{5-31}$$

where T_e = fin temperature at $y = y_{max}$

Performing the integration:

$$-\frac{q_r^2}{2\sigma\epsilon F_a \delta K} = \frac{T_e{}^4 - T_r{}^4}{5} - T_a{}^4 (T_e - T_r)$$

Thus, the fin thickness is found to be

$$\delta = \frac{q_r{}^2}{2\sigma\epsilon F_a K}\left[\frac{T_e{}^4 - T_r{}^4}{5} - T_a{}^4 (T_e - T_r)\right]^{-1} \tag{5-32}$$

With δ defined, the fin height can be from Equation 5-29:

$$y_{max} = \frac{T_r - T_e}{\frac{\pi D}{4E\delta K}\left(\frac{q}{A}\right)_{ref}} \tag{5-33}$$

For the conditions of interest here,

$T_r = 1000^\circ R$

$T_a = 500^\circ R$

The heater design presented earlier employs

$$\left(\frac{q}{A}\right)_{ref} = 144 \text{ Btu per hr-sq in.}$$

based on $T_{ref} = 360^0R$. For $T_r = 1000^0R$ maximum, the heat flux ratio E is approximately 3.0. The copper fin material has an average thermal conductivity K of 16.6 Btu per hr-sq in.-^{0}R per in., and the surface emissivity is taken to be 0.90.

The geometrical factor for radiation between two fins set at 90 deg is 0.25. Thus, the factor applying to radiation to the surroundings is:

$$F_a = 0.75$$

Applying these values to Equations 5-32 and 5-33 results in:

$$\delta = 42.7\ D^2 \left[1100 - 1.6 \times 10^{12} T_e^{\ 5} + 0.5T_e\right]^{-1}, \text{ in.}$$

$$y_{max} = 18.9D\ (1000 - T_e) \left[1100 - 1.6 \times 10^{12} T_e^{\ 5} + 0.5T_e\right]^{-1}, \text{ in.}$$

Thus, when T_e is specified, δ and y become functions of the basic heater diameter D alone. The fin weight per unit length is

$$\frac{W_f}{L} = \delta y_{max} \rho$$

where ρ = fin material density

Therefore, the optimum value of T_e can be found by investigating δy_{max}. When this was accomplished, it was found that the most desirable fin tip temperature was approximately 800^0R. This results in the fin thickness and height relations used in the Design Reference Manual:

$$\delta = 0.0445\ D^2, \text{ in.}$$

$$y_{max} = 3.87\ D, \text{ in.}$$

Fin thickness and height are plotted on Figure 5-13, and the total weight of four fins is presented on Figure 5-14.

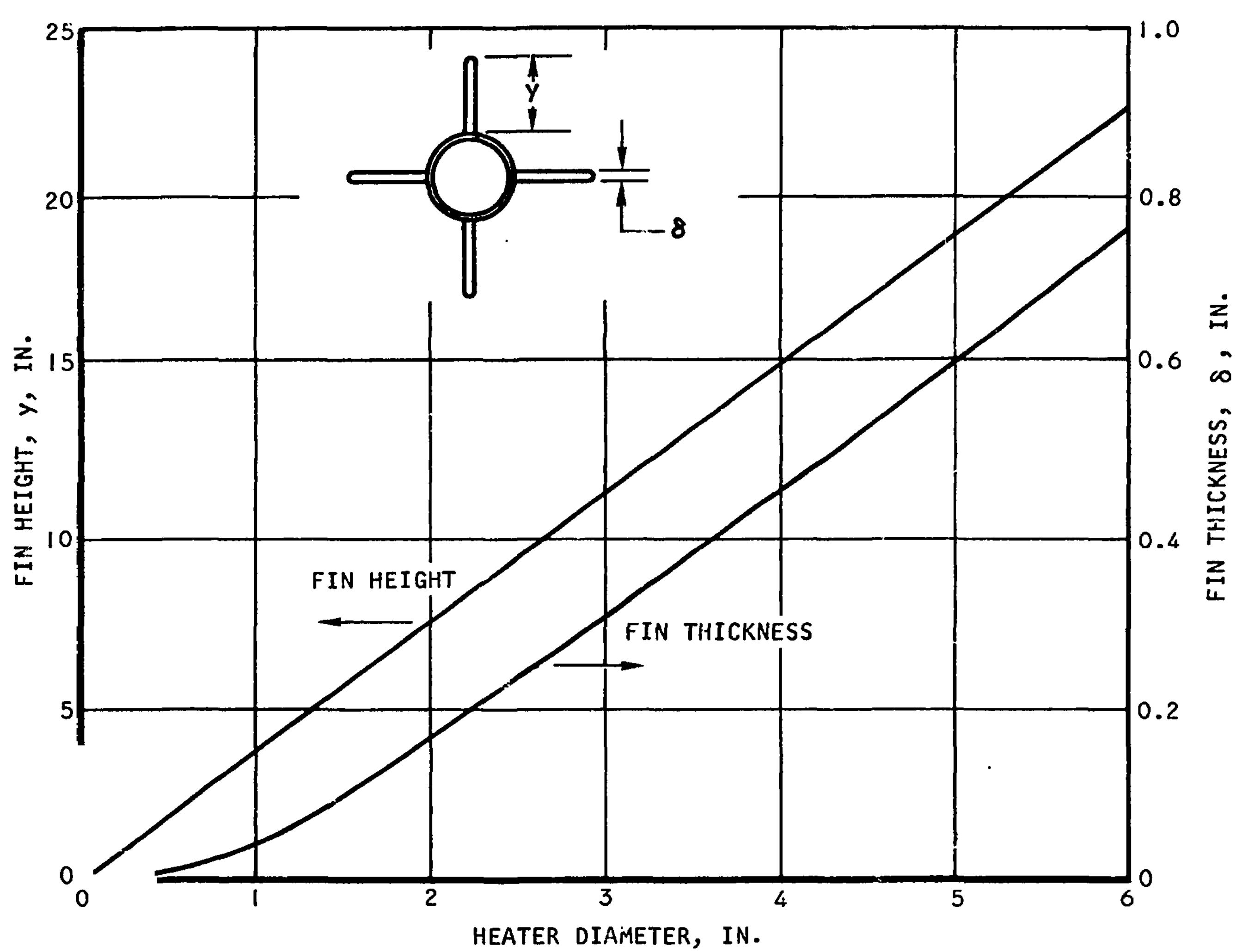

Figure 5-13. Radiation Fire Dimensions

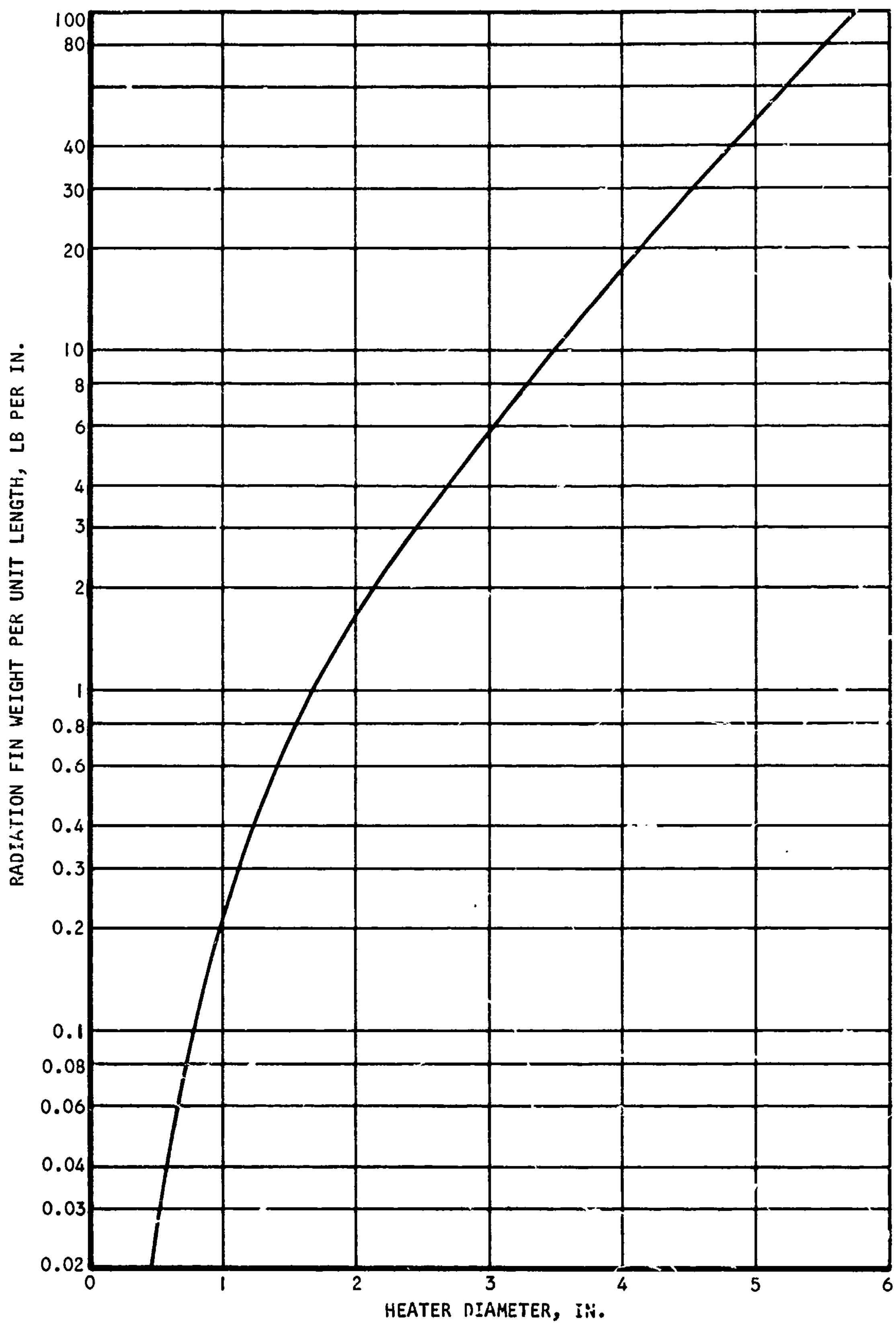

Figure 5-14. Radiation Fin Weight Characteristics

The Eff .. Varying the Heater Diameter

Since the heater design e.. :oys an annular flow channel, both its flow area and its heat transfer area are proportional to the diameter. Increasing the heater diameter will reduce the flow velocity. The net effect is a reduction in both the pressure drop and the convective heat transfer coefficient. Varying the heater diameter will also affect the thickness of the radiator δ. The heat input increases with the heat transfer area, which is proportional to the tube diameter. Therefore, the heat transfer rate per unit length of the heater is increased. The height of the radiator must then be increased to be able to dissipate the heat in emergency. The increase in radiator height will be accompanied by a shorter heater length such that the total radiating surface is essentially a constant. However, because the power per inch of heater increases and because the heat path to the radiators is larger (larger y), the radiator must be thicker in order to conduct the heat to the radiating surfaces at a given temperature drop. As the diameter is varied, it will produce significant changes in the pressure loss, the heating element temperature, and the radiator weight.

Total Heater Unit Costs

Due to the simple nature of the electrical heater unit, it was possible to prepare estimates for units of various diameters and lengths. Since both the basic heater and the radiation surfaces have character ics that are well-defined when these two variables are specified, it is felt that good parametric representation was obtained. The results of the cost estimation are presented in Figure 5-15, where the nonrecurring cost is taken to be independent of diameter.

TRANSPORT FLUID HEAT EXCHANGERS

As stated earlier, the transport fluid stream considered is FC-75, received at 30 to 100 psia and 50^0 to 700^0R. The flow rate of this stream may be chosen by the designer.

This heat transfer situation was found to be best handled by use of a shell-tube bundle heat exchanger of cross-parallel flow configuration. As shown in Figure 5-16a, typical shell-tube construction is considered with the

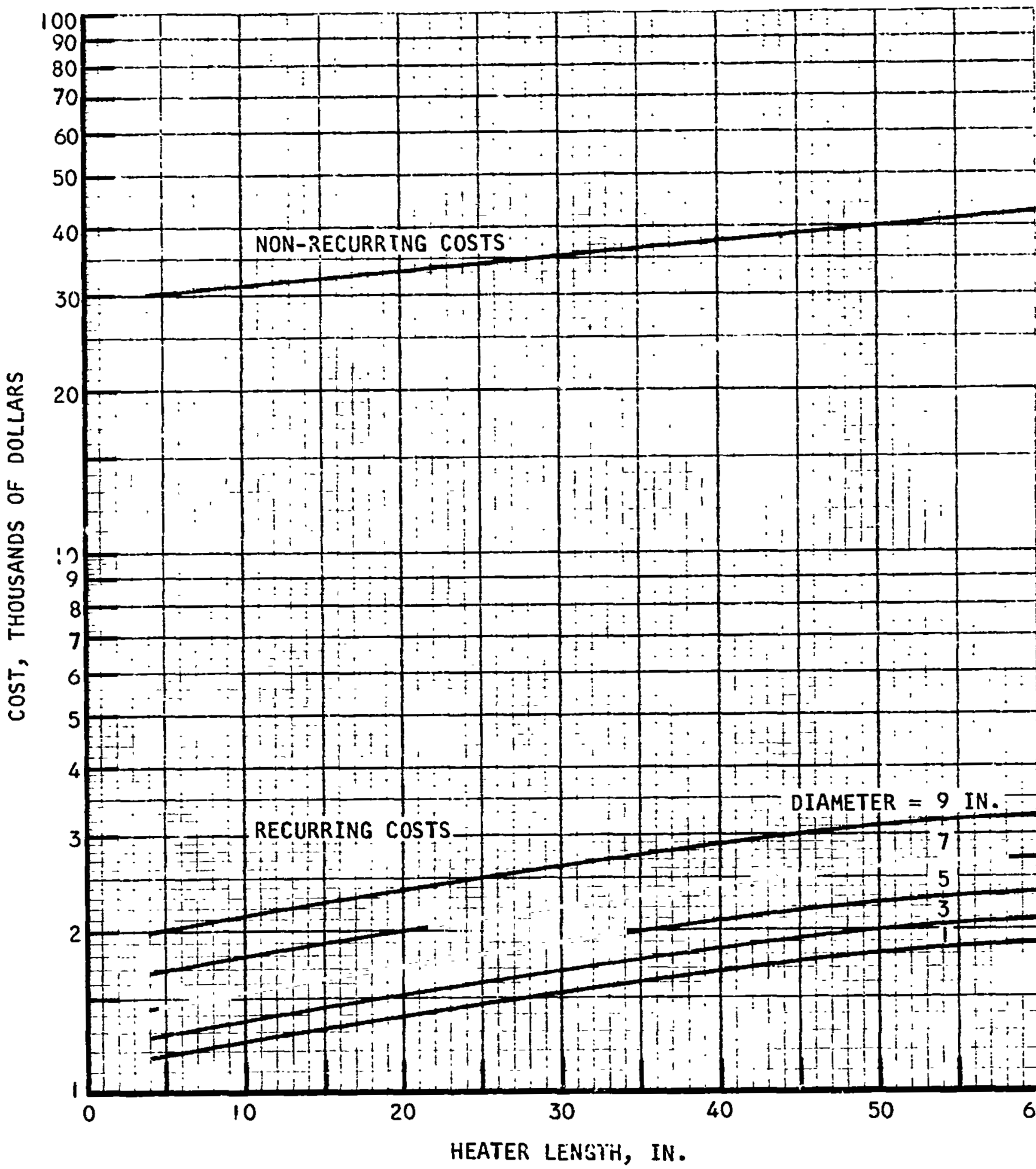

Figure 5-15. Electrical Heater Cost Characteristics

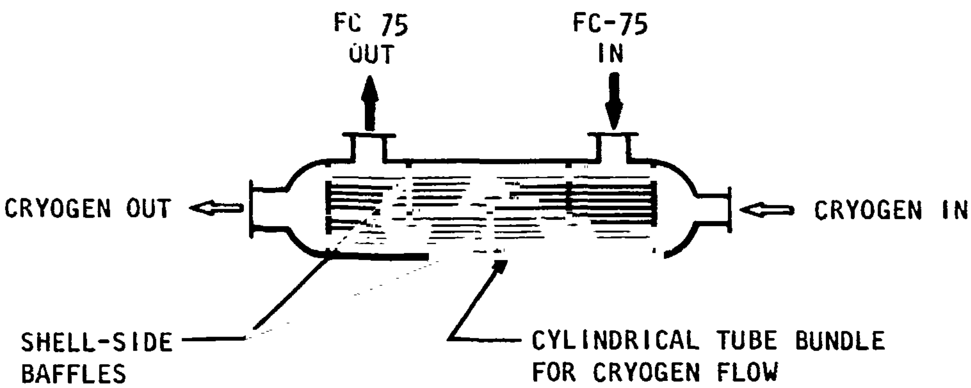

a. Cylindrical Cross-Parallel Flow Tubular Heat Exchanger Used with Transport Fluid Heat Source

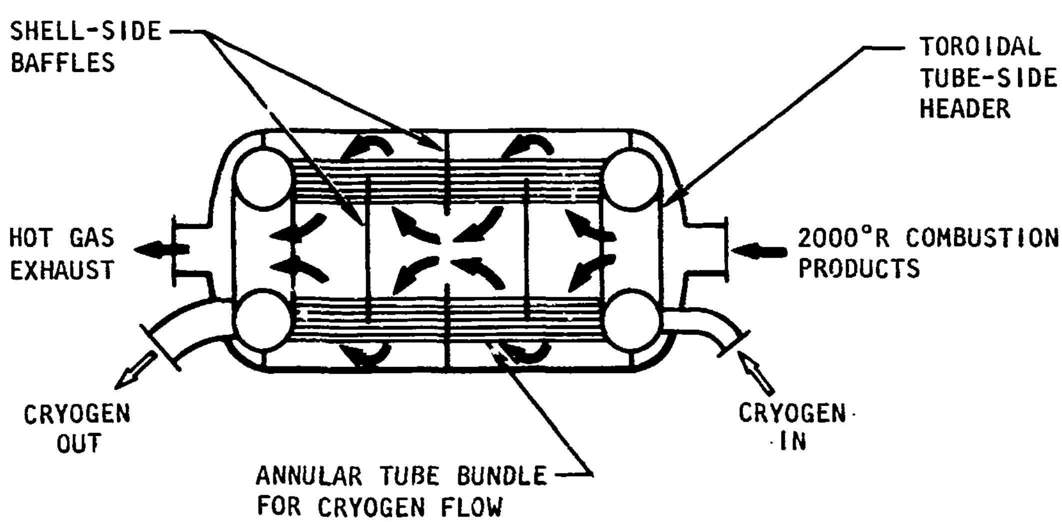

b. Annular Cross-Parallel Flow Tubular Heat Exchanger Used with Hot Gas Heat Source

S-67097

Figure 5-16. Heat Exchanger Configurations for Fluid Heat Sources cryogen flowing through the tube bundle in a single pass and the FC-75 flowing in multipass as required on the shell side. These units are of stainless steel construction. All tubes are 0.10-in. dia with ring dimples as turbulence promotors. Tube spacing is 0.03 in.

The parallel flow arrangement is necessary to avoid freeze-up of the transport fluid. No special features are required with the FC-75 source for oxygen heat exchangers.

Although the model considered here is somewhat constrained geometrically, no closed form solution for heat exchanger length and diameter is possible. A relatively simple design method was found to be available, employing an expression developed below. The iteration involved in the selected approach is not difficult, allowing designs to be established with reasonable speed.

Basic Design Tools

Consider a direct-transfer heat exchanger which exchanges heat between a hot stream and a cold stream. The heat transfer associated with an element dA of the heat transfer surface between the streams is given by:

$$dq = U(T_h - T_c)\ dA \tag{5-34}$$

where U = overall thermal conductance

T_h = hot stream temperature at dA

T_c = cold stream temperature at dA

The temperatures T_h and T_c are related to the total heat transfer rate by

$$T_h = T_{h_I} - \frac{q}{C_h} \tag{5-35}$$

$$T_c = T_{c_I} + \frac{q}{C_c} \tag{5-36}$$

where T_{h_I}, T_{c_I} = inlet temperatures for the streams

q = total heat transferred in flowing from the inlet to dA

$C_h = \dot{w}_h \overline{C}_{P_h}$, hot stream heat capacity rate

$C_c = \dot{w}_c \overline{C}_{P_c}$, cold stream heat capacity rate

$\dot{w}_h, \dot{w}_c$ = mass flow rates for the streams

$\bar{c}_{p_h}, \bar{c}_{p_c}$ = mean specific heat capacities for the streams

Thus, the temperature difference in Equation 5-34 is

$$T_h - T_c = T_{h_1} - T_{c_1} - q\left(\frac{1}{C_c} + \frac{1}{C_h}\right) \tag{5-37}$$

This allows that equation to be rewritten as:

$$\frac{dq}{dA} = U\,(T_{h_1} - T_{c_1}) - qU\left(\frac{1}{C_c} + \frac{1}{C_h}\right) \tag{5-38}$$

If the definitions are made:

$$\omega_1 = U\,(T_{h_1} - T_{c_1}) \tag{5-39}$$

$$\omega_2 = U\left(\frac{1}{C_c} + \frac{1}{C_h}\right) \tag{5-40}$$

Equation 5-38 can then be expressed as:

$$\frac{dq}{\omega_1 - \omega_2 q} = dA \tag{5-41}$$

Integration of Equation 5-41 results in

$$-\frac{1}{\omega_2}\ln\,(\omega_1 - \omega_2 q) = A + a_o$$

which can be rearranged to yield

$$q = \frac{\omega_1}{\omega_2} - \frac{a_1}{\omega_2}\,e^{-\omega_2 A} \tag{5-42}$$

When A = 0, q = 0 and the constant of integration a_1 is found to be

$$a_1 = \omega_1$$

The heat transfer rate is finally found to have the form:

$$q = \left(1 - e^{-\omega_2 A}\right)\frac{\omega_1}{\omega_2} \tag{5-43}$$

Or, returning to the definitions of ω_1 and ω_2:

$$q = \left\{1 - \exp\left[-\left(\frac{1}{C_c} + \frac{1}{C_h}\right)UA\right]\right\}\frac{T_{h_1} - T_{c_1}}{\frac{1}{C_c} + \frac{1}{C_h}} \tag{5-44}$$

Considering the cold stream alone, the heat transfer rate is given by

$$q = C_c\,(T_{c_2} - T_{c_1}) \tag{5-45}$$

Combination of these two expressions for q yields:

$$\exp\left[-\left(\frac{1}{C_c} + \frac{1}{C_h}\right)UA\right] = 1 - \frac{T_{c_2} - T_{c_1}}{T_{h_1} - T_{c_1}}\left(1 + \frac{C_c}{C_h}\right) \tag{5-46}$$

where the ratio of temperature differences on the right side is the cold-side temperature effectiveness:

$$\epsilon = \frac{T_{c_2} - T_{c_1}}{T_{h_1} - T_{c_1}} \tag{5-47}$$

It is convenient to define:

$$\phi_3 = \frac{1}{C_c} + \frac{1}{C_h} \tag{5-48}$$

and
$$\psi = 1 - \epsilon\left(1 + \frac{C_c}{C_h}\right) \tag{5-49}$$

This results in:

$$\phi_3 UA = -\ln\psi \tag{5-50}$$

The function given by Equation 5-50 is presented on Figure 5-17. The heat transfer area can be represented as

$$A = \frac{\phi_3 UA}{\phi_3 U} \tag{5-51}$$

If the capacity rates, the temperature effectiveness, and the overall thermal [illegible] can be found, ϕ_3UA can be evaluated and Equation 5-51 used for [illegible] the heat transfer area.

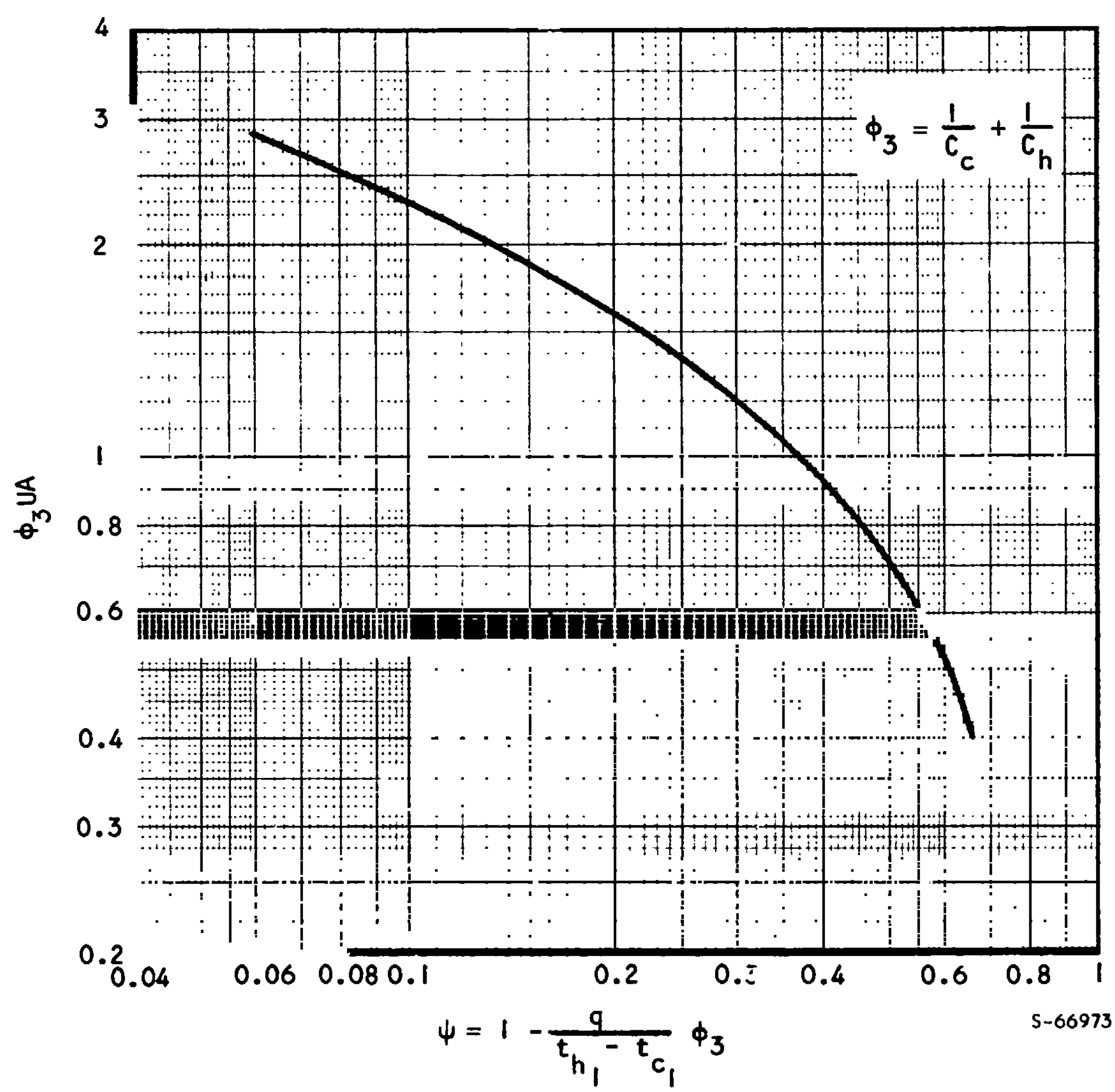

Figure 5-17. Design Function for Transport Fluid Heat Exchangers

The overall thermal conductance for the heat exchangers considered here can be obtained from:

$$\frac{1}{U} = \frac{1}{h_c} + \frac{1}{h_h} \qquad (5\text{-}52)$$

where h_c = cryogen stream thermal conductance

h_h = transport fluid thermal conductance

In Equation 5-52, the conductive resistance of the thin-walled dimpled tubing has been neglected.

The cryogen stream conductance is a function of the heat transfer characteristics of the selected tubing. As noted before, 0.10-in.-ID, ring-dimpled stainless tubing is employed. A wall thickness of approximately 0.004 in. will be satisfactory over the entire pressure range. The ring dimples serve as tubulence promoters. The dimple configuration is specified by the parameter ζ:

$$\zeta = \frac{\delta/d}{\sqrt{s/d}}$$

where d = tube diameter

δ = dimple depth

s = spacing along tube between dimples

For this application, a value of $\zeta = 0.05$ has been chosen. The Colburn modulus and Fanning friction factor of ring-dimpled tubing at $\zeta = 0.05$ is presented on Figure 5-18.

Using the dimpled tube data together with carefully averaged fluid properties, it was possible to define the cryogen-side conductance as a function of mass velocity and fluid pressure for the fluids studied here. Conductances for hydrogen are plotted on Figure 5-19; oxygen and nitrogen conductances are found on Figure 5-20.

The hot-side conductance represents a case of flow through an offset tube bank. Using standard relationships for this situation and averaged properties for the FC-75 stream resulted in the plot of h_h versus hot-side mass velocity provided in Figure 5-21.

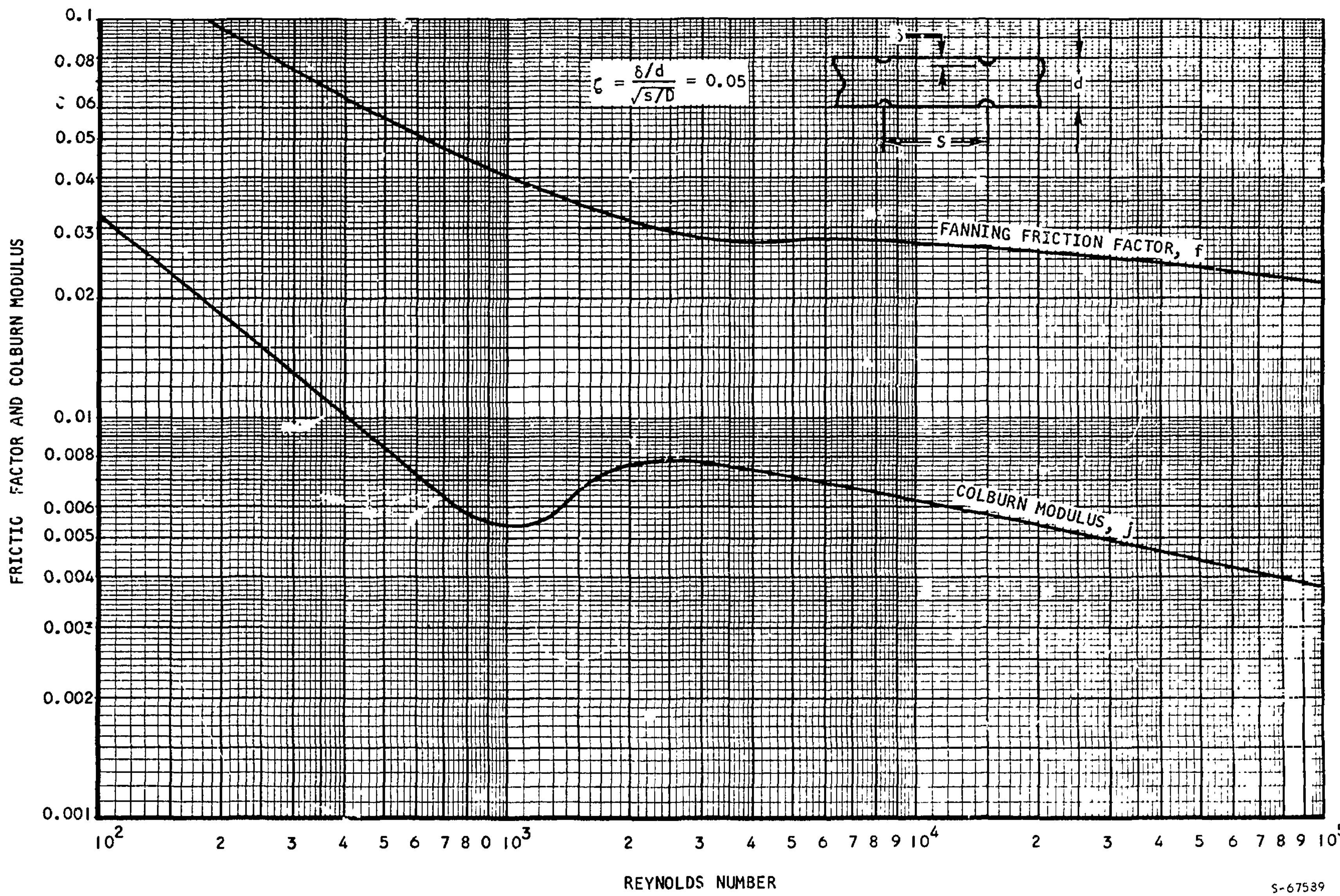

Figure 5-18. Heat Transfer and Friction Characteristics of Ring-Dimpled Tubes, at $\zeta = 0.05$

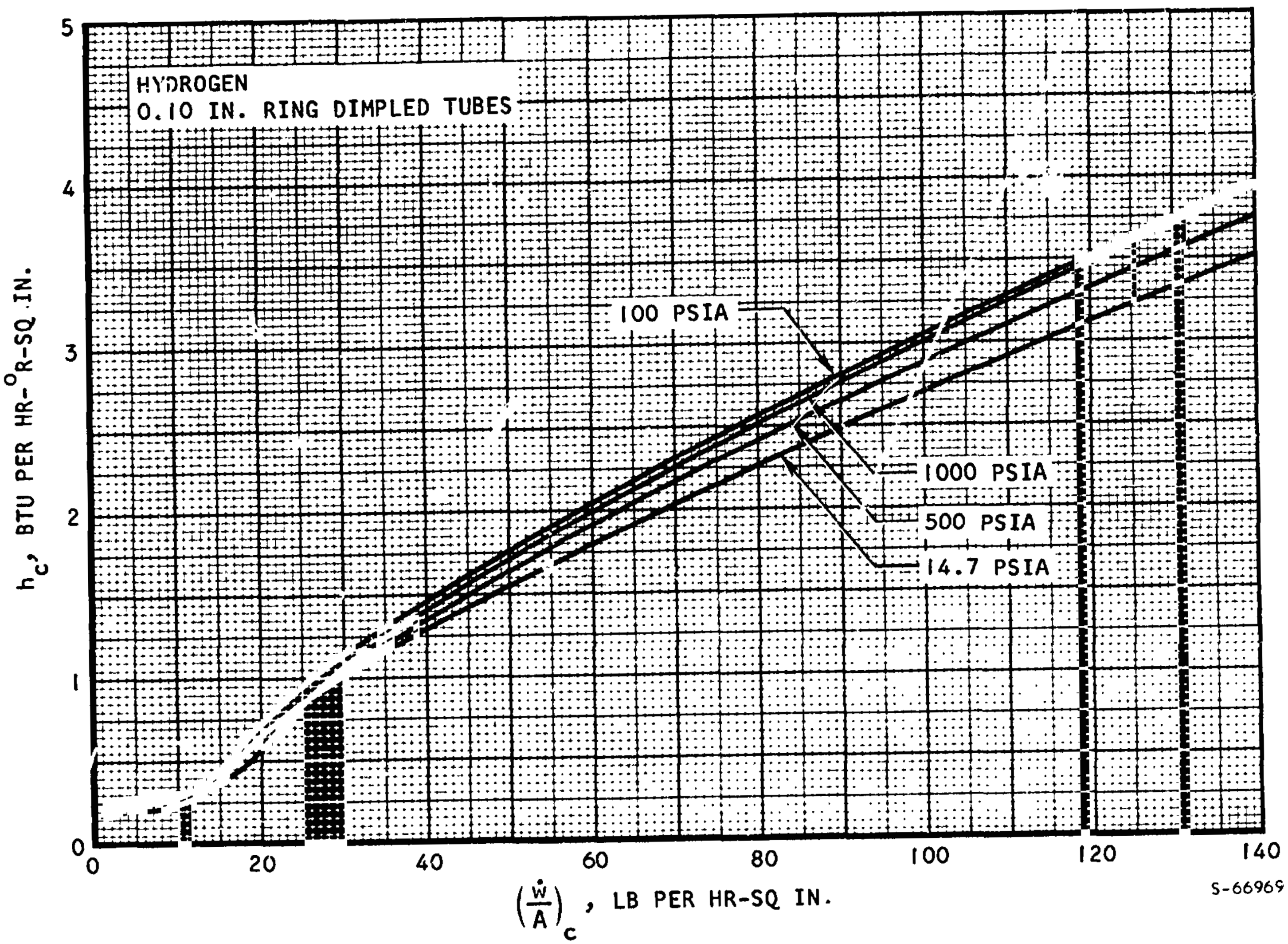

Figure 5-19. Cold-Side Thermal Conductances for Hydrogen

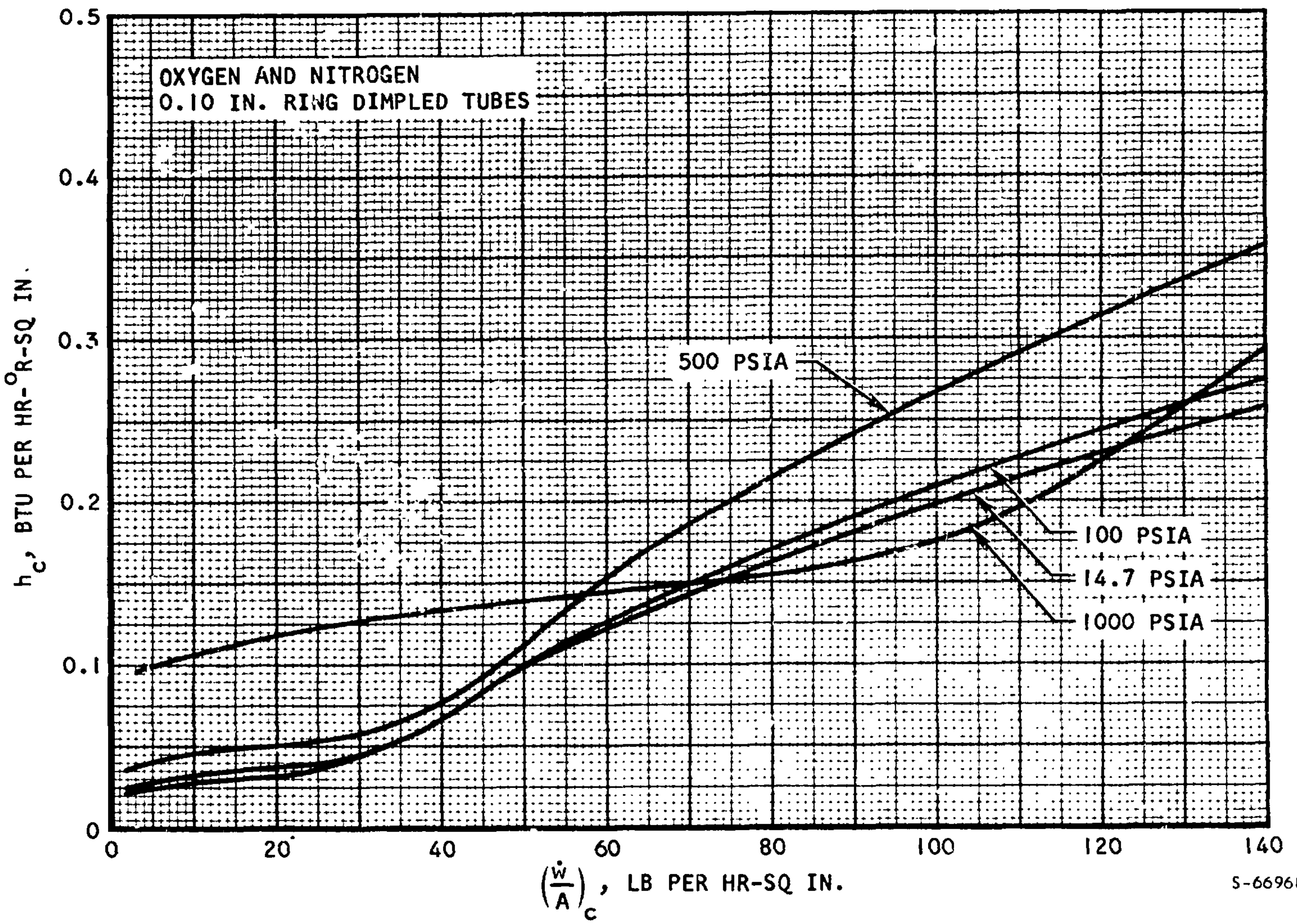

Figure 5-20. Cold-Side Thermal Conductances for Oxygen and Nitrogen

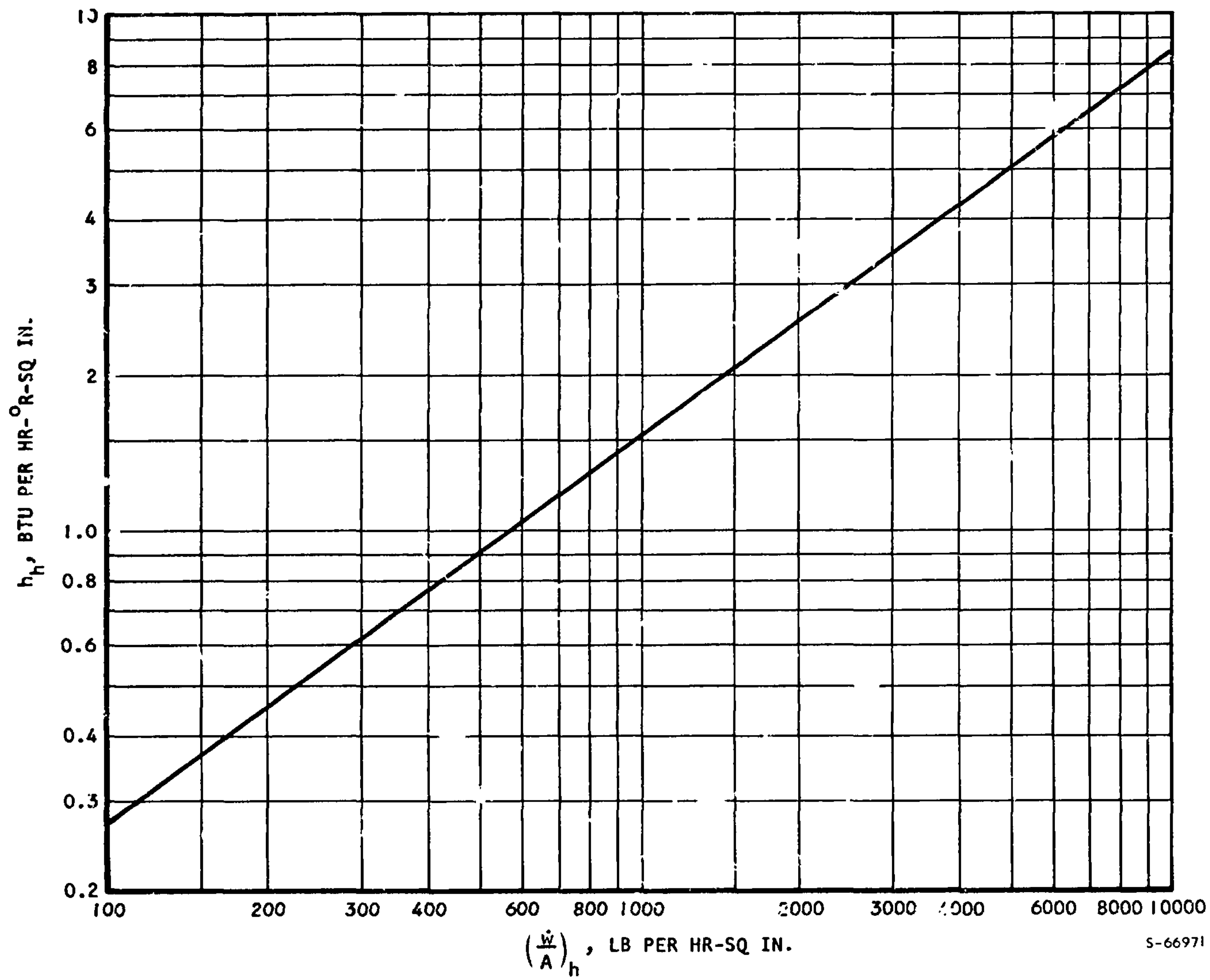

Figure 5-21. Hot-Side Heat Transfer Coefficient for Transport Fluid Heat Exchangers

With Figures 5-19 through 5-21, it is possible to evaluate the overall conductance U if the mass velocities of the two streams are available.

Design Procedure

The procedure established for this heat exchanger is summarized in Figure 5-22. The philosophy used here makes use of the thermal conductance ratio (TCR) to ensure selection of a design point not subject to freezeup. TCR is defined as:

$$TCR = \frac{h_c}{h_h} = \frac{T_h - T_w}{T_w - T_c} \tag{5-52}$$

where T_h = hot stream local bulk temperature

T_c = cold stream local bulk temperature

T_w = wall local temperature

To avoid freezing situations with FC-75, a reasonable minimum wall temperature is 400°R. Thus, the maximum value of TCR is given by:

$$TCR_{max} = \frac{T_{h_I} - 400}{400 - T_{c_I}} \tag{5-53}$$

As shown on Figure 5-22, the procedure requires specification of three independent variables about which the user has no prior knowledge. Fortunately, reasonable first guesses can be made which lead to rapid convergence on satisfactory designs.

The variables that must be assumed are:

$\left(\frac{\dot{w}}{A}\right)_c$ = Cold-side mass velocity

M = No. of hot-side passes per in. of heat exchanger length

m = Parameter used estimating the capacity rate ratio, C_c/C_h

The first two influence the geometric characteristics of the design, while the last parameter is important in satisfying the thermal conductance ratio criterion.

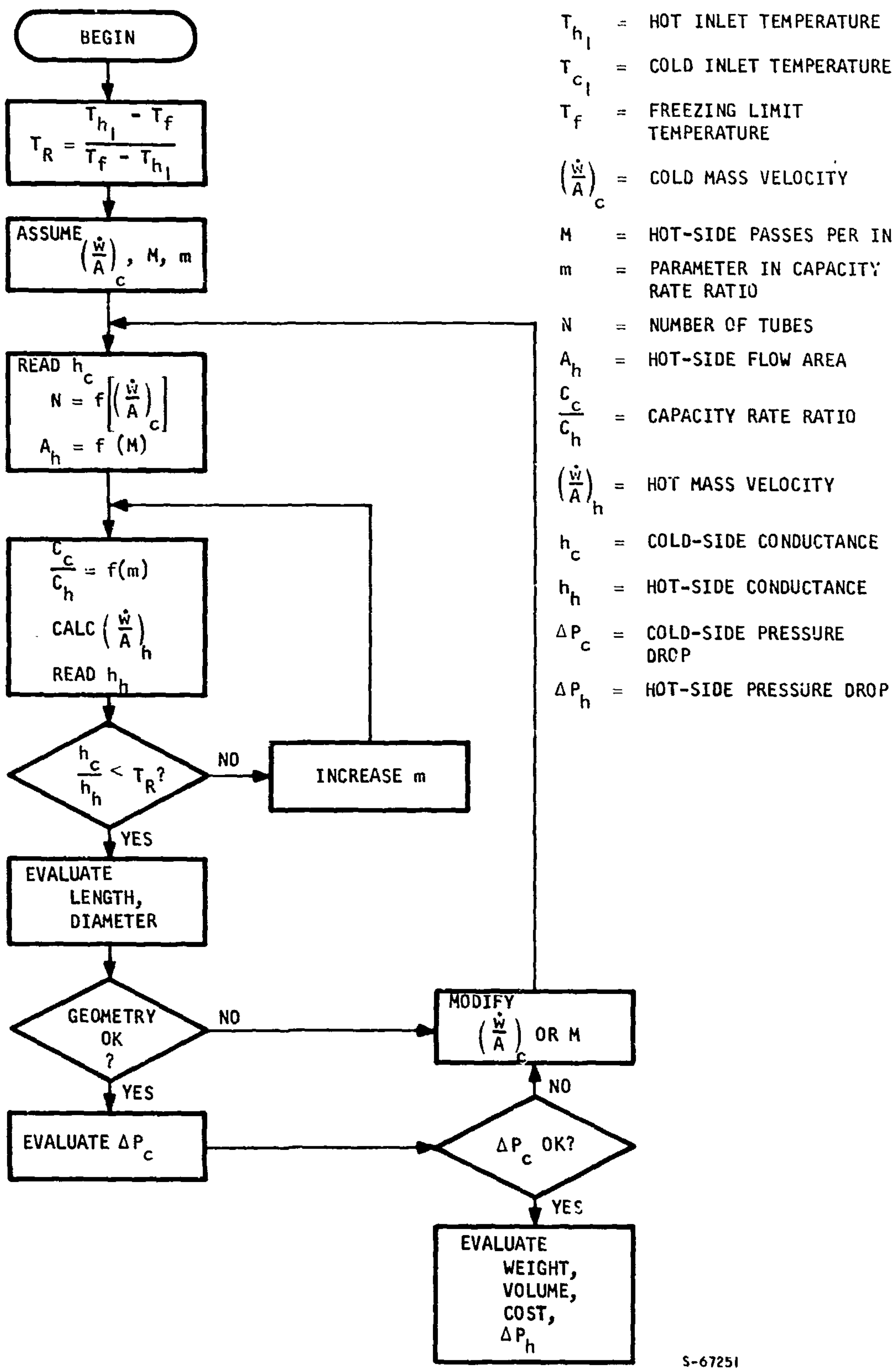

Figure 5-22. Design Procedure for Transport Fluid Heat Exchangers

The cold-side mass velocity permits h_c to be evaluated and also allows the required number of tubes N to be determined from

$$N = 128 \frac{\dot{w}_c}{\left(\frac{\dot{w}}{A}\right)_c} \tag{5-54}$$

The hot-side flow area A_h is then calculated from

$$A_h = 0.03\ (2 + \sqrt{N})/M \tag{5-55}$$

The capacity rate ratio is estimated with the relation

$$\frac{C_c}{C_h} = 1 - \frac{m}{\epsilon} \tag{5-56}$$

where $\epsilon = \frac{T_{c_2} - T_{c_1}}{T_{h_1} - T_{c_1}}$, cold-side effectiveness

Thus, in guessing m it is clear that some value less than ϵ must be chosen.

The FC-75 flow rate can now be found to have the value:

$$\dot{w}_h = \frac{C_c}{\overline{C}_{P_h}\left(\frac{C_c}{C_h}\right)}$$

If the hot-side mass velocity is now evaluated,

$$\left(\frac{\dot{w}}{A}\right)_h = \frac{\dot{w}_h}{A_h}$$

The hot-side thermal conductance h_h can be found using Figure 5-21.

TCR can be determined at this point from Equation 5-52, and compared with TCR_{max}. If TCR is too large, the parameter m must be increased and a new capacity rate ratio determined.

If TCR is satisfactory, the function

$$\psi = 1 - \epsilon\left(1 + \frac{C_c}{C_h}\right)$$

is calculated, and Figure 5-17 is used to obtain a value for $\phi_3 UA$.

The overall thermal conductance of the heat exchanger is given by

$$U = \frac{h_c}{1 + TCR} \tag{5-57}$$

and the definition of the parameter ϕ_3 is:

$$\phi_3 = \frac{1}{C_c} + \frac{1}{C_h}$$

Thus, the required heat transfer area A can now be determined from

$$A = \left(\frac{\phi_3 UA}{\phi_3 U}\right)$$

The tube bundle length necessary to satisfy this area requirement is

$$L = 3.18 \frac{A}{N} \tag{5-58}$$

At this point, the design is fully defined in terms of shell diameter and length. It is now appropriate to assess these characteristics. If the proportions are not reasonable, further iteration must be accomplished.

When satisfactory geometric results are obtained, Figures 5-23 and 5-24 can be entered to obtain the cold and hot stream pressure losses. If these are acceptable, the design can be considered completed; otherwise, iteration to achieve the desired pressure loss should take place.

In selecting values of $(\dot{W}/A)_c$ or M for new iterations, the following observations are useful:

Increase of $(\dot{W}/A)_c$: decreases length
decreases diameter
increases cold pressure loss

Increase of M: decreases length
decreases cold pressure loss
does not affect diameter

<u>Heat Exchanger Weight and Cost</u>

The estimated weight of heat exchangers of this type is presented on Figure 5-25. While the weights plotted here include allowances for ports and

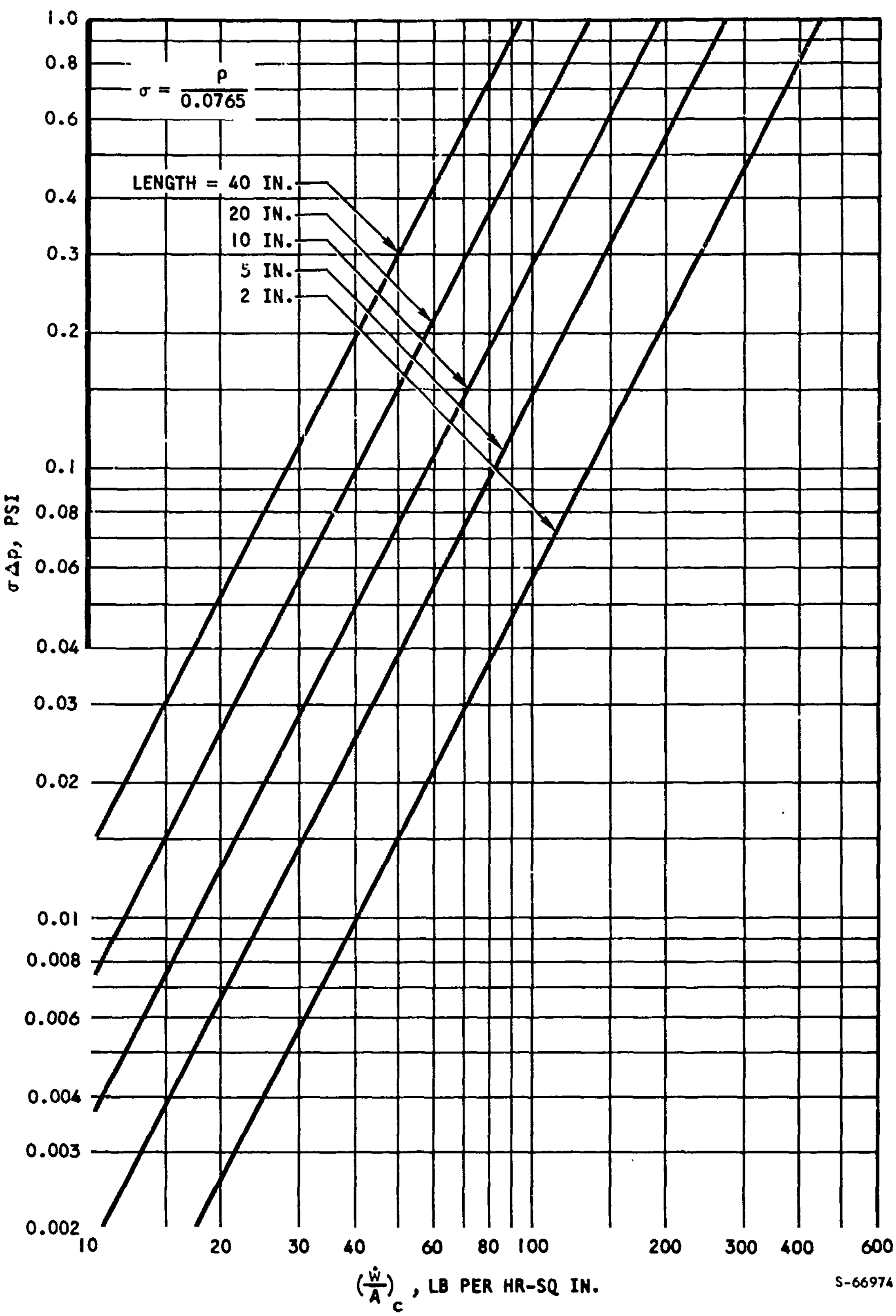

Figure 5-23. Cold Side Pressure Drop Characteristic for Transport Fluid Heat Exchangers

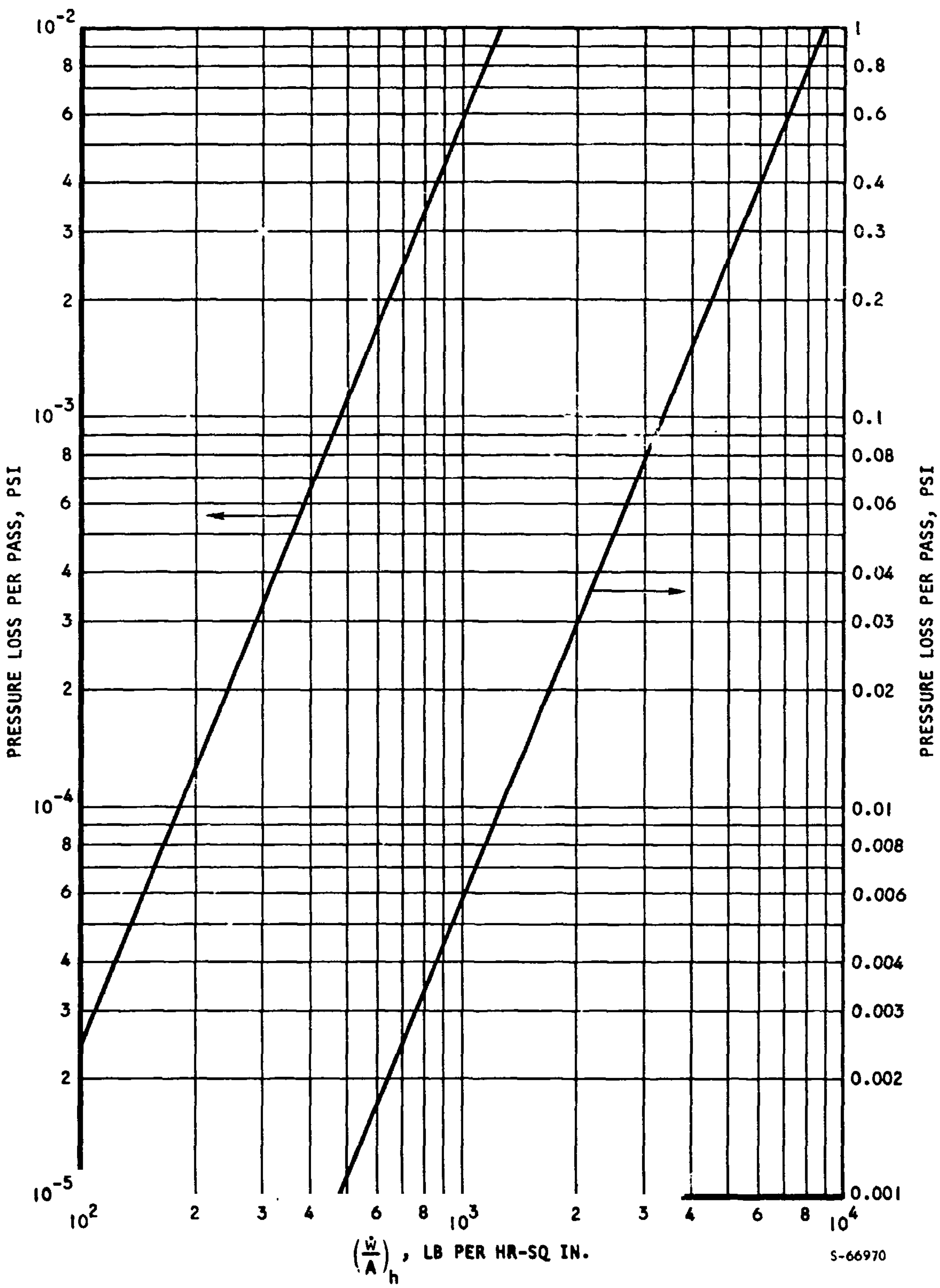

Figure 5-24. Hot-Side Pressure Loss Characteristic for Transport Fluid Heat Exchangers

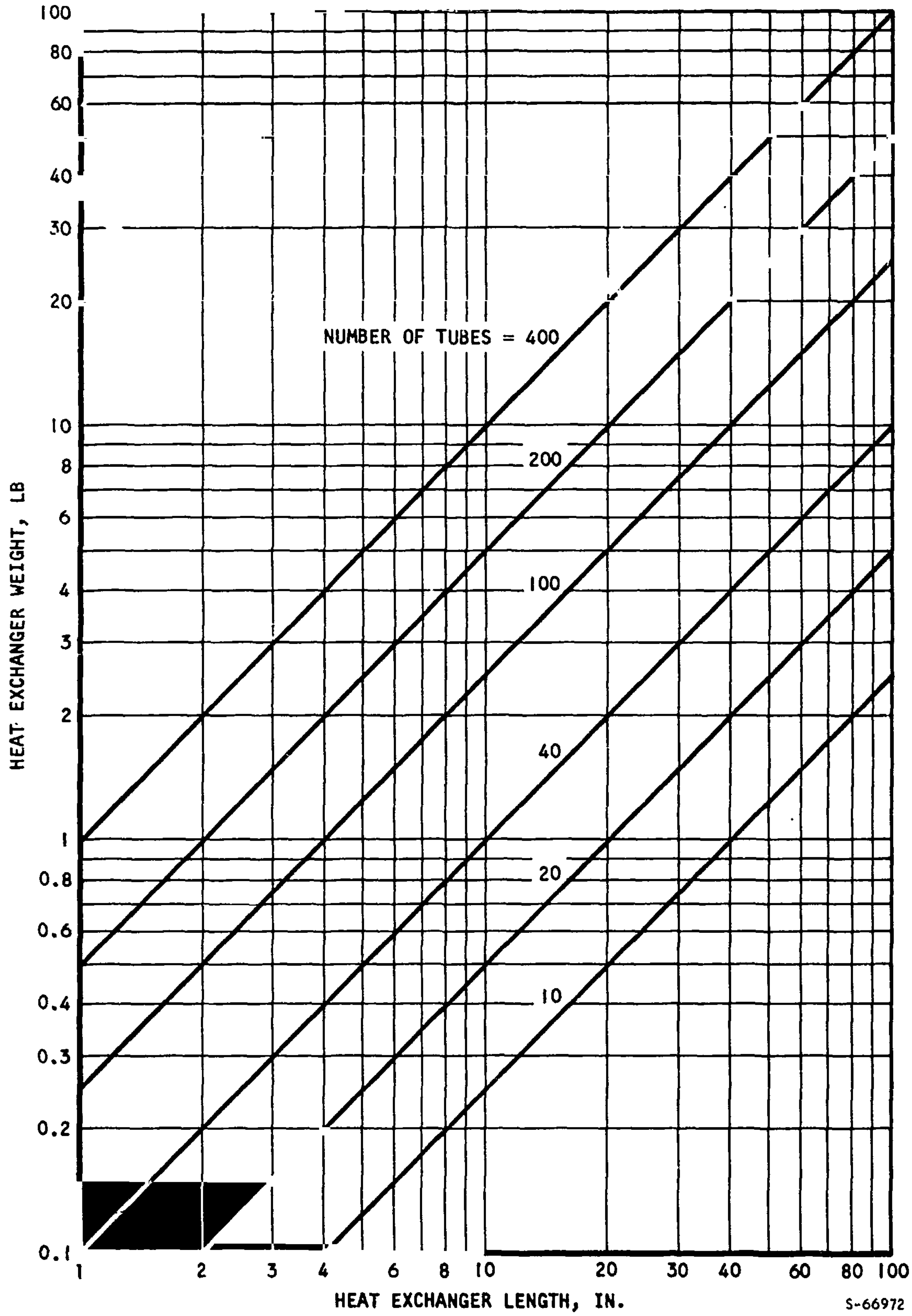

Figure 5-25. Weight of Transport Fluid Heat Exchangers

headers, these features and also mounting provisions become a large proportion of total weight for small units. Thus, it is suggested that 0.5 lb be considered the minimum weight for the transport fluid heat exchangers. All results under this value obtained from Figure 5-25 should be corrected to 0.5 lb.

The heat exchanger cost correlation has been established as a function of core volume. This characteristic is presented on Figure 5-26. This information was obtained by establishing a trend with respect to volume for shell and tube heat exchangers. After carrying out estimates for units of the type designed here, the characteristics were compared with those of the exchangers used to establish the cost-volume trend. After appropriate adjustment, Figure 5-26 was obtained.

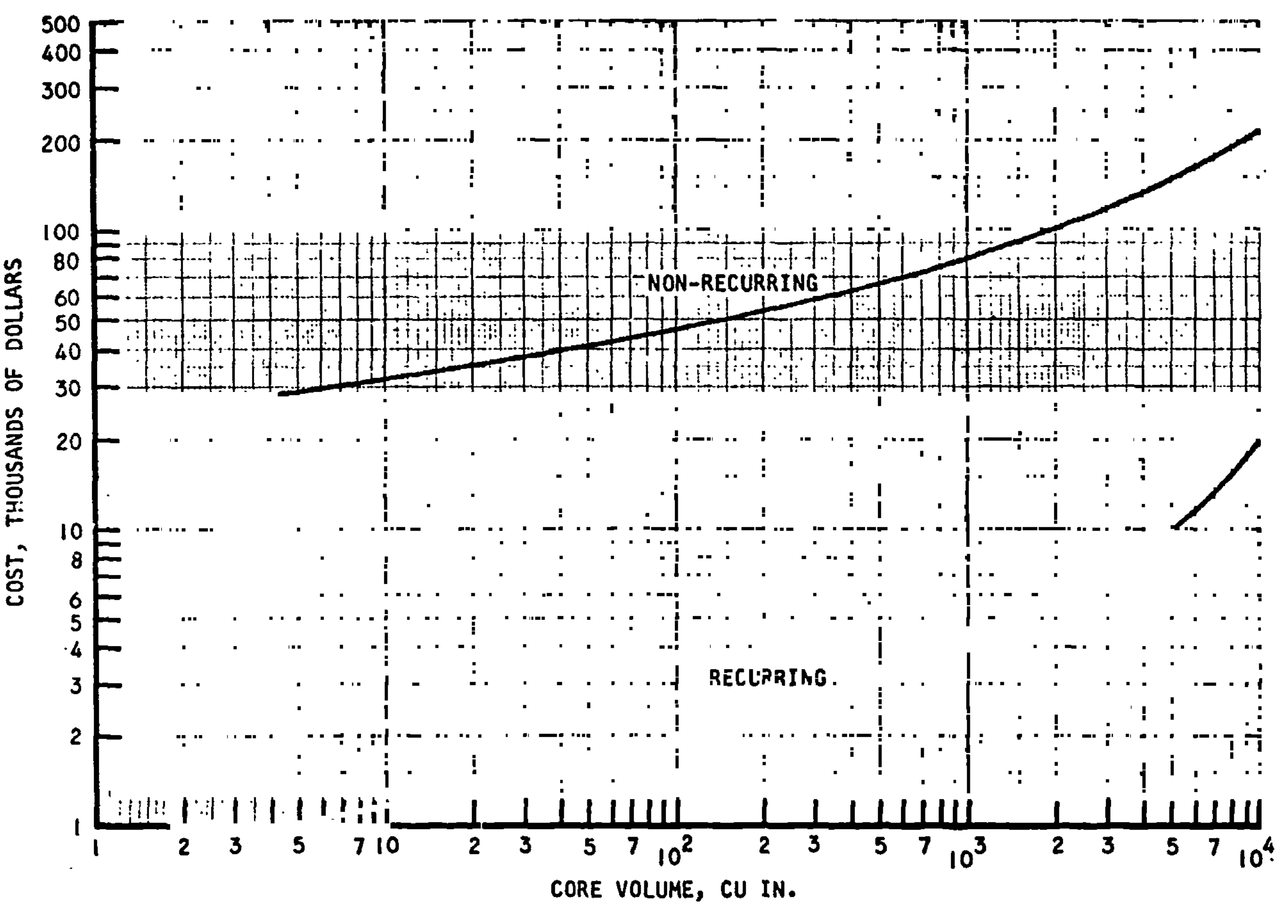

Figure 5-26. Cost Characteristics of Transport Fluid Heat Exchangers

HOT GAS HEAT EXCHANGERS

Introduction

Under this alternative, heat is supplied to the cryogen by a 100-psia, 2000°R stream of H_2-O_2 combustion products. Flow rate of the combustion products is assumed to be at the discretion of the user.

The stringent thermal and structural requirements imposed by this high-temperature heat source result in a significant departure in configuration for these units. Although the cross-parallel flow tubular heat exchanger is the choice here, as for the FC-75 units, to minimize freeze-up problems, the traditional cylindrical tube bundle configuration is not satisfactory.

A concept that minimizes the thermal stress problems of the tube bundle is the annular core configuration shown in Figure 5-16b. This approach has been investigated in several high-temperature heat exchanger development programs at AiResearch, including the fabrication and testing of developmental units. In this configuration, the tube bundle has the form of a hollow cylinder. Baffles are alternate disks and rings. The hot gas enters the open center of the tube bundle and is then caused to flow radially outward through the tubes. Ring baffles then turn the gas, directing it radially inward to the open center again. To clarify the construction used, a photograph of an annular tube bundle is shown in Figure 5-27. As mentioned, parallel flow is used unless high effectiveness is required; then, a parallel flow unit is followed by a counterflow section.

The tube bundle can be constructed as a completely free-floating core element, enhancing the safety of the unit. This feature allows close inspection and testing of the tube bundle prior to installation in the shell. In addition, double-wall tube construction can be considered, although the characterization presented here is based on single-wall, ring-dimpled tubes. The material used is Hastelloy-X.

The nominal hot gas inlet temperature is 2000°R, this being the highest temperature considered feasible for equipment using noncooled surfaces. Above this level, it is felt that provisions must be incorporated for active

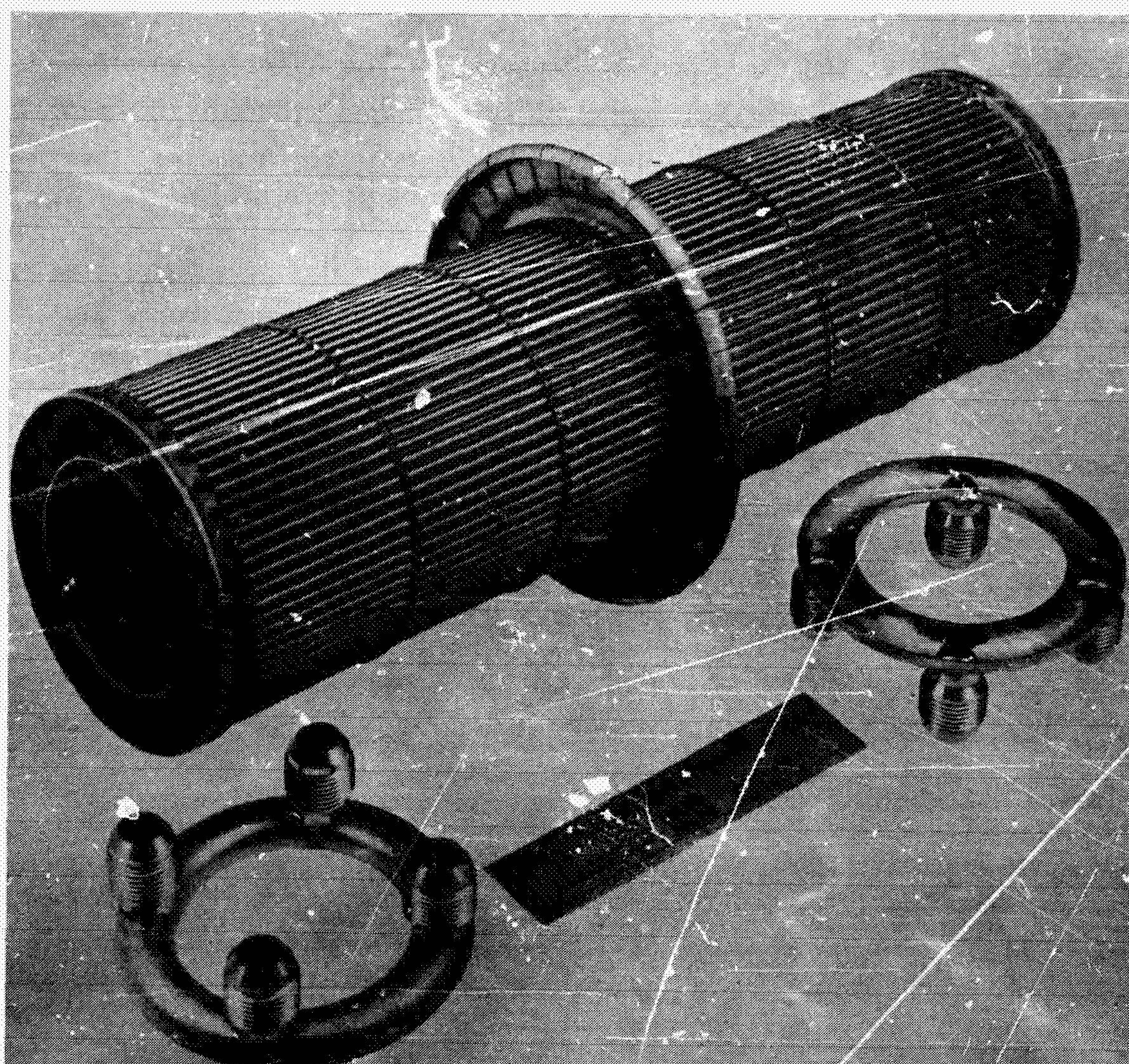

Figure 5-27. Typical Annular Tube Bundle and Headers

cooling of all surfaces impinged upon by the hot gas. However, the design procedure for these units will allow lower inlet temperatures to be investigated should these be of interest to the user.

As in the case of the FC-75 heat exchangers, an iterative design procedure is necessary for the combustion product units. Here, the hot-side outlet temperature and the pressure losses must be manipulated to define a heat exchanger with acceptable geometric characteristics.

With regard to the cost characterization of the annular tube bundle heat exchanger, the concept has been chosen here because of its great potential. Although developmental work has been accomplished, more technology development effort is needed to place it on the same cost basis as the two preceding types of heat source. Thus, the cost elements presented in Section 6 are projections of cost believed achievable after the needed basic development is carried out.

Selection of Design Model

The primary design considerations here are concerned with selecting a heat transfer matrix, establishing flow configurations, determining a core geometry, and adopting a basis for structural design.

I. Heat Transfer Matrix

There are a wide variety of heat transfer materials that can be utilized in heat exchanger design. Typical heat exchanger surfaces are illustrated in Figure 5-28. To minimize size and weight of heat exchangers, it is desirable to select the heat transfer matrix with the highest heat transfer area per unit volume consistent with other design constraints. The degree of compactness of various heat transfer surfaces are constrasted in Figure 5-29 and show a range of about two-and-one-half order of magnitude. Clearly there is an overlap between geometries of different types as the internal matrix parameters are varied over their available ranges. The types of surfaces that could be considered in these heat exchangers are the various tubular or plate-fin approaches. Very high heat transfer coefficients can be achieved with both types of surfaces. In general, however, the plate-fin types of heat exchanger, where they can be used, result in a smaller and lighter heat unit.

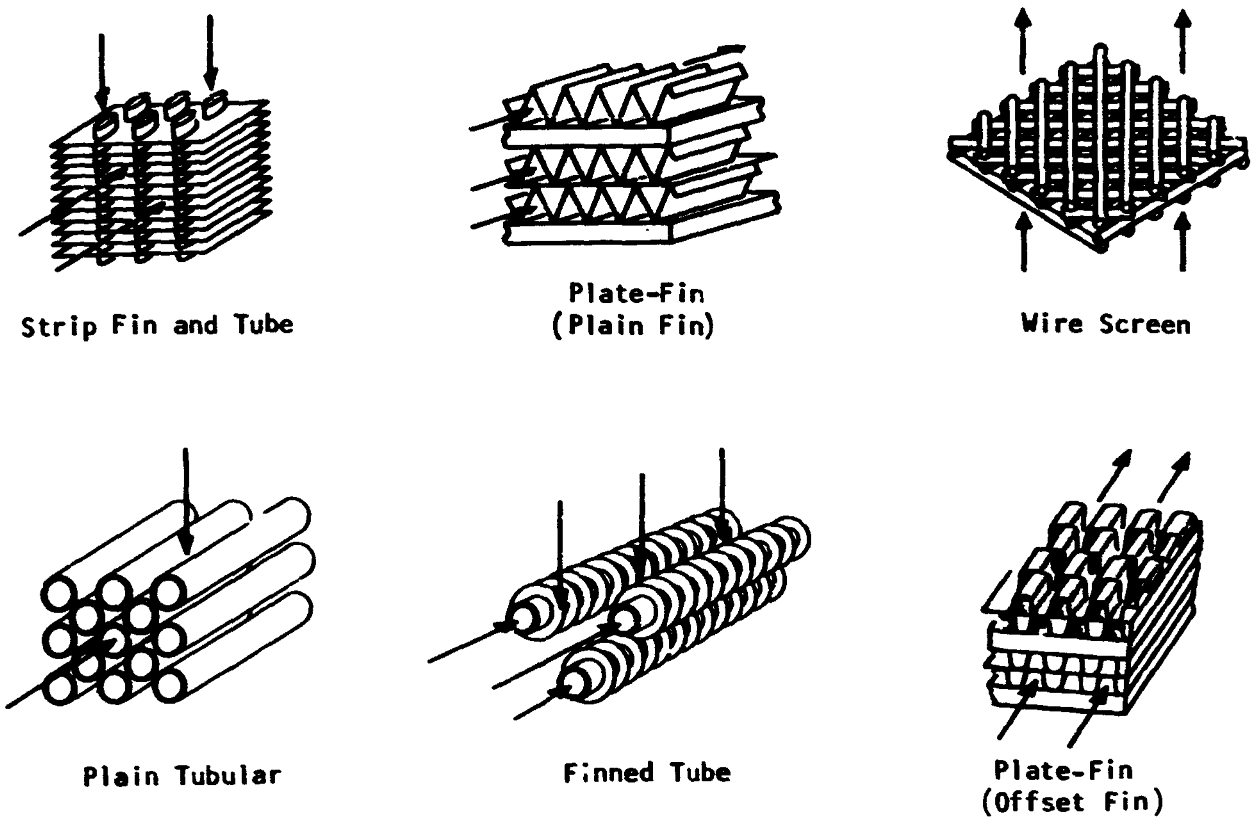

Figure 5-28. Types of Heat Transfer Surfaces

S-64847

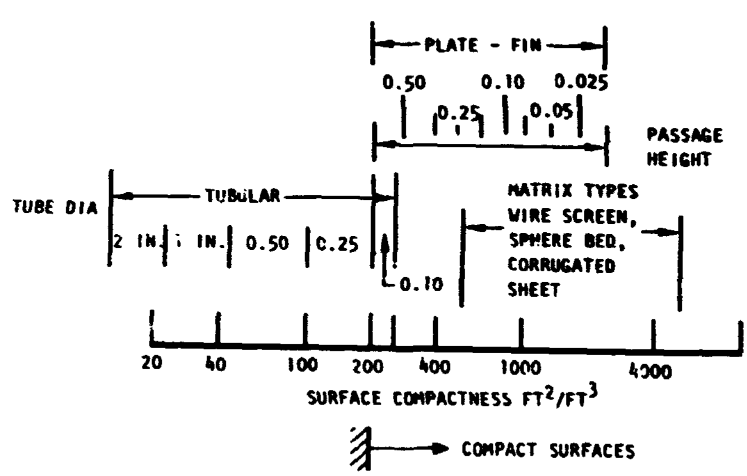

Figure 5-29. Surface Compactness Spectrum

S-64848

The high operating pressures associated with many of the units of this study restricts the selection of heat transfer matrixes. While the plate-fin type is optimum from a heat transfer point of view, the pressure containment capabilities of this type of construction are considerably poorer than offered by the tubular type construction. At the operating temperatures of interest, the plate-fin type of heat exchanger is probably restricted to pressure levels below 500 psi. Thus, the operating pressure level restricts the choice of the heat transfer matrix to the various types of tubular construction, at least for the high pressure heat exchangers.

An additional factor for the selection of a tubular matrix is concerned with leakage of the contained fluids. Since leakage of oxygen into high-temperature, hydrogen-rich combustion products would cause catastrophic failure, leakage becomes a major design consideration. Increased matrix compactness tends to increase the ratio of stream frontal to stream flow length. This means a greater summed length of braze or weld joint where direct leakage is most likely to occur between the two fluid streams. In tubular units the braze or weld joint between the tube and the header is less likely to leak than the header joint of a typical brazed plate-fin type construction. Furthermore, the tube joint generally is more conducive to test and corrective procedures than the typical brazed plate-fin construction.

With tubular heat exchangers, extended surfaces may be added to the outside of the tubes by employing fins. However, these fins can introduce large temperature gradients. These temperature gradients could result in freezing temperatures at the hot fin root. Furthermore, tightly spaced fins provide quasi-stagnation zones at the fin roots, and at the sharp corners would act as points of initial ice build-up on the combustion product side. In finned tubes, once this ice build-up occurs there exists an unstable situation whereby the loss of hot-side extended surface area from ice build-up sufficiently reduces the wall temperature to promote additional loss of effective heat transfer area. This can cause substantial reductions in overall heat transfer performance as well as sharp increases in hot fluid pressure drop. Bare tube matrixes allow better and more predictable metal temperature control, and do not provide the quasi-stagnation zones associated with extended surface matrixes.

Offset rather than in-line rows of tubes have been selected for two reasons: (1) the staggered tube rows create high turbulence in the fluid flowing over them, which results in a large heat transfer coefficient for a given pressure drop and thus a small heat transfer matrix for a given requirement; and (2) the tubulent mixing of the fluid flowing over the tubes eliminates cold stagnant areas associated with the in-line configuration. Thus, the possibility of ice formation is reduced when the staggered tube configuration is used.

2. Flow Configuration

Having selected a tubular matrix, an obvious conclusion is to flow the cryogen inside the tubes and the combustion products outside the tubes. The cryogen is consistently the highest pressure fluid; hence, the shell structural requirements are lessened when the shell is designed to contain the combustion products. In addition, the combustion products have a high percentage of the inlet total pressure available for promoting the high heat transfer coefficients of flow across tubes. Hence, multipassing of the combustion products can be used to achieve high velocity of the combustion products through the matrix, ensuring a high heat transfer coefficient. In addition, multipassing can be used to achieve a desirable shape for the matrix.

Another distinct advantage of flowing the cryogens through the tubes arises from the thermal stress loads in the advent of water vapor freezing. Consider a unit with the cryogen outside tubes and the combustion products inside the tubes. Assume an abnormal mode of operation that causes a frost build-up inside a tube. The flow in the tube would decrease, and the fluid in the tube would suffer a greater temperature drop. The wall temperature would drop, and freezing would continue until virtual or total blockage of the tube occurred. The combustion products and the mean wall temperature of the tube would approach the mean cryogen temperature. The resulting temperature gradient between the cold tube and adjacent tubes at the constraining header could be increased by more than 600°F and cause severe tensile thermal stress in the cold tube. This danger is prevented by flowing the combustion products across the tubes because the effect of partial blockage will not affect individual tubes.

3. Core Geometry

For all heat exchangers except the gas counterflow types, a cross-parallel flow configuration with the hot fluid multipassed was used. Justification for this, as well as justification for recommending use of a multipassed, cross-parallel flow configuration when the cold fluid is greather than 500°R, is given in the following paragraphs.

The performance of various types of heat exchanger flow configurations is illustrated in Figure 5-30. This curve plots heat exchanger effective, ness against NTU requirements (at a fixed capacity rate ratio) where the NTU requirement is a measure of heat exchanger size. As illustrated in this figure,, the smallest size heat exchanger can be achieved with a counterflow configuration.

When the temperature of the cold fluid is less than the freezing temperature of water, however, there is a possibility of ice formation, and the thermal gradients are more severe with the counterflow configuration. Figures 5-31 and 5-32 contrast the temperature distribution for parallel and counterflow heat exchangers. In the counterflow arrangement the temperature gradients along the tube wall are much more severe than in the parallel flow units. Thus, the parallel flow unit is more advantageous from both a structural standpoint and a reduction in the possibility of freezing. While these problems could be alleviated by reducing the combustion product temperature difference, this would require a large increase in the propellant requirements to provide the conditioning energy requirements. Therefore, parallel flow units are used for all heat exchangers where the temperature of the cold fluid is less than 500°R.

When the inlet temperature of the cold fluid is greater than 500°R, the possibility of freezing no longer exists, and the temperature gradient along the tube bundle is diminished, allowing the counterflow configuration to be employed. Since the counterflow configuration results in a smaller heat exchanger, its use is highly recommended when possible.

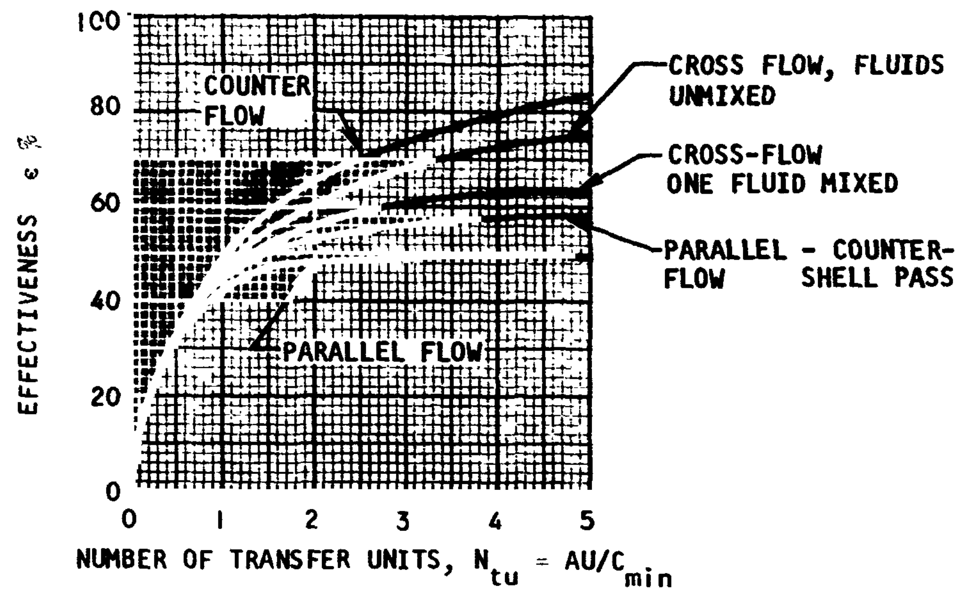

Figure 5-30. Heat Transfer Effectiveness as a function of Number of Transfer Units: Effect of Flow Arrangement for $C_{min}/C_{max} = 1$

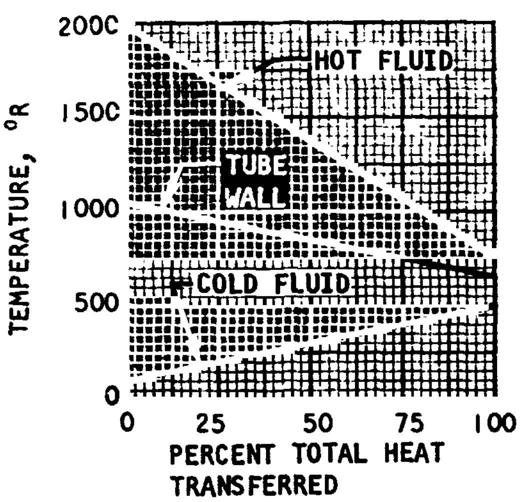

Figure 5-31. Parallel Flow Heat Exchanger Performance

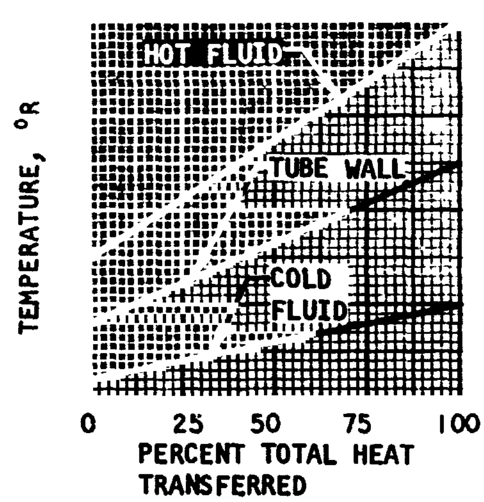

S-67579

Figure 5-32. Counterflow Heat Exchanger Performance

For most designs, the hot fluid combustion products make several crossflow passes. Each pass is of sufficiently low total temperature rise to avoid excessively cold corners within the matrix caused by the transverse temperature gradient inherent in crossflow heat exchangers. The multiple pass arrangement provides optimum use of the combustion products, but requires high pressure drop. It does result in a reasonable packaging shape.

The multipass configuration decreases the radial temperature gradient per pass as the number of passes increases. This relieves back heat flow and decreases thermal stresses at the point of baffle-tube contact.

4. Flow Stability and Maldistribution

Serious performance and structural difficulties will result from designs that have flow instabilities and flow maldistribution across the matrix face. Such instabilities stem from high flow acceleration-deceleration and kinetic losses relative to the frictional drag losses. Boiling and supercritical hydrogen and oxygen units suffer large changes in mean fluid density from inlet-to-outlet, and have relatively low friction loss in a highly turbulent flow condition, which can set up pressure and flow oscillations in the tubes. The present designs recognize such problems and utilize turbulators and severe ring dimpling in zones of high fluid density changes. Such devices further aid the predictability of heat transfer performance and generally reduce the tube wall temperature at the combustion product inlet.

Flow maldistribution can be introduced by poor duct design, core inlet and outlet effects, and by interpass turn geometries. Even in the preliminary parametric studies, core dimensions and volumes reflect interpass combustion product flow areas sufficiently high so as not to produce maldistribution. The incident kinetic head to any matrix must be much lower than the matrix frictional loss, and the core diameter, shell diameter, and ducting are all established to maintain the kinetic head at less than 10 percent of the frictional pressure loss.

5. Structural Considerations

All components of the heat exchanger are considered to be fabricated from high-temperature, oxidization-resistant alloys. Although the most suitable alloy has not yet been established, Haynes Alloy 188 and Hastelloy X are the leading candidates. The thickness of the materials used for the various components depends on design stress levels and minimum gages for manufacturability.

Selecting design stress levels for the components depe ds on many factors; typically, these factors include the temperature of the materials, the temperature gradients in the material, the number of thermal cycles the material experiences, the design life of the material, the number of pressure cycles the material experiences, and such other factors as vibration levels. Obviously, many of these factors cannot be defined in a parametric study. The approach taken, therefore, was to establish a relationship between design stress and operating temperature, which is representative for most applications. These design stresses are used to determine component thicknesses based on pressure containment.. Design stress as a function of temperature is shown on Figure 5-33. The initial design and development effort for the sophisticated heat exchangers considered here must include an extensive analytical and experimental program aimed at verification of the structural design basis.

The design stress levels presented in Figure 5-33 are based on creep-rupture data on Hastelloy X, and are considered representative of any of the structural materials which are suitable for this application. The design stress levels represent a life to failure of about 10,000 hr over the temperature range shown. For the actual heat exchangers, in which design life is probably closer to 1000 hr, this represents a safety factor of 10 on operating life, corresponding to a factor of safety of 1.5 on stress.

The heat exchangers must be satisfactory for sustained pressure loads of up to 1000 psi for the operating life. For the preliminary sizing required subsequent to the initial heat transfer design, material thicknesses are determined by simplified analyses such as using membrane loads of cylindrical and spherical shells. For the final design a detailed stress analysis would include determination of discontinuity stresses such as those due to pressure deflection mismatches at a heater, cylindrical shell, and spherical end cap joint.

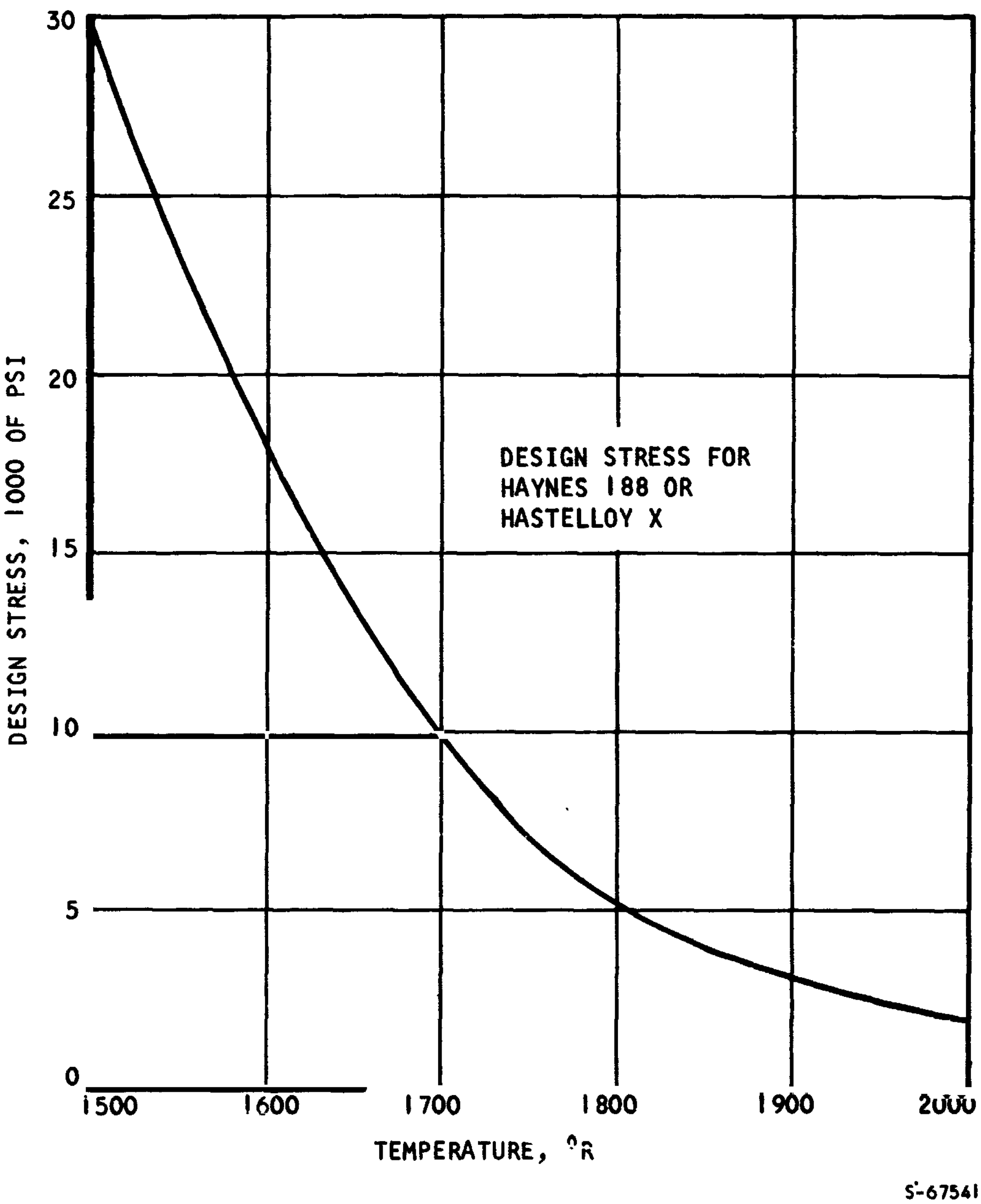

Figure 5-33. Temperature Dependence of Design Stress for Heat Exchanger Material of Construction

If the inlet temperature of the combustion products is 2000°R or less and if environmental considerations allow the shell to be at the same temperature as the combustion products, then the shell can be constructed of a single layer of sheet metal. If the inlet temperature of the combustion products is greater than 2000°R, or if environmental considerations require that the shell must remain cool, then the shell must be actively cooled. This is accomplished by using double-wall construction for the shell. Coolant--generally a portion of the cryogen to be warmed--flows in the passage between the inner and outer walls, maintaining both walls at an acceptable temperature. Fins are inserted in the cooling passage between the two walls to promote heat transfer and improve the structural integrity of the shell. No weight or volume penalty is incurred for using double-wall construction for the shell. The shell is provided with bellows to allow it to expand longitudinally as required.

Baffles are located within the heat transfer matrix to force the combustion products to flow across the tubes several times. This technique, which is known as multipassing, increases the velocity of the combustion products as they flow over the tubes, which raises the convective conductance between the tubes and the combustion products and prevents ice formation on the tubes while reducing the matrix size. The baffles consist of a single layer of sheet metal when the inlet temperature of the combustion products is less than 2000°R. In heat exchangers using inlet temperatures greater than 2000°R, all baffles experiencing temperatures greater than 2000°R are actively cooled in the same manner as the shell

For oxygen service, leakage of the oxygen into the combustion products will cause a catastrophic failure of the heat exchanger. To ensure against this, a double-walled header may be used in the region where the tubes penetrate the toroidal header ducts. Typically the space between the two walls would be pressurized with nitrogen to a level slightly higher than that of the oxygen so that any leaks between the header ducts and tubes would result in a small nitrogen leak into the oxygen rather than a catastrophic leak of oxygen into the combustion products.

In assigning working stresses to the various components, each component is assumed to be at operating temperature, and the components are designed to contain pressure according to the design stresses in Figure 5-33. Design temperature and stresses for each component are given below.

a. Tubes

Tubes must operate at temperatures as high as 1800°R, which corresponds to a working stress of 5000 psi. Tube thicknesses and minimum gages are shown on Figure 5-34.

b. Shells

It is assumed that there will be at least a 200°F temperature drop in the combustion products across the first pass of the tubes when the inlet temperature of the combustion products is 2000°R. Therefore, the design temperature of the shell is 1800°R, which corresponds to a working stress of 5000 psi.

The minimum shell thickness is 0.032 in. The expansion bellows, if required, are not considered to affect shell weight.

c. Combustion Products Ducts

The combustion products ducts must operate at combustion products inlet temperature unless they are actively cooled. Since the temperature of combustion products can be as high as 2000°R in heat exchangers that do not use cooled ducts, the design temperature of the ducts must be 2000°R. Therefore, all combustion products ducts use a design stress of 2000 psi.

If the heat exchanger operates with combustion products hotter than 2000°R, the ducts must have double wall construction, and the coolant flowing between the walls must cool the inner wall to 2000°R. The double wall construction will have the same weight as a single wall duct designed to a 2000-psi working stress. The minimum duct thickness is 0.032 in.

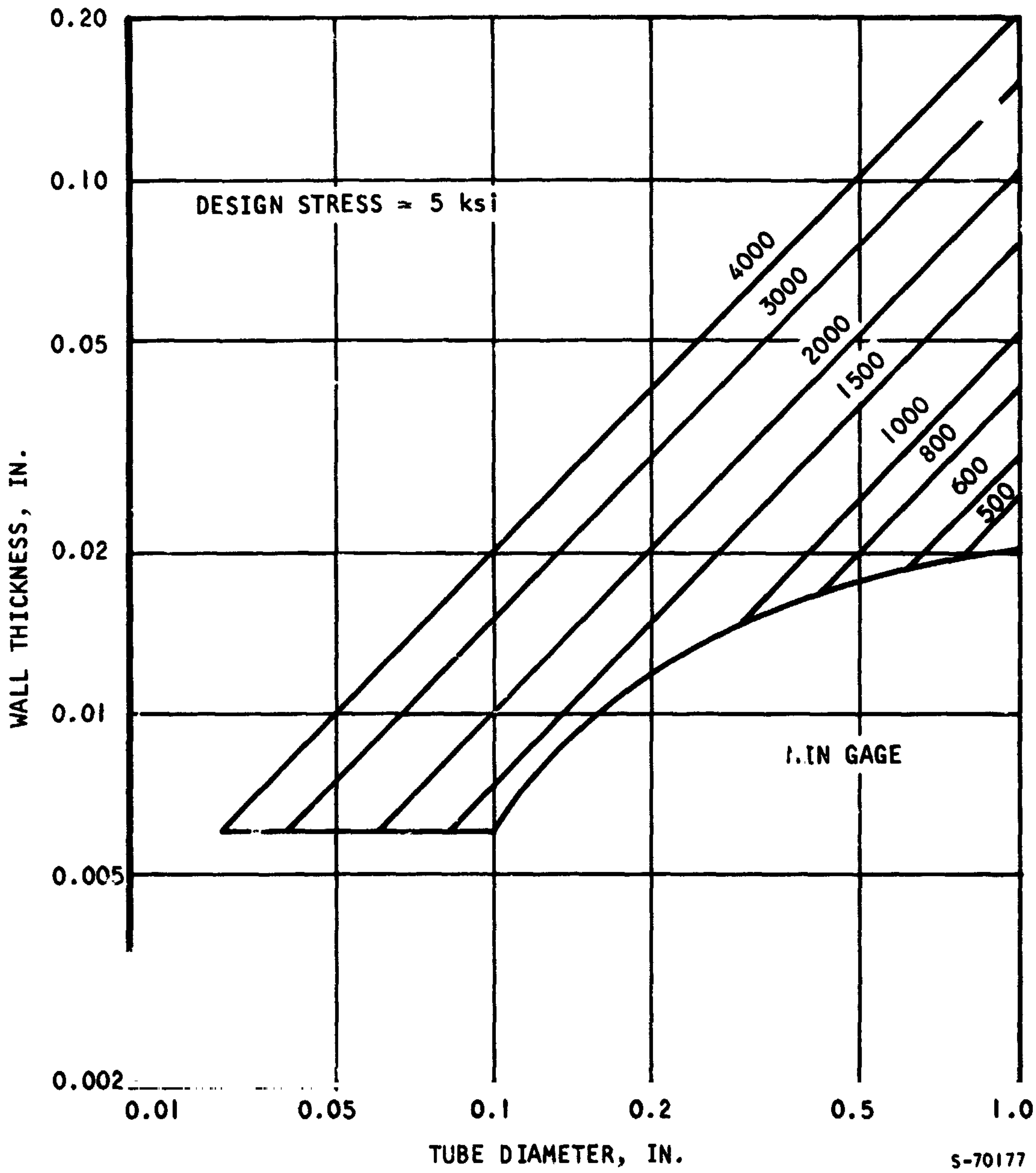

Figure 5-34. Tube Wall Thicknesses for 1700°R Maximum Temperature

d. Toroidal Header Duct

The toroidal header duct has two thicknesses associated with it: (i) the region where the tubes penetrate the duct, and (2) the remaining material of the duct.

The ring-shaped region where the tubes penetrate the duct can experience temperatures that are close to the inlet temperature of the combustion products. Furthermore, it must be stiff to prevent the formation of leaks at the tube-duct interface. To contain the cryogen pressure and provide stiffness, the thickness of this portion of the header duct is set at 2 times the shell thickness, with a minimum thickness of 0.064 in. The weight of this portion of the header duct is based on this thickness and should be reasonably accurate whether a thick single wall or a double wall is employed.

The remaining material in the toroidal header duct operates at temperatures much closer to that of the cold fluid. It is unlikely that the remainder of the duct will approach 1600°R; however, 1600°R has been used as the design temperature of this portion of the duct. Consequently, the remaining portion of the duct uses a design stress of 20,000 psi. Minimum material thickness is 0.032 in.

e. Baffles

The baffles are constructed of 0.032-in.-thick sheet metal. If the heat exchanger operates with combustion products at temperatures greater than 2000°R, some of the baffles will require cooling. This necessitates double-wall construction, which would double the weight of the baffle. This extra weight has not been accounted for in the study, but the baffles represent a small portion of heat exchanger weight so this inaccuracy in high-temperature heat exchangers has little effect on overall weight.

6. State-of-the-Art Evaluation

The heat exchangers just described can be built with very high reliability coupled with light weight using existing engineering, design, fabrication, and test techniques. Enough data on cryogenic heat transfer, properties of materials at high and low temperature, and fabrication of compact heat exchangers involving severe temperatures and thermal gradients have been generated from previous development programs to sharply reduce, if not eliminate, any further development efforts required before the above described heat exchangers could be used. These statements apply both to heat exchangers using simple, single-walled shells and ducts and to heat exchangers requiring active cooling of the shell and duct surfaces.

However, any heat exchanger of the type described in this section is considered to be specially designed to a particular application. Therefore, each heat exchanger to be built will require extensive effort in engineering and testing, despite the fact that the technology required to build it exists.

Heat Transfer Analysis

The methods and equations used to establish the size of the heat exchangers is presented in the following paragraphs.

1. Heat Exchanger Design Variables

As given in Section 2, the design variables required for a heat exchanger design are:

$\dot{w}_c$ = cold stream mass flow rate

$T_{c, in}$ = cold stream inlet temperature

$P_{c, in}$ = cold stream inlet pressure

$\dot{w}_h$ = hot stream mass flow rate

$T_{h, in}$ = hot stream inlet temperature

$P_{h, in}$ = hot stream inlet pressure

Hot fluid properties

Cold fluid properties

ΔP_h = hot stream pressure loss

ΔP_c = cold stream pressure loss

These variables are combined and manipulated in the following manner.

For two-fluid heat exchangers using conventional surfaces, there are three basic governing equations relating the significant parameters. They are:

1. The overall heat transfer rate equation

$$\frac{dQ}{dA} = U\,(T_h - T_c)$$

where:

$\frac{dQ}{dA}$ = heat flux per unit transfer area

$(T_h - T_c)$ = the driving temperature potential at location of the heat flux,

U = overall thermal conductance referenced to the driving temperature potential (this term is a grouping of terms to be defined later)

2. The geometric constraint equation represented by the effectiveness equation

$$\epsilon = \frac{q}{q_{max}} = MAX\left[\frac{T_{h,in} - T_{h,out}}{T_{h,in} - T_{c,in}},\ \frac{T_{c,out} - T_{c,in}}{T_{h,in} - T_{c,in}}\right]$$

where:

$\frac{q}{q_{max}}$ = ratio actual rate of thermal energy transfer to the maximum rate of thermal energy transfer that is theoretically possible

Effectiveness is a functional of the following thermodynamic and geometric variables

$$\epsilon = \phi\,(N_{tu},\ C_r,\ \text{flow configuration})$$

where:

$N_{tu} = \int_0^A \frac{U}{C_{min}}\, dA$ = number of heat transfer units which is the overall conductance normalized by the minimum stream capacitance, C_{min}.

Flow arrangement = the particular geometric relationship of the fluid streams, c.g., counterflow, parallel flow, or crossflow.

$C = Wc_p$, fluid capacity rate

$C_{min} = \mathrm{MIN}\ (C_h,\ C_c)$

$C_{max} = \mathrm{MAX}\ (C_h,\ C_c)$

$C_r = C_{min}/C_{max}$

To a good approximation, N_{tu} can be integrated to give:

$$N_{tu} = \frac{UA}{C_{min}}$$

The following relationships express the relationship between ϵ, N_{tu}, C_r, and flow configuration. For parallel flow configurations, the relationship is:

$$\epsilon = \frac{1 - \exp\ (1 + C_r)}{1 + C_r}$$

For counterflow configurations, the relationship is:

$$\epsilon = \frac{1 - \exp\ \left[-N_{tu}\ (1-C_r)\right]}{1 - C_r \exp\ \left[-N_{tu}\ (1-C_r)\right]}$$

For boilers, C_c is infinite; hence, C_r is zero. The expression then becomes:

$$\epsilon = 1 - \exp\ (-N_{tu})$$

3. The allowable pressure drop equation within a core at low Mach number:

$$\Delta P = \frac{5.35 \times 10^{-10} G^2}{2 g_c \rho_{in}} \left[(K_c + 1 - \sigma^2) + 2 \left(\frac{\rho_{in}}{\rho_{out}} - 1 \right) + \frac{f \rho_{in} L}{\rho_m r_h} - (1 - \sigma^2 - K_e) \frac{\rho_{in}}{\rho_{out}} \right] \tag{5-59}$$

where:

$G = \frac{\dot{w}}{A}$, mass velocity

f = friction factor dependent on the nature of the heat transfer matrix, fluid mass velocity, and fluid viscosity

$\frac{5.35 \times 10^{-10} G^2}{2 g_c \rho_{in}}$ = inlet velocity head

$2 \left(\frac{\rho_{in}}{\rho_{out}} - 1 \right)$ = flow acceleration

$f \frac{L \rho_{in}}{\rho_m r_h}$ = frictional pressure loss

$K_c + 1 - \sigma^2$ = entrance head loss

$1 - \sigma^2 - K_e$ = exit head loss

K_c = contraction pressure loss coefficient

K_e = expansion pressure loss coefficient

σ = ratio of flow area to frontal area

These equations show the interrelationship between a given heat transfer requirement, the overall conductance, and the heat transfer area. The problem definition fixes the heat rate, the temperature potential, and the effectiveness. Heat exchanger weight is optimized by maximizing the conductance and minimizing the area within the limitations of specified pressure allowances. Weight arises both from that weight attributed to the matrix surface area and from the external structure required both to support and connect the inner heat transfer matrix and to duct and contain the fluids. Matrixes that are compact (high area density per unit volume) and give high performance (yielding a high conductance per unit of pumping power) are the most desirable.

Further information on the nature of heat exchanger optimization can be found by investigating the following conductance equation:

$$\frac{1}{UA} = \frac{1}{(hA)_h} + \frac{a}{(kA)_w} + \frac{1}{(hA)_c} \tag{5-60}$$

The first and third terms on the right hand side are the fluid convection contribution; the second term, usually negligible, is the conduction contribution of the metal walls. It may be concluded that increasing the convection coefficients increases U and decreases the required area and weight. There is a limit, however, to the benefits of a relatively high coefficient on a given side because the individual contributions are related in such a manner that one side may be dominant.

The convective conductance h is dependent on the mass flux velocity; the fluid Prandtl number, specific heat, and viscosity; and the size and nature of the heat transfer matrix. Thus, there is an interrelationship between fluid properties, pressure drop, and matrix properties which determines the magnitudes of h_h and h_c.

There are also additional conditions that must be met. "Reasonableness" of final design geometry limits the final arrangement of hot and cold side matrixes. Units that are theoretically acceptable may not be manufacturable, packagable, or may impose fluid flow problems. Flow distribution and stability are severely limited by the relative magnitude of the right hand terms of the pressure drop equation as well as the inlet and outlet velocity heads. Generally, it is beneficial to both distribution and stability to have frictional component dominate by a factor of 5 or greater.

In the heat exchangers of this study there are also maximum and minimum wall temperature limitations imposed upon the heat exchanger designs based on structural and freezing considerations, respectively. The following equation determines wall temperature:

$$T_w = \frac{T_h + T_c\ (TCR)}{1 + TCR} \tag{5-61}$$

where the thermal conductance ratio (TCR) is defined as:

$$TCR = \frac{(hA)_c}{(hA)_h} = \frac{T_h - T_w}{T_w - T_c} \tag{5-62}$$

For the heat transfer matrixes used in this study, the heat transfer areas of the hot and cold sides are nearly the same, i.e., the tube wall area. Thus,

$$TCR = \frac{h_c}{h_h} \tag{5-63}$$

Therefore, for a given wall temperature there is an additional limit imposed on the relative magnitudes of h_c and h_h.

2. Data Correlations

The values of friction factor f and convective conductance h are based on nondimensional experimental data correlations for the particular heat transfer matrix used. The nondimensional correlations depend on the exact nature of the inside and outside heat transfer surfaces.

In this study many combinations of internal and external heat transfer surfaces are used, with the exact combination depending on the combination of heat transfer region (boiling, supercritical or gaseous), P_h, P_c, ΔP_h, ΔP_c, $\dot{w}_h$ and $\dot{w}_c$ specified. Consequently it is impractical to present the correlations for all the heat transfer surfaces investigated in this study. The data used are obtained from gaseous tests on actual cores, and apply to any fluid with a Prandtl number near 1.0, such as the gases, vapors, and supercritical fluids of this study, upon using the appropriate equations relating h and f to the dimensionless test data.

Computer techniques were used to generate parametric heat exchanger data over a broad range of operating conditions. Existing heat exchanger performance and design computer programs were modified to handle the peculiar heat transport properties of the combustion products and cryogenic hydrogen and oxygen. The accuracy of the heat exchanger performance prediction in all single phase units is limited by the following two major effects:

(1) Nonlinear bulk, stream transport property behavior, especially specific heat during instances of supercritical oxygen and hydrogen heat transfer.

(2) Extremely high wall-to-bulk stream temperature gradients (ratios exceeding 20 to 1 in some designs) impose severe density and other property gradients on the velocity and thermal boundary layer.

As discussed earlier, simple tubular heat transfer matrixes were selected for the designs. To establish consistency, generality, and reasonable accuracy for the parametric study, AiResearch test data for fluids with Prandtl number of the order of one were assumed applicable. This assumption was based on previous experience; this data can be modified by suitable calculation techniques to relate it to the fluids under consideration.

The use of turbulators and flow-orificing at the cryogenic fluid inlet can be used to promote flow stability and minimize the impact of some uncertainties in performance predictions. Also, in certain designs the predictable side (i.e., hot or cold side of a heat exchanger) was the controlling side, and large discrepancies on the more ambiguous opposing side are tolerable.

In conclusion, the basic data correlation that was used incorporated classic Colburn modulus and Fanning friction factor data modified to include variation in properties across the boundary layer.

The general form of the correlations used depends on the properties of the fluids involved. The variation in properties requires use of three different sets of correlation equations: (1) gaseous, (2) boiling, and (3) supercritical. The boundaries of these regions are given in Table 5-1 for the cold fluids. The combustion products are considered to always be gaseous. The boundaries on heat transfer regions for the cold fluids is based on information in Reference 6.

The governing equations for the data correlations are presented below by heat transfer region.

TABLE 5-1

BOUNDARIES OF HEAT TRANSFER REGIONS

Region	Min. Pressure, psia			Max. Pressure, psia			Min. Temperature, ^oR			Max. Temperature ^oR		
	N_2	O_2	H_2	N_2	O_2	H_2	N_2	O_2	H_2	N_2	O_2	H_2
Supercritical	500	800	200	2000	2000	2000	140	160	35	260	320	90
Boiling	15	15	15	450	700	180	140	160	35	Sat. Vap	Sat. Vap	Sat. Vap
Gas Parallel-Flow	15	15	15	2000	2000	2000	Sat. Vap: $P<P_{crit}$ 260: $P>P_{crit}$	Sat. Vap: $P<P_{crit}$ 320: $P>P_{crit}$	Sat. Vap: $P<P_{crit}$ 90: $P>P_{crit}$	$\Sigma\epsilon\leq 0.91$	$\Sigma\epsilon\leq 0.91$	$\Sigma\epsilon\leq 0.91$
Gas Counter-Flow	15	15	15	2000	2000	2000	500	500	500	$\epsilon<0.9$	$\epsilon<0.9$	$\epsilon<0.9$

a. Gaseous Heat Transfe! Region

This region includes the combustion products as well as the regions for the cold fluids defined in Table 5-1. Special considerations for the combustion products are presented in subheading d.

Convective conductance is obtained from the following equation:

$$h = \frac{G_b \; j_b \; C_{pb}}{Pr_b^{\;2/3}} \left(\frac{T_w}{T_b} \right)^n \tag{5-64}$$

The correction factors for variations in fluid properties are taken from Chapter 12 of Reference 7. All properties are based on the temperature of the bulk fluid. The Colburn heat transfer modulus j is a function of Reynolds number for the particular heat transfer surface employed, and is based on test data:

$$j_b = \Phi \left(Re_b \right) \tag{5-65}$$

where

$$Re_b = \frac{4 G_b r_h}{\mu_b} \tag{5-66}$$

The Fanning friction factor f is corrected for property variations according to the procedures outlined in Reference 7.

$$f = f_b \left(\frac{T_w}{T_b} \right)^m$$

where

$$f_b = \Phi \left(Re_b \right) \tag{5-67}$$

Values for m and n are given in Table 5-2.

TABLE 5-2

EXPONENTS FOR VARIATION IN PROPERTIES
IN GASEOUS HEAT TRANSFER

Mode of Heat Transfer	Heating ($T_w > T_b$)		Cooling ($T_w < T_b$)	
	m	n	m	n
<u>Inside Tubes</u>				
Laminar	1.0	0.0	1.0	0.0
Turbulent	-0.1	-0.5	-0.1	0.0
<u>Outside Tubes</u>				
No distinction between laminar and turbulent	0.0	0.02	0.0	0.02

b. <u>Boiling Heat Transfer Region</u>

The convective conductance h is based on Equations 3.9 and 3.12 of Reference 8 for flow inside a smooth tube:

$$\frac{Nu_{exp}}{Nu_{calc,\ vsp}} = \Phi\left(X_{tt}\right)$$

$$Nu_{calc,\ vsp} = 0.026\ Re_{vsp}^{0.8}\ Pr_v^{0.33}\left(\frac{\mu_v}{\mu_w}\right)^{0.14}$$

$$Re_{vsp} = \frac{4\ \rho_v\ U_{avg}\ r_h}{\mu_v} = \frac{4Gr_h}{\mu_v}\ \frac{\rho_v}{\rho_{avg}}$$

$$Pr_v = \frac{C_{pv}\ \mu_v}{k_v}$$

The average density ρ_{avg} is obtained from

$$\rho_{avg} = \frac{2\rho_l\ \rho_v}{\rho_l + \rho_v}$$

The above expression for Nu can be rewritten in terms of the Colburn j factor:

$$j_{calc,vsp} = \frac{0.026}{Re_{vsp}^{0.2}} \left(\frac{\mu_v}{\mu_w}\right)^{0.14}$$

Data points corresponding to the above relationship were used in the computer program. Convective conductance is given by:

$$h = \frac{j_{calc,vsp} G C_{pv}}{Pr_v^{2/3}}$$

In determining h, $j_{calc,vsp}$ was set equal to j_{exp}. Examination of the relationship between $Nu_{exp}/Nu_{calc,vsp}$ and χ_{tt} indicates that $Nu_{exp}/Nu_{calc,vsp}$ varies from 2.0 at the heat exchanger inlet to 0.5 at the outlet, and averages 1.0 over the length of the heat exchanger. Normally the critical tube wall temperature for freezing is located at the outlet, where the actual value of h on the inside of the tube is one-half its calculated value. Consequently, the probability of freezing at the outlet is diminished by the use of average values of h. At the inlet the temperature difference between the two fluids is greatest, so that a higher-than-average coefficient can be tolerated

The Fanning friction factor was based on data for severely dimpled tubes to simulate an orifice at the outlet. The Reynolds number used was Re_{vsp}.

c. Supercritical Heat Transfer Region

The convective conductance was based on the Shitsman correlation taken from Reference 6 for near-critical fluids:

$$Nu = Nu_b = 0.023 \, (Re_b)^{0.8} \, (Pr_{min})^{0.4}$$

where Pr_{min} refers to the smaller of the Prandtl number evaluated at the bulk temperature and the Prandtl number evaluated at the wall temperature. Rewriting this expression in terms of a Colburn j factor and convective conductance gives

$$h = \frac{j_b \; G_b \; C_{pb}}{{Pr_b}^{2/3}} \left(\frac{Pr_{min}}{Pr_b} \right)^{1/3}$$

where j_b is the value of the Colburn modulus evaluated at Re_b.

The friction factor is evaluated at Re_b and corrected by a viscosity ratio, as explained in Reference 7 for property corrections in liquids:

$$f = f_b \left(\frac{\mu_w}{\mu_b} \right)^m$$

where

$$m = 0.58 \quad \text{(Laminar)}$$

$$m = 0.09 \quad \text{(Turbulent)}$$

d. Compressed Liquids

Compressed liquids must be warmed from their compressed state to either a saturated or near-critical state before the heat transfer relationships presented in subheadings b and c above rigorously apply. The enthalpy change the liquid undergoes in reaching either of these states is much smaller than the enthalpy change it would undergo to arrive at the maximum energy limit of these states. Hence, it is assumed that little error is generated in using either boiling or supercritical heat transfer phenomena to apply to subcooled liquid.

e. Combustion Products

This subheading discusses special phenomena associated with the combustion products; heat transfer relationships are given in subheading a. The combustion products contain a condensable and freezable component in their water component. To avoid the flow instability and potential freezing problems which could arise from allowing water to condense on the tubes in a macroscopic scale, the outlet temperature of the combustion products is kept hotter than the dew point of the water component. However, the tube wall temperature is allowed to be as cold as 550°R, which will often be below the dew point of the water component. In this situation, some water will condense in local areas of the tube, only to reevaporate as the droplets rejoin the mainstream of the combustion products.

These areas of local condensation are transient because a local condensation will raise the external heat transfer coefficient, which in turn will raise the wall temperature, thus enhancing evaporation of the condensate. Allowing the tube wall temperature to locally fall below the dew point of the water component of the combustion products therefore is not expected to cause problems.

3. Equations for the Supercritical Heat Transfer Region

It was found that the supercritical heat exchangers tended to operate at very high cold fluid Reynolds numbers and had very high convective conductances for the cold fluid. These phenomena cause nearly all the cold fluid pressure drop to be due to flow acceleration. The large internal heat transfer coefficient causes the actual TCR to be independent of cold fluid pressure drop so that TCR can be set at nearly any desired value by addition or removal of insulation on the tubes, or using a noncompact core such as a spiral tube configuration.

a. Pressure Drop of Cold Fluid

From Equation 5-59, all pressure drop becomes due to flow acceleration when Reynolds number becomes very large; hence,

$$\Delta P = \frac{5.35 \times 10^{-10}\, G^2}{g_c}\left(\frac{1}{\rho_{out}} - \frac{1}{\rho_{in}}\right)$$

For supercritical fluids, $\rho_{out} \ll \rho_{in}$. Hence,

$$\Delta P = \frac{5.35 \times 10^{-10}\, G^2}{g_c\, \rho_{out}}$$

For the high pressure gaseous units the cold fluid pressure drop was also found to be due to flow acceleration. Hence, the above equation can be written

$$\frac{\Delta P_x}{\Delta P_o} = \frac{\rho_{o,out}}{\rho_{x,out}}$$

where the subscript "o" refers to the gas heat transfer region and the subscript "x" refers to the supercritical heat transfer region.

At the heat exchanger outlets, the density of both the high pressure gas and the supercritical fluid can be approximated by:

$$\frac{P}{\rho} = \frac{RT}{M}$$

Hence, for a given fluid at a given pressure

$$\frac{\Delta P_x}{\Delta P_o} = \frac{T_{x,out}}{T_{o,out}}$$

Parametric Study

The design model was studied parametrically over a wide range using the relationships and data discussed above. The parametric computer analysis was conducted as part of Contract NAS 9-11330, under subcontract from the Lockheed Missiles and Space Company (Reference 9). The insight and conclusions drawn from that program allowed the establishment of a convenient format for the computer results for use in the handbook-type procedure desired here.

The approach used in the parametric study is to give the user complete freedom in varying the 11 variables required to define a heat exchanger design, subject to the temperature limitations placed on the tube walls. To accomplish this with a data set of finite size, it is necessary for the user to determine the UA required for his particular heat exchanger. Calculating the required UA eliminates flow rates and temperatures from the list of independent variables. This leaves pressures, pressure drops, and fluid characteristics as the independent variables, which must be included in the data presentation. Consequently, the weight and volume data can be presented in the form of (W/UA) and (V/UA) as functions of fluid type, heat transfer region, fluid pressure, and fluid pressure drops.

The limitations on allowable temperatures of the heat transfer matrix requires that the thermal conductance ratio TCR also be presented in the same manner. Acceptable designs possess values of TCR within the TCR range defined by the maximum material temperature and the minimum wall temperature for avoidance of freezing. When this criterion is met, the UA for that design is calculated. The user then can calculate the heat exchanger weight and volume by multiplying (W/UA) and (V/UA) by UA.

It was found that (W/UA) is independent of flow rates of the fluids; however, (V/UA) is dependent on both W_c and P_h. Consequently, it is necessary to correct (V/UA) for P_h and W_c before multiplying by UA to obtain volume.

A typical set of TCR, (W/UA) and (V/UA) are presented as Figures 5-35, 5-36, and 5-37. The set shown is for gaseous oxygen in parallel flow with combustion products at 100 psia. Similar sets of curves are provided in the Design Reference Manual for the case of boiling. Gaseous and boiling heat transfer cases are also covered for hydrogen there. The data provided for oxygen is applicable to nitrogen due to the great similarity of these fluids.

I. Generation of Parametric Data

The data curves in Section 2 were generated in the following manner. A particular cold fluid is selected, and the heat transfer relationships applicable to the particular heat transfer region of interest are input to the heat exchanger design computer program. Then enough different combinations of hot fluid pressure, cold fluid pressure, hot fluid pressure drop, and cold fluid pressure drop are established to cover the entire range of parametric data. Next, fluid flow rates and inlet and outlet temperatures are selected which will result in a reasonable heat exchanger design. Then the computer program is used to determine the weight, volume, and thermal conductance ratio of an optimum heat exchanger at each combination of fluid pressures and pressure drops.

At each combination of pressures and pressure drops the computer generates over 400 separate heat exchanger designs covering all combinations of heat transfer surfaces inside the tube, tube spacings, tube diameters, and number of passes of the combustion products across the tubes which are considered reasonable. The weight, volume, and thermal conductance ratio of the optimum heat exchanger are then selected for use in the parametric data set.

The criteria for an optimum heat exchanger are light weight coupled with a core configuration and overall shape which is reasonable and easy to build.

The weight of the optimum heat exchanger is divided by the UA of the heat exchanger to generate one point for the (W/UA) data. The TCR of the optimum

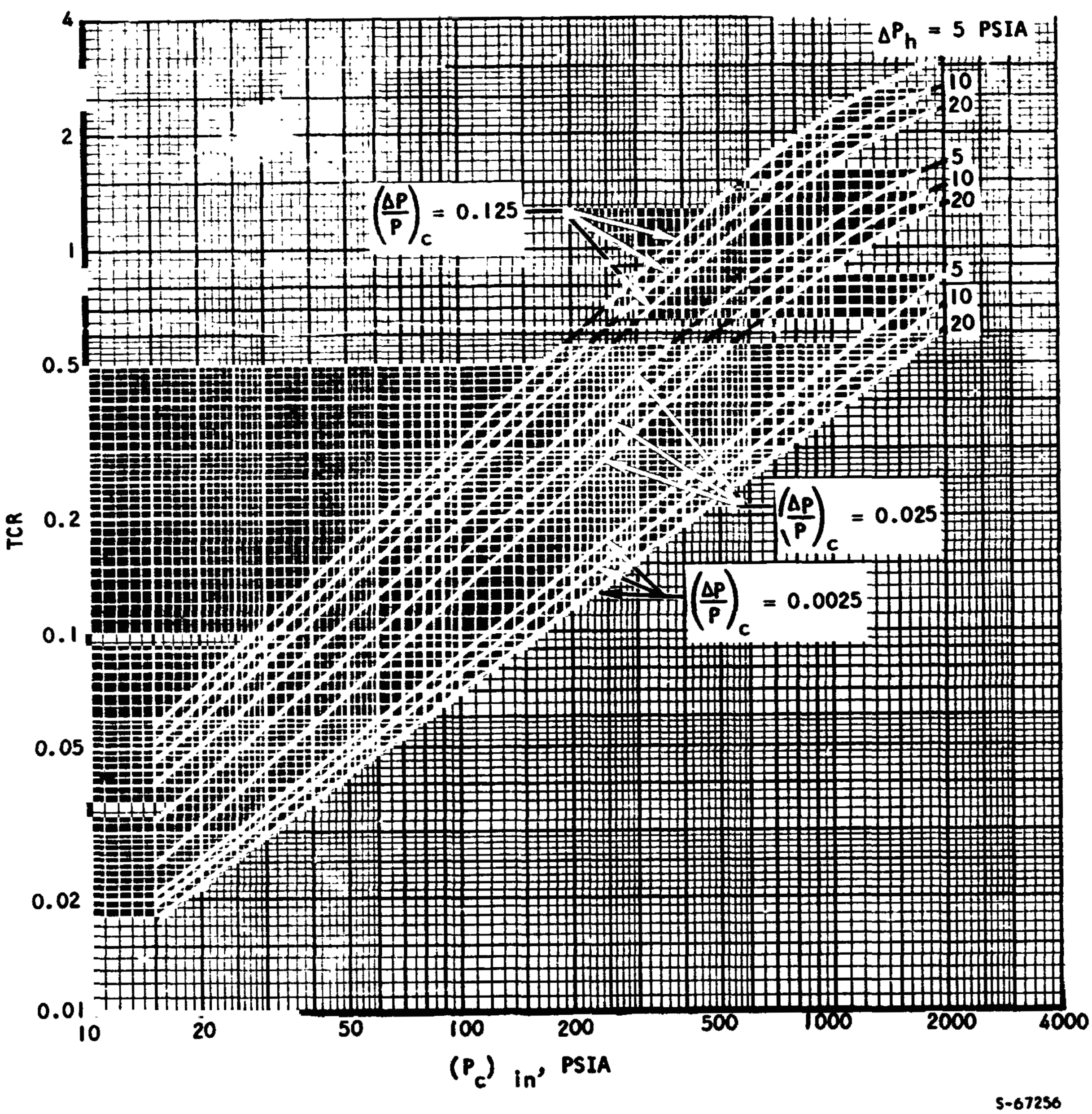

Figure 5-35. Thermal Conductance Ratio for Gaseous Oxygen with Combustion Products at 100 psia

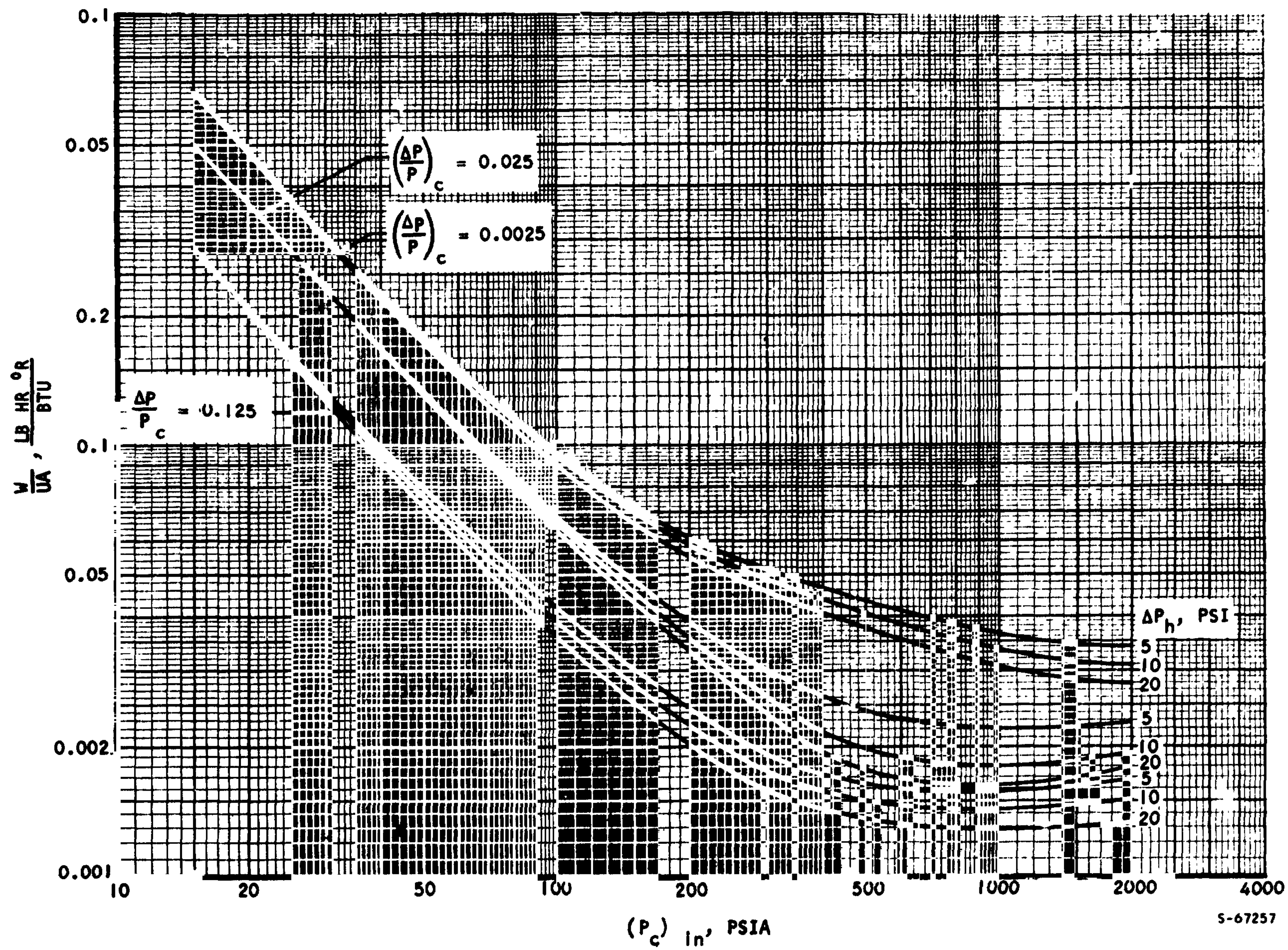

Figure 5-36. Weight Factor for Gaseous Oxygen with Combustion Products at 100 PSIA

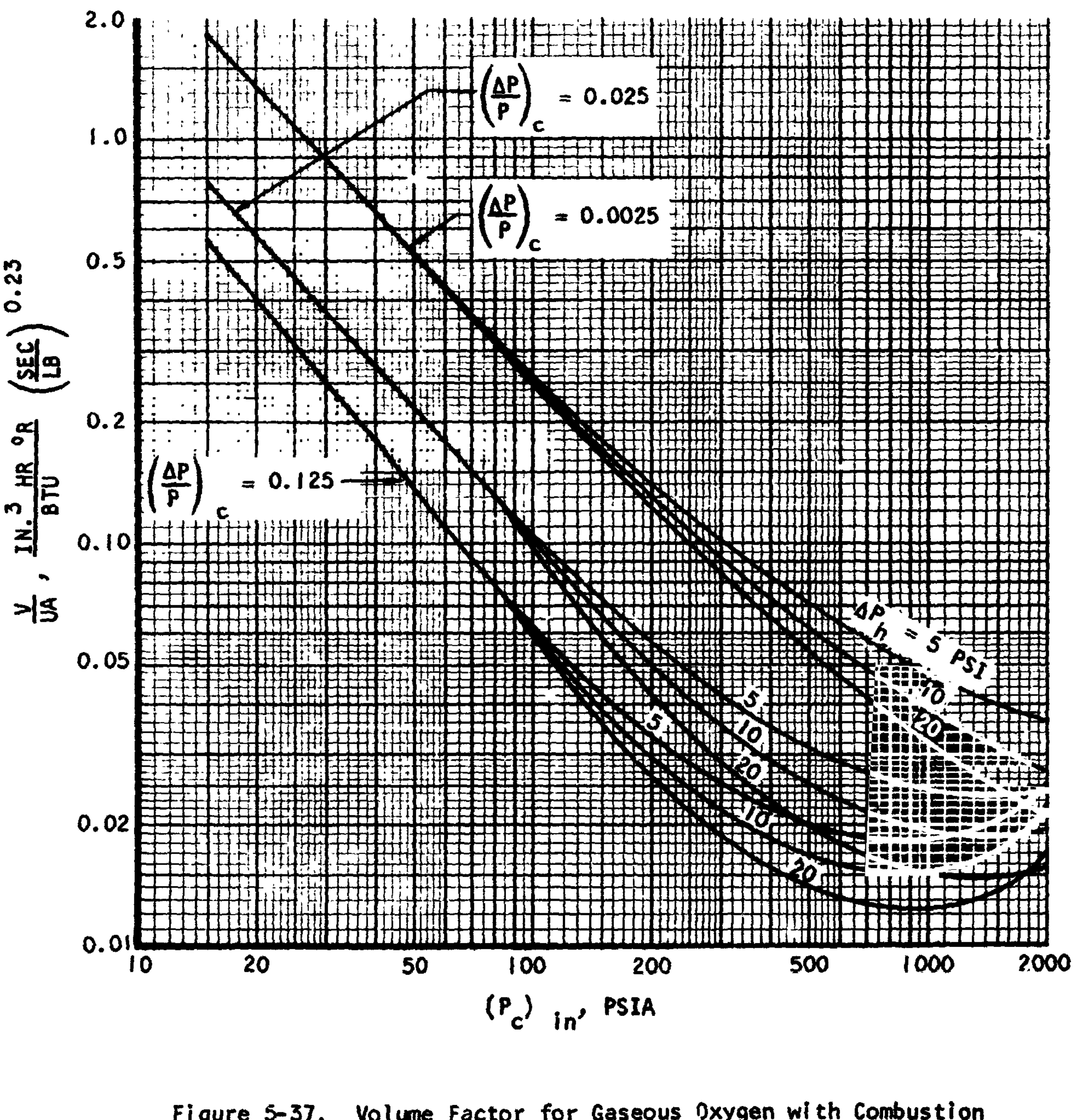

Figure 5-37. Volume Factor for Gaseous Oxygen with Combustion Products at 100 psia

heat exchanger is used as one point of the TCR data. Once the dependence of (V/UA) on cold fluid flow rate and combination products pressure is known, the heat exchanger volume is divided by UA, and the resulting quotient is multiplied by the appropriate factor for flow dependence to generate (V/UA). This value is used as one point of the (V/UA) parametric data.

The above procedures were repeated for all fluids and heat transfer regions of the study. The data points were then plotted, resulting in the curves presented in the Design Reference Manual.

2. Heat Exchanger Design Points

The values of inlet temperatures, outlet temperatures, and oxidizer-to-fuel ratio employed in generating the parametric data are chosen to be representative of a heat exchanger in the middle of a particular heat transfer region. Using an average heat exchanger permits substantial deviation in either direction without loss of accuracy.

a. Oxidizer-to-Fuel Ratio

An oxidizer-to-fuel ratio (OF) of 1.0 was used to generate the data curves. This value results in a combustion temperature of roughly 2000°R. If OF is doubled, the combustion temperature is about 35000°R, which is the maximum allowable value for the study. If OF is halved, the combustion temperature is 1200°R, which is approaching a minimum value practical for this class of heat exchanger. Therefore, OF = 1.0 represents a middle of OF values likely to be encountered.

b. Fluid Temperatures

It is expected that the majority of heat exchangers will be parallel flow units with N_{tu} between 0.5 and 2.2. Therefore, the heat exchangers used to generate the parametric data used an N_{tu} of roughly 1.0. This is obtained with an effectiveness range between 0.5 and 0.6, and a capacity rate ratio between 0.0 and 0.25. This is accomplished by using $T_{h,in}$ = 2000°R, $T_{h,out}$ = 1000°R, and $T_{c,in}$ as determined by Table 5-1. Cold fluid outlet temperature is established by Table 5-1 for the boiling and supercritical heat transfer regions.

For the gas parallel flow region, the cold fluid outlet temperature is set so that the temperature rise is in the middle of a band of reasonable cold fluid temperature rises. Table 5-3 presents outlet temperatures of the cold fluid.

TABLE 5-3

COLD FLUID OUTLET
TEMPERATURES FOR GAS PARALLEL
FLOW HEAT EXCHANGERS

Gas	Pressure, psia	Outlet Temperature, $^{\circ}R$
Oxygen	< 1000	400
	≥ 1000	500
Hydrogen	10 to 2000	350

No counterflow heat exchangers were designed. The counterflow core is identical to the gas parallel flow core in pressure drops, (W/UA), (V/UA), and convective conductances generated for a given pressure drop. Consequently, the gas parallel flow parametric data can be applied to gas counterflow cores.

c. <u>Fluid Flow Rates</u>

Except for cases involving flow surveys, the fluid flow rates are set so that heat exchanger weight is between 5 and 30 lb.

3. <u>Range of Pressures and Pressure Drops</u>

The range of pressures and pressure drops covered varies among heat transfer regions. Therefore, each heat transfer region will be discussed separately.

The pressure of the combustion products is always less than the cold fluid pressure for the cases investigated. For example, the hot gas pressures covered for gaseous oxygen at 1000 psia would be 7.5, 15, 30, 75, 150, 300, and 750 psia. All combinations of pressure drops would be covered at $P_{c,in}$ = 1000 psia, and all the above values of $P_{h,in}$. If the oxygen pressure were 40 psia, then all combinations of pressure drops would be investigated for $P_{c,in}$ of 40 psia and $P_{h,in}$ of 7.5, 15, and 30 psia. It was found that the minimum (W/UA) for all fluids and design cases consistently occurred at values of $P_{h,in}$ on the order of 100 psia. Thus, the plots presented are based on this combustion products inlet pressure.

a. Gaseous Oxygen

Hot fluid pressures investigated are 7.5, 15, 30, 75, 150, 300, 750, and 1500 psia. Cold fluid pressures investigated are 10, 20, 40, 100, 200, 400, 1000, and 2000 psia. Hot fluid normalized pressure drops $(\Delta P/P)_h$ investigated are 0.05, 0.10, and 0.20. Cold fluid normalized pressure drops $(\Delta P/P)_c$ investigated are 0.0025, 0.025, and 0.125.

b. Gaseous Hydrogen

Hot fluid pressures investigated are 7.5, 15, 30, 75, 150, 300, 750, and 1500 psia. Cold fluid pressures investigated are 10, 20, 40, 100, 200, 400, 1000, and 2000 psia. Hot fluid normalized pressure drops $(\Delta P/P)_h$ investigated are 0.05, 0.10, and 0.20. Cold fluid normalized pressure drops $(\Delta P/P)_c$ investigated are 0.002, 0.01, 0.05, and 0.20.

c. Boiling Oxygen

Hot fluid pressures investigated are 7.5, 15, 30, 75, 240, and 560 psia. Cold fluid pressures investigated are 10, 100, 300, and 700 psia. Hot fluid normalized pressure drops $(\Delta P/P)_h$ investigated are 0.05, 0.10, and 0.20. Cold fluid normalized pressure drops $(\Delta P/P)_c$ investigated are 0.0025, 0.025, and 0.125.

d. Boiling Hydrogen

Hot fluid pressures investigated are 7.5, 15, 30, 75, and 150 psia. Cold fluid pressures investigated are 10, 50, 100 and 180 psia. Hot fluid normalized pressure drops $(\Delta P/P)_h$ investigated are 0.05, 0.10, and 0.20. Cold fluid normalized pressure drops $(\Delta P/P)_c$ investigated are 0.002, 0.01, 0.05, and 0.2.

e. Supercritical Oxygen

It was found that supercritical heat exchangers would often not use a normal compact heat transfer matrix. The cases run on the computer to find this are as follows. Hot fluid inlet pressure is 600 psia. Cold fluid inlet pressure is 800 psia. Hot fluid normalized pressure drops $(\Delta P/P)_h$ investigated are 0.05, 0.10, and 0.20. Cold fluid normalized pressure drops $(\Delta P/P)_c$ investigated are 0.0025, 0.025, and 0.125. No further cases were run after inspection of the heat exchanger characteristics for the above cases indicated that the parametric data for the gas parallel flow heat transfer region could be used instead.

f. Supercritical Hydrogen

Comments applying to supercritical oxygen apply here as well. The cases run on the computer are as follows. Hot fluid inlet pressure is 150 psia. Cold fluid inlet pressure is 200 psia. Hot fluid normalized pressure drops $(\Delta P/P)_h$ are 0.05, 0.10, and 0.20. Cold fluid normalized pressure drops $(\Delta P/P)_c$ are 0.002, 0.01, 0.05, and 0.20.

4. Flow Dependence

In addition to the cases just presented, additional cases were run for the gas parallel flow heat transfer region to determine whether (W/UA), (V/UA), and TCR depended on fluid flow rates. To accomplish this, cases were run at several hot and cold fluid pressures, and the fluid flow rates were allowed to vary over the range of interest in the parametric study. It was found that (W/UA) and TCR display little if any dependence on flow rate. It was found that (V/UA) depends on both cold fluid flow rate and hot fluid pressure. These dependences are combined into a corrective factor.

The parameters used to investigate flow dependence varied in the following manner. Cold fluid pressures varied from 10 to 1000 psia; hot fluid pressures varied from 7.5 to 750 psia. Normalized pressure drops for the hot fluid varied from 0.05 to 0.2, and normalized pressure drops for the cold fluid varied from 0.001 to 0.20. Hydrogen flow rates varied from 0.2 to 8.0 lb per sec, and oxygen flow rates varied from 1.0 to 40 lb per sec.

5. <u>Parametric Cost Information</u>

The discussion thus far presented has noted that, while the design concept represents the state of the art in lightweight, reliable, high-temperature heat exchangers, considerable development effort remains to be accomplished. In particular, analytical and experimental verification of the structural design approach is necessary before the annular tube bundle concept at the 2000°R level can be considered fully developed.

This posed a problem in the establishment of cost trends for these heat exchangers. If the development effort known to be required were included in the nonrecurring cost trend, the costs evaluated by use of the Design Reference Manual would become extremely high for this heat exchanger type, resulting in an unfair comparison with the other heat sources. In addition, the nature of technology development programs makes these costs difficult to estimate.

Since the costs associated with verification of the concept and approach apply only to the first few designs executed at the 2000°R level, it was clear that the nonrecurring cost presented in the Design Reference Manual should be based on the assumption that the needed development has been carried out. Thus, the cost trends presented in Figure 5-38 are projections of the cost ultimately achievable for annular tube bundle designs based on AiResearch experience with tubular heat exchangers and evaluation of the design and development problems which can be expected in any unit of this level of sophistication.

<u>Use of Parametric Data</u>

Detailed instructions on use of the parametric data, including calculation forms, are provided in the Design Reference Manual. This information will not be reproduced in full here. The procedure employed is summarized in the logic diagram of Figure 5-39.

The technique used consists of five steps:

(1) Define interfaces of heat exchanger with remainder of system and combustion products source.

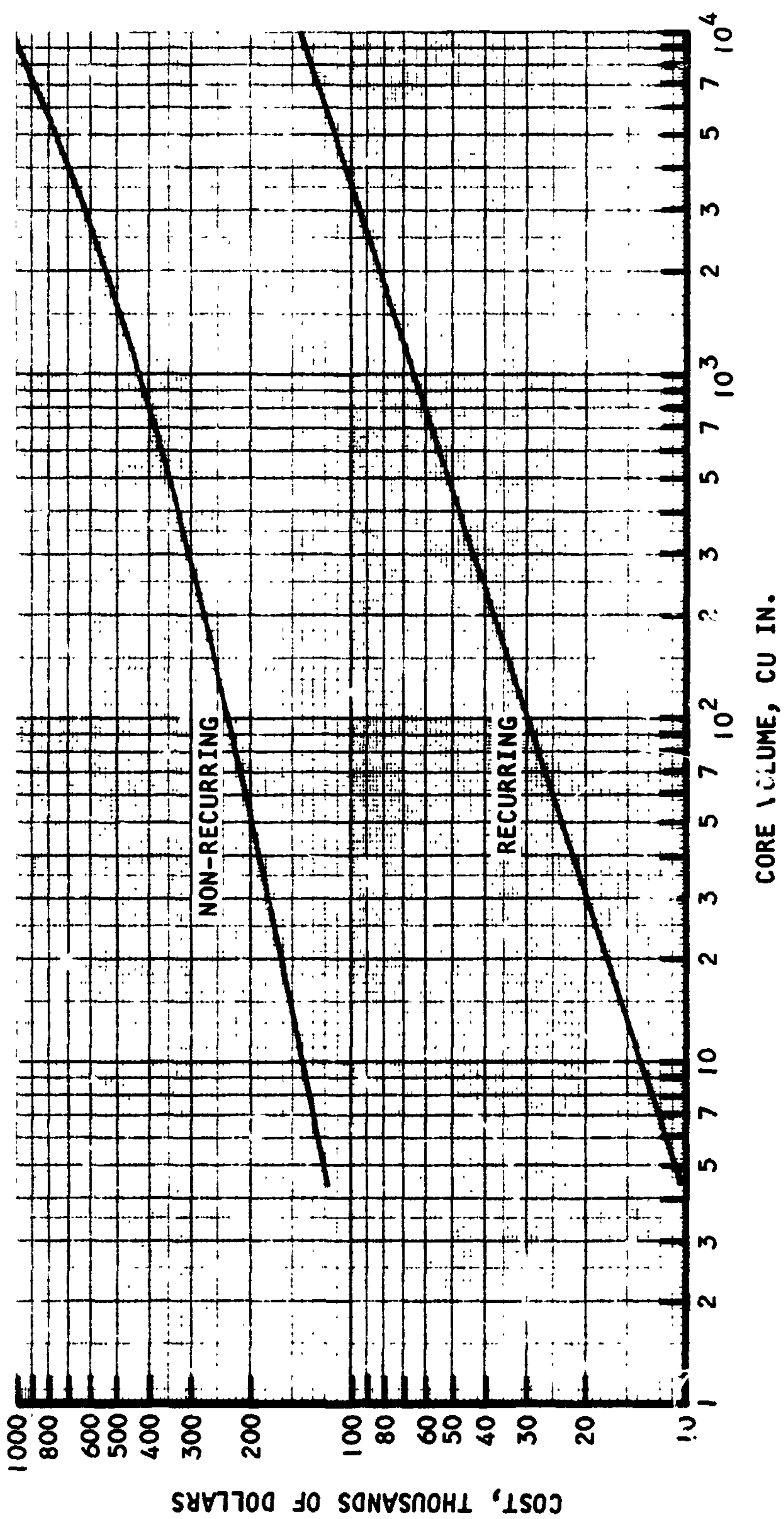

Figure 5-38. Cost Characteristics for Hot Gas Heat Exchangers

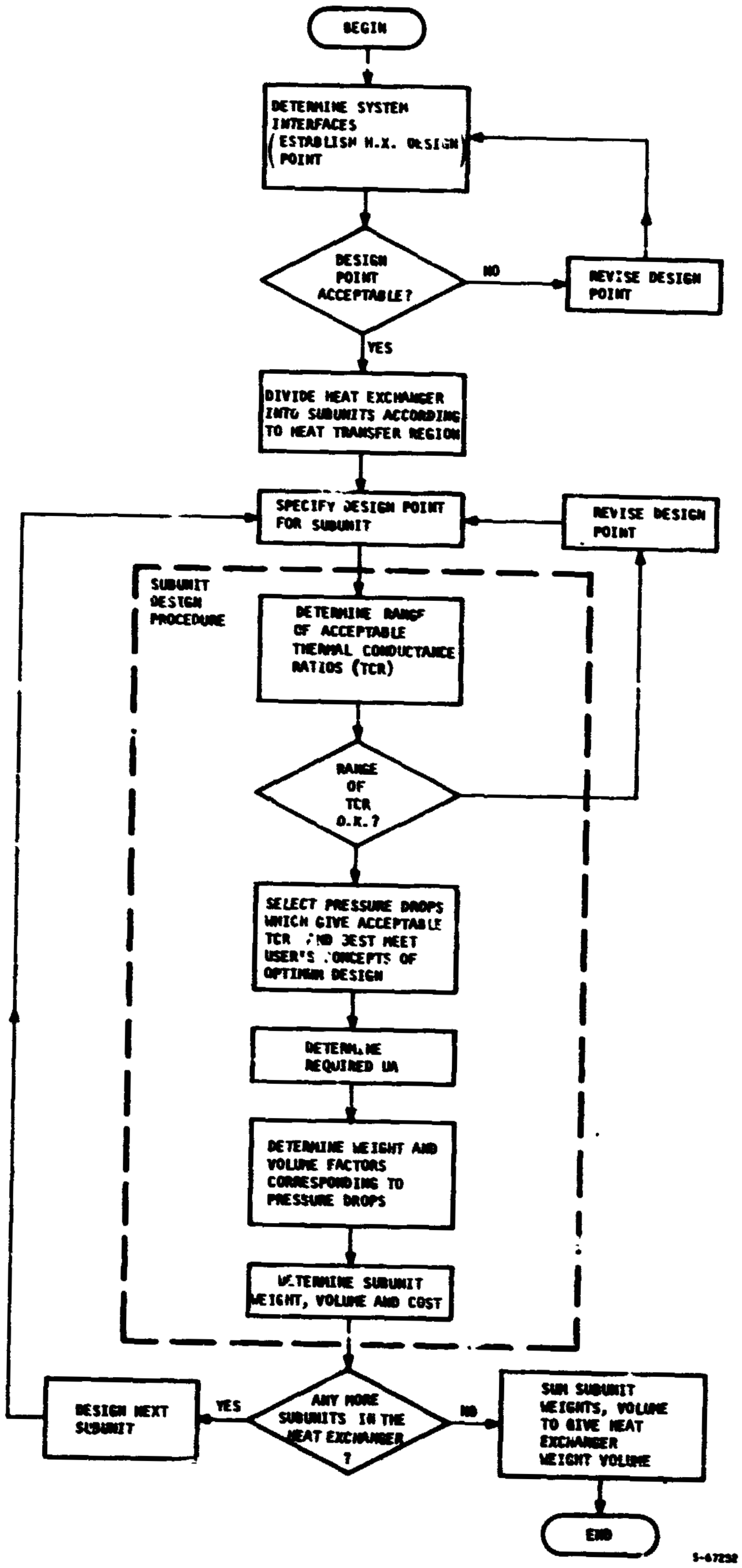

Figure 5-39. Hot Gas Heat Exchanger Design Procedure

(2) Divide heat exchanger into subunits according to heat transfer region.

(3) Define individual subunit design points.

(4) Obtain subunit designs.

(5) Sum subunit characteristics to establish weight, volume, and cost of complete heat exchanger.

The heat transfer regions which are treated here are:

- Boiling
- Supercritical
- Gas (parallel flow)
- Gas (counterflow)

The boiling or supercritical regimes may or may not be present. In any case, only one of these regimes will exist in a particular heat exchanger. Thus, at most, three subunits are possible. Many cases will result in one or two subunits.

Design of each subunit is based on establishment of a TCR range which ensures that the tube wall temperatures do not exceed the maximum temperature (1800°R) or present potential combustion products freezing problems. Figure 5-35, or its appropriate counterpart from the Design Reference Manual, is entered and pressure drops are selected such that the thermal conductance ratio range is satisfied. This may require revision of the pressure loss goals of the user. In the Manual, techniques are defined for extrapolation beyond the regions plotted. If this is necessary, correction of the final results will be required.

When hot and cold stream pressure drops have been selected in this manner, Figures 5-36 and 5-37 (or the appropriate counterparts) may be used to obtain (W/UA) and (V/UA) for the design point conditions considered. The overall conductance-heat transfer area product UA is then calculated, and subunit weight and volume (for all except supercritical subunits) is found from:

$$W = F_c F_h (W/UA)(UA), \text{ lb} \qquad (5\text{-}68)$$

and

$$V = F_c F_h \dot{w}_c^{\,n} (V/UA)(UA), \text{ cu in.} \qquad (5\text{-}69)$$

where

UA = calculated conductance-area product, Bt per hr-^{o}R

F_c = scaling factor resulting from extrapolation of cold fluid pressure drop

F_h = scaling factor resulting from extrapolation of hot fluid pressure drop

$\dot{w}_c$ = cryogen mass flow rate, lb per sec

n = 0.265 for hydrogen

n = 0.23 for oxygen and nitrogen

For supercritical units, the weight and volume are given by:

$$W = (W/UA)\ (UA) \left(\frac{1 + TCR_o}{1 + TCR_{max}}\right)\left(\frac{TCR_{max}}{TCR_o}\right) \qquad (5\text{-}70)$$

and

$$V = (V/UA)\ (UA)\ (\dot{w}_c)^n \left(\frac{1 + TCR_o}{1 + TCR_{max}}\right)\left(\frac{TCR_{max}}{TCR_o}\right) \qquad (5\text{-}71)$$

where

TCR_o = thermal conductance ratio selected from the applicable TCR plot

TCR_{max} = upper limit of thermal conductance ratio range

In addition, the cold stream pressure drop requires correction for supercritical subunits. The relations to be used are:

$\Delta P = 0.00286\ \Delta P_o\ (T_{c,out})$ for hydrogen

$\Delta P = 0.002\ \Delta P_o\ (T_{c,out})$ for oxygen or nitrogen where

ΔP_o = cold fluid pressure drop chosen from applicable TCR curve

$T_{c,out}$ = cold stream outlet temperature for complete heat exchanger

After weight and volume of each subunit is defined, these characteristics are summed to obtain total heat exchanger weight and volume. The total volume is then used to estimate the unit recurring and nonrecurring cost on Figure 5-38.

Heat exchanger weight is obtained from the following expression:

$$W_{tot} = \sum_{j=1}^{m} W_j$$

where j identifies each individual subunit and m is the total number of subunits in the heat exchanger. If W_{tot} is less than 5 lb, set W_{tot} equal to 5 lb. This value should represent a minimum weight of superalloy shell-and-tube, high-temperature heat exchangers, and accounts for mounting brackets, expansion bellows and interface fittings, all of which become increasingly significant when the basic heat exchanger weight falls below 5 lb.

Heat exchanger volume is obtained as follows:

$$V_{tot} = \sum_{j+1}^{m} V_j$$

If W_{tot} is less than 5 lb, heat exchanger volume should be modified as follows:

$$V = 5.0 \frac{V_{tot}}{W_{tot}}$$

where V_{tot} and W_{tot} refer to the unrevised values.

The calculated value of combustion products pressure drop may vary among subunits; however, the actual hot fluid pressure drops must be equal to the largest hot fluid pressure drop in the group. Thus,

$$\Delta P_{h,tot} = MAX\ (\Delta P_{h,j})$$

where $\Delta P_{h,j}$ refers to the pressure drop in the combustion products in any particular subunit. Outlet pressure of the combustion products is given by:

$$P_{h,out} = P_{h,in} - \Delta P_{h,tot}$$

The pressure drop of the cold fluid is equal to the sum of the pressure drops in the subunits. Thus, the outlet pressure of the cold fluid is given by:

$$P_{c,out} = P_{c,in} - \sum_{j=1}^{m} \Delta P_{c,j}$$

where $\Delta P_{c,j}$ is the cold fluid pressure drop of the jth subunit.

SECTION 6

PUMPS

The external pressurization system model requires characterization of fluid-moving devices over a very wide range. The maximum recirculation flow rates of Table 2-2 imply volumetric flows of approximately 100 cfm for oxygen and 200 cfm for hydrogen if vapor is recirculated to satisfy the liquid delivery requirements. Fortunately, examination of some typical line and heat exchanger pressure losses indicate the pump pressure rise will generally be of the order of 10 psi. The requirements call for single stage pumps of the centrifugal and Barske types.

All pumps are assumed to be driven through a magnetic coupling. This approach is considered mandatory in the case of the oxygen pumps and is beneficial, in terms of cost and power consumption, for the hydrogen and nitrogen pumps. The coupling, which employs samarium-cobalt magnets, allows submerged operation of the motor to be avoided. Thus, development costs are reduced and windage losses are minimized.

BASIC PUMP CHARACTERIZATION

The range of flow requirements for the recirculation loop appear to be satisfied by pumps having specific speeds ranging from 150 to 5000, where specific speed is defined as

$$N_s = \frac{N\sqrt{Q_g}}{H^{3/4}} \tag{6-1}$$

and N = rotational speed, rpm

Q_g = volumetric flow rate, gpm

H = head rise, ft-lb_f per lb_m

Or, if the volumetric flow rate is expressed in cfm rather than gpm:

$$N_s = 0.365\,\frac{N\sqrt{Q}}{H^{3/4}} \tag{6-2}$$

Under the incompressible flow assumption applying to this study, the head rise is adequately represented by

$$H = 144 \frac{\Delta P}{\rho_I} \qquad (6\text{-}3)$$

where ΔP = pump pressure rise, psi

ρ_I = inlet fluid density, lb_m per cu ft

The specific speed range noted covers the regimes of Barske pumps (N_S from 150 to 380) and centrifugal pumps (N_S from 380 to 5000). Above specific speeds of 5000, pump configurations would be of the axial-flow type.

Typical impellers for the two dominant types are shown in Figure 6-1. While the centrifugal design is familiar to users, the Barske pump is less common. Like the centrifugal machine, fluid enters at the eye, or center, of the impeller and is discharged at the periphery. Head rise is accomplished by rigid-body rotation of the mass of fluid within the housing, which need not have close clearances. The fluid is discharged through one or more venturi-like passages, thus effecting pressure recovery. The simplicity and loose impeller-to-housing clearances make this pump attractive in providing substantial head rises in low-flow situations, since small-scale units are readily designed.

The pump characterization adopted for this program is presented in Figure 6-2. Here, peak efficiency and head coefficient are plotted against specific speed, as composite curves for the three types of machines. The head coefficient is a dimensionless dynamic similarity parameter defined as:

$$\psi = \frac{g_c H}{U^2} \qquad (6\text{-}4)$$

where U = impeller tip speed, fps

The dimensionless data of Figure 6-2 is sufficient to define the overall geometric and performance characteristics of the pump types depicted. However, since the peak effic ·ıcy is presented, the efficiency of individual designs will require correction for degradation due to low Reynolds number or small impeller size.

The Barske pump information incorporated in Figure 6-2 is due to Balje' (Reference 10), while the centrifugal pump data i‿ drawn from Reference 11 and

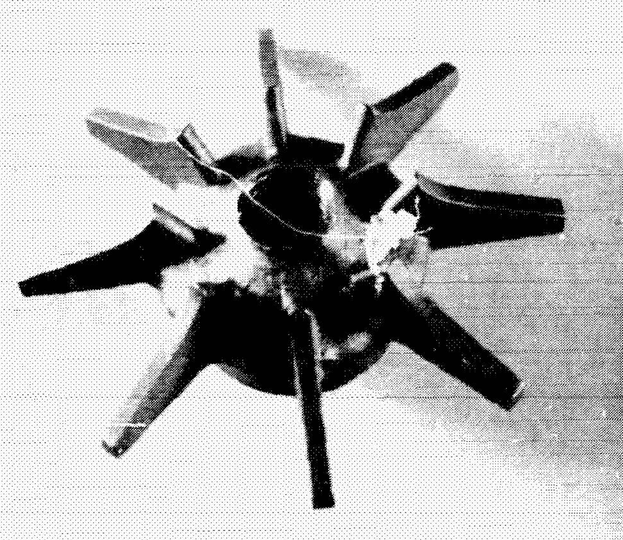

a. TYPICAL BARSKE IMPELLER

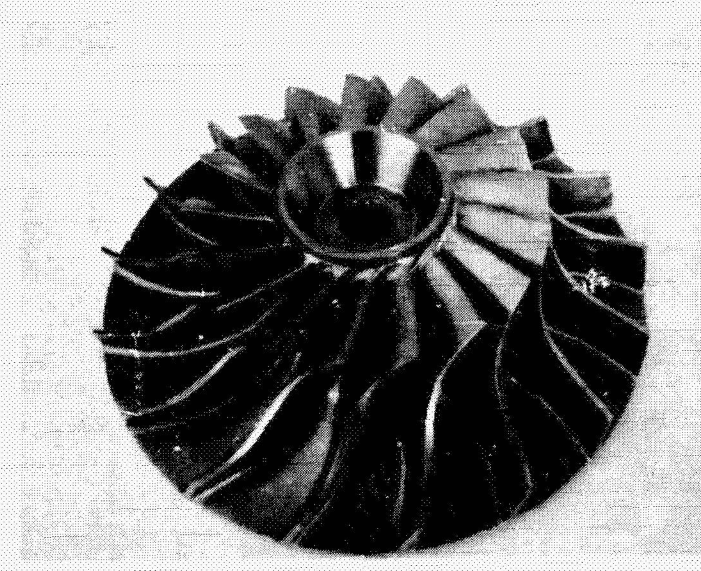

b. TYPICAL CENTRIFUGAL IMPELLER

F-13628

Figure 6-1. Pump Types Characterized

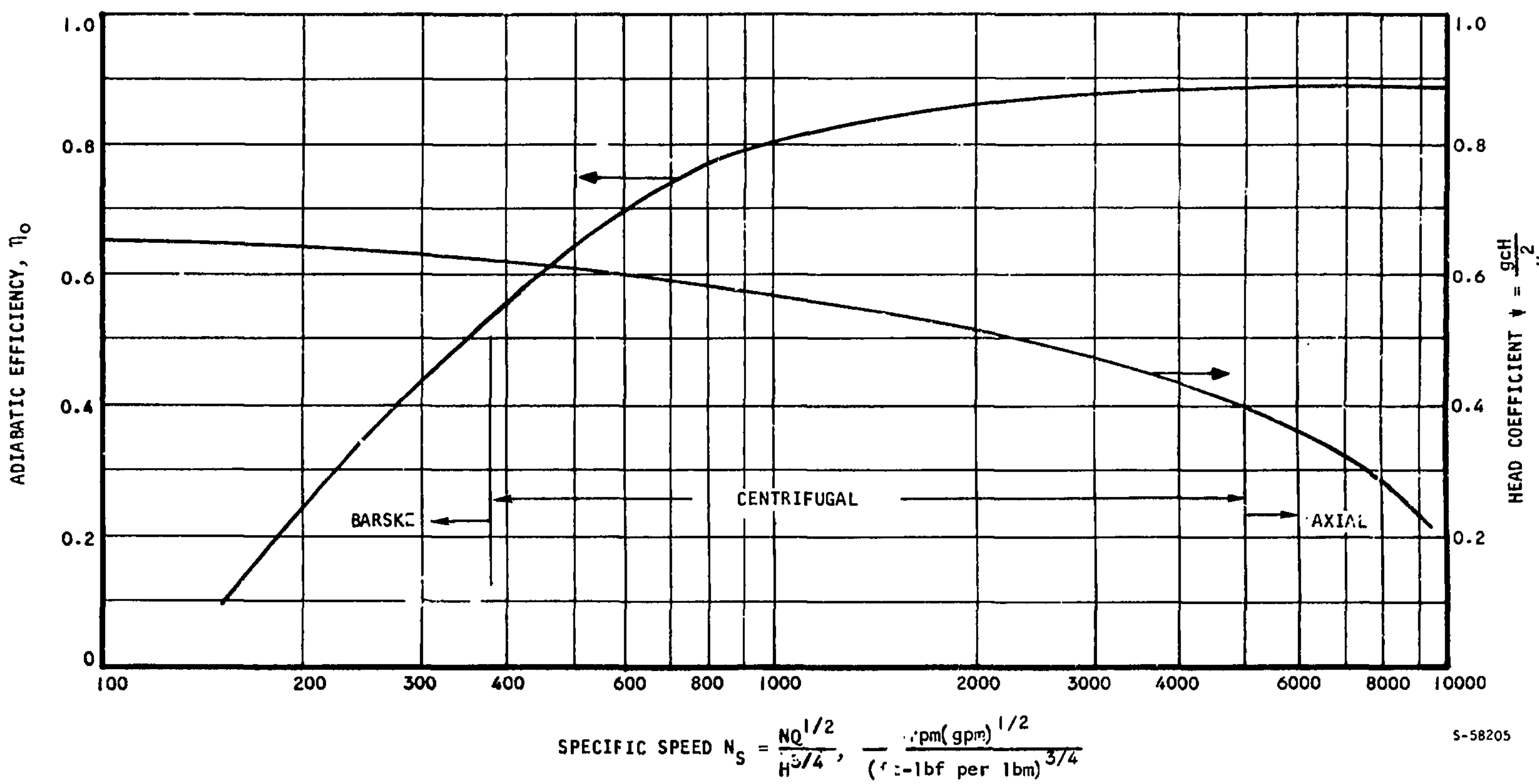

Figure 6-2. Pump Efficiency and Head Coefficient, at a Reynolds Number of 10^6

AiResearch experience in this field. The axial machine characteristics are taken from Eckert and Schnell (Reference 12).

PUMP DESIGN CHART

While there is no difficulty in the direct application of Figure 6-2 in the design of pumps for this program, it is possible to recast the basic design data in a form much more convenient for preliminary analysis. This is accomplished by observing that if the rotational speed dependence of the head coefficient curve is made explicit, a family of curves results. The impeller tip speed is given by:

$$U = \frac{\pi DN}{720} \tag{6-5}$$

where D = impeller tip diameter, in.

Using this definition in Equation 6-4, it is found that the ratio of head rise to the square of D is a function of ψ and N:

$$\frac{H}{D^2} = \left(\frac{720}{\pi}\right)^2 \frac{\psi N^2}{g_c} \tag{6-6}$$

Thus, for constant rotational speeds, H/D^2 may be plotted as a function of N_s/N.

This has been accomplished on curve 3 of Figure 6-3, resulting in the family of curves represented by the solid lines.

Since lines of constant specific speed can readily be superimposed on the family of H/D^2 curves, it is possible to base a canted set of coordinates on these lines. The efficiency curve of Figure 6-2 can then be incorporated into curve 3.

Noting that the head rise can be written as:

$$H = \frac{Q^{2/3}}{(N_s/N)^{4/3}}$$

and recalling Equation 6-3, it is possible to develop curves 1 and 2. Curve 4 requires only the obvious observation that H/D^2 can be plotted as a function of H and D.

When arranged as presented in Figure 6-3, the four curves represent a complete pump sizing tool. Note that all adjacent coordinate axes are identical, allowing orthographic projection of lines from one curve to the next. The information needed to employ Figure 6-3 is:

(a) Fluid inlet density, ρ_l, lb per cu ft

(b) Pump pressure rise, ΔP, psi

(c) Volumetric flow rate, Q:

$$Q = \frac{\dot{w}_c}{60\ \rho_l}\ ,\ \text{cfm}$$

As shown schematically in Figure 6-3, the curves are used as follows:

(a) Curve I is entered with ρ_l and ΔP, defining the head rise, H.

(b) From the point, a line should be parallel to the abscissa, across curve 2 to the 45-deg fold line.

(c) The volume flow, Q, is located along the projected line in curve 2. From this point, a line is projected down across curve 3, parallel to the ordinate.

(d) The permissible pump operating points lie along the line across curve 3. Selection of a speed on this curve fixes the pump design point.

(e) From any permissible operating point, it is possible to read the corresponding peak efficiency by projecting a line, parallel to the lines of constant specific speed, to the dashed efficiency curve. Comparison of the efficiency possible at permissible design points allows the speed to be rapidly chosen.

(f) Projection of lines from the chosen design point across curve 4 and from the point defined by the head rise line on the 45-deg fold line across curve 4 define the impeller diameter at their intersection on that curve.

Thus, Figure 6-3 allows H, N, N_s, η and impeller diameter D to be evaluated quickly. The pump design task is completed after applying several checks and corrections to the results obtained graphically on this chart.

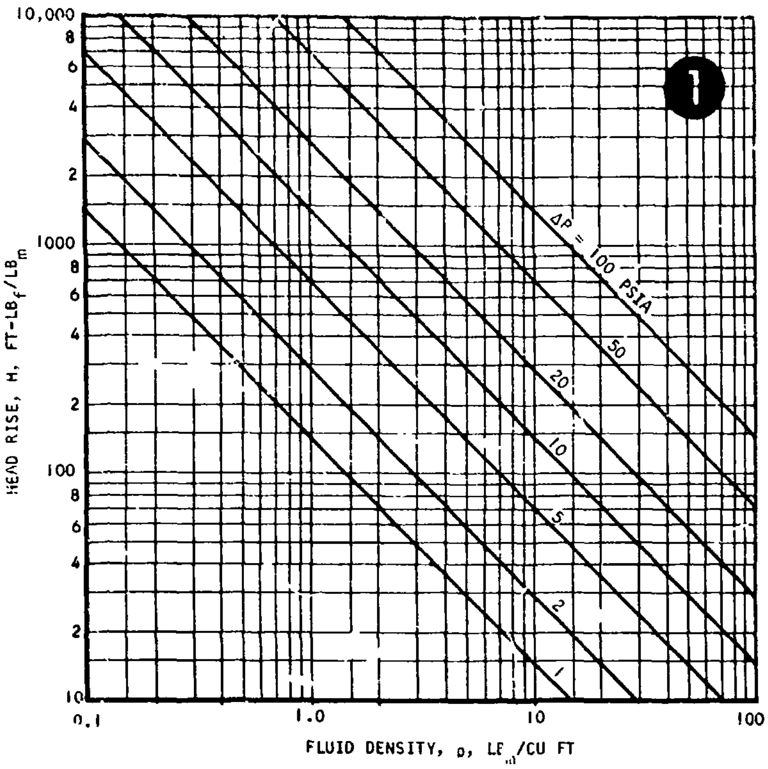

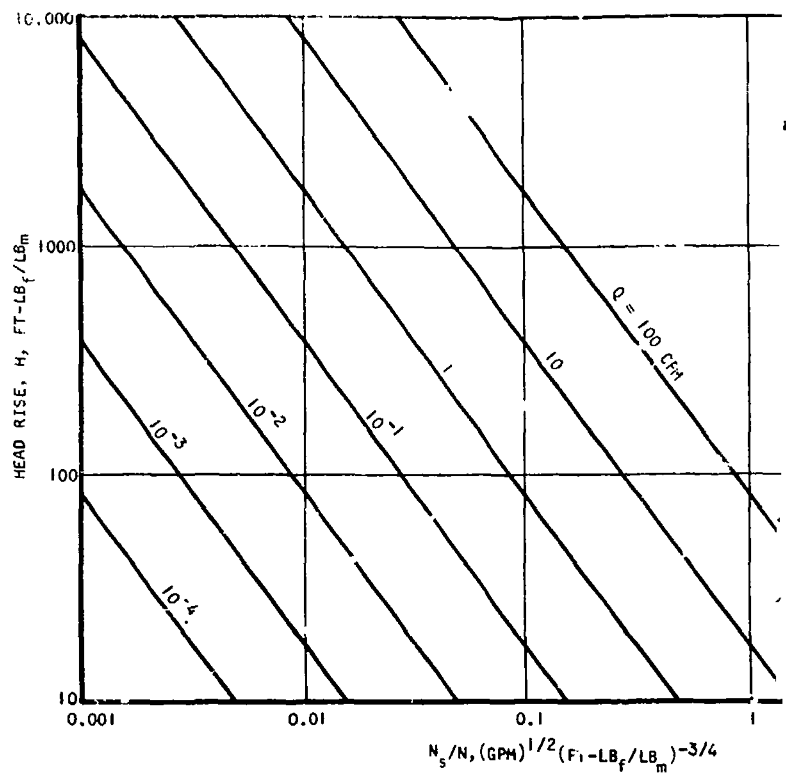

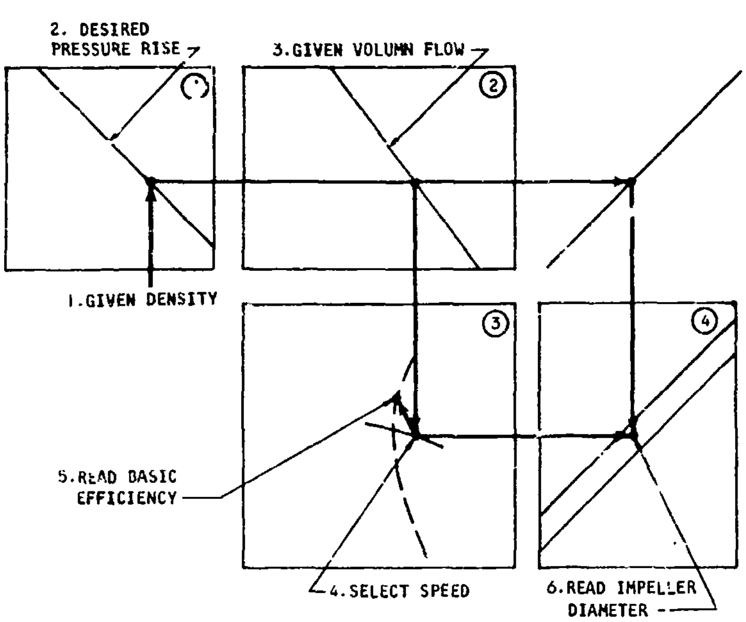

SCHEMATIC INSTRUCTIONS FOR USE OF CHART

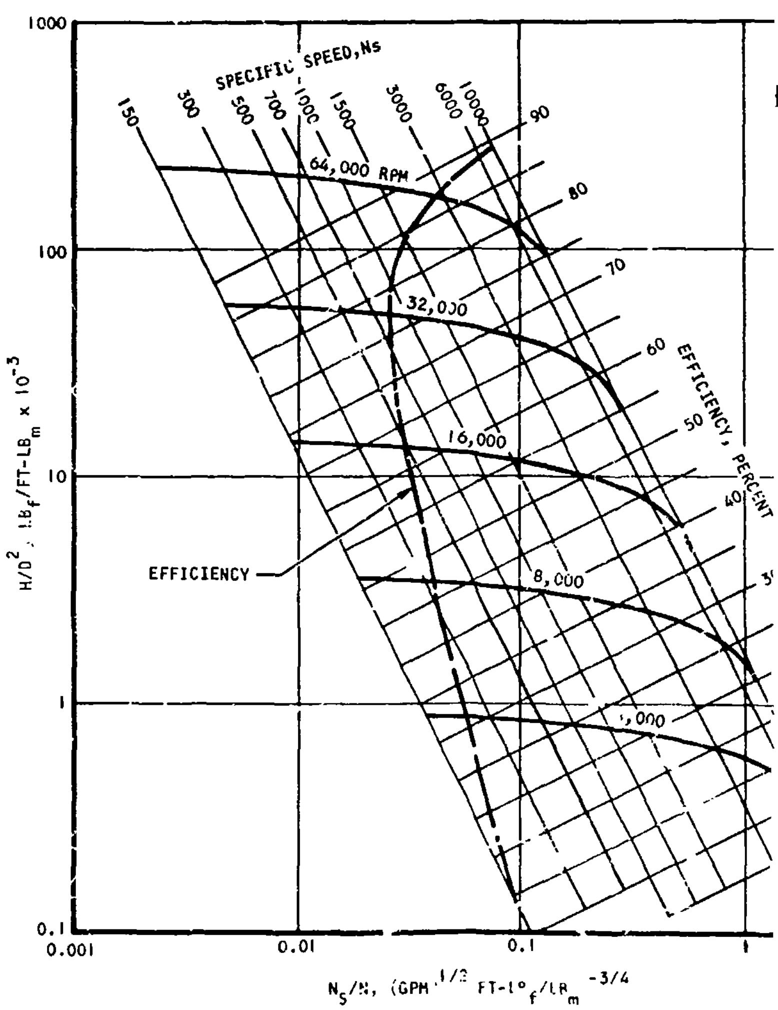

FOLDOUT FRAME 2

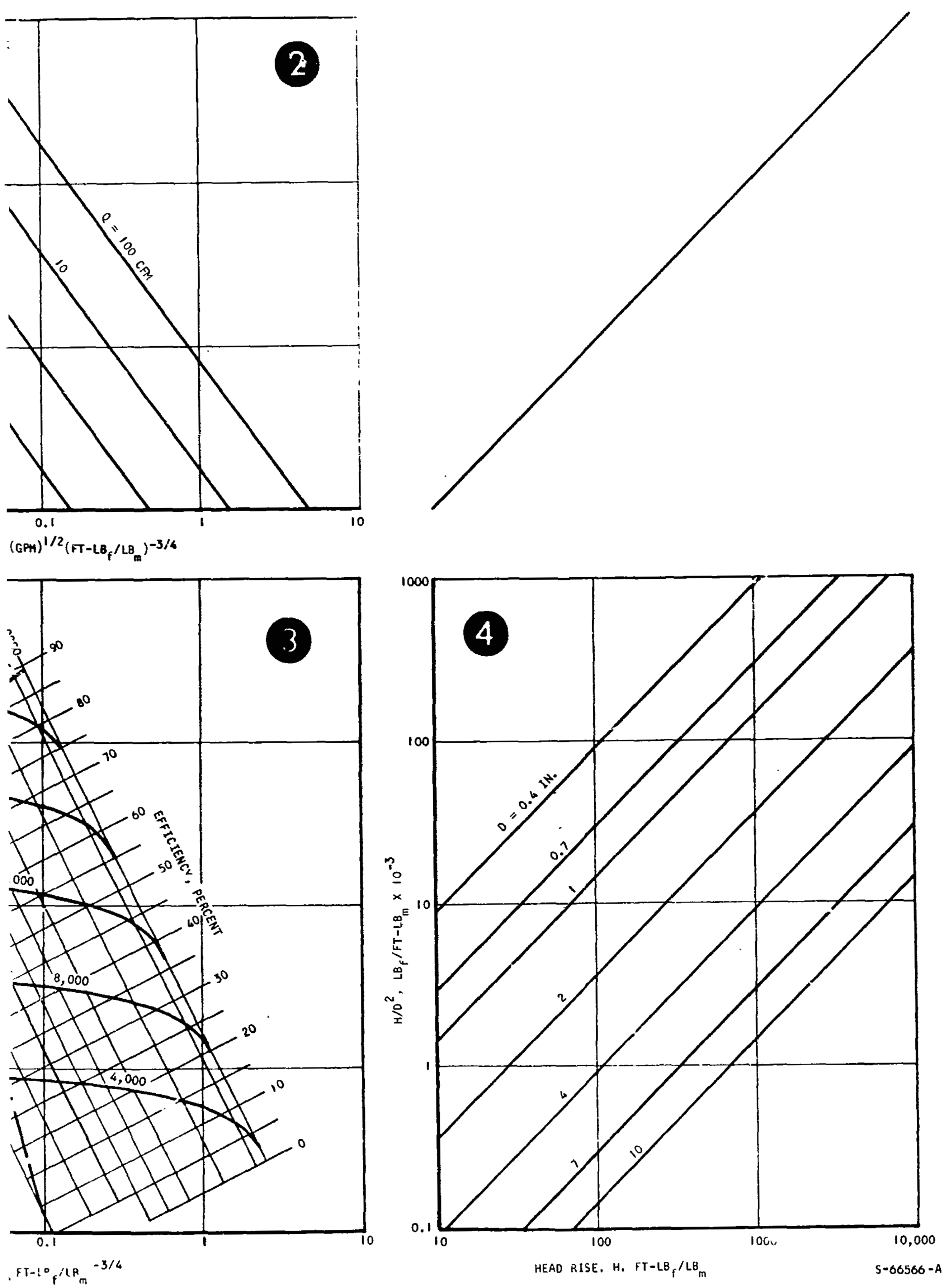

Figure 6-3. Basic Pump Characteristic Curves

PRECEDING PAGE BLANK NOT FILMED

The pump type selected is indicated by the specific speed. The approximate boundaries for the types available are:

Type	N_s Range
Barske	150 to 380
Centrifugal	380 to 5,000
Axial	5,000 to 10,000

In selecting the speed at the design point, the motor type to be chosen must be considered. With the brushless dc motor, any speed in the 4,000 to 64,000 rpm range characterized can be selected. In the case of the 400 Hz induction motor, six discrete speeds are available, corresponding to pole numbers from 2 to 12. The permissible speeds for induction motor-driven pumps are:

Number of Poles	Speed, rpm
2	22,800
4	11,400
6	7,600
8	5,700
10	4,560
12	3,800

CORRECTION OF DESIGN POINT

Impeller Tip Speed

After es ablishing a design point in Figure 6-3, the impeller tip speed must be checked. For pumps of the types presented here, a tip speed of 1500 ft per sec represents the boundary of well-developed technology. By comparing the data of Figure 6-4 with the impeller diameter and the shaft speed, it can be determined if this limit has been exceeded. If so, a lower speed should be selected in Figure 6-3.

In extreme cases reduction in speed will not suffice to satisfy this limit. When this occurs, a multi-stage pump is required. Such designs can be investigated by dividing the total pressure rise among two or more stages. The volume flow for each succeeding stage must be based on the fluid inlet conditions for that stage. If the multi-stage unit is considered to be driven by a single motor, the speed must be chosen at the same value for each stage and stage power values then summed to obtain the total motor power rating.

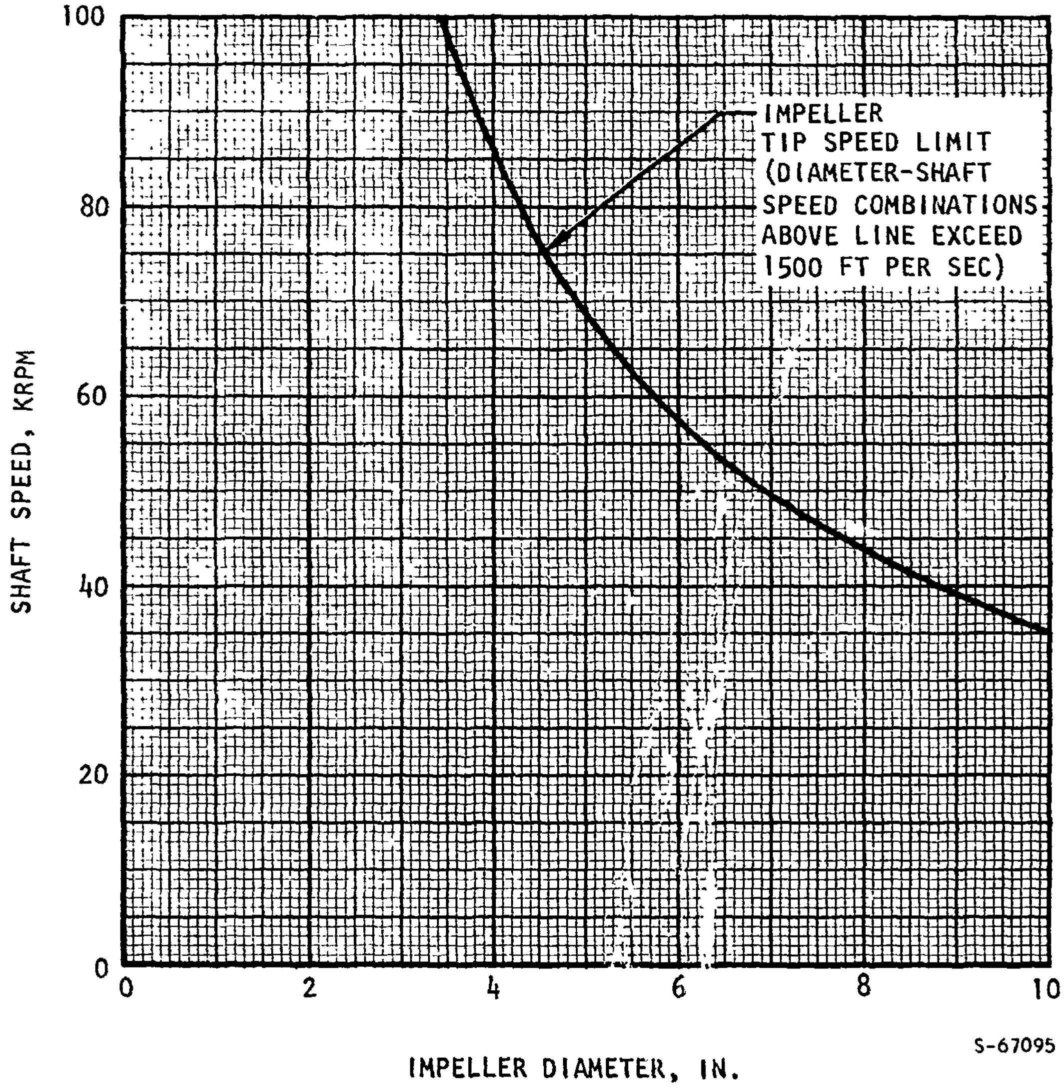

Figure 7-3. Impeller Tip Speed Limit Check

Efficiency Corrections

Two corrections may have to be applied to the peak efficiency value obtained in Figure 6-3. In Figure 6-5, the effect of impeller Reynolds number is shown, as a function Reynolds number and specific speed. For our purposes, the impeller Reynolds number is given by:

$$Re_i = 5411 \frac{D^2 N\rho_I}{\mu_I} \qquad (6\text{-}7)$$

where μ_I = dynamic viscosity at inlet conditions

Figure 6-6 represents the effect of impeller size on efficiency of wheels below 4-in. diameter. The corrected efficiency is thus found to be:

$$\eta = \left(\frac{\eta}{\eta_o}\right)_R \left(\frac{\eta}{\eta_o}\right)_S \eta_o \qquad (6\text{-}8)$$

where $\left(\frac{\eta}{\eta_o}\right)_R$ is the factor obtained from Figure 6-5

$\left(\frac{\eta}{\eta_o}\right)_S$ is the factor obtained from Figure 6-6

Using the corrected efficiency, the shaft power requirement can be calculated from:

$$PWR_S = 5.05 \times 10^{-7} \frac{\dot{w}_c H}{\eta}, \text{ hp} \qquad (6\text{-}9)$$

For small pumps, a lower limit on shaft power should be set, since Equation 6-9 will be found invalid in the regime where parasitic losses are dominant. As a rule of thumb, 30 w is the lowest power level that will be observed. Thus, if

$PWR_S < 0.04$ hp

set $PWR_S = 0.04$ hp

The design procedure discussed above is summarized, in schematic form in Figure 6-7.

Cavitation Considerations

Investigation of the pump requirements of external pressurization systems indicates the pressure rise will generally be well within the 100 psi range provided. Under these conditions, cavitation in liquid-handling pumps does

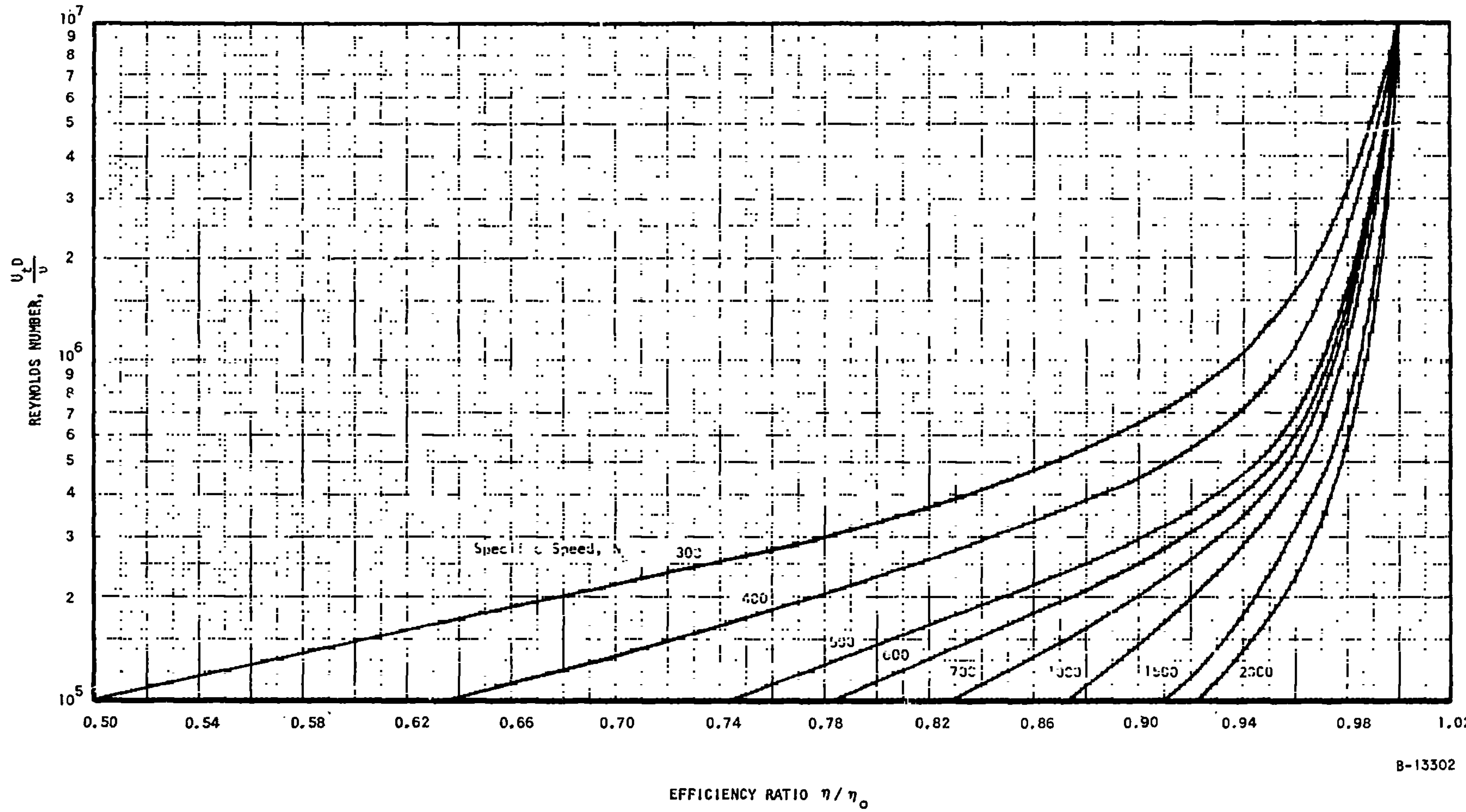

Figure 6-5. Reynolds Number Efficiency Correction

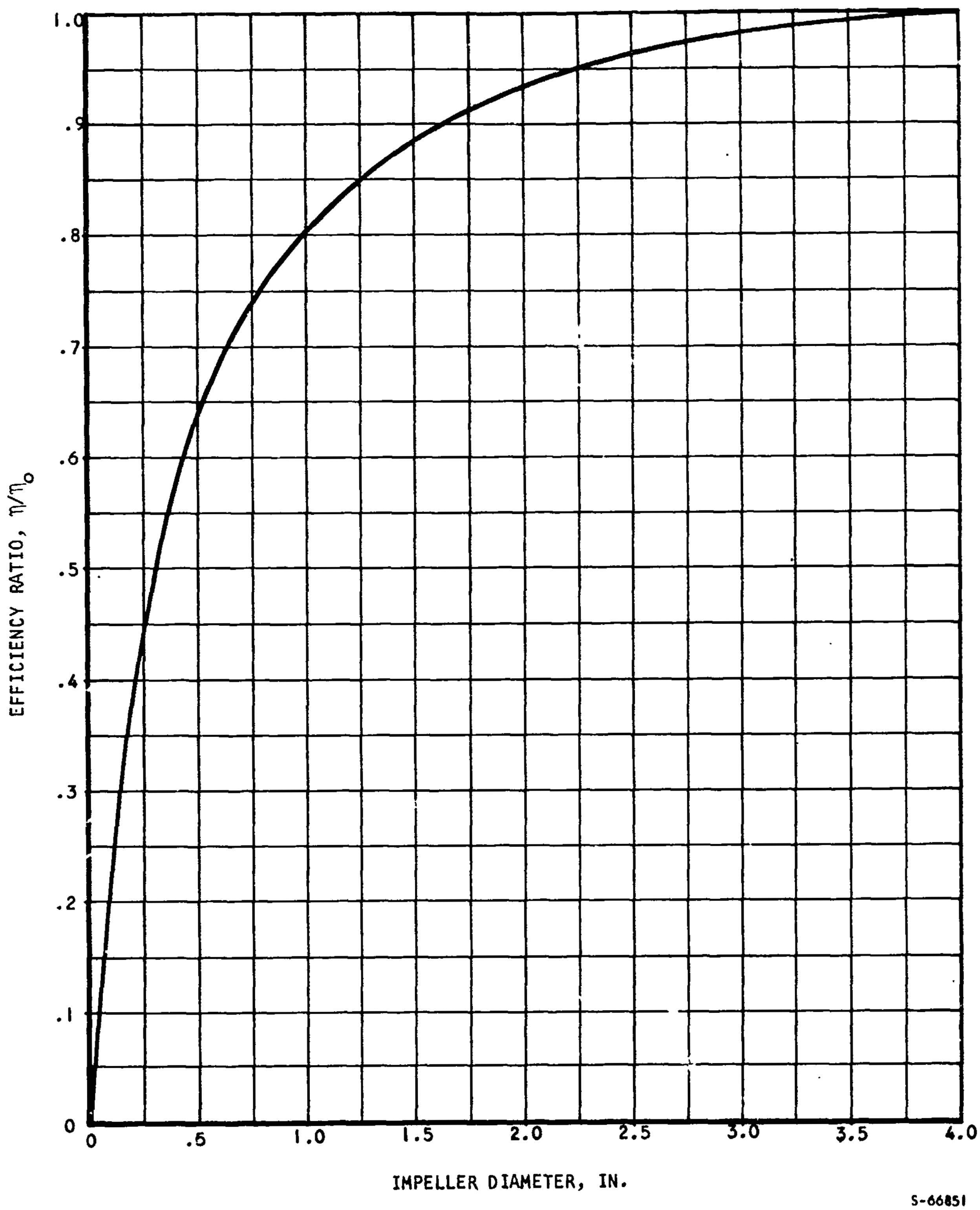

Figure 6-6. Efficiency Correction Factor for Pump Impellers Smaller than Four Inches

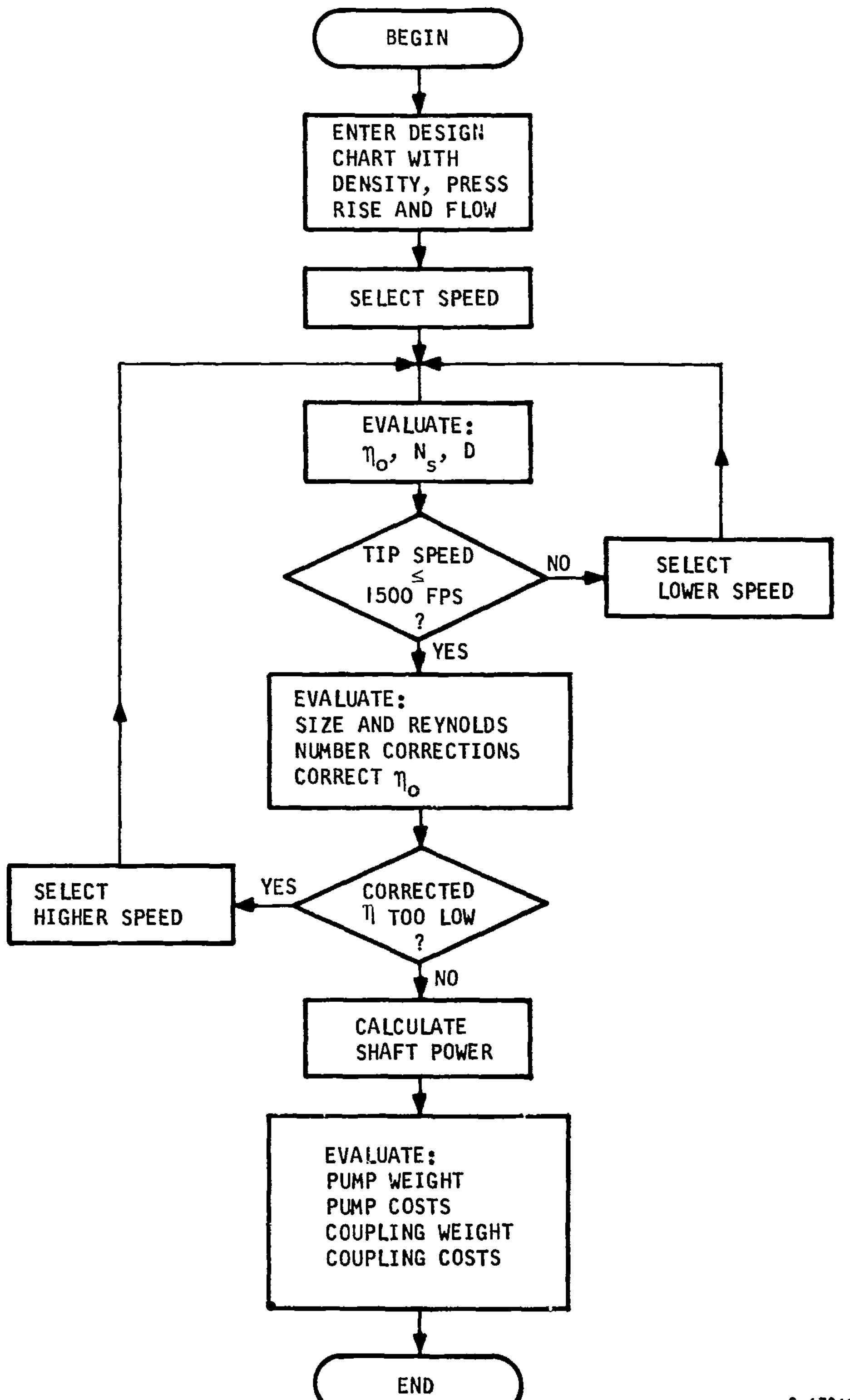

Figure 6-7. Pump Design Procedure

not present a problem. This can be verified in Figures 6-8 and 6-9, where the net positive suction pressure (NPSP) required at the pump inlet is shown for hydrogen, and oxygen and nitrogen, respectively. Figure 6-8 is based on a suction specific speed of 100,000, while the oxygen and nitrogen NPSP in Figure 6-9 is based on a value of 50,000. The suction specific speed is defined as

$$S = \frac{N\sqrt{Q}}{\left(\frac{NPSP}{\rho_l}\right)^{3/4}} \qquad (6\text{-}10)$$

The values referenced for the three fluids represent those readily achievable by the available approaches to inlet and inducer design.

Weight and Cost Characteristics

Weight of the pump alone, including the housing but excluding the magnetic coupling and drive motor, is presented in Figure 6-10. This information is taken from Reference 13, which is a study of pumps similar to those considered here.

Pump cost, also as a function of impeller diameter, is shown in Figure 6-11. These trends are assembled from historical cost data for AiResearch centrifugal and Barske pumps. The slight rise in recurring (or hardware) cost indicates the relative insensitivity of the Barske design to clearance ratios.

MAGNETIC COUPLING CHARACTERISTICS

Many pumps and compressors require that the aerodynamic or hydrodynamic section be sealed from the driving elements. Typical applications of this type are air turbine-driven refrigerant compressors and oxygen pumps and compressors. Although shaft seals have been developed for such machines, they are usually mechanically complex and eventually permit significant leakage. Safety implications do not allow reliance on seals for oxygen systems.

The magnetic coupling offers a convenient solution to this design problem. This device consists of two magnetic halves arranged so that the driving half induces rotary motion of the driven half. A diaphragm may be located between the halves, allowing hermetic sealing of the driving and driven sections. To use magnetic couplings effectively, AiResearch initiated a company-sponsored

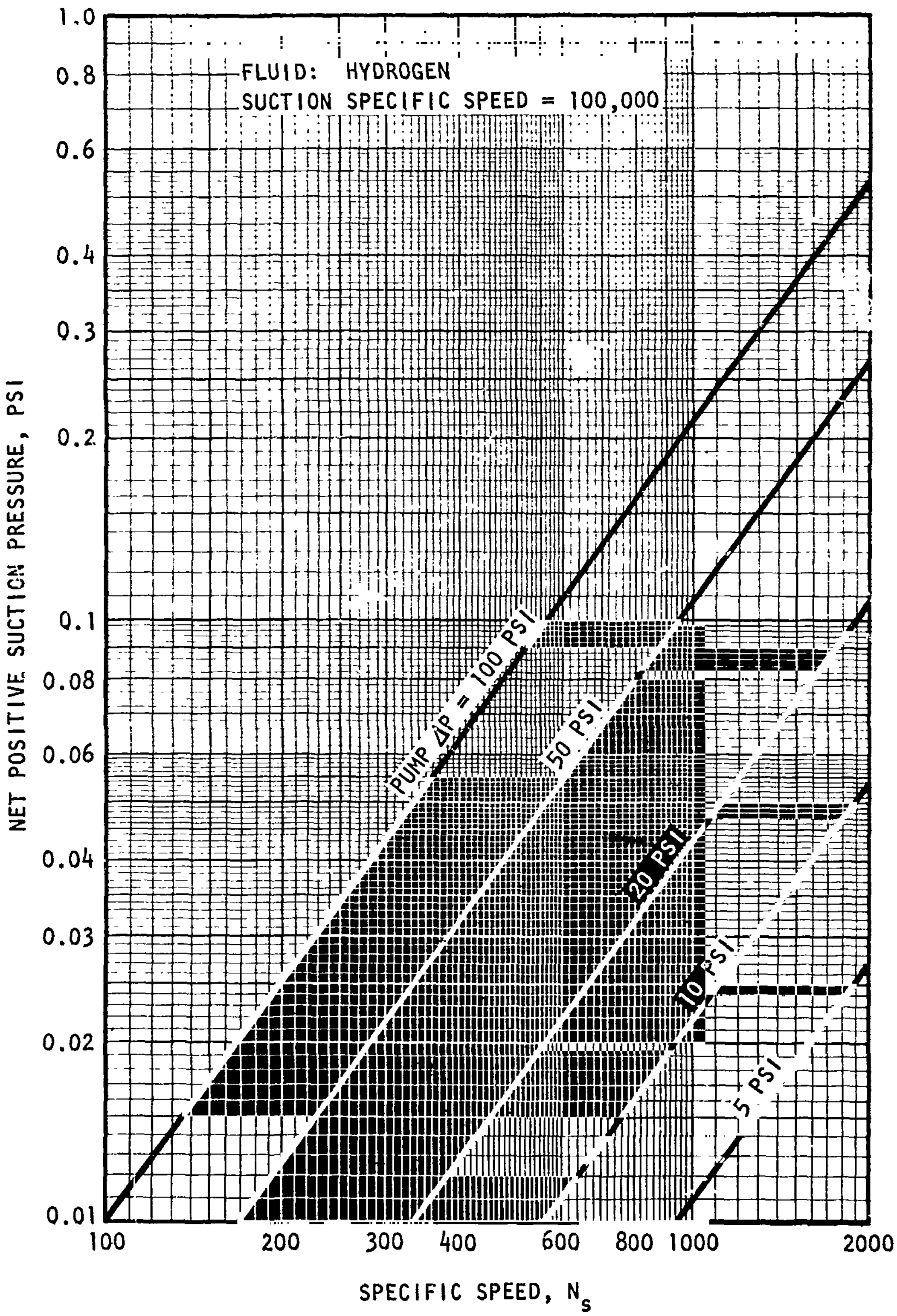

Figure 6-8. Net Positive Suction Pressure for Liquid Hydrogen Pumps

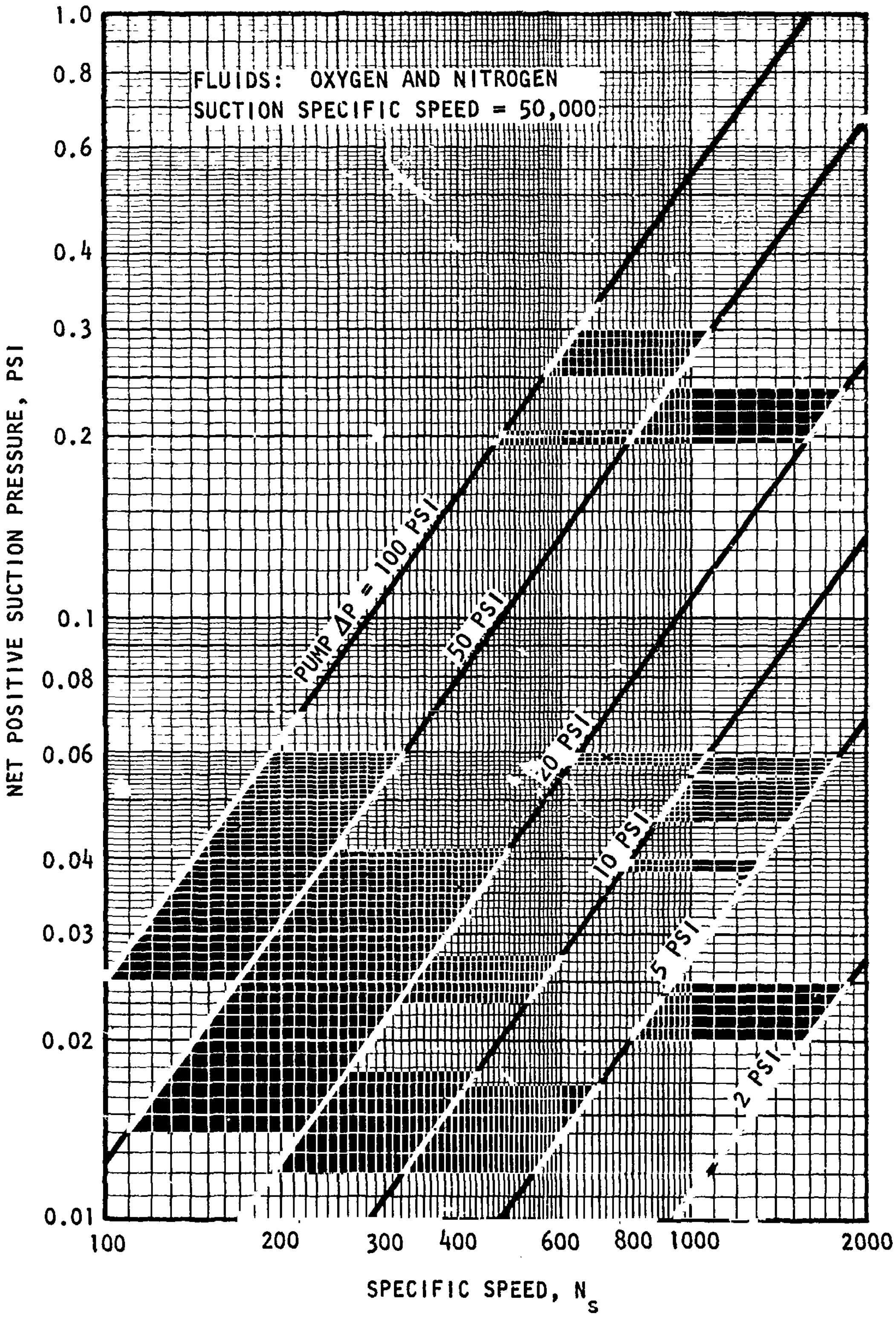

Figure 6-9. Net Positive Suction Pressure for Liquid Oxygen and Nitrogen Pumps

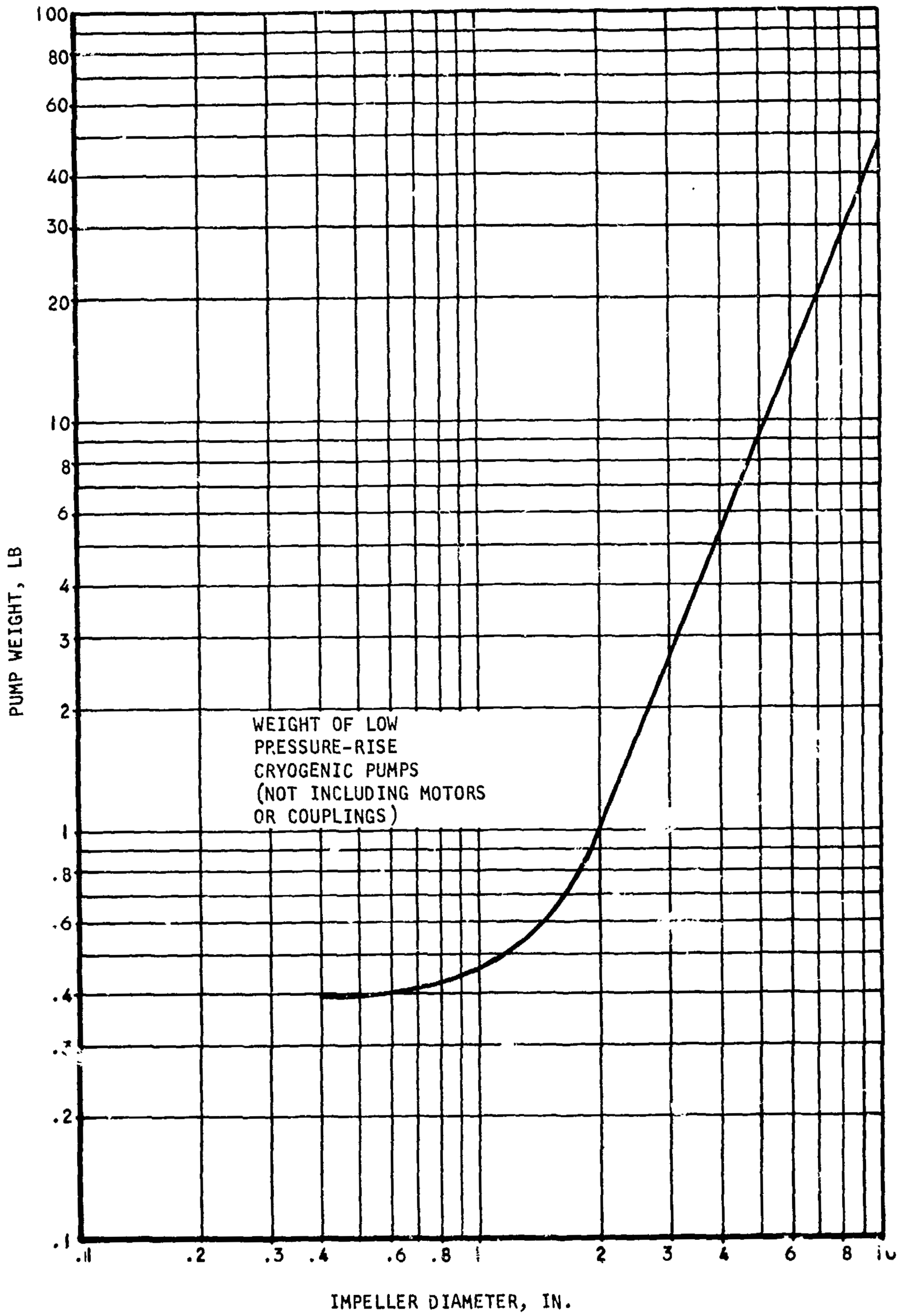

Figure 6-10. Pump Weight Characteristics

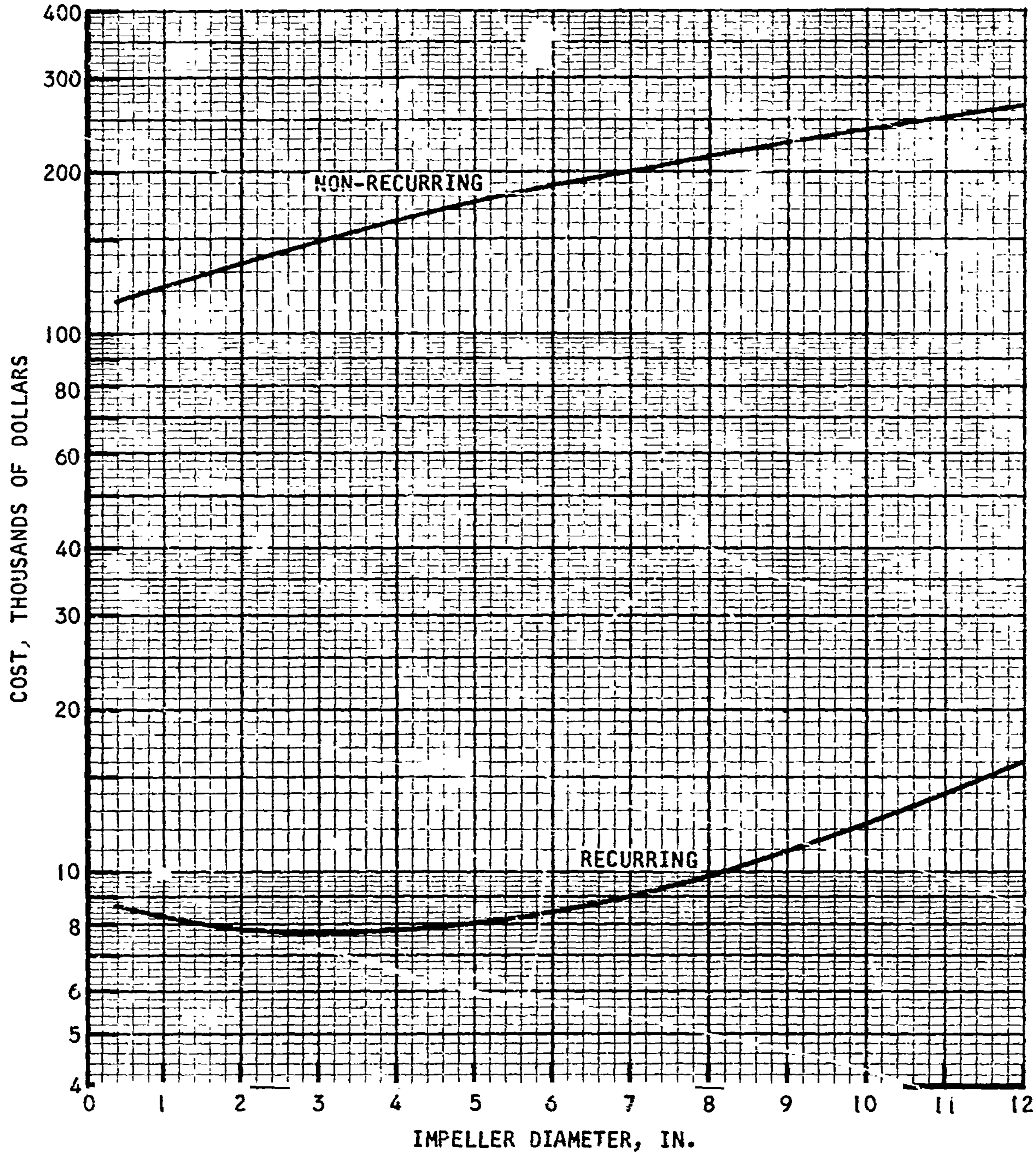

Figure 6-11. Pump Cost Characteristics

R&D program to define optimum designs in 1967. This program, the source of the data presented here, included studies of weight, torque, size and upper limits of power transmission capability.

For driving of the pumps characterized in this study, the permanent magnet coupling has been chosen. Typical coupling configuration is shown in Figure 6-12. The magnets, fabricated in the shape of cylindrical buttons, are contained in a structural rotor which also comprises part of the magnetic circuit. The magnets are samarium-cobalt, a relatively new permanent magnet material that combines high magnetic energy product with reasonable cost.

It is recommended that couplings be used on old pump units considered under this study. Use of the coupling for hydrogen and nitrogen pumps has the advantage of permitting motor design to be simplified and allows minimization of motor windage losses.

Weight of these coupling units is presented in Figure 6-13 as a function of shaft speed and power transmission level. With samarium-cobalt, the tip speed at the magnets must be limited to 575 fps. This limit, apparent in Figure 6-13, may impose some constraint on pump design.

The cost characteristics of the coupling is considered to be primarily dependent on transmitted power capacity. The estimated coupling recurring and nonrecurring cost is plotted in Figure 6-14.

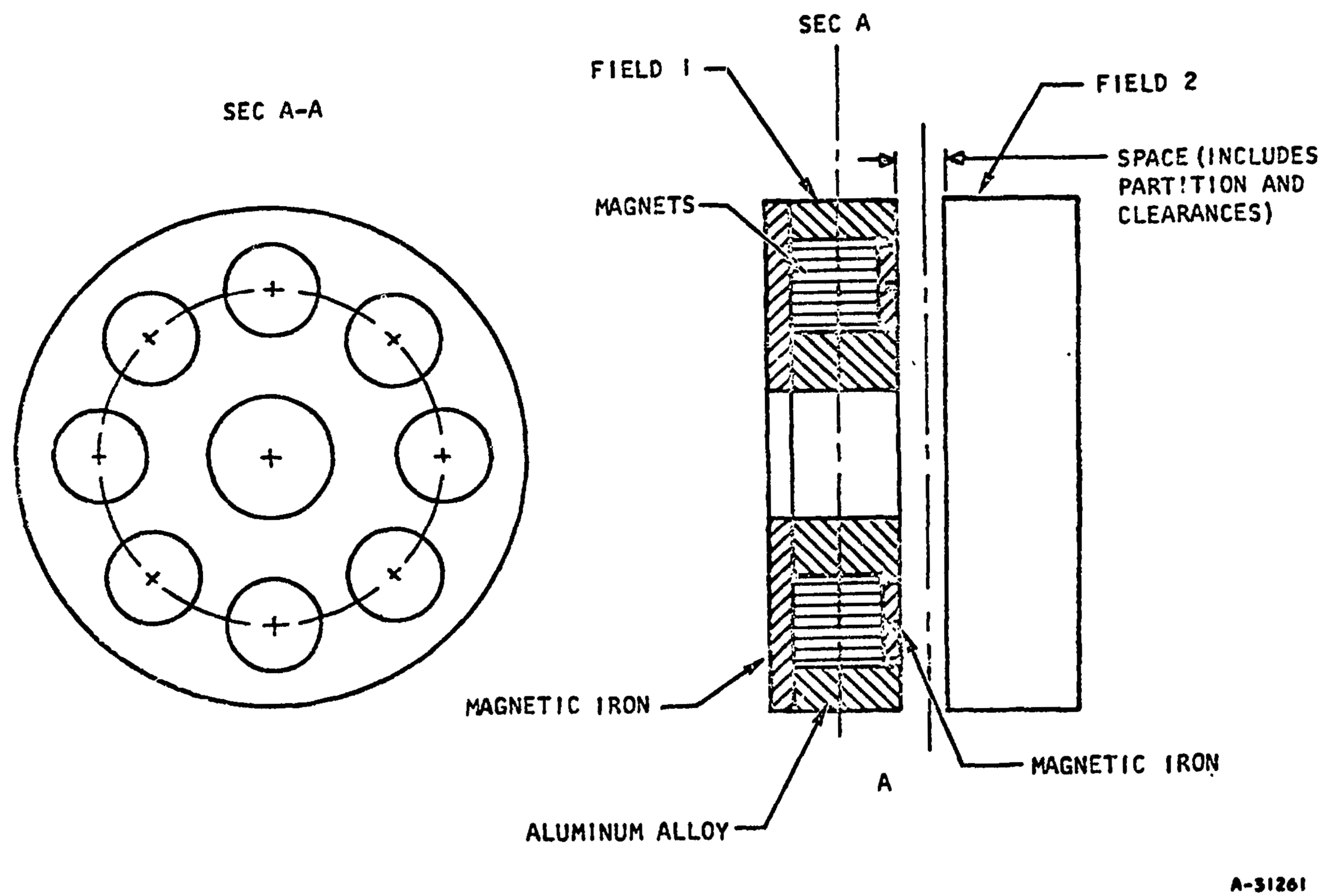

Figure 6-12. Structure of a Magnetic Coupling

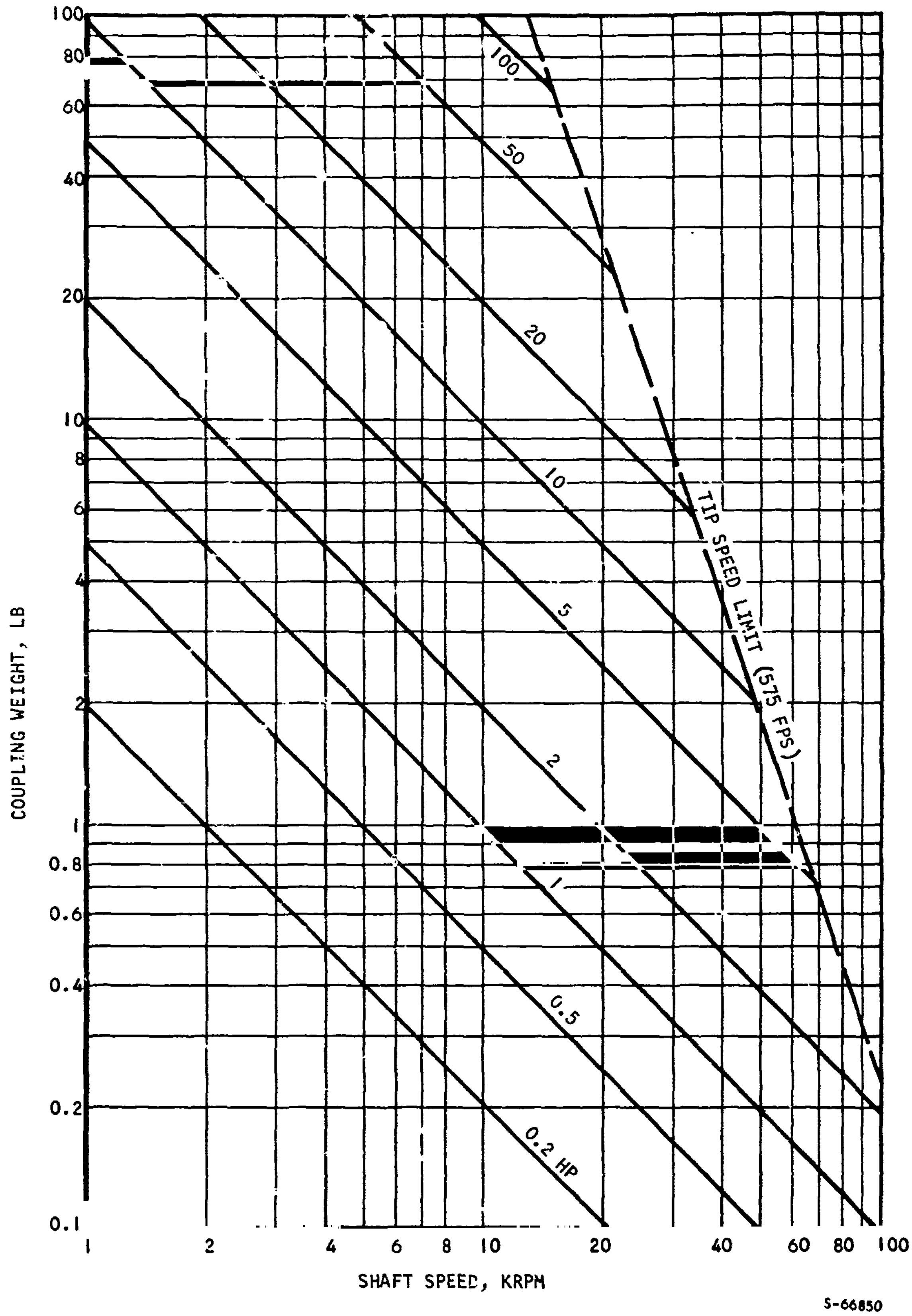

Figure 6-13. Weight of Samarium-Cobalt Magnetic Couplings

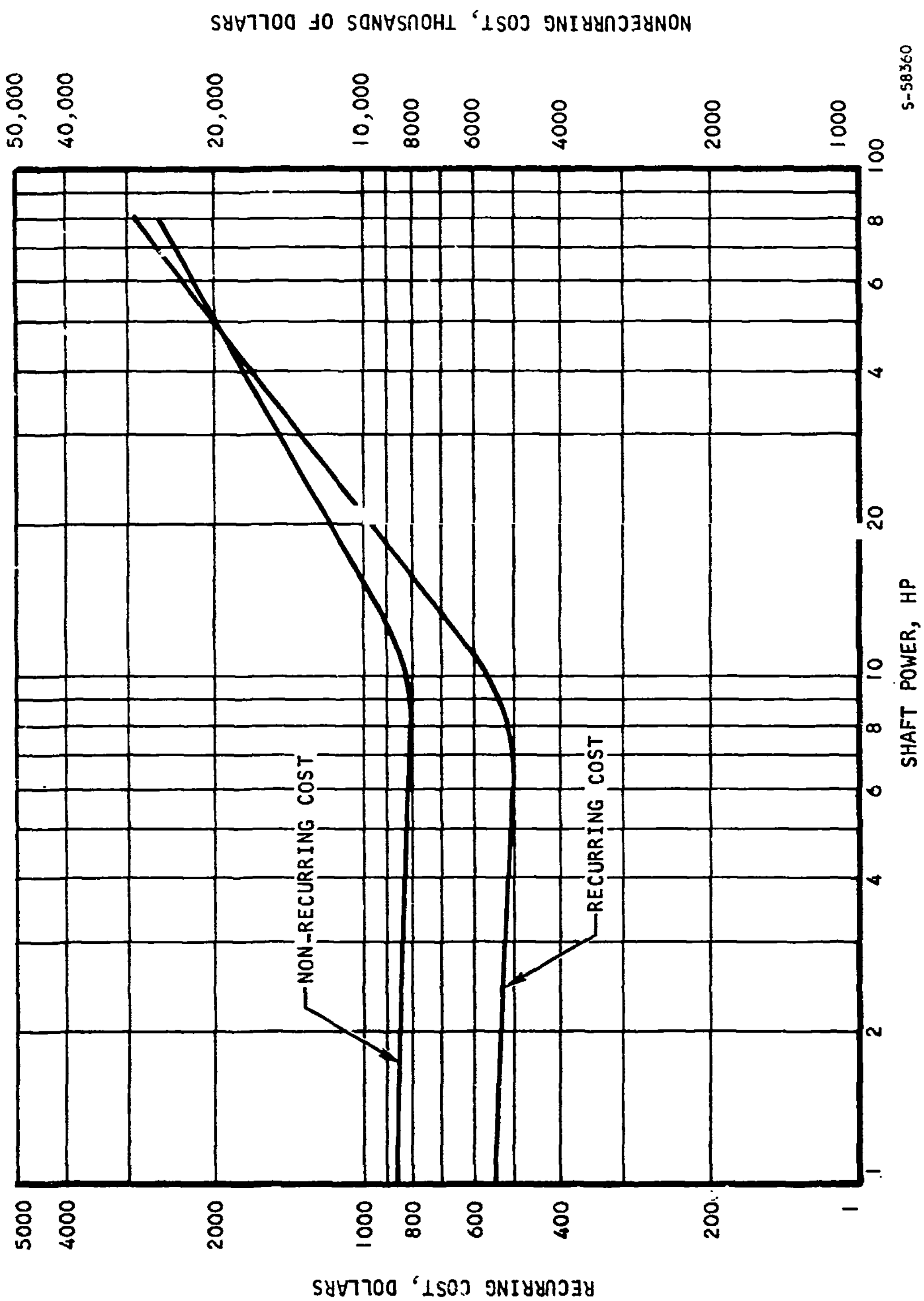

Figure 6-14. Magnetic Coupling Cost Data

SECTION 7

DRIVE MOTORS

Two types of pump drive motors are represented in this section: the ac induction motor and the brushless dc motor. These two motors provide considerable latitude in selection of speed, weight and cost for the pump drive function.

INDUCTION MOTOR

Since considerable design information is available for the induction motor, this characterization was obtained by statistical analysis of the characteristics of a number of motors. The basic assumptions are as follows:

(a) The rotor is of the squirrel-cage construction, using aluminum or copper alloy for the rotor bar.

(b) The lamination is silicon steel.

(c) The stator has a cooling capability of 10 to 20 w/cu in.

(d) The maximum allowable tip speed is 600 fps.

(e) The power source is 3-phase, 115 v, 400 Hz.

(f) Designs ranging from 2 to 12 poles are of interest.

The motor assembly weight, which includes housing, bearings and shaft provisions for mounting of the magnetic coupling, is presented in Figure 7-1. The efficiency of this design, including bearing and windage losses, is found in Figure 7-2. Power factor for fully-loaded induction motors is given in Figure 7-3.

The input power requirement for the motor can be evaluated from

$$PWR = 746 \frac{PWR_S}{\eta_m \, PF} \text{, watt} \qquad (7\text{-}1)$$

where PWR_S = shaft power, hp

η_m = motor efficiency

PF = power factor

Cost elements for the induction motor are provided in Figure 7-4.

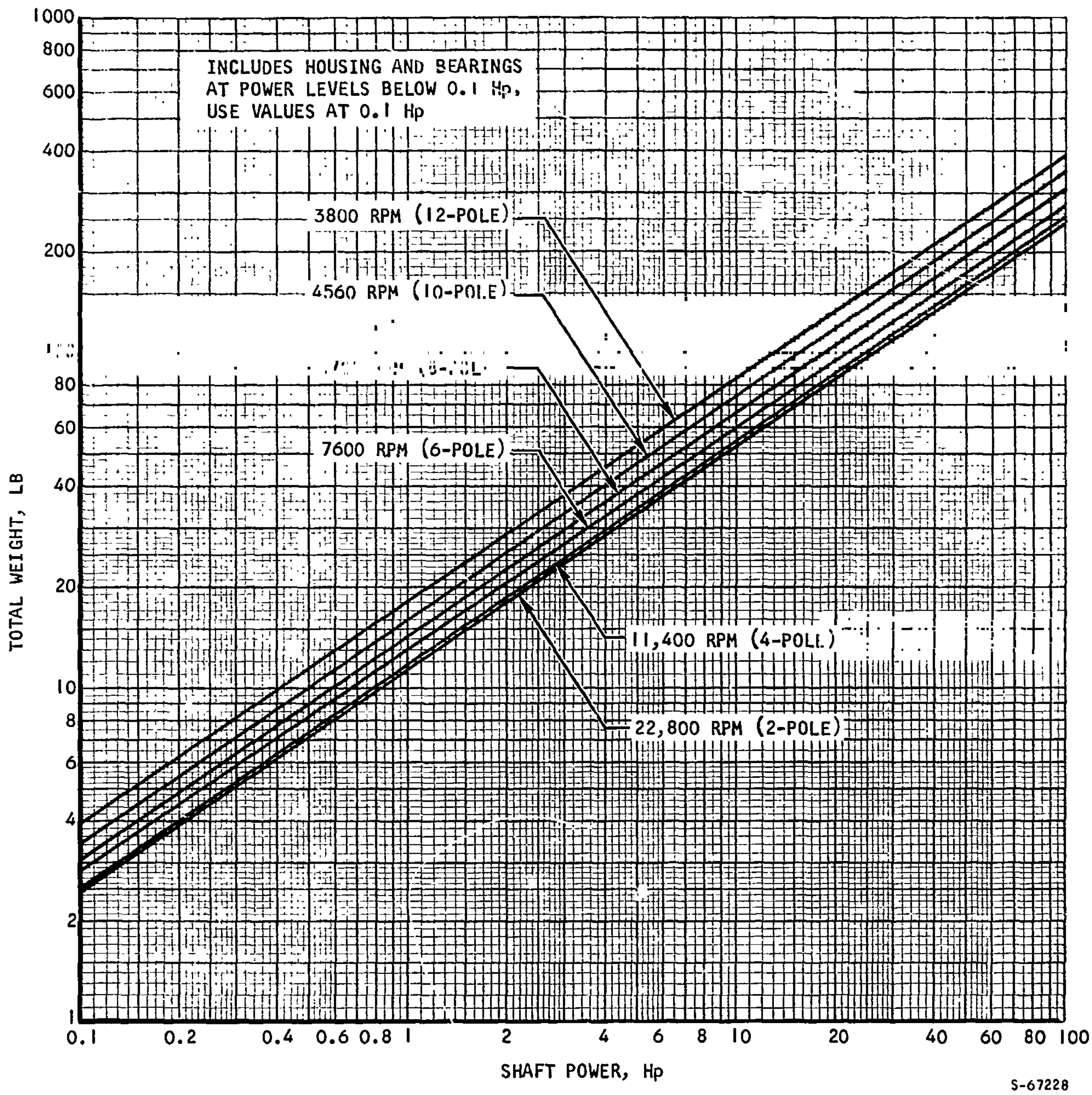

Figure 7-1. Weight of 400 Hz Squirrel-Cage Induction Motors

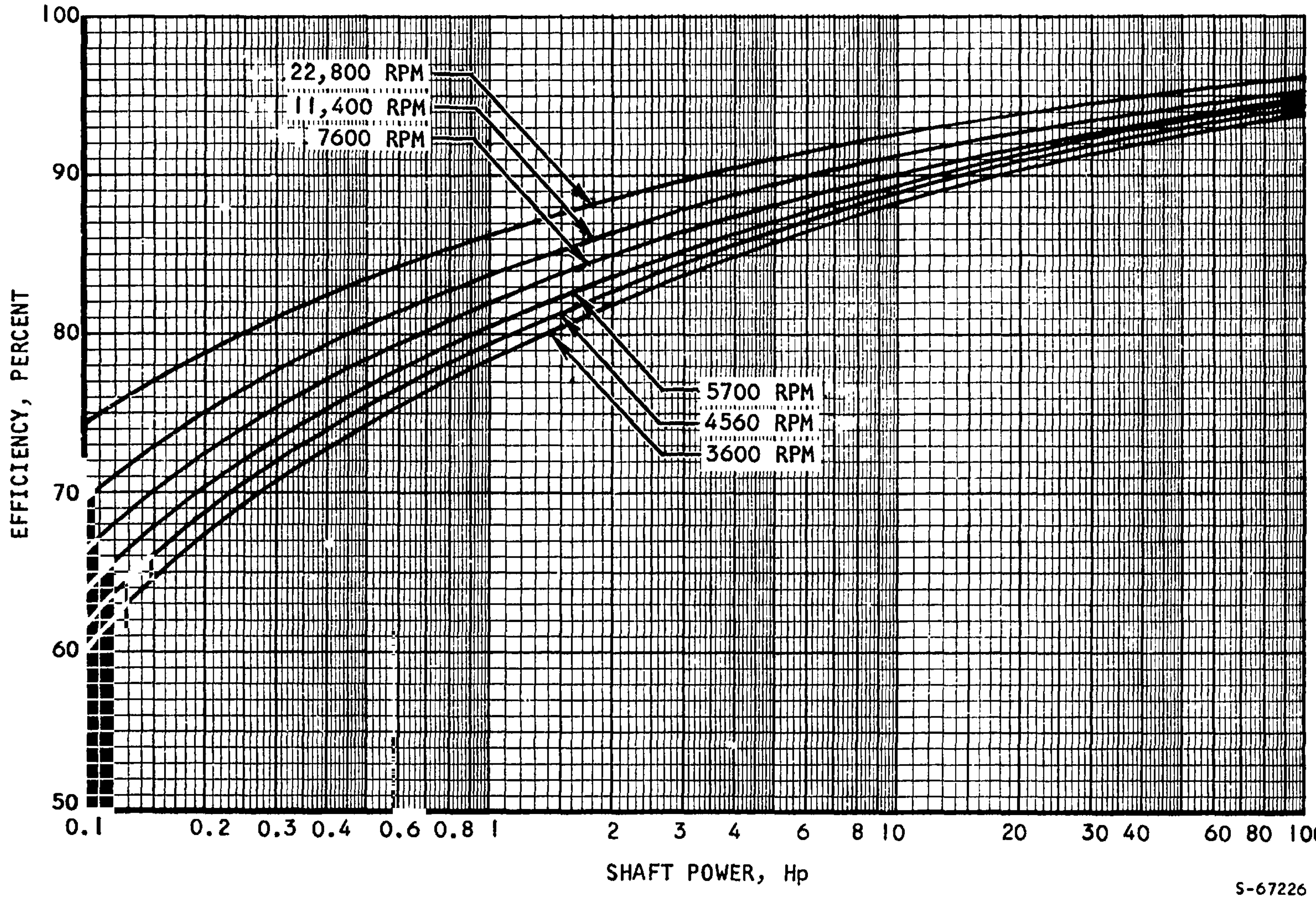

Figure 7-2. Efficiency of 400 Hz Cage Rotor Induction Motors

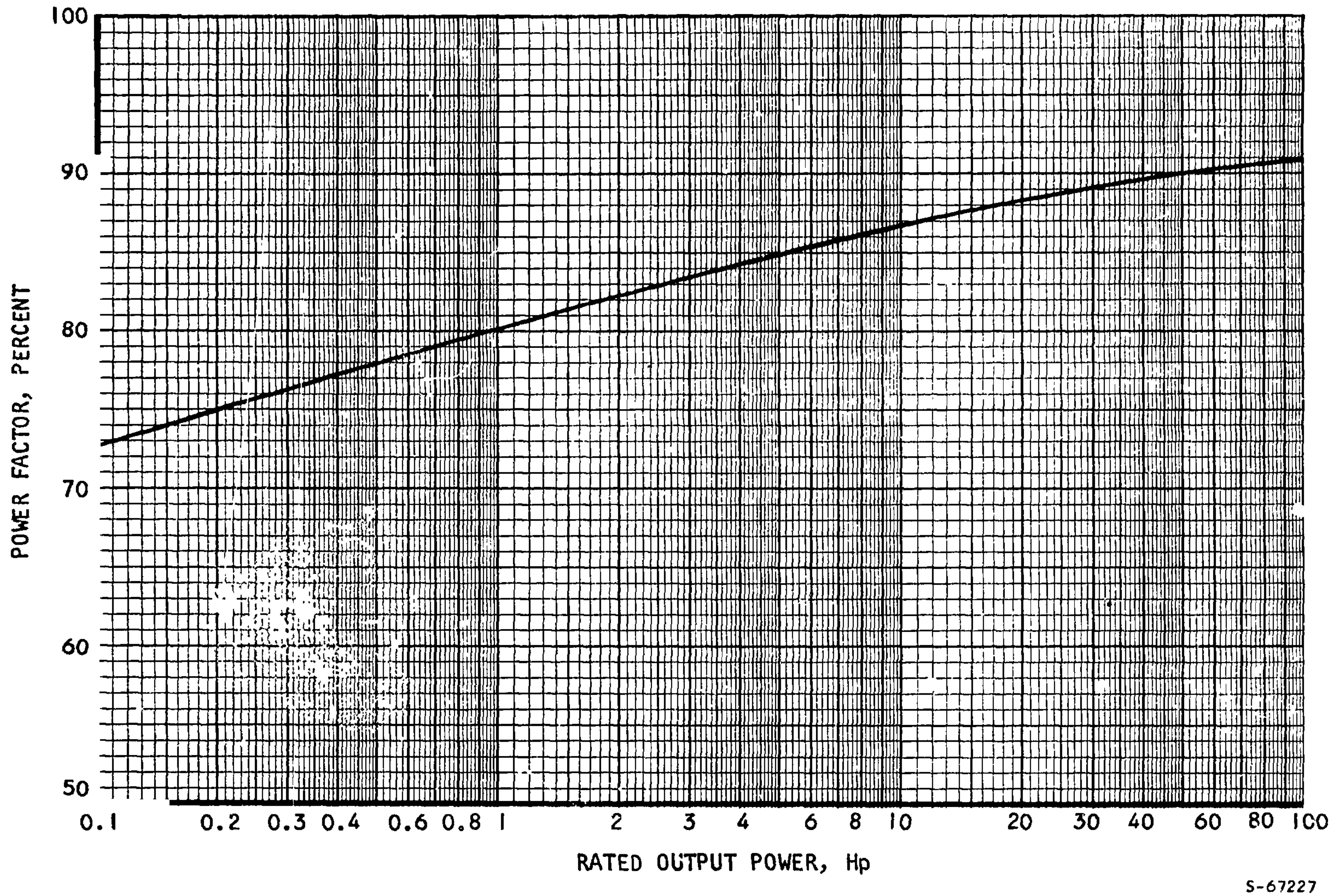

Figure 7-3. **Full-Load Power Factor of 3-Phase Induction Motors**

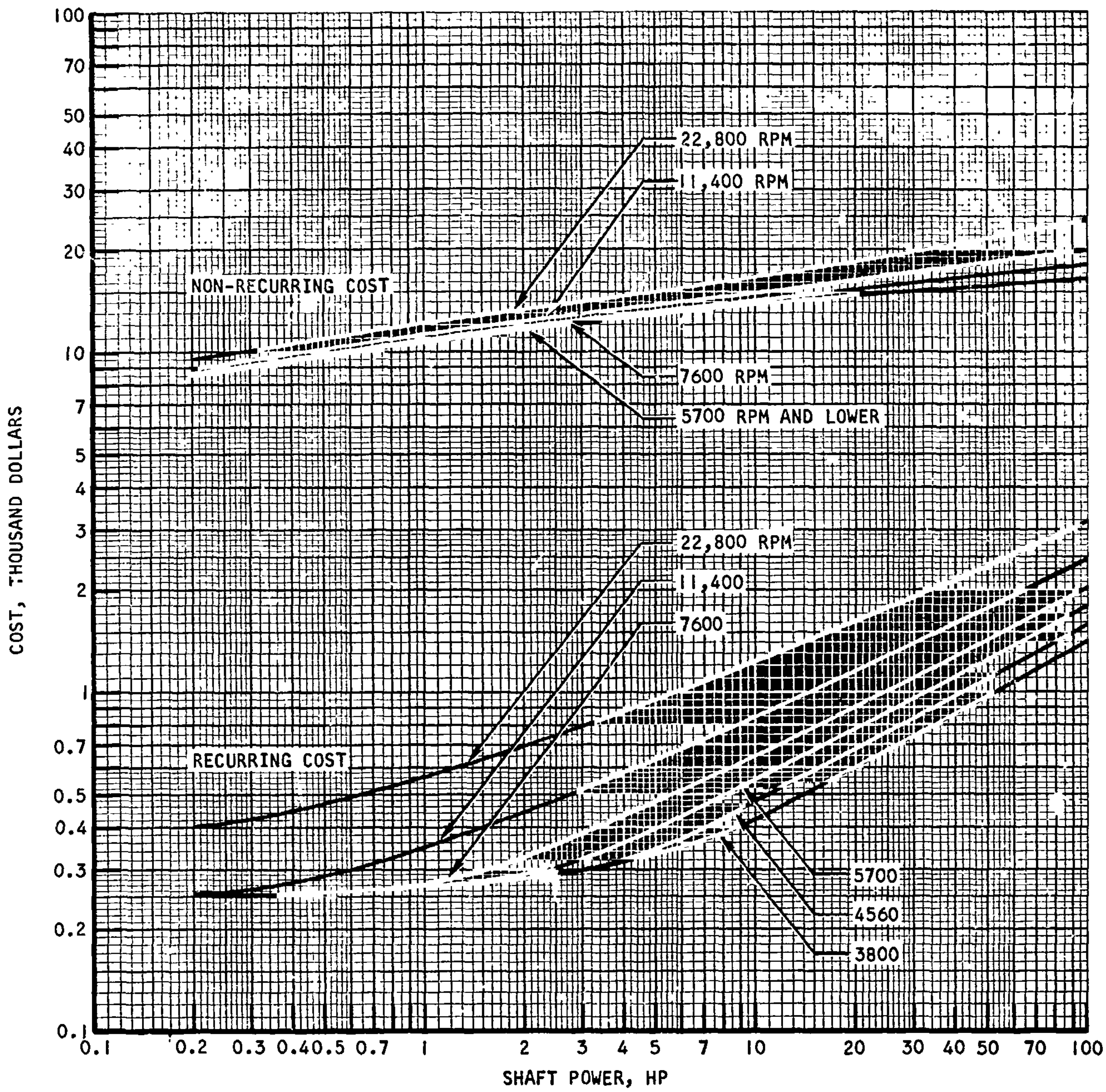

Figure 7-4. Cost Characteristics of 400 Hz Cage Rotor Induction Motors

BRUSHLESS DC MOTOR

The following description characterizes a permanent magnet-type brushless dc motor which will allow power levels up to 100 hp to be supplied at speeds ranging from 4,000 to 64,000 rpm. Although considerably more expensive than three-phase induction motors, the brushless dc motor offers a high degree of flexibility in application.

There are two permanent magnet alloys which can be used in an ironless construction: platinum-cobalt and samarium-cobalt. The use of platinum-cobalt in machines up to 100 hp seemed unrealistic from a cost and availability standpoint. The material is 77 percent platinum by weight. Samarium-cobalt is a new material which has twice the magnetic energy product of platinum-cobalt but has low mechanical strength in tension. Samarium-cobalt or similar materials will probably compose the magnets of the 1970's. This study is based entirely on the use of samarium-cobalt.

Because of the lack of tensile strength in samarium-cobalt, it is necessary to support the rotor magnets. Past analysis of support of permanent magnets in radial-gap rotor assemblies has indicated that a high-strength steel sleeve shrunk over the fabricated rotor is the best means of support. The study was therefore based on the use of a nonmagnetic Inconel 718 sleeve, which must use up some of the allowable airgap region. It was determined by brief iteration that a rotor support using 30 percent of the gap would approximate an optimum condition.

From this configuration, various relations were established. By using a suitable sizing process based on a certain design, the performance of the machine as a function of output power and speed can be determined. The following are the basic assumptions for the analysis.

(a) The alternators are all designed as four-pole machines, representing a practical compromise between fabrication and electromagnetic considerations.

(b) The maximum allowable tip speed of the rotor is 640 fps. This is determined from the loading of the support ring based on a 20-percent overspeed requirement and an Inconel 718 yield strength of 150,000 psi.

(c) When the size of the machine varies, a certain proportionality is maintained.

(d) The magnet material, samarium-cobalt, has twice the magnetic energy product of platinum-cobalt.

(e) The cooling capability is 20 w/cu-in. If this limit is exceeded, the capacity of the machine is derated while maintaining the same weight.

Weight of motor assemblies, which include housing, bearings, provisions for the magnetic coupling and the solid state electronics required by the motor circuit, are presented in Figure 7-5. Overall motor assembly efficiency estimates are provided in Figure 7-6.

Input electrical power is given directly by

$$PWR = 746 \frac{PWR_S}{\eta_m} \qquad (7\text{-}2)$$

The cost information for the brushless dc motor assembly is presented in Figure 7-7.

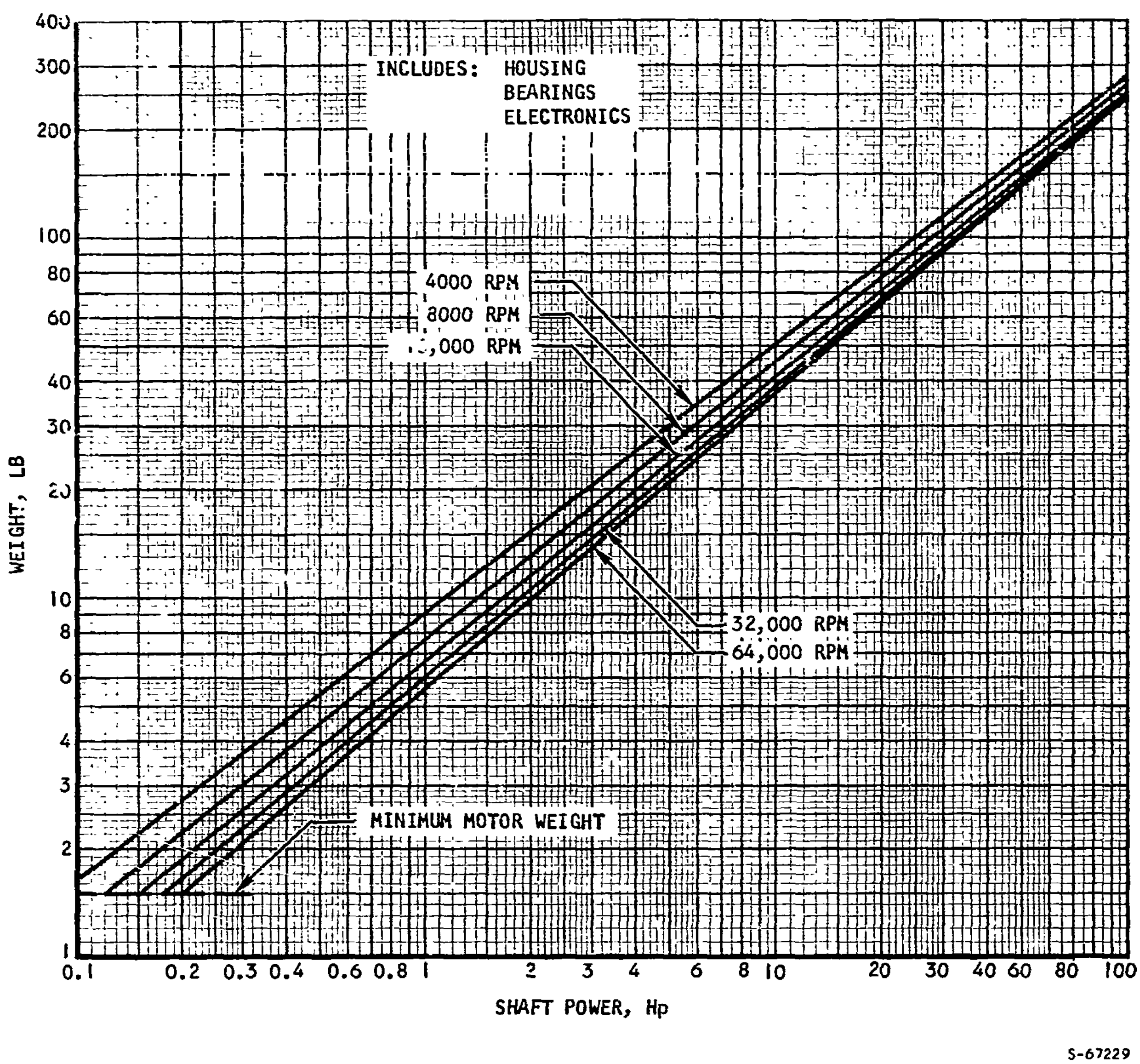

Figure 7-5. Weight of Brushless DC Motors

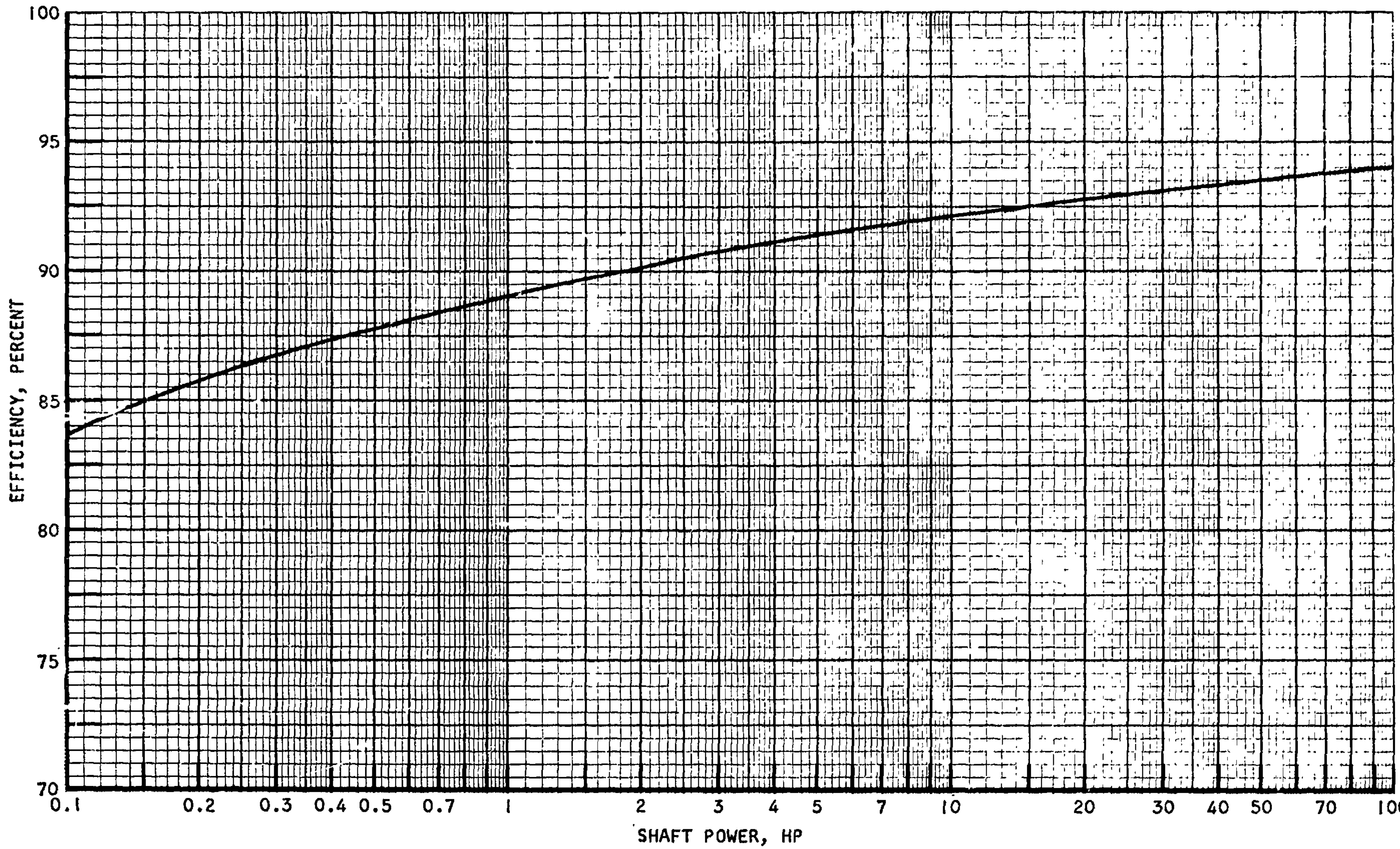

Figure 7-6. Average Efficiency of Samarium-Cobalt Permanent Magnet Brushless DC Motors

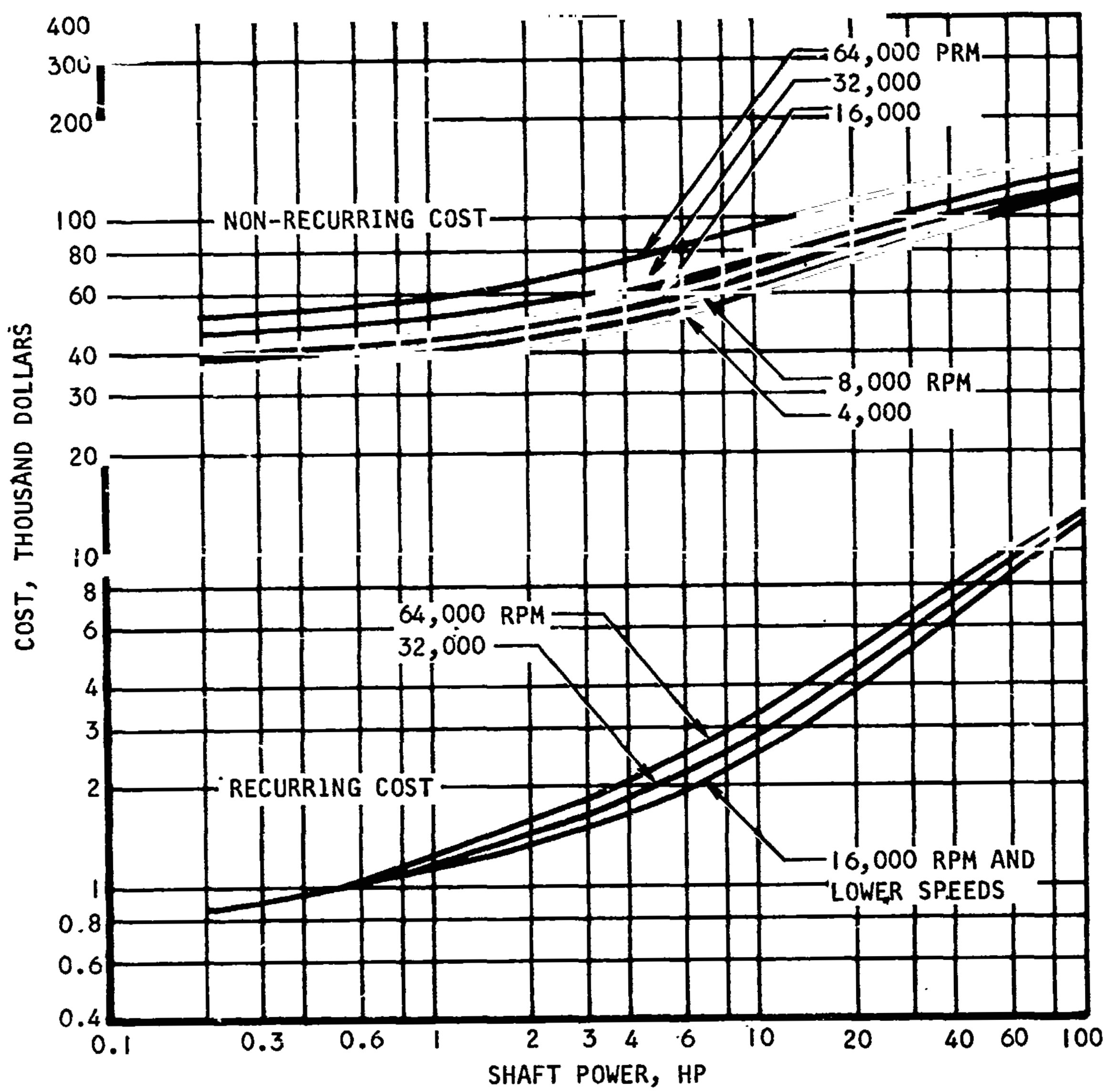

Figure 7-7. Cost Characteristics of Samarium-Cobalt Permanent Magnet Brushless DC Motors

SECTION 8

REFERENCES

1. Wapato, P. G., A. W. Keeley, L. N. Jew and C. F. Young, External Pressurization Systems for Cryogenic Storage Systems - Design Reference Manual, AiResearch Manufacturing Co., Report 71-7535, June 1971.

2. Flow of Fluids, Crane Co., Technical Paper No. 410, 1965.

3. SAE Aero-Space Applied Thermodynamics Manual, SAE Committee A-9, New York.

4. Vennard, J. K., Elementary Fluid Dynamics, Wiley, 1959.

5. ASHRAE Guide Data Book--Equipment, ASHRAE, 1969.

6. Hendricks, R. V., R. J. Simoneau, and R. V. Smith, Survey of Heat Transfer to Near Critical Fluids, NASA TN D-5886, November 1970.

7. Kays, W. M. Convective Heat and Mass Transfer, McGraw-Hill, New York, 1966.

8. Brentari, E. G., P. J. Niarratano, and R. V. Smith, Boiling Heat Transfer for Oxygen, Nitrogen, Hydrogen and Helium, NBS TN-317, September 20, 1965.

9. Shuttle Cryogenic Supply System (CSS) Optimization Study - Final Report; Vol. 10, Heat Exchanger Parametric Data; AiResearch Manufacturing Co., Report 71-7505-10, Prepared for Lockheed Missiles and Space Company under Subcontract 28-7447, June, 1971.

10. Balje, O. E., "A Study on Design Criteria and Matching of Turbomachines: Part B - Compressor and Pump Performance and Matching of Turbocomponents," Trans ASME, 84, Series A, 103-114, 1962.

11. "Centrifugal Pumps for Power Transmission", Air Force Report AFAPL-TR-66-12, January 1966.

12. Eckert, B., and E. Schnell, Axial-und Radialkompressoren, Springer-Verlag, Berlin, 1961.

13. Sanders, J. L., and R. E. Forrette, Orbital Refueling Pump Study Program, AiResearch Manufacturing Co., Report 67-2529, July 1967.

APPENDIX

UTILIZATION OF STORAGE PRESSURE DECAY FOR LIQUID CRYOGEN DELIVERY

It is of interest to investigate the use of decay of storage pressure as alternative means of effecting delivery of liquid from a cryogenic storage system. Assuming that the nominal storage pressure is above the minimum delivery pressure acceptable to the using system, it is clear that this pressure potential will allow some delivery rate to be supported. The objective is to determine the liquid delivery rates that could be obtained for the tank specified in the Design Reference Manual example problem.

PRESSURE DECAY PROCESSES

The first law of thermodynamics for the case of delivery of fluid from a constant volume tank is

$$dQ = dH - Vdp + h_a dm \qquad \text{(A-1)}$$

where

dQ = infinitesimal quantity of heat input to the system

H = total enthalpy of the stored fluid

V = fluid storage volume

p = stored fluid pressure

h_a = specific enthalpy of exiting fluid

m = total stored fluid mass

If the tank is well-insulated, dQ can be considered negligible. The pressure change is then

$$dp = \frac{dH + h_a dm}{V} \qquad \text{(A-2)}$$

and if the tank content consists of a well-mixed, single-phase fluid, the process takes place isentropically.

However, if the tank contains both liquid and vapor, h_a may be considerably different from the average specific enthalpy of the tank contents. Thus, the decay process will depart from the isentropic. Referring to Equation A-2 and noting that for withdrawal dm is negative, it is seen that when the exit stream enthalpy is less than that of average stored fluid, as it is for the case of liquid delivery, pressure decrease will be less than the isentropic process. Thus, entropy must increase.

The rate of pressure change must be dependent on the vapor fraction, or quality, of the tank contents at a point in the process. As the quality increases, the specific enthalpy representing the average stored fluid condition also increases. Since as pressure falls saturated liquid enthalpy decreases, the enthalpy of the departing stream represents a decreasing fraction of the average enthalpy as the tank is depleted. The pressure decay rate dp/dt therefore decreases throughout the delivery period. This is shown in Figure A-1, where several liquid delivery pressure decay processes are presented on a general temperature-entropy plot. All start at the same tank quantity, or initial density, but at successively higher pressures. The delivered fluid flow rate is identical for each process. Each continues until the minimum delivery pressure p_F is reached.

At the beginning of delivery for processes A, B, and C, vapor fraction is relatively small; this results in rapid decay of pressure, however, which is rapidly reduced as quality rises. Process D begins at a supercritical pressure level; decay is very rapid, following a line of constant entropy until the tank contents become two-phase. From that point on, decay resembles that of processes A, B, and C.

The nature of these delivery processes as the liquid portion of the stored fluid is depleted is noteworthy. When the liquid phase has been exhausted and the contents consists of single-phase fluid, the decay path must again become isentropic. However, isentropic expansion from a point along the saturated vapor boundary must produce a small liquid fraction. If it is possible to deliver the liquid produced in preference to vapor (e.g., a gravity field is present such that liquid is directed to the tank outlet), the rate of decay will fall drastically until the liquid phase is again exhausted. At that time, isentropic decay again takes place, producing more liquid phase fluid.

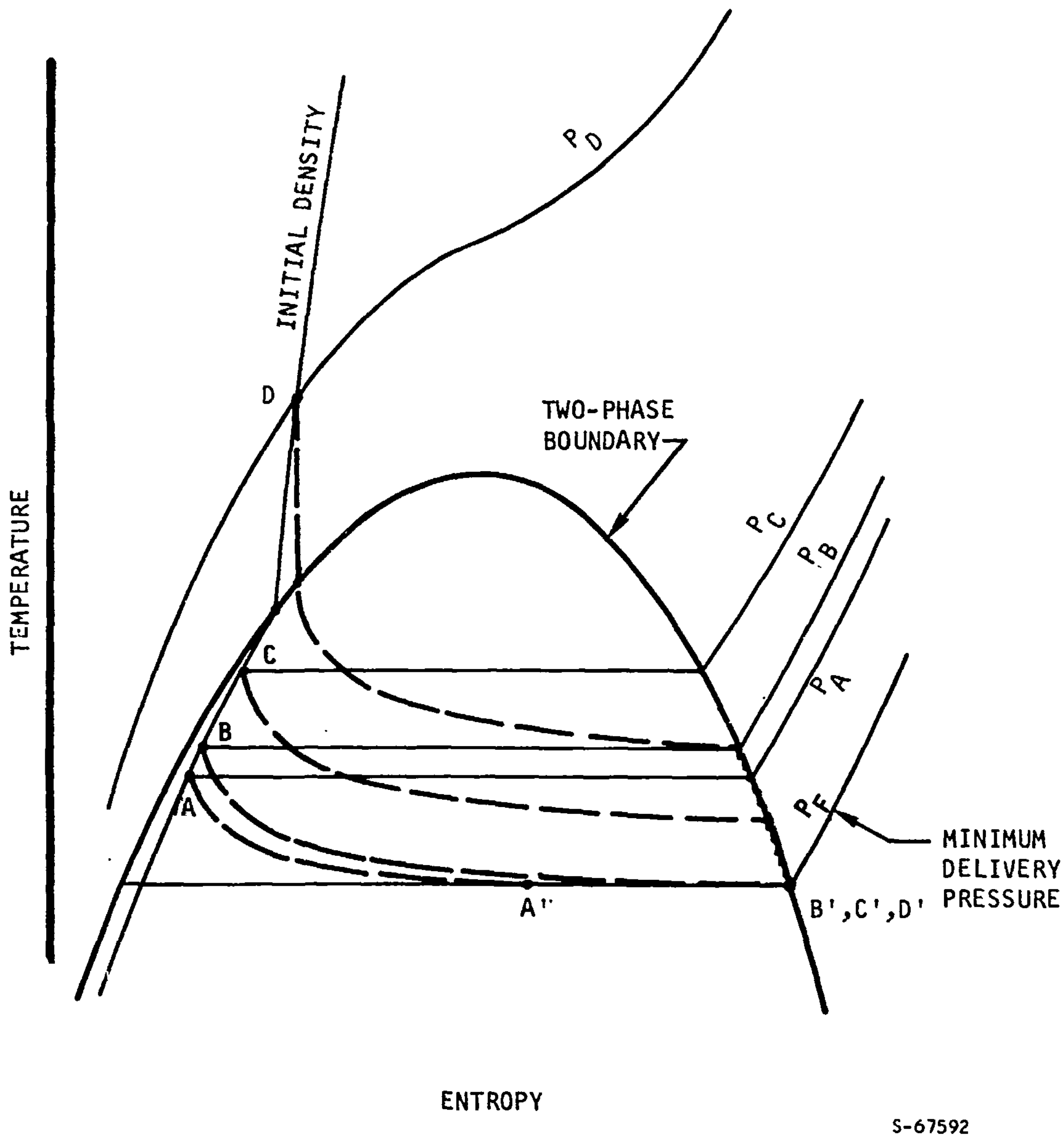

Figure A-1. Liquid Delivery Processes With Pressure Decay

The behavior described above takes place until the delivery period ends, when the pressure p_F is reached. Thus, processes C and D in Figure A-1 are constrained to follow the saturated vapor line once the delivery has caused the liquid phase to be depleted. This causes processes B, C, and D to share the same final stored fluid condition, that of saturated vapor at the pressure p_F. Since identical quantities of mass have been removed at the same flow rate, the flow period sustained by the three processes is also identical.

It is clear from the foregoing that in selecting the initial pressure level for pressure decay liquid delivery processes, there is no advantage in pressures significantly above that of process B. That is, processes which decay to the saturated vapor boundary at pressures well above the minimum delivery pressure only increase pressure containment requirements without increasing flow capability.

On the other hand, lower initial pressures, such as shown for process A, result in higher final fluid density at p_F, and hence a shorter flow period.

ANALYSIS OF EXAMPLE PROBLEM TANK

To quantify these effects for a case of interest, flow capability of the Design Reference Manual example problem tank was investigated using a tank dynamics computer program. The program used considers the following form of the first law written for finite changes:

$$Q = h_2 m_2 - h_1 m_1 + h_a (m_2 - m_1) - CV_o (p_2 - p_1) + m_s c_{p_s} (T_2 - T_1) \quad \text{(A-3)}$$

where V_o = nominal tank volume

m_s = inner shell mass

c_{p_s} = inner shell specific heat capacity

T = fluid temperature

and the subscripts 1 and 2 identify the beginning and end of the time period considered. The final term of Equation A-3 accounts for the effect of thermal storage in the inner shell. The coefficient C applied to the nominal volume accounts for tank volume changes due to pressure and temperature. C is given by

$$C = 1 + \frac{3D_o}{8Et_s}(p_1 + p_2 - 2p_o) + \frac{3\alpha}{2}(T_1 + T_2 - 2T_o) \tag{A-4}$$

where D_o = nominal inner shell inside diameter, based on V_o

p_o = pressure at which $V = V_o$

T_o = temperature at which $V = V_o$

E = Young's modulus for inner shell material

α = thermal expansivity for inner shell material

t_s = inner shell thickness

For the situation examine here, the computer program calculates h_a for single-phase regions as

$$h_a = \frac{h_1 + h_2}{2} \tag{A-5}$$

where h_1 and h_2 are the initial and final average specific enthalpies of the stored fluid. After the two phase region is entered, liquid delivery is to take place; for this case,

$$h_a = \frac{h_{L_1} + h_{L_2}}{2} \tag{A-6}$$

where h_{L_1} and h_{L_2} are the initial and final saturated liquid enthalpies.

The example problem tank was defined as:

Fluid	Oxygen
Tank volume, cu ft	225
Tank geometry	Spherical
Storage pressure, psia	50
Storage delivery rate, lb per sec	5
Delivered fluid phase	Liquid

Since this information was originally established as a problem statement for an external pressurization system, the thermal characteristics of the tank were not defined. To permit calculation of thermal characteristics, the following assumptions were adopted:

(1) The tank is insulated with 2 in. of evacuated aluminized mylar superinsulation.

(2) Inner vessel support employs tension members which can be represented as having:

Total conduction area/length ratio = 0.045 $in.^2$ per in.

Mean thermal conductivity = 7 Btu per hr-ft-^{0}R

(3) Inner vessel is constructed of stainless steel.

After applying the above data and assumptions to a tank design computer program, the following tank characteristics were defined:

Inner shell I.D.	90.60 in.
Inner shell wall thickness	0.055 in.
Outer shell O.D.	94.91 in.
Line and support heat leak	10.8 Btu per hr
Total heat leak	63.0 Btu per hr
Vent flow rate at design point	56.5 lb per hr

For examination of pressure decay delivery, the minimum delivery pressure was assumed to be 30 psia. A range of flow rates encompassing the specified 5 lb per sec was investigated. It was desired to determine the minimum initial pressure required for decay to the saturated vapor condition at 30 psia as a function of flow rate. This required analysis of a number of initial conditions until the proper final state was obtained.

The results of this brief study are presented on Figure A-2, where it is found that the minimum initial pressure for flows as high as 10 lb per sec is well below the nominal tank pressure of 50 psia. In the situation examined, capability exists for the delivery of very large liquid flow rates.

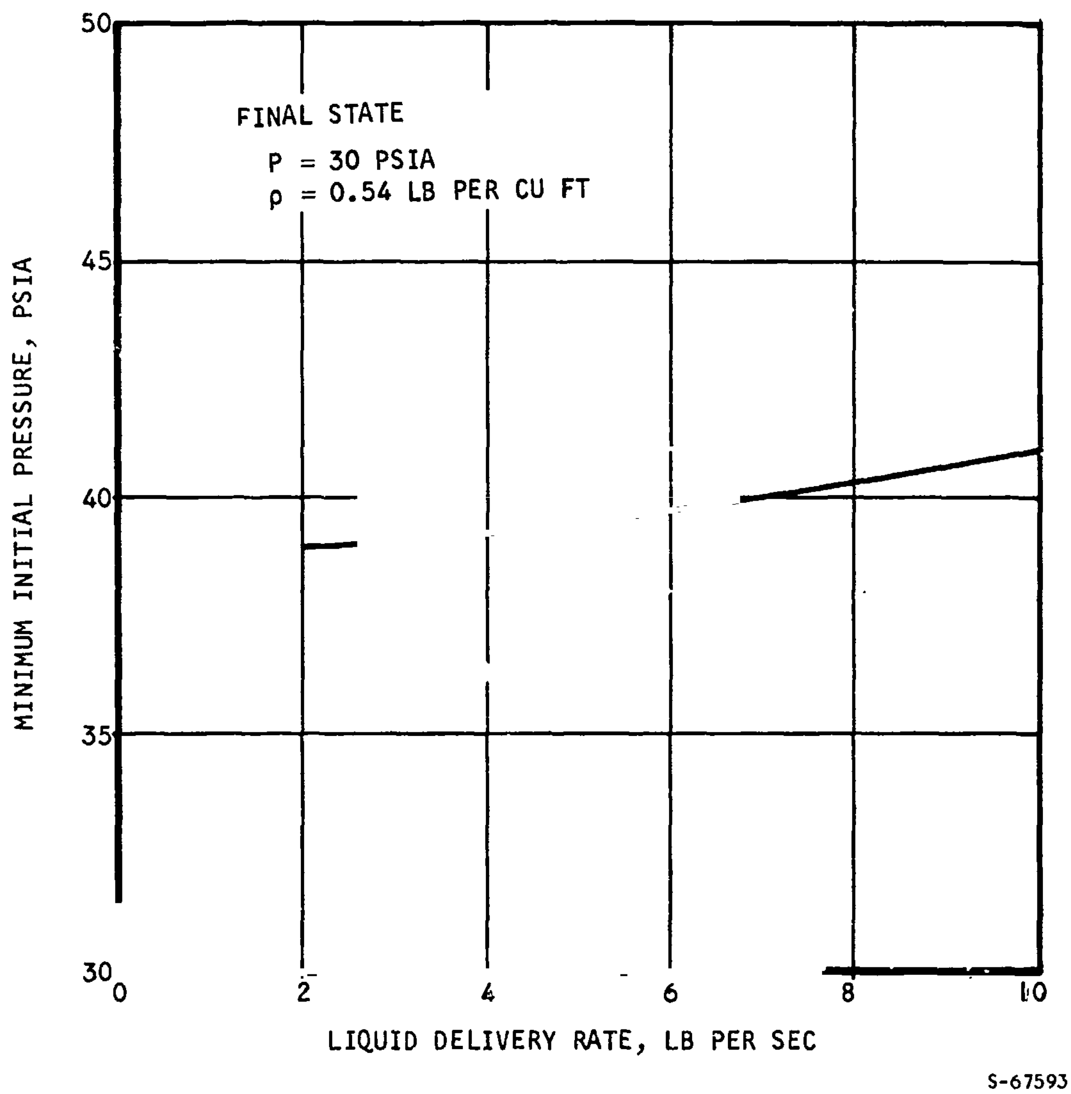

Figure A-2. Pressure Decay Liquid Delivery Performance of Example Problem Oxygen Tank

CONCLUSION

While it would appear that the pressure decay technique can offer an attractive alternative to external pressurization systems for delivery of liquid, several aspects of this analysis must be considered.

First, it must be remembered that the considerations of this appendix are purely thermodynamic. While the flow capacity indicated above is available so far as the thermodynamics of the storage vessel are concerned, the entire delivery process must be studied in detail to define the true flow capacity. Line friction losses undoubtedly place the real limit on this type of delivery process, and since two phase flow must occur at some point in the delivery lines, the limit is likely to be far lower than that permitted by the tank thermodynamics.

Second, the type of delivery discussed here, unlike the external pressurization system, precludes the possibility of providing NPSH for using equipment. When the storage system supplies large high-pressure rise pumps, this consideration may be crucial.